Alma Mater Studiorum – Università di Bologna

DOTTORATO DI RICERCA IN

Scienze della Terra, della Vita e dell’Ambiente

Ciclo XXIX

Settori Concorsuali di afferenza: 04/A2 (prevalente) e 04/A4

Settori Scientifico disciplinari: GEO/02 (prevalente) e GEO/10

TITOLO TESI

The remote sensing-stratigraphic approach applied to the reconstruction of Holocene sedimentary evolution in coastal areas: case studies from Arno and Po delta plains (Italy)

Presentata da: Serena Giacomelli

Coordinatore Dottorato

Prof.ssa B. Mantovani

Relatore

Dott.ssa V. Rossi

Co-Relatore

Prof.ssa M. Sgavetti

Esame finale anno 2017

ABSTRACT

The improvement reached over time in remote sensing (RS) technology, for both airborne and spaceborne products, together with the growing availability of open-access databases, made the remote-sensed data and analyses to be increasingly employed in several geological research fields, including Quaternary and Environmental Geology. Satellite imagery, in particular, can furnish a higher amount of data, more manageable and often at free-of-charge (such as Landsat, Sentinel 2a, etc.), with respect to airborne photos, even though usually with a lower geometric resolution (e.g., Landsat visible and infra-red bands 30 meters *versus* few meters of aerial photos). The possibility to process multi/hyperspectral satellite images facilitate indeed the detection of diverse features/objects from the same scene.

In modern alluvial-coastal plains, the false color composition (FCC-combination of electromagnetic spectral bands in red, green, blue-RGB space) is commonly used to highlight, based on brightness (i.e., reflectance) contrast patterns on the scenes, the soil moisture distribution emerging in the form of surface “traces” (e.g., dark colors: wet/saturated conditions; bright colors: dry conditions). In an alluvial-coastal plain such variations of moisture can help to detect stagnant *versus* well-drained areas, that are past wetlands and paleochannels, respectively. Despite the fact that this type of investigation has been frequently applied in paleohydrographic reconstructions, the relationship existing between RS-derived traces and shallow subsurface stratigraphy remains underexplored.

The present PhD thesis represents a contribution to this open issue, through the application of a multidisciplinary methodology integrating remote-sensed analyses (optical multi/hyperspectral images and DTM LiDAR) with sedimentologic and stratigraphic field data in the study of paleodrainage traces detected in two coastal-deltaic areas from the Ligurian and Adriatic sea: the San Rossore (SR-Arno plain) and the Mezzano Valley (MV-Po plain) sites, respectively.

The processing (FCC, Principal Component Analysis–PCA and Unsupervised classification, basically) and interpretation of several Landsat 7 ETM+, Landsat 8 OLI, Sentinel 2a, ASTER and Hyperion scenes, supported by the use of the high resolution DTM LiDAR, allowed to identify and map in the two sites traces of paleochannels.

Field surveys and soil sampling campaigns performed on selected RS-detected traces permitted to analyze their surface sedimentological and optical characteristics, matching invariabily with silty-clayey lithology .

Thereafter, the investigation was extended to the shallow subsurface (i.e., uppermost 10 m) through the collection of auger drillings and continuous core data on which facies analysis and stratigraphic correlations were undertaken. The cross-reference between RS-identified features (traces) and surface-subsurface deposits (cores) allowed to couple morphologies and deposits, shedding new light on the relationships between surface geological features and the corresponding subsurface stratigraphic architecture and then, to reconstruct extending along traces the “stratigraphic calibration”, the paleodrainage evolution.

In croplands, the combined use of free-of-charge satellite imagery and DTM LiDAR, led to the identification and mapping on the surface of buried (2-4m bgl) landforms (paleochannels). The surface visibility of the traces related to contrasting brightness patterns depends on the surface moisture spatial distribution that, in turn, is influenced by the distribution of organic-rich deposits and/or by the shallow subsurface stratigraphic architecture. In coastal wetlands (MV-site), indeed, the development of a dense, meandering paleodrainage networks produced micro-morphologies that guided the shallow subsurface and surface spatial distribution of organic-rich clays (i.e., saltmarsh and then swamp) while in prograding alluvial-delta plain contexts (SR-site), the occurrence of less organic lithofacies and more variable facies heteropies with respect to the wetlands, can be responsible for a lower degree of the traces visibility.

As documented by litho-facies correlations performed on stratigraphic sections involving previous and newly drilled cores, along with radiocarbon dating carried out on cores, during highstand conditions (after ca. 7000 yr BP) the two sites follow different mechanism of lagoon infilling and delta growth. In Pisa, the transgressive lagoon experienced a “sheltered” delta phase (ca. 6000-3000 yr BP), with sinuous distributary channels crossing swampy area, gradually disappearing with the beginning of the wave-dominated delta progradation (from ca. 3000 yr BP on). In Mezzano, the lagoon experienced a tidally-influenced phase (ca. 6000-3000 yr BP) mainly favored by the local morphologies (i.e., low topographic gradient) and delta lobe dynamics. The Po di Spina delta lobe activation (around 2800 yr cal BP) in the MV-site induced the isolation of the basin that turned into a stagnant paludal environment just recently reclaimed.

RIASSUNTO

I progressi fatti dal telerilevamento, sia aereo che da piattafroma satellitare, insieme alla crescente disponibilità di database open-access, hanno incentivato l'uso di dati telerilevati in diversi campi della geologia, incluso il Quaternario e la Geologia Ambientale. Le immagini satellitari, in particolare, spesso *free-of-charge* (quali Landsat, Sentinel 2a, etc…), possono fornire un quantitativo di dati maggiore, più facilmente gestibile rispetto alle foto aeree, sebbene con una risoluzione geometrica in genere minore (es: Landsat nel visibile e infra-rosso è 30m *versus* pochi metri delle foto aeree). La possibilità di elaborare immagini multi/iperspettrali infatti agevola l'identificazione dei diversi elementi presenti all'interno della stessa scena. Nelle pianure alluvionali-costiere attuali, composizioni in falsi colori (combinazioni di bande elettromagnetiche spettrali nei canali R-G-B) sono comunemente usate per mettere in evidenza la distribuzione superficiale dell'umidità del suolo, restituita sotto forma di "tracce", sulla base dei contrasti di luminosità che caratterizzano l'immagine (ovvero, colori scuri: condizioni di umidità/suolo saturo; colori chiari condizioni drenate). Tali variazioni di umidità consentono di distinguere aree umide rispetto ad aree ben drenate, e quindi in ambiente alluvionale-costiero consentono di identificare, rispettivamente, tracce di antiche paludi e paleocanali. Nonostante il fatto che questo tipo di indagine sia stato frequentemente utilizzato nelle ricostruzioni paleoidrografiche, resta poco esplorato il rapporto esistente fra tracce telerilevate e la stratigrafia del primo sottosuolo.

La presente tesi di dottorato rappresenta un contributo alla comprensione di tali rapporti, attraverso l'applicazione di una metodologia multidisciplinare che integra analisi da telerilevamento (immagini satellitari ottiche multi/iperspettrali e modelli digitali del terreno-DTM da LiDAR) con dati sedimentologici di campagna e stratigrafici di sottosuolo nello studio di paleodrenaggi identificati in due aree costiere che si affacciano sul Mar Ligure e sul Mar Adriatico: il sito di San Rossore (pianura dell'Arno) e la Valle del Mezzano (Delta del Po), rispettivamente. L'elaborazione (tra cui composizione in falsi colori, analisi delle componenti principali e classificazione non-supervisionata) ed interpretazione di diverse immagini (Landsat 7 ETM+, Landsat 8 OLI, Sentinel 2a, ASTER e Hyperion), affiancata dall'uso di DTM ad alta risoluzione, hanno permesso di identificare e mappare nei due siti diverse tracce di paleocanali.

Il rilevamento di campagna ed il campionamento di suoli effetuato su tracce telerilevate opportunamente selezionate hanno consentito di caratterizzarle dal punto di vista sedimentologico e ottico, risultando invariabilmente associate a litologie siltose-argillose. Le indagini sono state successivamente estese al primo sottosuolo (primi 10m) attraverso l'acquisizione di dati stratigrafici (carote) tramite perforazione con trivella a mano e carotiere a percussione (vibracore), sui quali sono state effettuate analisi di facies e correlazioni stratigrafiche. L'incrocio tra tracce telerilevate e depositi superficiali di sottosuolo ha consentito di associare depositi a forme, chiarendo il rapporto esistente fra elementi geologici superficiali e architettura stratigrafica di sottosuolo e di ricostruire, estendendo la calibrazione stratigrafica lungo lo

sviluppo planimetrico delle tracce, l'evoluzione del paleodrenaggio. Nelle aree agricole, l'uso combinato di immagini satellitari gratuite e di DTM da LiDAR, ha consentito di identificare e mappare sulla superficie tracce di paleocanali sepolti (2-4m dal piano campagna). La visibilità in superficie di queste tracce è legata a contrasti di luminosità che dipendono dalla distribuzione superficiale dell'umidità che, a sua volta, è influenzata dalla distribuzione spaziale dei depositi ricchi in materia organica e/o dalla architettura stratigrafica del primo sottosuolo. Nelle aree umide costiere (sito MV) infatti, lo sviluppo di un paleodrenaggio fitto e meandriforme ha prodotto micro-morfologie che hanno guidato la distribuzione superficiale e nel primo sottosuolo di argille ricche in materia organica (es: paludi salmastre e dulcicole) mentre in contesti alluvionali-deltizi progradanti (sito SR), la presenza di litofacies meno organiche e la maggiore variabilità delle eteropie rispetto a contesti palustri, sembrano essere responsabili per una minore visibilità delle tracce in superficie.

Come documentato dalle correlazioni di facies realizzate sulle sezioni stratigrafiche che coinvolgono dati di sottosuolo pregressi e di nuova acquisizione, e dalle datazioni radiocarbonio realizzate su carota supportate da dati esistenti, durante l'highstand (dopo 7000 anni fa) nei due siti studiati (SR e MV) meccanismi di tipo diverso hanno portato al riempimento delle lagune trasgressive e alla crescita dei delta. A Pisa, la laguna si configura come protetta (tra i 6000 e i 3000 anni fa), con canali distributori sinuosi che attraversano aree paludose, che scompaiono gradualmente con l'inzio della progradazione del delta dell'Arno (attorno ai 3000 anni). Nella Valle del Mezzano, la laguna attraversa una fase tidale-influenzata (tra i 6000 e i 3000 anni fa) favorita principalmente dalla morfologia locale (es: basso gradiente topografico) e dalle dinamiche di sviluppo dei lobi deltizi. L'attivazione del lobo deltizio del Po di Spina (attorno a 2800 anni fa), in particolare ha indotto nel sito del Mezzano l'isolamento del bacino trasformandolo in un ambiente stagnante, solo recentemente bonificato.

“In the middle of difficulty lies opportunity.”

A. Einstein

RINGRAZIAMENTI

In queste poche righe, scritte volutamente nella mia madrelingua, desidero ringraziare tutti coloro che mi hanno aiutato nella realizzazione del mio progetto di ricerca e tutti quelli che in qualche modo hanno fatto parte di questo percorso durato tre anni.

Comincio con il ringraziare di cuore la mia tutor, la dott.ssa Veronica Rossi con la quale ho condiviso ogni fase di questa ricerca. La ringrazio per l'immancabile sostegno, scientifico e umano, e per la fiducia ricevuti, per la straordinaria disponibilità, per la pazienza e per la sua amicizia. E la ringrazio soprattutto per aver continuato a credere in questa ricerca anche nei momenti meno facili, supportandomi sempre e non abbandonandomi mai.

Ringrazio molto la Prof. ssa Maria Sgavetti, la mia co-tutor in questo Dottorato. Maria mi ha inziata alla disciplina del telerilevamento della quale è esperta da sempre, facendomi appassionare a questo lavoro sempre più. La ringrazio per avermi spronata e sostenuta in ogni momento, per avermi supportata da tutti i punti di vista, per aver appoggiato le mie scelte e per avermi dato la possibilità di confrontarmi con lei ogni qualvolta ne sentissi il bisogno.

Grazie di cuore al Prof. Alessandro Amorosi per l'infinita disponibilità, per la pazienza e per la sua preziosa supervisione e per essere stato un riferimento.

Ringrazio il Prof. Roberto Carlos de Souza Filho per la disponibilità dimostrata durante il mio periodo di fomazione all'estero, dove grazie a lui ho avuto modo di approfondire le mie conoscenze sul telerilevamento. Grazie anche a Saeid Asadzadeh, stimato collega e amico prezioso col quale ho avuto la fortuna di condividere la mia permanenza all' IG_ Instituto de Geociências presso UNICAMP (San Paolo).

Ringrazio i revisori di questa Tesi di Dottorato, il Prof. Roberto Tinterri e la dott.ssa Dilce Fatima Rossetti per la disponibilità, per gli utili consigli e gli stimoli ricevuti.

Ringrazio il Dipartimento di Scienze della Terra di Pisa, nelle persone del Prof. Giovanni Sarti, della Prof.ssa Marta Pappalardo e della dott.ssa Monica Bini per aver dato disponibilità e supporto logistico.

Ringrazio il Comune di Pisa, nella persona del dott.geol. Marco Redini per la concessione dei dati LiDAR, insieme al Ministero dell'Ambiente e della Tutela del Territorio.

Dico un grazie speciale ai ragazzi del Dipartimento di Scienze della Terra (ci tengo a chiamarlo così!) dell'Università di Parma, tutti, ed in particolare i ragazzi del dente E dove da ormai 4 anni a questa parte ho l'opportunità di lavorare e dove ho avuto la fortuna di trovare non solo stimati colleghi ma amici.

Ringrazio Mirko Carlini per tutti i costruttivi confronti, per gli stimoli, per il supporto, l'aiuto e per la sua sincera amicizia. Grazie a Giovanna Serventi, collega ma soprattutto amica con la quale condivido quotidianamente la mia vita lavorativa…grazie per la pazienza, per il sostegno, l'aiuto e per tutto ciò che condividiamo, cose buone e meno buone…non so come farò l'anno prossimo! Ringrazio Elisa Galli ed Arianna Secchiari per l'amicizia e l'affetto dimostrato durante il mio percorso.

Grazie ad Andrea Civa, fondamentale presenza nelle mie campagne di acquisizione dati ma soprattutto amico. Lo ringrazio per il supporto e la disponibilità, e per tutte le leccornie messe a disposizione della sottoscritta che hanno, non solo deliziato il palato, ma stimolato la mente!

Ringrazio Katia Carbonara per essersi presa cura di me, non lasciandomi mai senza cena quando ho dovuto fare *tour de force* diurno/notturni lontana da casa. Grazie per l'amicizia.

Ringrazio Alberto Piazza per avermi fatto sorridere sempre con le sue battute, anche in momenti difficili…l'umore per me è molto importante per la buona riuscita di un lavoro!

Grazie a Mahtab Mozafari, persona ricca e matura, con la quale ho potuto confrontarmi negli ultimi periodi e che mi ha certamente aiutato a fare training con l'inglese!

Ringrazio anche tutti quelli che del Dente E non ho nominato, per nome e cognome, Michele, Rosalia, Flavio, etc. ma che mi sono stati comunque vicini spesso tirandomi su di morale..

Ringrazio Teresa Trua, con la quale ho condiviso tanto tempo soprattutto durante i nostri viaggi da pendolari. Grazie per l'amicizia, il supporto morale ed i preziosi consigli.

Grazie ai colleghi di Dottorato del XXIX ciclo del BiGeA dell'Università di Bologna coi quali ho condiviso momenti ufficiali (presentazioni) e anche ludici (soprattutto pranzi!!), ed in particolare all'amico Andrea Cau col quale ho potuto spesso scientificamente e umanamente confrontarmi durante questi tre anni.

Ringrazio Francesco Rinaldi, Luigi Bruno, Bruno Campo per la loro disponibilità….senza di loro non sarebbe stato possibile acquisire dati e quindi fare ricerca!

Grazie alla mia famiglia, per aver accettato sempre le mie scelte lavorative, e per avermi appoggiata in ogni modo. Ma soprattutto li ringrazio per avermi insegnato a credere in quello che faccio.

Ed infine ringrazio Michele, una persona che considero straordinaria e che ho avuto la fortuna di avere accanto anche in questo mio percorso di Dottorato. Lo ringrazio per aver condiviso con me tutto, per avermi sostenuta sempre, per avermi aiutata fisicamente nelle mie campagne, per avermi sopportata e supportata, per non avermi mai abbandonata. Per avermi insegnato ad affrontare con semplicità piccoli e grandi difficoltà. Lo ringrazio per l'infinita pazienza, per non essersi mai lamentato di tutti i weekend non goduti e per molte delle vacanze “saltate” per via dei miei impegni. Senza di lui sarebbe stato molto difficile riuscire a concludere questo mio percorso. Gliene sarò sempre grata.

TABLE OF CONTENTS

CHAPTER 1_INTRODUCTION

CHAPTER 2_THE SATELLITE OPTICAL MULTI-HYPERSPECTRAL IMAGERY AND DIGITAL TERRAIN MODEL (DTM): PRINCIPLES AND DATA PROCESSING

CHAPTER 3_THE INTEGRATED REMOTE SENSING (RS)-STRATIGRAPHIC APPROACH

CHAPTER 4_PISA PLAIN (ARNO DELTA) RS-STRATIGRAPHIC RESULTS

CHAPETR 5_ MEZZANO VALLEY (PO DELTA PLAIN) RS-STRATIGRAPHIC RESULTS

5.1 Paleodrainage RS-detected traces (MV west area)

5.2 Beach-ridges RS-detected traces (MV east area)

CHAPETR 6_ MEZZANO VALLEY (PO DELTA PLAIN) RS-STRATIGRAPHIC RESULTS

APPENDIX A - SATELLITE IMAGES: PCA and FCC examples (Pisa Plain and Mezzano Valley study areas)

APPENDIX B - STRATIGRAPHIC LOG AND PHOTOGRAPHIC REPORT OF VIBRACORES (Pisa Plain and Mezzano Valley study areas)

APPENDIX C - PUBLISHED PAPER (Pisa Plain)

CHAPTER 1_INTRODUCTION

1.1. Background

The improvement reached over time in remote sensing (RS) technology, for both airborne and spaceborne products, paralleled by the expanding availability of open-access databases, led the RS data and analyses to be increasingly employed in several geological research fields, including Quaternary and Environmental Geology.

Beside the widespread use of RS in geological mapping, hydrological and land-use studies, mining exploration and environmental monitoring (Bakkeret al., 2009), many RS data as aerial photographs, satellite images and digital elevation model (DEM) have been often used also in urban and extra-urban geoarchaeological contexts (Arnaud-Fassetta et al., 2003; Fouache et al., 2005; Stefani and Vincenzi, 2005; Vött, 2007; Ghilardi et al., 2010; Mozzi et al., 2010; Bisson and Bini, 2012; Bini et al., 2012b; Furlani et al., 2012; Amorosi et al., 2013a). When used as a support to geomorphological and geological surveys, these data commonly succeed in the identification of past natural (alluvial and/or coastal) and/or anthropogenic landforms, which interacted with the growth phases of the archaeological site. The approach combining RS images (aerial photographs, satellite images) with DEM has been more frequently adopted also for reconstructing past drainage networks in many alluvial-delta plains (Ghilardi et al., 2008; Piovan et al., 2010, 2012; Ravazzi et al., 2013), and fluvial systems, especially in areas where the acquisition of field data is difficult due to a dense forest cover (Rossetti et al., 2008a, 2009, 2015; Mantelli et al., 2009).

It is well known that satellite images can furnish a higher and more manageable volume of geological data at free-of-charge with respect to airborne photos (Landsat, Sentinel, Hyperion, and recently also ASTER are free-of-charge), even if the geometric resolution is usually lower (e.g., Landsat visible and infra-red bands 30 meters *versus* few meters of aerial photos). Indeed, the processing of satellite images permits to produce different combinations of spectral bands (constituting the electromagnetic spectrum-EM, i.e., sunlight spectrum), highlighting diverse features/objects from the same scene.

In modern alluvial-coastal plains, false color composition (combination of spectral bands in red, green, blue-RGB space) is commonly used to highlight different soil moisture contents emerging in the form of surface “traces” (e.g., dark colors: wet/saturated conditions; bright colors: dry conditions). Such variations of moisture can help to identify stagnant *versus* well-drained areas, which in an alluvial-coastal plain environment can be useful for detecting past wetlands and paleochannels, respectively (Bisson and Bini, 2012; Bini et al., 2012a; Sgavetti, 1974; Sgavetti and Ferrari, 1988). Despite the fact that this type of investigation has been applied in paleohydrological reconstructions, the use of RS data in stratigraphic analysis, particularly at the shallow subsurface, remains underexplored.

In particular, if and in which way shallow subsurface stratigraphy influences trace's visualization it is still an open issue. Indeed, the electromagnetic spectrum (sunlight) detected by satellite sensors is known to be influenced by Earth's surface features, but few studies (Amorosi et al., 2013; Quintanar et al., 2013) have recently documented the occurrence of buried paleochannels in correspondence of the remote-sensed traces suggesting that also RS optical systems can be a valuable tool to infer what occurs underneath the surface (Bakker et al., 2009; Wang et al., 2012).

Thus, a deeper investigation into the relationship existing between RS-derived traces and shallow subsurface stratigraphy is necessary to explore and especially test the potentiality of satellite imagery as a tool for a plan-view identification of buried sedimentary bodies in different alluvial-coastal contexts. If successful, it may be a strong support to high-resolution core stratigraphic analyses in the three-dimensional reconstruction of facies spatial distribution patterns, improving our knowledge about the recent past evolution of alluvial-coastal plains.

1.2. Aims of the research project and study areas selection

This research wants to be a contribution to the open issue concerning the effectiveness of optical RS data and analyses in subsurface coastal stratigraphy, through the application of a multidisciplinary methodology integrating remote-sensed images analyses with sedimentologic and stratigraphic field data carefully collected from the selected traces.The main purposesof the project are:

(i) to assess both the effectiveness and the potentiality of free-of-charge RS data analysis (optical multispectral/hyperspectral satellite images), supported by DTM LiDAR- Light Detection And Ranging, in the identification of past landforms buried beneath coastal-deltaic plains, hosting urban areas as well;

(ii) to analyze to what extent the vertical stacking of sedimentary units with contrasting lithofacies characteristics and its variations over short distances may influence the visibility of landforms from satellite sensors;

(iii) to assess the role played by an integrated RS-high resolution stratigraphic approach in reconstructing the recent past genesis of coastal plains and, as a consequence, furnish new insights into the sedimentary evolution of two selected Mediterranean delta plains during the highstand phase (ca. 7000 cal yr BP onwards). Specific attention is paid on the depositional dynamics involved into the transition from late transgressive lagoons to present-day wave-dominated delta systems.

To reach these purposes, two Italian coastal sites have been selected: the Pisa Plain (North Tuscany) and the Mezzano Valley in the southern Po Plain. The former is located in the Arno River wave-dominated delta system overlooking the north Tyrrhenian Sea/Ligurian Sea, the latter belongs to an ancient Po River wave-dominated delta, not more active, in the north Adriatic Sea (fig. 1).

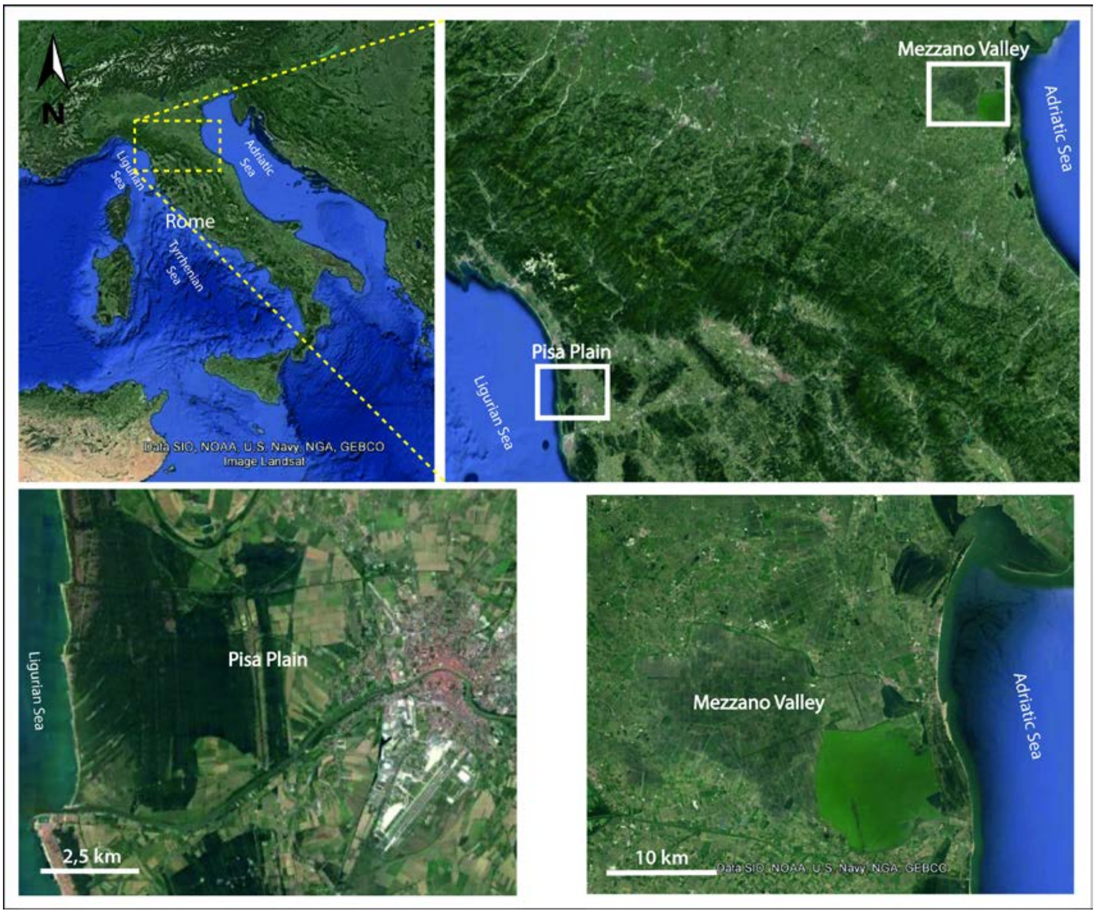

Figure 1_ Study areas (Pisa Plain and Mezzano Valley) locations (images from Google Earth)

The Pisa Plain and the Mezzano Valley have been selected since they meet several requirements, reported as follows:

- Availability of free-of-charge optical multispectral and hyperspectral satellite images from USGS and ESA websites, and high-resolution digital terrain model (DTM LiDAR) kindly furnished by the MATTM (Ministero dell'Ambiente e della Tutela del Territorio) and the local authority (Pisa Municipality) in the framework of active scientific collaborations.
- Good potentialities for detailed RS investigations, as shown by previous works (Sgavetti & Ferrari, 1988; Bini et al., 2012a, b; Bruni and Cosci, 2003; Amorosi et al., 2013).

- Availability of wide and valuable subsurface geognostic databases, mainly composed of CPT-Cone Penetrometer Test/CPTU-piezocone tests and cores. The Arno database is mainly composed of data provided by the Geological Survey of Pisa Province. The Mezzano database mainly derives from the on-line dataset provided by the Geological Survey of Regione Emilia Romagna-RER.
- Good knowledge of late Quaternary type facies stratigraphy and architecture (Amorosi et al., 2003, 2008, 2013a).
- Belonging to wide marine delta systems developed during the mid-late Holocene period after the filling of lagoon basins, which generally characterized wide portions of the Mediterranean coastline at the end of the Holocene sea-level transgression (around 8000-7000 cal yr BP; Anthony et al., 2014; Vacchi et al., 2016).
- Different geomorphological settings: the Pisa Plain is located within a still prograding alluvial-delta plain fed by the Arno River, while the Mezzano Valley corresponds to the reclaimed delta plain portion of an abandoned lobe belonging to the Po Delta system.

This research started from the Pisa plain, where in the framework of the collaboration experienced inside the research project MAPPA-Methodologies Applied to Archaeological Potential Predictivity (http://www.mappaproject.org/), to which I belonged, an approach combining RS and subsurface geological data was successfully applied to reconstruct paleoenvironmental changes occurred in the Pisa city area during historical times (Amorosi et al., 2013a).

From the urban zone the investigation has been extended seawards/westwards, in the cropland area of Pisa San Rossore (SR site) in order to cover the knowledge gap between the city and the outcropping beach-ridges (outer delta plain/sandy strandplain of the Arno Delta; Della Rocca et al., 1987), that have been morphologically studied in detail by Pranzini (2007) through LiDAR. The newly study portion of the Pisa plain is bordered to the south by the Arno River and to the north by the Serchio River, and likely characterized by a dynamic paleodrainage system attributable to ancient branches of the Arno and Serchio rivers as suggested, but still not documented from a stratigraphic point of view, by historical sources and geomorphological works (Strabo, V, 2, 5, C 222; Della Rocca et al., 1987; Marchisio et al., 1999; Bruni and Cosci, 2003).

The second study area, the Mezzano Valley-MV, is a low-lying coastal basin located behind a set of outcropping or sub-outcropping beach-ridges, the easternmost attributed to an ancient delta strandplain fed by ancient Po River branches (i.e., Po di Spina and Po di Primaro delta lobes; Bondesan et al., 1995; Stefani and Vincenzi, 2005). These beach-ridges are generically dated to the Etruscan and pre-Etruscan periods on the basis of archeological remains (Bondesan et al., 1995; Stefani and Vincenzi, 2005). The MV shows evident channelized traces, that have been already partially identified on satellite images by Sgavetti and Ferrari (1988). Nonetheless, the sedimentological expression and age of activity of these traces are still unknown and have been investigated in the present thesis. In MV area, the same integrated methodology was applied, performing a detailed analysis of the remote-sensed traces on satellite images with different spectral and geometric resolution, fully integrated with surface and subsurface stratigraphic data.

1.3. Thesis outline

The research work carried out during the PhD Program is presented in the thesis as follows:

- Chapters 2-3, following the present introduction, are focused on the adopted methodology. Specifically, Chapter 2 reports the main technical information and basic principles about passive optical remote sensing systems as well as the state-of-art of data processing for optical satellite images and DTM. Chapter 3 is focused then on the explanation of the workflow, furnishing a detailed description of the integrated RS-stratigraphic methodological approach applied to the two study areas;

- Chapters 4-5 concern with the results obtained in the Pisa plain (Chapter 4) and the Mezzano Valley (Chapter 5) in terms of RS-detected morphologies, facies associations and 3D subsurface stratigraphy of the uppermost ca. 7-10 m. For each chapter a scientific article reporting the main part of the results is presented along with paragraphs on completion of the data. The article concerning the Pisa plain urban area (pilot area) has been published in “Palaeogeography, Palaeoclimatology, Palaeoecology” by Sarti et al. 2015, while the article about the MV paleodrainage has been prepared for a forthcoming submission to “Geomorphology”, a journal concerning with remote sensing applications in geologic fields.

- In Chapter 6 the results obtained from each study area are discussed and compared in order to present conclusive considerations about *(i)* the effectiveness of the application of a RS-stratigraphic approach for high-resolution subsurface stratigraphic studies in different coastal settings and *(ii)* the evolution processes/dynamics of Mediterranean microtidal coastal plain areas from lagoonal basins to wave-dominate deltas under Holocene highstand sea-level conditions.

- In Appendix A, B and C additional materials are reported, in particular:

  A) the processed imagery (PCA) employed in this thesis for the RS-investigation of the Pisa plain and Mezzano Valley sites;

B) stratigraphic logs and photographic reports of the vibracores drilled in the two study areas (SR and MV);

C) the paper titled: "*The Upper Pleistocene Isola di Coltano Sands (Arno Coastal Plain, Tuscany, Italy): review of stratigraphic data and tectonic implications for the southern margin of the Viareggio Basin"* dealing with the Pisa coastal plain stratigraphic-depositional evolution, published by Sarti et al in 2015, to which I contributed as coauthor.

References

Amorosi A., Centineo M.C., Colalongo M.L., Pasini G., Sarti G., Vaiani S.C., (2003). Facies architecture and Latest Pleistocene–Holocene depositional history of the Po Delta (Comacchio area) Italy. *The Journal of Geology*, 111, 39–56.

Amorosi A., Sarti G., Rossi V., Fontana V., (2008). Anatomy and sequence stratigraphy of the late Quaternary Arno valley fill (Tuscany, Italy). In: Amorosi, A., Haq, B.U., Sabato, L. (Eds.), Advances in Application of Sequence Stratigraphy in Italy, *GeoActa*, Special Publication 1, 55-66.

Amorosi A., Bini M., Giacomelli S., Pappalardo M., Ribecai C., Rossi V., Sammartino I., Sarti G., (2013a). Middle to late Holocene environmental evolution of the Pisa coastal plain (Tuscany, Italy) and early human settlement. *Quaternary International* 303, 93-106.

Anthony E.J., Marriner N., Morhange C., (2014). Human influence and the changing geomorphology of Mediterranean deltas and coasts over the last 6000 years: From progradation to destruction phase?, *Earth-Science Reviews*, 139, 336-361.

Arnaud-Fassetta G., Landure´ C., (2003). Hydroclimatic hazards, vulnerability of societies and fluvial risk in the Rhone Delta (Mediterranean France) from the Greek period to the Early Middle Ages. In: Fouache, E. (Ed.), *The Mediterranean World Environment and History*. Elsevier, Paris, pp. 51–76.

Bakker W.H., Feringa W., Gieske A.S.M, Gorte B.G.H, Grabmaier K.A., Hecker C.A., Horn J.A., Huurneman G.C., Janssen L.L.F., Kerle N., van der Meer F.D., Parodi G.N., Pohl C., Reeves C.V., van Ruitenbeek, Schetselaar E.M., Templfi K., Weir M.J.C, Westinga E., Woldai T., (2009). *Principles of Remote Sensing-* Editors: Templfi K., Kerle N., Huurneman G. C., Janssen L. L. F.

Bini M., Brückner H., Chelli A., Pappalardo M., Da Prato S., Gervasini L., (2012a). Palaeogeographies of the Magra Valley coastal plain to constrain the location ofthe Roman harbour of Luna (NW Italy). *Palaeogeogr. Palaeoclimatol. Palaeoecol.* 337-338, 37-51.

Bini M., Capitani M., Pappalardo M., Pocobelli G.F., (2012b). Vecchi e Nuovi dati dalla fotointerpretazione aerea. In: Anichini F., Fabiani, F. Gattiglia, G.,Gualandi, M.L. (Eds.), Metodologie applicate alla predittivita' del potenziale archeologico, *1 Edizioni Nuova Cultura*, Roma, 131-156.

Bisson M. and Bini M., (2012). A multidisciplinary approach to reveal palaeohydrographic features: the case study of Luna archaeological site surroundings. *Int. J. Geogr. Inf. Sci.* 26, 327–343.

Bondesan M., Favero V., Viñals M.J, (1995). New evidence on the evolution of the Po-delta coastal plain during the Holocene, *Quaternary International. Int.*, 29/30, 105–110.

Bruni S. and Cosci M., (2003). Alpheae veterem contemptlor originis urbem, quam cingunt geminis Arnus et Ausuraquis. Il paesaggio di Pisa etrusca e romana: materiali e problemi. In: Bruni, S. (Ed.), *Il porto urbano di Pisa. La fase etrusca. Il contesto e il relitto ellenistico*, Pisa, 29–43.

Della Rocca R., Mazzanti R., Pranzini E., (1987). Studio geomorfologico della Pianura di Pisa (Toscana). *Geogr. Fis. Din. Quaternaria* 10, 56-84.

Fouache É., Dalongeville R., Kunesch S., Suc J. P., Subally D., Prieur A., Lozoue P., (2005). The environmental setting of the harbor of the classical site of Oeniades on the Acheloos delta, Greece. *Geoarchaeology*, 20, 3, 285-302.

Furlani S., Antoniolic F., Biolchia S., Gambine T., Gaucie R., Lo Prestig V., Anzideih M., Devotod S., Palomboi M., Sullig A., (2012). Holocene sea-level change in Malta. *Quatenary International*, 288, 146-157.

Furlani S., Monegato G., Stinghen A., Rova E., Kuparadze D., Boschian G., Massironi M., Bondesan A., (2012). «Paleohydrographic Evolution and its Influence on Human Settlement in the Karthaliny Basin (Georgia)». Alpine and Mediterranean Quaternary 25, 57-66.

Ghilardi M., Kunesch S., Styllas M., Fouache E., (2008). Reconstruction of Mid-Holocene sedimentary environments in the central part of the Thessaloniki Plain (Greece), based on microfaunal identification, magnetic susceptibility and grain-size analyses. *Geomorphology*, 97, 3-4, 617-630.

Ghilardi M., Genç A., Syrides G. , Bloemendal J, Psomiadis D., Paraschou T., Kunesch S., Fouache E., (2010). Reconstruction of the landscape history around the remnant arch of the Klidhi Roman Bridge, Thessaloniki Plain, North Central Greece. *Journal of Archaeological Science* 37, 178–191.

Mantelli L.R., Rossetti D. F., Albuquerque P. G., Valeriano M.M., (2009). Applying SRTM digital elevation model to unravel Quaternary drainage in forested areas of Northeastern Amazonia, Computers and *Geoscience*, 35, 12, 2331-2337.

Marchisio M., Cosci M., D'Onofrio L., Biagioni A., Ciuffi P., Lancucci N., Saviozzi F., (1999). Ricostruzione degli antichi corsi fluviali nella pianura di Pisa con metodi geofisici. "*Science and Technology for Cultural Heritage*", 8, 59-75.

Mozzi P., Piovan S., Rossato S., Cucato M., Abba' T., Fontana A., (2010). Palaeohydrography and early settlements in Padua (Italy). *Il Quaternario Italian Journal of Quaternary Science*s, 23(2Bis), 387-400.

Piovan S., Mozzi P., Stefani C., (2010). Bronze Age palaeohydrography of the southern Venetian Plain. *Geoarcheology* 25-1, 6-35.

Piovan S., P. Mozzi, M. Zecchin, (2012). The interplay between adjacent Adige and Po alluvial systems and deltas in the late Holocene (Northern Italy). *Géomorphologie : relief, processus, environnement*, 4, 427-440.

Pranzini E., (2007). Airborne LiDAR survey applied to the analysis of historical evolution at the Arno River delta (Italy) in *«Journal of Coastal Research»*SI 50 (Proceedings of the 9th International Coastal Symposium), 400 – 409 http://www.griffith.edu.au/conference/ics2007/pdf/ICS078.pdf

Quintanar J., Khan S. D., Fathy M. S., Zalat A. A., (2013). Remote sensing, planform, and facies analysis of the Plain of Tineh, Egypt for the remains of the defunct Pelusiac River. *Sedimentary Geology* 297, 16–30.

Ravazzi C., Marchetti M., Zanon M., Perego R., Quirino T., Deaddis M., De Amicis M., Margaritora D., (2013). Lake evolution and landscape history in the lower Mincio River valley, unravelling drainage changes in the central Po Plain (N-Italy) since the Bronze Age. *Quaternary International*, 288, 195-205.

Rossetti D.F., Valeriano M.M., Góes A.M., Thalles M., (2008a). Palaeodrainage on MarajóIsland, northern Brazil, in relation to Holocene relative sea-level dynamics. *The Holocene* 18, 923–934.

Rossetti D.F., Valeriano, M. and Furini C. H., (2009). Evaluating remote sensing products to delineate palaeodrainages in forested areas of southwestern Marajo Island, Anais XIV, Simposio Brasilerio de Sensoriamento Remoto, Natal, Brasil, 25-30, INPE, 3333-3339, April 2009.

Rossetti D.F.,Palloti S., Polizela M. C., Cohenb L. C., Pessendac R., (2015). Late Pleistocene–Holocene evolution of the Doce River delta, southeastern Brazil: Implications for the understanding of wave-influenced deltas. *Marine Geology*, 367, 1 September 2015, 171–190.

Stefani M. and Vincenzi S., (2005). The interplay of eustasy, climate and human activity in the late Quaternary depositional evolution and sedimentary architecture of the Po Delta system, *Marine Geology*, 222-223, 19-48.

Sgavetti M., (1974). Le caratteristiche di riflettività spettrale di una zona della pianura Padana su immagini ERTS-1, Anno XXXII-Bollettino di Geologia e Scienze Affini, n.3.

Sgavetti M. and Ferrari C., (1988). The use of TM data for the study of a modern deltaic depositional system. *Int. J. Remote Sensing*, 9, nos. 10 and 11, 1613-162.

Vacchi M., Marriner N., Morhange C., Spada G., Fontana A., Rovere A., (2016). Multiproxy assessment of Holocene relative sea-level changes in the western Mediterranean: Sea-level variability and improvements in the definition of the isostatic signal, *Earth-Science Reviews*, 155, 172-197.

Vött A., Schriever A., Handl M., Brückner H., (2007). Holocene palaeogeographies of the central Acheloos River delta (NW Greece) in the vicinity of the ancient seaport Oiniadai. *Geodinamica Acta* 20/4, 241–256.

Wang X.Y., Guo Z.Y., Wu L., Zhu C., He H., (2012). Extraction of palaeochannel information from remote sensing imagery in the east of Chaohu Lake, China. Front *Earth Sci. Chin*. 6 (1), 75–82.

CHAPTER 2_THE SATELLITE OPTICAL MULTI-HYPERSPECTRAL IMAGERY AND DIGITAL TERRAIN MODEL (DTM): PRINCIPLES AND DATA PROCESSING

2.1 The Remote Sensing process

The term 'Remote Sensing' is a generic definition that includes those instruments and techniques that deal with the acquisition (through real-time or recording energy devices) of both qualitative and quantitative information and data about objects or phenomena, without coming directly in physic contact with them (fig. 2.1).

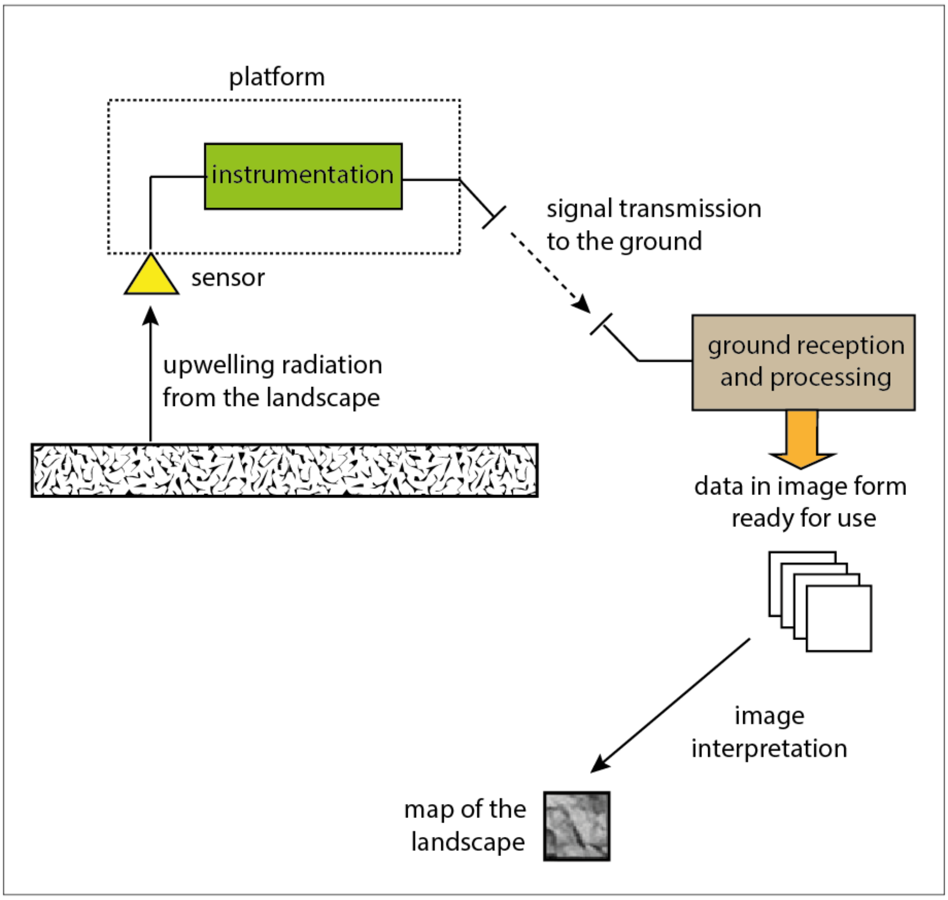

Figure 2.1_ Sketch of the remote sensing process (modified from Richardson and Xiuping, 2006)

In the RS the information vehicle is the energy transported by the electromagnetic (EM) radiation, including light, force field or acoustic energy, that interacting with objects furnishes information about their physical-chemical characteristics. Based on this principle, the fields of applications of RS can be various such as archeology, climatology, oceanography, glaciology, Earth Science, forest monitoring, environmental pollution, land use, urban mapping, and many others (Richards and Jia, 2006). In Earth Science, in particular, RS is focused on the Earth's surface investigation as landform characterization and mapping, landscape evolution, ecological studies, hazard prediction, surface survey, resources management and exploiting, generally based on remote sensed imagery.

Along with aerial photos, the satellite imagery, indeed, provides a fundamental basis for the photointerpretation and mapping of the geological features at different scales and combined with the use of GIS (Geographic Information System), represents a powerful tool for the management and analysis of interdisciplinary issues.

Most common RS systems for the Earth's surface observation are optical, since they record the reflected Sun radiation (RS passive system, fig. 2.2 a, b) from the visible up to the mid-infrared range (see section 1.2) of the EM spectrum, that represents only a portion of the recordable wavelengths but suitable for most of the RS mapping purposes. Other RS systems, known as active systems (fig. 2.2 c), are able to record backscattered energy from a platform emitting a radiation and to collect data from further portions of the EM spectrum (e.g., the radar system works with microwaves).

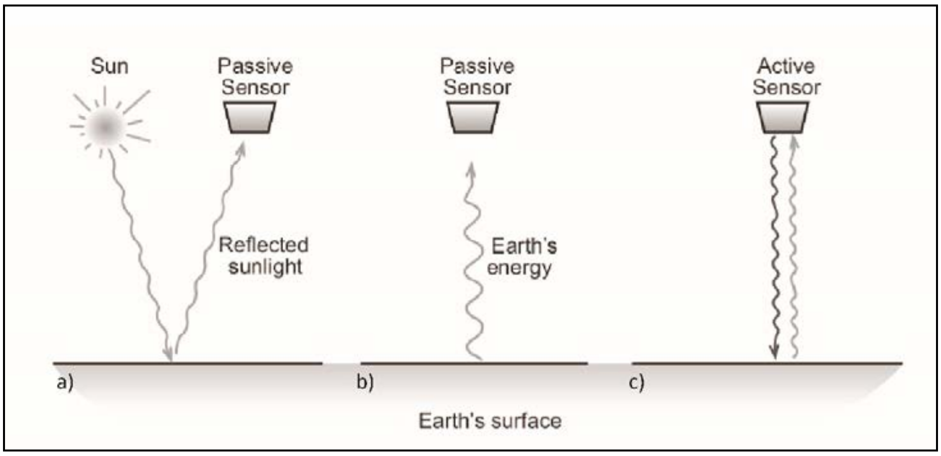

Figure 2.1_ Sketch of a,b) remote sensing passive systems, exploiting respectively the energy coming from the Sun (sunlight) and the energy emitted from Earth through the surface; c) remote sensing active system, where the energy is produced by an active sensor that also record the reflected energy .(from Bakker et al., 2009)

2.2 The Electromagnetic radiation

As stated in the previous section in RS the vehicle of information is the EM radiation, that can be modeled by waves or photons (radiant energy bearing particles). According to the wave theory defined in the 17th century, the light/EM radiation travels at approximately 300,000 km/s, following a straight line (light ray) with energy constantly changing between its two perpendicularly oscillating components: the electrical and the magnetic energy.

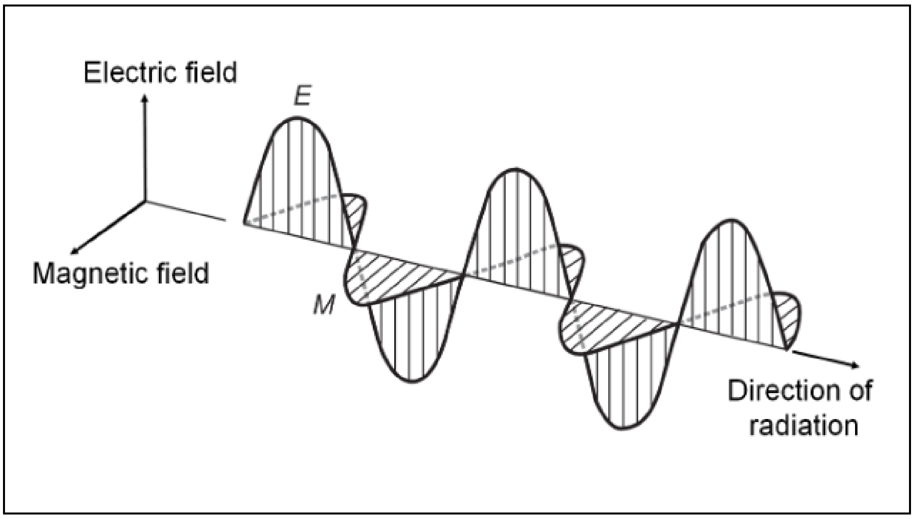

Figure 2.2_ Electromagnetic radiation: electric and magnetic components (from Bakker et al., 2009)

The light, as a wave, can be characterized by three parameters: wavelength, amplitude and phase (fig. 2.4). The wavelength (λ) is the distance, usually measured in µm (= 10^{-6} m) travelled by the light between two consecutive maxima (or minima) of energy in a cycle of oscillation; the amplitude (α) is the wave peak value and it is proportional to the amount of energy; the phase (φ), ranging from 0 to 2π, expresses the difference between the wave start point and the origin of counting distance.

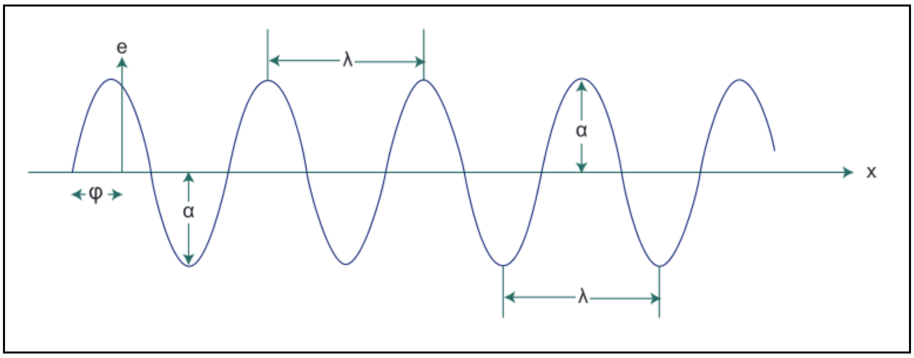

Figure 2.3_ Characteristics of an electric wave: λ=wavelenght; α=amplitude; φ=phase (from Bakker et al., 2009)

The frequency is the inverse of the time needed by a wave to complete one cycle (period) and it is usually measured in hertz-HZ (1HZ= 1cycle per second).

As the speed of the light (c) is constant, the relationship between wavelength and frequency (ν) is:

$$c = \lambda \times \nu \qquad [1]$$

Each body with an absolute temperature (°K) above zero (-273,15°C) emits EM energy because of molecular agitation. In particular, the Sun can be considered a black-body, that is an (theoretical) object capable to totally adsorb the incoming radiation and to entirely re-emit it, at every wavelength but with a maximum wavelength (λ_{max} Wien's law) that is function of the temperature of the body.

The Sun and the Earth have two different emissions maxima at respectively 0,483µm and 9,66µm (fig.2.5). Generally, the intensity of the radiation emitted (exitance) is proportionally dependent to temperature (fig.2.5).

The entire continuous range of wavelengths is defined as EM spectrum, conventionally gathered into regions, or spectral bands, such as X-ray, Ultraviolet (UV), Visible (VIS), Infrared (IR), microwave (fig. 2.6). Each spectral region has different relevance for the Earth observation; for example, UV-VIS bands reveal rocks and mineral properties, the IR region is suitable to discriminate vegetation and its stress state (by near infrared- NIR) or for the monitoring of environmental phenomena (thermal infrared bands-TIR), while the microwave portion of the spectrum provides information on moisture content of soils (Bakker et al., 2009).

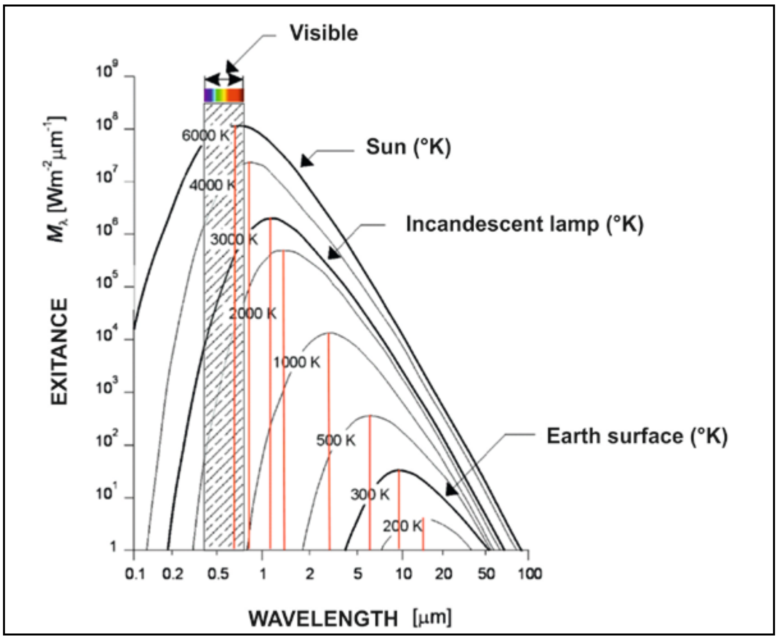

Figure 2.4_Radiation curves for different surfaces at different temperatures (modified from http://dipsa.unibo.it/catgis/pdf/Vol_3_1.pdf)

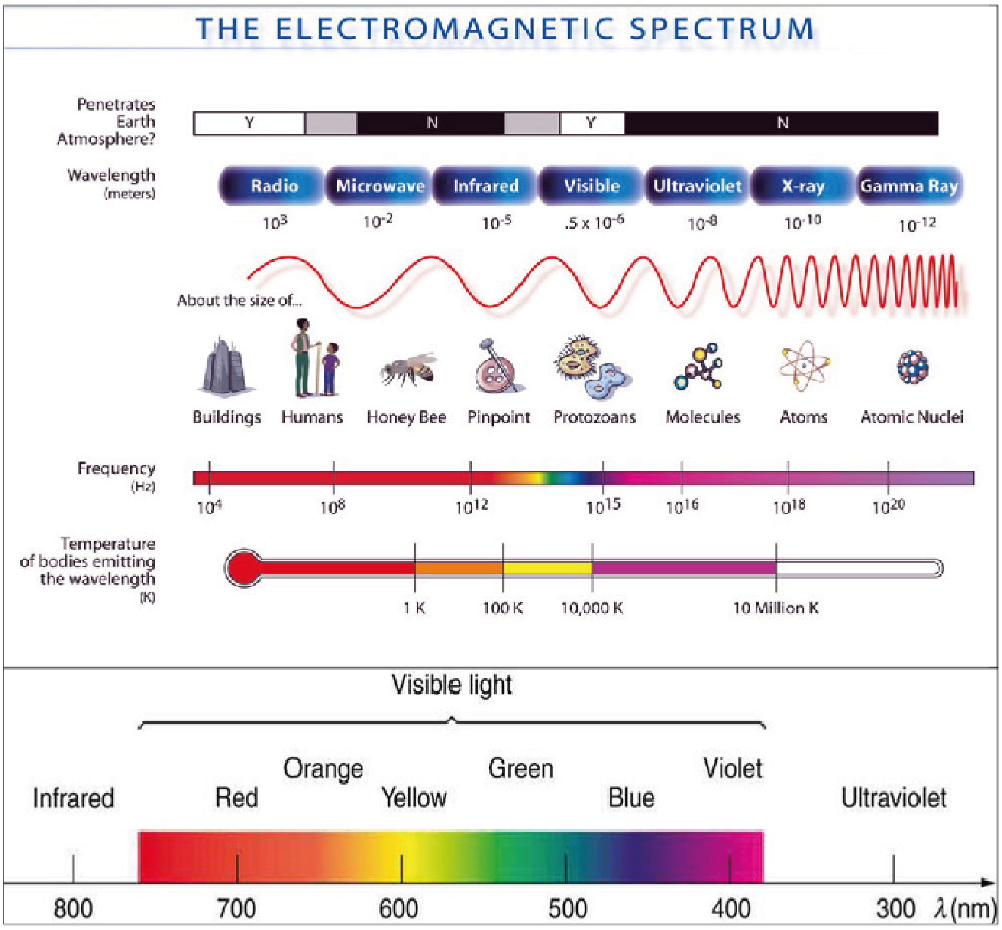

Figure 2.5_The Electromagnetic spectrum (modified from: http://www.scienceinschool.org/sites/default/files/articleContentImages/19/chemiluminescence/issue19chemiluminescence19_xl.jpg; https://figures.boundless-cdn.com/16334/large/figure-2025-03-10a.jpeg).

Before reaching the Earth’s surface, the Sun radiation interacts with the atmosphere where, due to adsorptions and scattering, the amount of energy decreases (fig. 2.7a). Ozone (O_3), water vapor (H_2O) and carbon dioxide (CO_2) molecules are responsible mostly for the absorptions. Therefore, only some portions of the EM spectrum, known as atmospheric windows, can be employed for the RS of the surface (fig. 2.7b) as they let the radiation pass through the atmosphere reaching the Earth’s surface.

Because of the presence of aerosol, gas and vapor in the atmosphere the incident radiation is deviated in different directions and scattering occur. The scattering effectivness is variable, depending on the aerosol, gas and vapor concentrations, the radiation wavelength and the distance the radiation travels through the atmosphere.

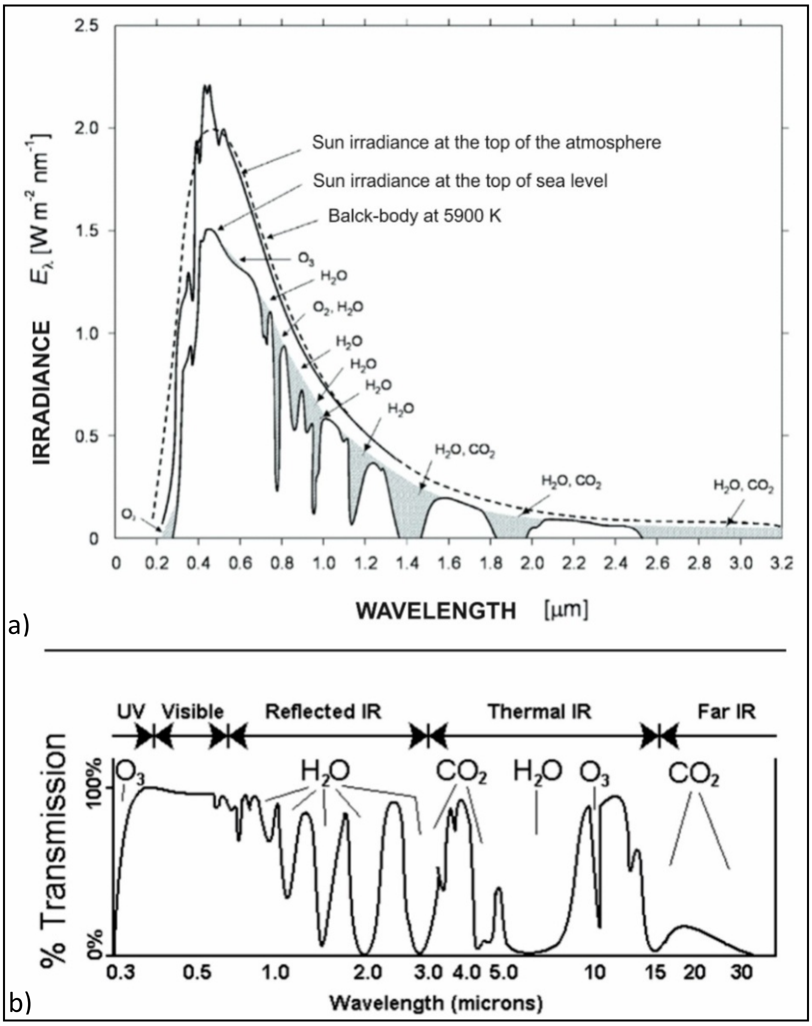

Figure 2.7_a) Effect of the atmosphere on the Sun electromagnetic (EM) radiation; b) atmospheric windows in the EM spectrum.

On the basis of the object characteristics (physical nature and roughness) occurring on the surface, the incident radiation (ϕ_i) can be reflected, absorbed or transmitted (ϕ_r, ϕ_a, ϕ_t respectively). These interactions can be expressed by the following coefficients (ρ=reflected; α=adsorbed; τ=transmitted):

$$\rho = \phi_r/\phi_i \qquad [2]$$

$$\alpha = \phi_a/\phi_i \qquad [3]$$

$$\tau = \phi_t/\phi_i \qquad [4]$$

Based on the principle of conservation of energy:

$$\alpha+\rho+\tau=1 \qquad [5]$$

The proportion of reflected, absorbed and transmitted energy varies with the wavelength and the material type. In RS land and water applications, the reflected radiation is the most useful because it is informative of the surface characteristics, as the physical nature and roughness. Reflection can be: *i)* specular, which is typically connected to smooth surfaces, where all the energy is reflected in one direction; and *ii)* diffuse, typical of rough surfaces, where the energy is reflected almost homogenously in all the directions (fig. 2.8 a, b).

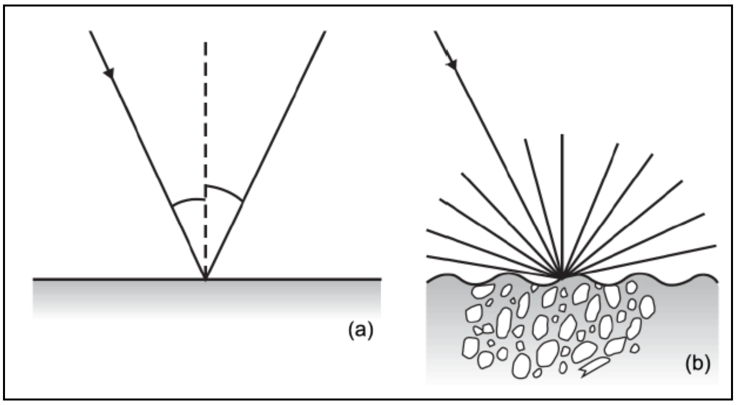

Figure 2.8_Sketch of different type of reflection: a) specular; b) diffuse (from Bakker et al., 2009). Incident energy is indicated with a black arrow.

In conclusion, the energy recorded by the sensor is the result of interactions of EM radiation with both the atmosphere and the Earth's surface (fig. 2.9).

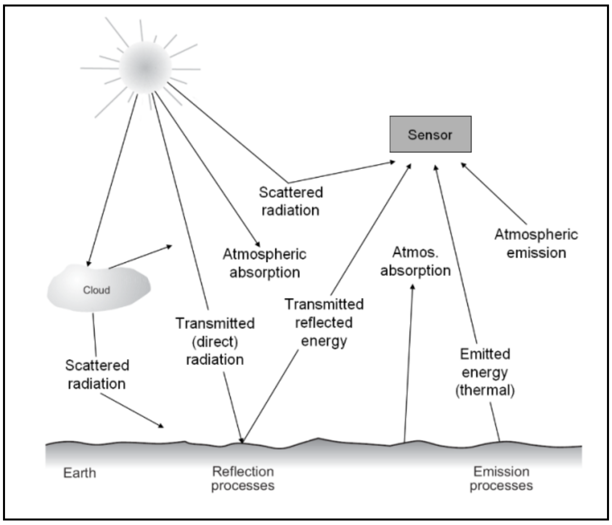

Figure 2.9_ Possible interactions among Sun radiation, atmosphere and Earth's surface (from Bakker et al., 2009)

The EM energy recorded from a RS system from a surface in a specific time interval (*radiant power Φ*, W=joule x second) can be quantified by the radiometric units. The most used in the RS field are the *irradiance (E)*, *exitance (M)* and *radiance (L),* defined as follow:

- $\Phi=\frac{dQ}{dt}$ (W), Q=energy, t=time [6]

  

  The radiant power (Φ) represent the energy spreading in all the directions, defined as the rate of flow of EM energy

- $E=\frac{d\Phi}{dA}$ (Wm^{-2}), A=area, Φ= incident radiant power [7]

  

  The irradiance (E) is defined as the radiant power incident upon a surface, per unit area.

- $M=\frac{d\Phi}{dA}$(Wm^{-2}), A=area, Φ= outcoming radiant power [8]

  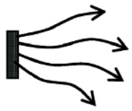

  The exitance (M) is the radiant power emitted by a unit area of a source around all its hemisphere

- $L=d\left(\frac{d\Phi}{dAcos\theta}\right)*\frac{1}{d\omega}$ ($Wm^{-2}sr^{-1}$), A=area [9]

  

  The radiance (L) is the radiant power, in a given direction, per unit solid angle per unit of projected area of the source, as viewed from the given direction.

2.3 Spectral signature and image spectroscopy

As previously stated (section 2.2), each surface, depending on its own physical-chemical characteristics, interacts with the EM radiation, at various wavelengths, in different ways. The interactions are expressed by a spectral response patterns that can be thought as the "finger print", the "signature" of each surface. Hence, the reflectance curve representing the energy observed at different wavelengths for a given surface is defined as its "spectral (reflectance) signature".

Evident local reflectance values decreases along the spectral curve highlight the range of wavelengths in which a material selectively adsorb the incident energy (*adsorption bands*). The adsorption bands are usually described by three spectral parameters (i.e., depth, center and width) that together with the adsorption positions (wavelength) allow to discriminate among different types of materials (fig. 2.10).

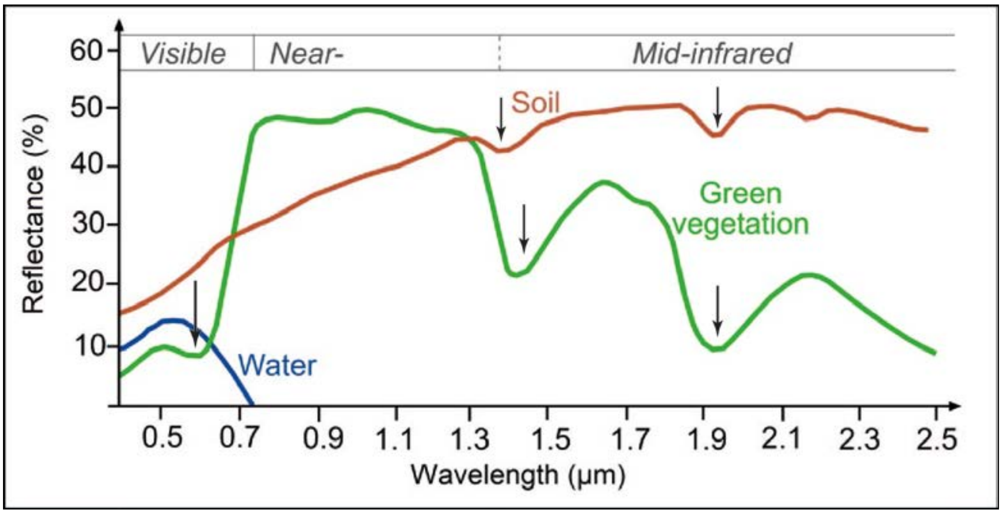

Figure 2.10_Some ideal spectral response patterns ("spectral signatures") for vegetation, water and dry bare soil; black arrows represent typical absorption features for these materials (modified from: http://www.seos-project.eu/modules/classification/classification-c00-p05.html).

Therefore, radiation from the Earth's surface permits to distinguish various features and study their geographic distributions (fig. 2.11). To obtain these information many airborne and spacecraft sensors, besides the Global Positioning System (GPS), have been equipped with imaging spectrometers.

The image spectrometer is a devices able to acquire data simultaneously in numerous narrow and contiguous spectral bands (hyperspectral data) for the restitution of the spectral patterns related to the various features occurring on the Earth's surface. Hyperspectral sensors collect data as a set of images (hundreds), each in a given wavelength interval, containing both spatial and spectral information from materials (occurring within the scene). For each pixel, the entire EM spectrum is acquired, then the spectral reflectance and the diagnostic spectral adsorption features are employed to identify and map differences in the surface composition.

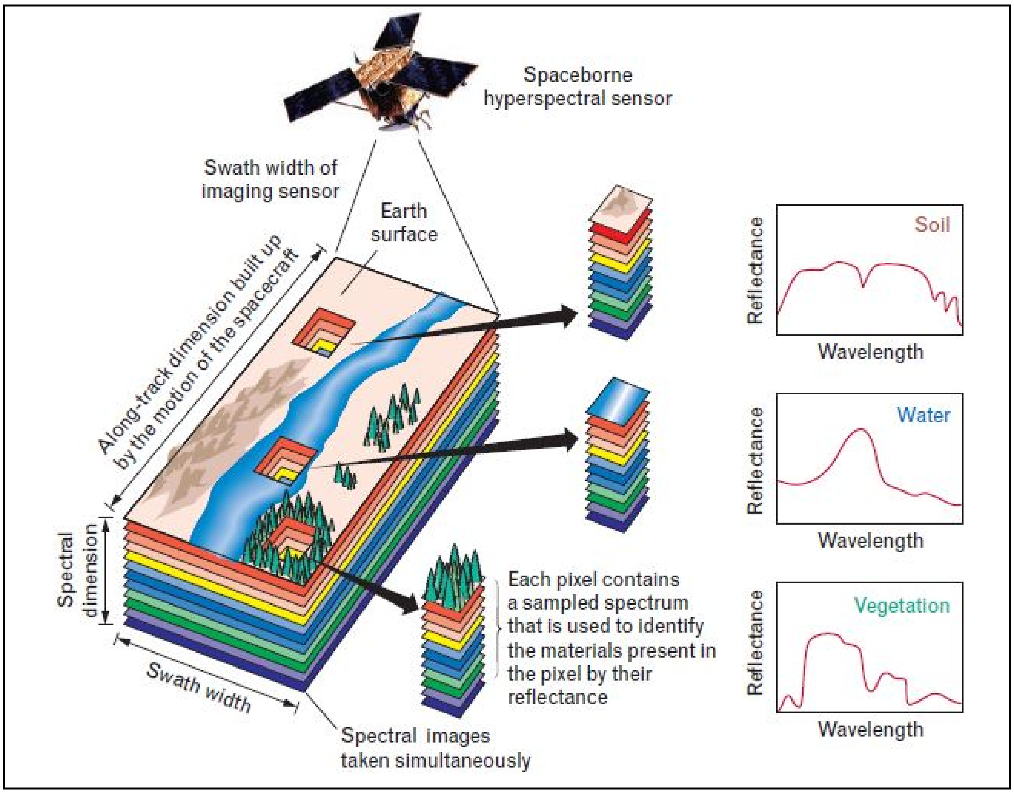

Figure 2.11_ Sketch of the operational principles of hyperspectral image spectroscopy from a remote sensing system: data acquisition and spectral signatures (from http://www.markelowitz.com/Hyperspectral.html)

2.4 Remote-sensed data

2.4.1. Satellite images

Satellite images are digital remote-sensed raster, which are matrix of picture elements (pixels) organized in columns and rows. Each pixel, whose dimension defines the geometric resolution of the image, represents a portion of the Earth's surface and it is characterized by a numeric value. Each value corrisponds to the radiance (see par. 1.1) recorded for each pixel in a specific spectral band (range of wavelengths) and it is expressed as digital number (DN) stored with a finite number of bits (binary system).

The number of bits determines the radiometric resolution of the image. Thus, in an 8-bit images the DNs range from 0 to 255 (i.e. 0- 1, 2^8) that are the possible grey gradation in a black (0) and white (255) color scale representation of the DNs (fig. 2.12).

Sensors can record energy in different wavelength ranges, at various spectral resolutions. The spectral resolution expresses the capability of a sensor to discriminate subtle wavelength intervals; the narrower the wavelength range for a specific band, the higher is the spectral resolution.

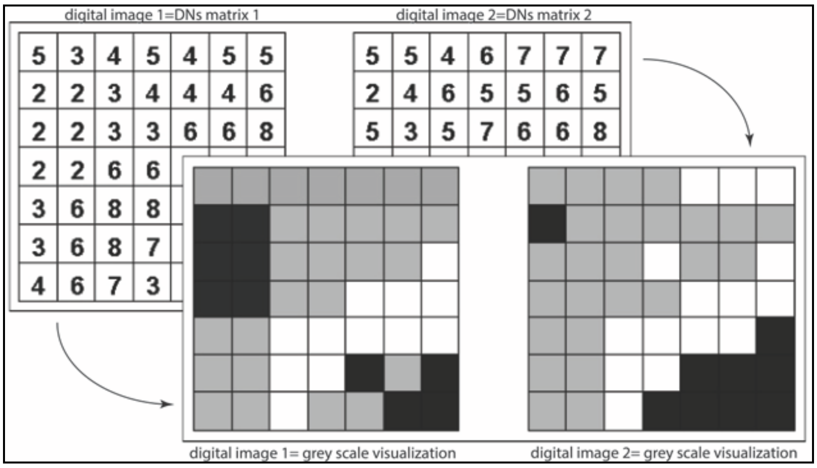

Figure 2.12_Digital images as matrix of numbers (brightness values) recorded by sensors and digital images grey-scale representations (modified from class lectures 2015-2016 by R. Salvini- Principi di Telerilevamento- Centro di GeoTecnologie di Siena)

Hence, an image acquired by a multispectral sensor will consist of a few image layers (generally 3-10) whose numbers correspond to the number of EM bands recorded by the RS sensor. On the contrary, an image recorded by a hyperspectral sensor will consist of many DNs matrices recorded for about hundred or more-contiguous narrow spectral bands (fig. 2.13). The complete spectral information carried by a hyperspectral image with respect to the multispectral image enables a better characterization and identification of targets.

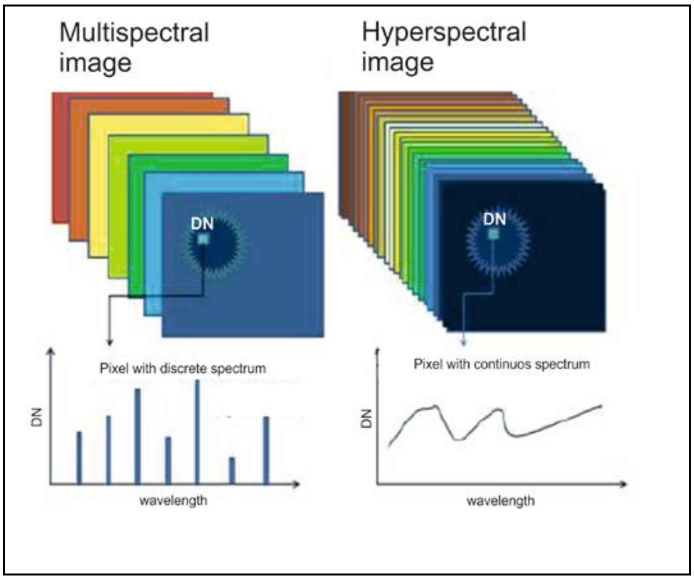

Figure 2.13_Data format from multispectral and hyperspectral images and relative spectral curves (modified from https://www.researchgate.net/publication/281067356_).

The geometric resolution of the images, and hence the ground pixel size, corresponds to the smallest object that can be resolved on the ground and it depends on the sensor Instantaneous Field of View (IFOV), i.e. cone of visibility (fig. 2.14). “High resolution” and “low resolution“ are referred to images with small and large geometric size of the pixel (e.g., 1m and 90m respectively). The width of the whole surface area covered by the sensor is defined as the scene swath (fig. 2.14), that usually for satellite platforms varies between tens and hundreds of km.

The satellite images are also characterized by the temporal resolution that expresses the revisiting time interval of a satellite sensor for a specific location. Revisiting frequency greater than 16 days or smaller than 3 days are defined respectively as low and high temporal resolution.

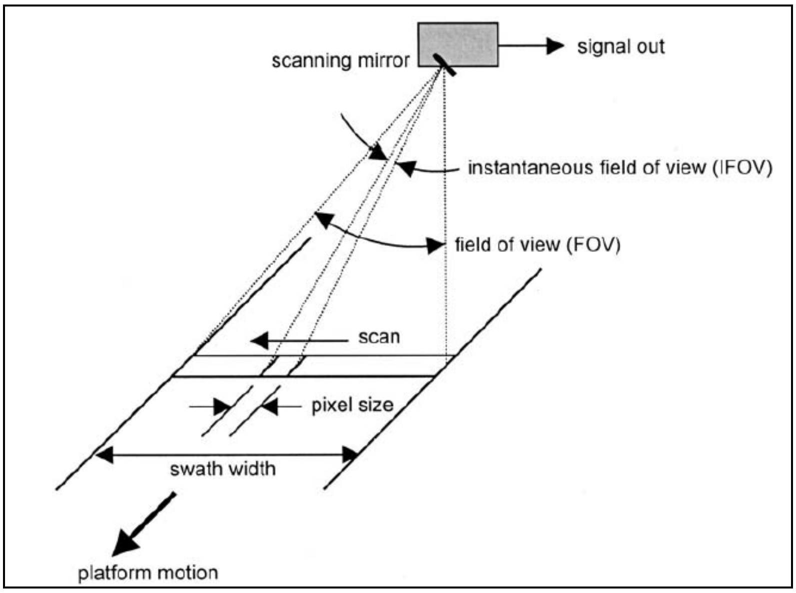

Figure 2.14_Instantaneous Field of View (IFOV) of a sensor and relative swath of the covered scene on the ground (https://www.researchgate.net/figure/283355006_fig10_Figure-12-Instantaneous-Field-Of-View-IFOV-Richards-J-Remote-Sensing-Digital-Image).

2.4.2. Images analysis

Remote sensed images before being analyzed need a series of corrections (*pre-processing*) aimed to reduce or delete the geometric and/or brightness value errors introduced by the sensor during the data recording and transmission.

Geometric distortions can be connected to various factors that generate systematic and non-systematic errors. Systematic errors refer mainly to predictable causes, such as the satellite’s positioning on its orbit, the Earth rotation during the acquisition (*skewing*), the Earth's surface curvature, difference in platform-scan acquisition speeds, etc.

Non-systematic distortions concern with unpredictable factors, such as the effect of the topography on the acquisition. Specific procedures and software have been developed by the satellite acquisition centers to compensate these errors and many satellite available data are furnished by the producer, e.g., USGS-Earth Explorer for Landsat, geometrically correct and georeferenced (correctly assigned to the coordinate system).

Sources of radiometric errors in the RS data are usually connected both to the malfunction of the instruments and to the atmospheric effect. Theoretically, an ideal detector system should be characterized by a linear transfer function between radiation in and signal out, but real detectors have a certain degree of non-linearity (fig. 2.15), causing alteration in the brightness returned values (DNs).

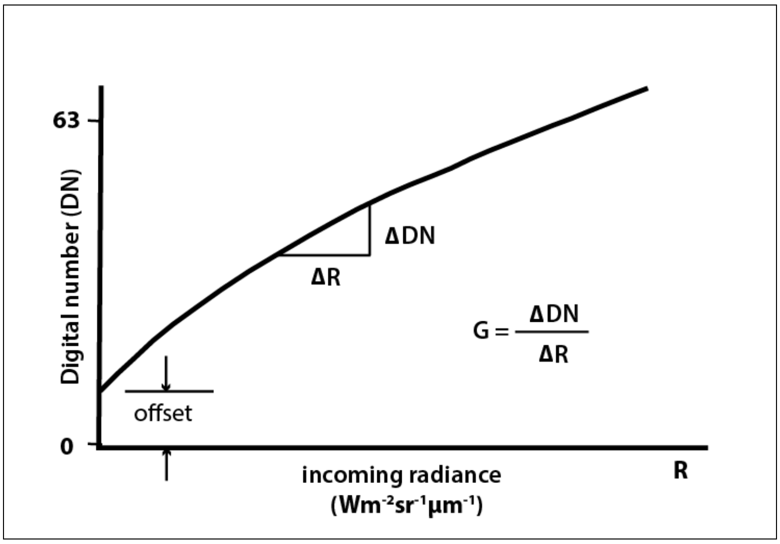

Figure 2.15_Non-linear relationship between radiance recorded by the sensors and converted DNs (modified from class lectures 2011-M. Sgavetti DiFeST-Univeristy of Parma).

Therefore, the out coming signal (DN_{mes}) must be correct (*sensor calibration*) for each pixel in each band to obtain the real values of the radiance at the sensor(DN_{rad}). Considering the "radiation in-signal out" graph (fig. 2.15), the DN_{rad} can be calculated extracting the intercept (offset-O) and the angular coefficient (gain-G):

$$DN_{rad}= (DN_{mes}-O)/G$$

where O is the offset (i.e., ordinate value of the graph intercept) and G is the gain (i.e., angular coefficient of the graph).

As stated in section 2.1, the Sun radiation interacts with the atmosphere and the scattering has the maximum effect in the VIS blue band (450-495 μm) with a progressive decrease towards the IR (> 700 μm) region of the EM spectrum.

To remove the atmospheric effect (*haze*) on radiance data two different approaches are possible, depending on the availability of the atmospheric condition parameters at the time of the acquisition:

1. if the parameters are known, the correction can be performed using specific algorithms and software that model the atmosphere (e.g., MODTRAN, ACORN, ATREM, ENVI-FLAASH);
2. if the parameters are not available, it is possible to correct the data through an image-based method suitable at least for cloud-free images, that is the "darkest pixel", also known as the histogram minimum method (Hadjimitsis et al., 2004a). This method is based on the assumption that not-zero radiation from an expected to be totally dark pixel (on Earth's surface) represents the atmospheric effect at visible wavelengths, since the surface radiance of a dark object can be approximated to zero. The brightness value (DN) associated to the darkest pixel is hence subtracted, for each band, to the DN of all the other pixels composing the scene.

In both cases, *atmospheric corrections* allow to obtain, for each band, the spectral radiance at the surface and hence the surface reflectance as it was at the top of the atmosphere (= ratio between the energy reflected from an object and the incident radiation, i.e. irradiance).

Once the RS data pre-processing is completed, the images can be analyzed and interpreted, both visually and digitally. Visual interpretation (*photointerpretation*) involves a human analyst collecting information by visual inspection, based on his/her experience and ability to connect colors and patterns to features from the real world. In detail, the study and interpretation of images in most RS applications rely on some fundamental features as shape, size, pattern, tone, texture, shadows, site, association, and spatial resolution (Olson, 1960).

On the other hand, digitally interpretation allow to extract information in a quantitative way using computer-based tools, that analyze the images on the basis of pixels' attributes (e.g., brightness).

In both cases, to be interpreted, the images must be visualized. As explained in section 1.3, satellite images are digital images that can be represented through a grey color-scale. In the case of multispectral (and hyperspectral) images, data can be visualized, exploiting the red-green-blue (RGB) coding of the PCmonitor, through the color composition (i.e., *bands combination*-fig. 2.16) that, merging together the different information (linked to each band) favor the possibility of discriminate features on the scene.

If the composition involves one or more bands outside the VIS-region (natural colors) of the EM, e.g. NIR and SWIR (short wave infrared), the bands combination produces a False Color Composition (FCC), very effective in highlighting and discriminating as much as possible the features occurring in the scenes.

Besides, it is possible to promote the visibility of an image also through the contrast enhancement, that amplifies also small differences in the data and allow to better differentiate features.

The image interpretation can be also improved by another radiometric manipulation technique that is the "density slice" that allows to discriminate brightness values differences subtle for the human eye sensitivity and/or to highlight significant region of interest reducing possible effect of noise, mapping the brightness ranges through the "segmentation" of the scene in sections with similar levels of grey (fig. 2.17).

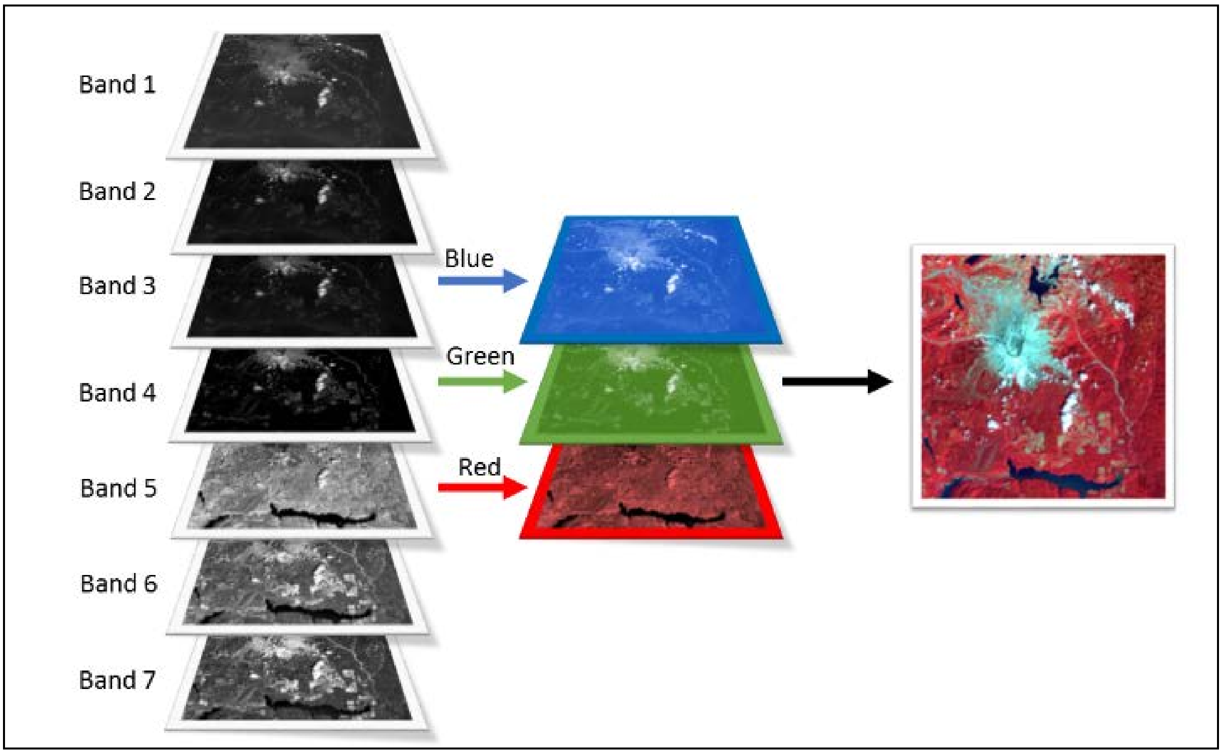

Figure 2.16_Example of bands acquired from a sensor represented as grey scale images and colour composite image through RGB representation (bands combination) _from http://gsp.humboldt.edu/OLM_2016/Courses/GSP_216/lessons/composites.html.

An effective images transformation aimed to enhance the visibility of differences on remote-sensed scenes is the Principal Component Analysis (PCA) of the bands collected for a single image. The purpose of the

PCA, that is a linear transformation technique used for the data recognition and compression, is to reduce a set of correlated multivariate measurements (RS multispectral/hyperspectral data) to a smaller set in which the features are not correlated to each other.

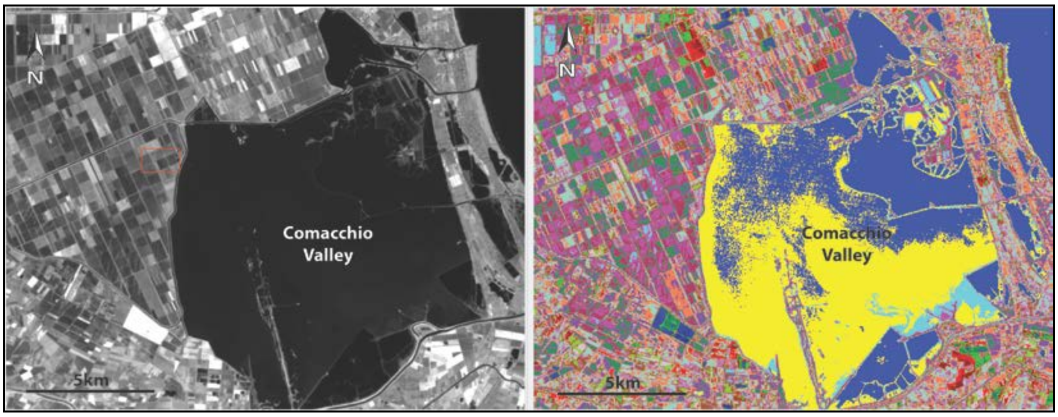

Figure 2.17_Clip of Landsat 7 ETM+ band 4 (NIR) scene from the Comacchio Valley (Po Plain, Italy) and the same image processed with ENVI for the ”Density slicing”.

It involves a mathematical procedure that transforms several (possibly) correlated variables into a (smaller) number of uncorrelated variables called “principal components (PC)” (fig. 2.18). The first PC concerns with most of the data variability. For multispectral data, it is common to find that the first two or three (orthogonal) components explain all the original variability in reflectance values. The others components thus tend to be dominated by noise effects. By not considering the “noisy” components, the volume of data can be considerably reduced without substantial information loss.

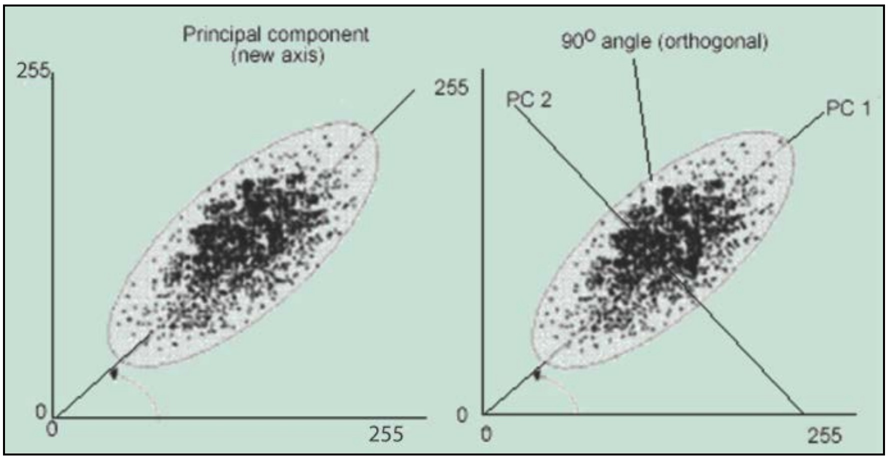

Figure 2.18_Principal Component transformation: the Principal Component Analysis (PCA) process produces in the data-space a number of “new axis” equal to the orginal EM bands, that allow to better distinguish especially data displaying strong correlations, as the ones shown in the picture (from http://nptel.ac.in/courses/105104100/lectureD_27/D_27_8.htm). In the diagrams X and Y axises represent brightness values (from 0 to 255) in two different electromagnetic bands.

Besides the visual interpretation, a computer-assisted interpretation of the digital images is also possible such as the "image classification". The image classification is aimed to group, through the use of various suitable algorithms, pixels on the basis of their values affinity into significant categories. Two kind of classifications can be followed to interpret the images: unsupervised and supervised.

The unsupervised classification does not require previous information about the classes of interest (i.e., categories) because this tool analyzes the dataset (image) and breaks it into the most prevalent natural spectral groupings (clusters) based on the reflectance properties of the pixels. Spectral classes derived from unsupervised classification usually need to be then reclassified into classes of information to complete the intepretation, connecting them to a real data (e.g., water, vegetation, clouds, buildings, etc..).

On the contrary, the supervised classification is guided by the user that introduces specific informative classes (e.g., land cover types) and defines portions of the scenes (i.e., *training sites*) representative of the introduced classes (i.e., *ground truth*). The software extract the spectral signature of the pixel belonging to each training site and uses it to recognize and group all other pixels in the scene that closely match with the training sites.

2.5 Digital terrain model (DTM)

In the Earth Science, the DTMs constitute the base for the geographical information system (GIS), often employed to investigate the geomorphologic characteristics of the surface at different scales. DTMs have been used in geoscience applications since 1950s (Miller and Laflamme, 1958), furnishing the base for the display and analysis of the topographic surface. Elevation was traditionally derived by direct survey of the terrain and derived through photogrammetry techniques with pairs of stereoscopic images.

Today, it is possible to acquire elevation data with different geometric resolution and height accuracy, for wide areas, through satellite radar system (e.g. SRTM, InSAR) and even high resolution elevation data through LiDAR system. LiDAR is an optical RS technique that involves an active sensor, on airborne or spaceborne platforms, transmitting laser pulses that bounce off the Earth's surface and then measured as first return (and others) and ground return (fig.2.19). LiDAR provides dense "clouds" of x,y,z points from which high quality digital surface model (DSM) and DTM models can be generated.

From elevation data, it is possible to derive different kinds of surface models as DEM, DSM (Digital Surface Model) and DTM (Digital Terrain Model). They all are raster data describing the surface topography but, while the term DEM is used as generic term used to refer to all types of topographic data describing the earth surface, DSM, that measures the height values of the first surface on the ground, referring to a surface model including buildings, vegetation, power lines, etc. Differently, the term DTM refers to a bare

Earth surface model, usually derived from DSM by digital removing of buildings, vegetation, power lines etc. (fig. 2.20).

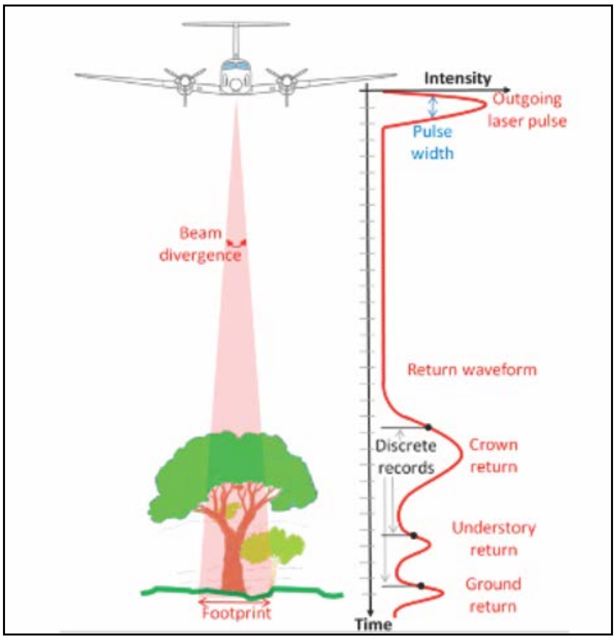

Figure 2.19_ Path of the laser pulse (mod. from Diaz et al., 2014) and interactions with different objects occurring on the Earth'surface.

The most common use of elevation data is for 3D-visualizations but they are also very useful for the extraction of terrain parameters, the creation of relief map, the investigation of the drainage and for geomorphologic analyses (qualitative and quantitative).

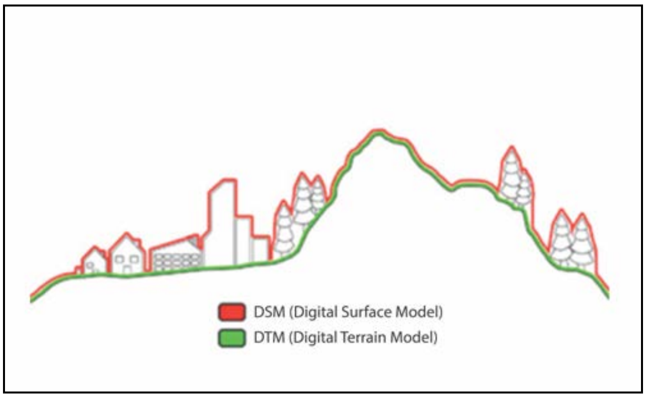

Figure 2.20_ Difference between Digital Surface Model (DSM) and Digital Terrain Model (DTM) (from *http://www.geoimage.com.au/DEMS/dems-overview*)

References

Bakker W.H., Feringa W., Gieske A.S.M, Gorte B.G.H, Grabmaier K.A., Hecker C.A., Horn J.A., Huurneman G.C., Janssen L.L.F., Kerle N., van der Meer F.D., Parodi G.N., Pohl C., Reeves C.V., van Ruitenbeek, Schetselaar E.M., Templfi K., Weir M.J.C, Westinga E., Woldai T., (2009). *Principles of Remote Sensing*- Editors: Templfi K., Kerle N., Huurneman G. C., Janssen L. L. F.

Hadjimitsis D. G., Clayton C. R. I., Hope V. S., (2004a). An assessment of the effectiveness of atmospheric correction algorithms through the remote sensing of some reservoirs, *Int. J. Remote Sens*., 25, 3651–3674.

Miller C. L. and Laflamme R.A., (1958). The digital terrain model: Theory and application. Photogrammetric, Engineering & Remote Sensing, 24(3), 433-442.

Olson C.E. ,(1960). Elements of photographic interpretation common to several sensors. *Photogrammetric Engineering & Remote Sensing*, 26(4), 651-656.

Richards J.A.and Jia X., (2006). Remote Sensing Digital Image Analysis, 4th edition, *Springer*, 439 p.

CHAPTER 3_THE INTEGRATED REMOTE SENSING (RS)-STRATIGRAPHIC APPROACH

Reconstructing the paleoenvironmental evolution of an area means to define the three-dimensional relationships existing among depositional/sedimentary environments over time and space. A reliable and accurate reconstruction is possible through the observation and interpretation of sedimentary bodies and facies, since each depositional environment is characterized by typical physical, chemical, and biological conditions that are responsible for specific type of deposits (Krumbein and Sloss, 1963) and morphologies.

In the case of modern alluvial-coastal plains, borehole stratigraphies and cone penetration tests (CPT) are considered the most informative data furnishing a continuous and almost undisturbed record of the subsurface vertical succession of deposits (Amorosi and Marchi, 1999; Amorosi et al., 2014; Styllas, 2014). However, the discrete, and in the case of CPT, indirect nature of these data prevents a direct observation of the morphology of buried sedimentary bodies and, as a consequence, it is commonly inferred on the basis of facies correlations along a grid of stratigraphic sections.

In order to test the possibility to obtain the missing morphologic information in a relatively easy, fast and low-cost way starting from the Earth’s surface observation, a fully integrated RS-stratigraphic methodological approach is developed and applied to the two study areas selected.

Following the aims of this research project, passive optical satellite imagery was selected among the available RS data as it represents a powerful tool for the visual mapping (on the x, y plane) and interpretation of surface geological and geomorphological features, also over wide areas, based on their optical behavior (spectral radiance/reflectance; Chapter 2). The combination of satellite multi/hyperspectral imagery with DTMs introduces, besides the plan-view, the elevation (z) datum allowing to define the 3D-shape of the mapped features (fig. 3.1 a,b).

Moving from the surface to the subsurface, field surveys and soil sampling campaigns were performed on selected RS-detected traces in order to analyze the sedimentological and optical characteristics of the on-trace and out-of-trace areas (fig. 3.1b). The knowledge of soil spectral signatures is indeed essential to calibrate the spectra extracted from the hyperspectral satellite images. Thereafter, the investigation was extended to the shallow subsurface (i.e., uppermost 10 m) through the collection of auger drillings and continuous core data (on-trace and out-of-trace cores; fig. 3.1c, fig. 3.2) on which facies analysis and stratigraphic correlations were undertaken.

Thus, the cross-reference between RS-identified features (traces) and surface-subsurface deposits (cores) firstly allowed to couple morphologies and deposits, shedding new light on the relationships between surface geological features and the corresponding subsurface stratigraphic architecture.

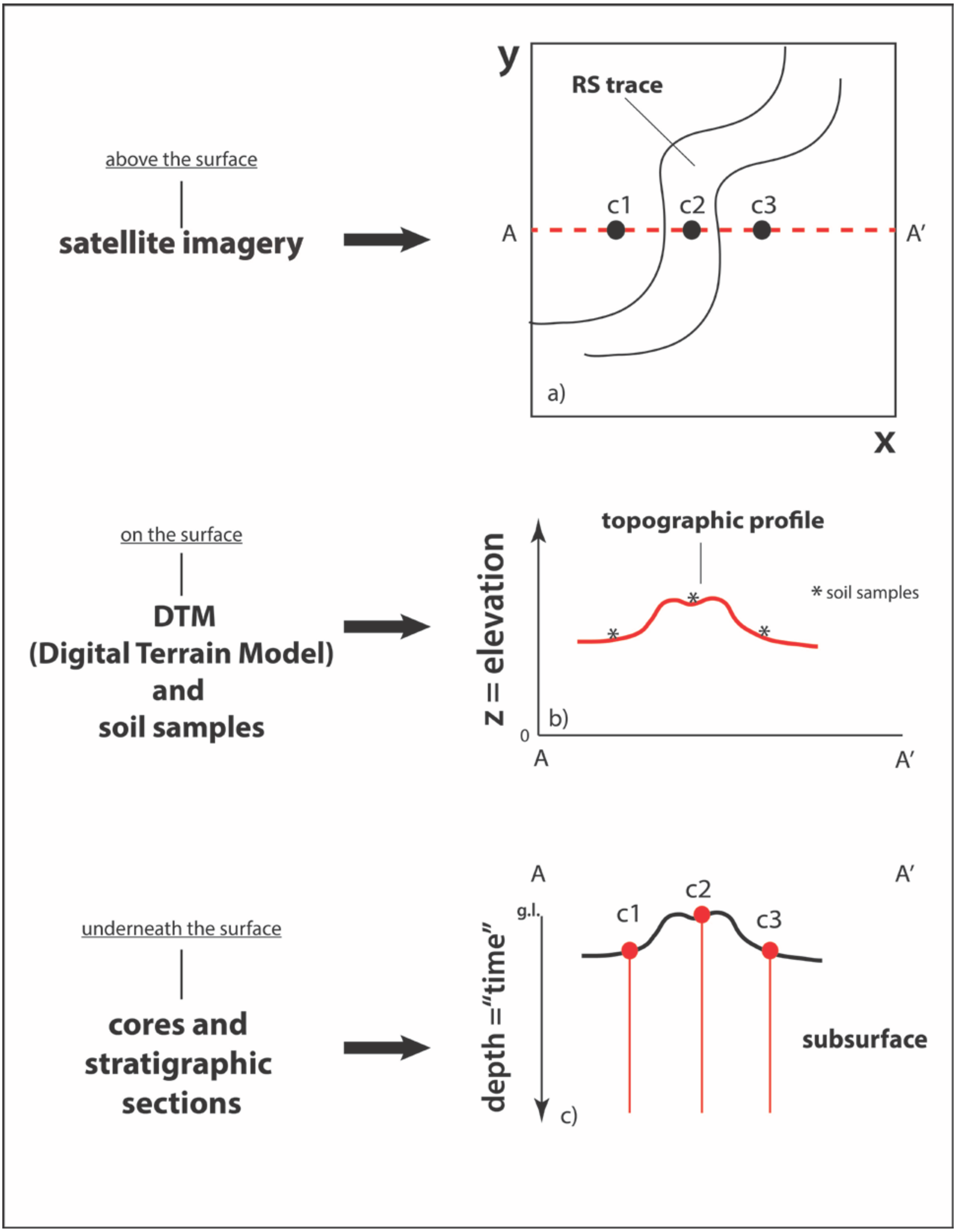

Figure 3.1_Scketch of the methodological approach followed in the present work.

The methodological approach applied to both the study areas (Pisa Plain and Mezzano Valley-southern Po Plain) is presented in detail in the next sections (3.1 and 3.2), where each step of the workflow depicted in the following figure 3.2 is described.

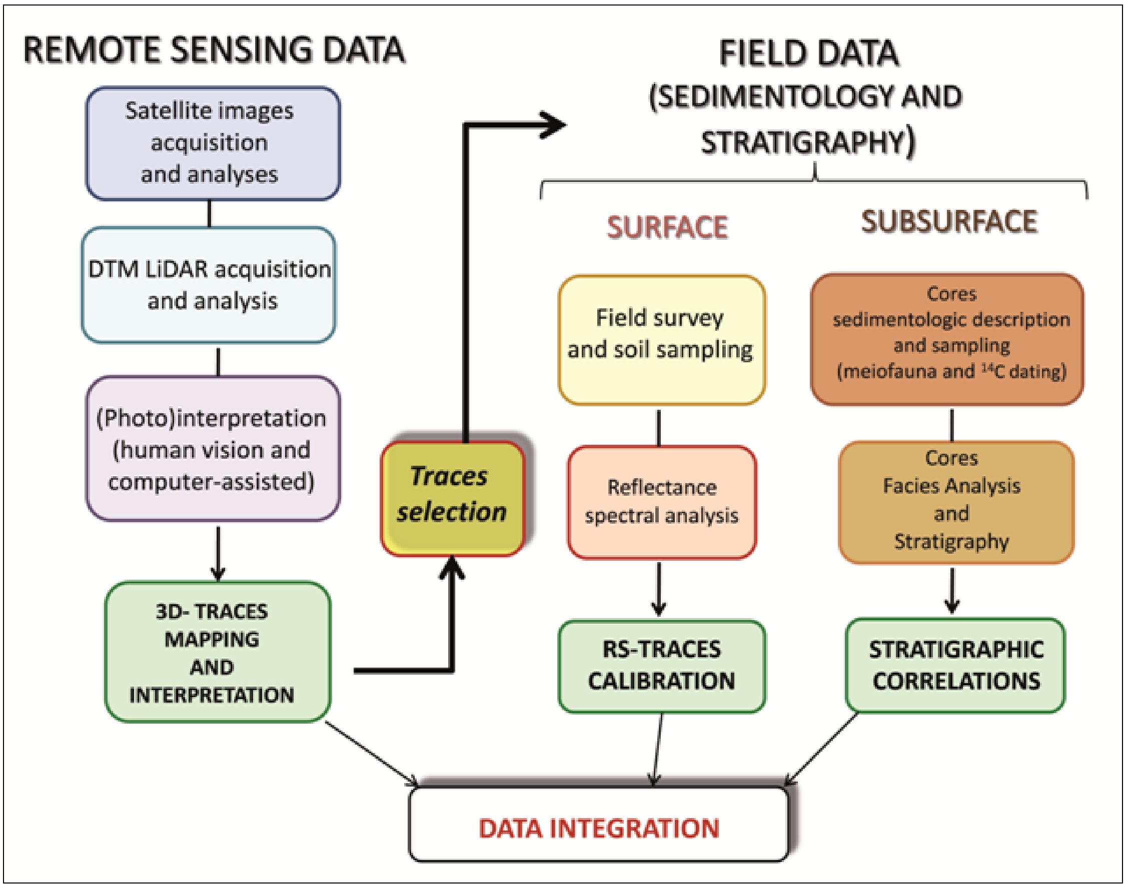

Figure 3.2_Workflow of the integrated methodological approach followed in the present work

However, concerning the Pisa Plain study area, it has to be said that it was not possible to rigorously apply the methodology showed in figure 3.2 in the urban area (Pisa city site), due to the widespread occurrence of a multilayered anthropogenic soil (Bini et al., 2015), which prevented surface samples collection/analysis and got more difficult the analyses of satellite images. For this reason, airborne photos analyzed by Dr. Monica Bini (Department of Geological Science, University of Pisa) were also used for the Pisa city site.

3.1. Remote sensing data (satellite imagery and LiDAR) and analyses

The analysis and interpretation were carried out using free-of-charge satellite imagery (Tab. 3.1). The advantage of using satellite images with respect to aerial photos is that multispectral (and hyperspectral) images can be enhanced and processed to extract the desired informative data carried by the different recorded EM bands.

Since clouds and vegetation canopy represent obstacles for the effectiveness in detecting surface geological features (such as paleochannel traces), only scenes recorded under the best atmospheric conditions and related to mainly outcropping bare soils were selected from the on-line NASA Land Processes Distributed Active Archive Center (LP DAAC), United States Geologic Survey (USGS), European Space Agency (ESA)-Copernicus imagery datasets.

To increase the amount of information achievable for the study areas, a multitemporal analysis was performed on Landsat imagery collected from different seasons of several years (http://earthexplorer.usgs.gov/).

Before being analyzed, the scenes were pre-processed for the atmospheric correction to obtain from the total radiance (energy recorded by the sensor for each pixel of the scene) the "Top of Atmosphere" (TOA) reflectance, which corresponds to the percent of energy reflected from the surface with respect to the incident energy (i.e., solar irradiance). This operation allowed to extract information about pixels' spectral signature and to compare spectral data among different images. No pre-processing was needed for the Sentinel-2 Multispectral Instruments (MSI) imagery, as the data were level-1C type, representing the ToA reflectance itself. The images were then converted to GeoTIFF format using the Sentinel Application Platform (SNAP) by ESA on-line toolbox, so that the georeferenced reflectance data could be processed with ENVI software and integrated with other referenced data.

Afterwards, all the images were radiometrically (e.g., histogram stretching and density slicing) and geometrically enhanced (e.g., pan-sharpening) to improve the perceived quality of the images and facilitate the recognition of different elements constituting the scenes, and hence the visual interpretation. The recognition was mainly based on the pixels' brightness contrast, that is related to different reflectance values, and on the spatial/geometrical arrangement of bright pixels corresponding to shapes.

In addition, appropriate EM spectral bands were chosen for the false color composite (FCC) RGB visualization to further highlight and distinguish features. In particular, considering the lithological characteristic of the areas (cohesive fine-grained *versus* coarse-grained unconsolidated deposits), the FCC were carried out using EM spectral bands particularly sensitive to lithology and moisture content, such as the ones from NIR and SWIR regions of the EM spectrum. Even though Thermal Infrared bands (TIR) are commonly employed to estimate soil moisture (Hulley et al., 2010; Mallik et al., 2009; Mira et al., 2010;

Zhang and Zhou, 2016), these bands were excluded from the image analysis due to their low geometric resolution (Tab. 3.1) with respect to the investigated targets.

The multitemporal georeferenced set of both Landsat 7 ETM+ and Landsat 8 OLI scenes was analyzed to study and compare the spectral response of the identified traces over time, and thence in different atmospheric conditions.

To further support and integrate the visual interpretation of the scenes, semi-automatic processing (unsupervised digital image classification and Principal Component Analysis - PCA) of the optical multispectral imagery was performed. The Iterative Self-Organizing Data Analysis Technique (ISODATA, Tou and Gonzalez, 1974) algorithm for the unsupervised classification was employed to put in evidence the spectral similarities inside each scene, grouping pixels in classes on the basis of their reflectance affinity. The PCA, calculating statistic correlation properties of the electromagnetic spectral bands, was performed to enhance differences among bands and the dataset variability through the extraction of the most informative components (Richards, 1986). The first principal component (PC1) was particularly significant, because it shows the greatest variance (Lillesand et al., 2004) and thus it allows the best distinction among the features inside each scene, maximizing the spectral differences.

Concerning the hyperspectral data from Hyperion satellite, even though the swath of the available images covered only a portion of the study area (Tab.3.1), it was possible to collect spectral signatures from the traces identified inside the Hyperion scenes and compare them with the USGS spectral library to correlate and interpret the extracted spectra. Imagery from Google Earth, provided mostly by the Digital Globe (2013) company that is the owner of Quick Bird, World View-1 and 2 satellites, were also employed to refine the visual interpretation as they display high geometric resolution (pixel size < 1m) even though no processing of the scenes was possible. All the traces highlighted by the image analysis were then mapped in GIS environment and georeferenced in the UTM-WGS84 projection system.

A 1m-resolution DTM from the aerial laser-scanning survey (undertaken by MATTM in 2008) was also used for the geomorphologic characterization of the study areas. For the Pisa Plain, the DTM was kindly provided by the Municipality of Pisa, within active scientific collaborations. The elevation data were acquired by an ALTM 3100AE Gemini laser-scanner that recorded data at a flight altitude ranging between 1050m and 1300m above the ground level, with an average density of acquisition of 0.8 and 1.5 points/m^2 for coastal and inland areas, respectively (http://ambiente.regione.emilia-romagna.it/geologia/temi/costa/il-rilievo-lidar). In order to extract high-reslution topographic profiles and perform measurements, the DTM was projected to WGS84-UTM Zone 32N and inside GIS environment geologic features were mapped. The resulting shapefiles were compared and integrated with the results obtained from the satellite image analysis.

Satellite	Sensor	Launch year	Orbit inclination (from Equator)	Height (km)	Swath width (km)	Revisit time (days)	Number of spectral bands	Spectral resolution (bits)	Spatial resolution (m)	Bands and wavelength ranges (nm)		Description	Ownership
LANDSAT 7	ETM+ (Enhanced Thematic Mapper Plus)	1999	98.2°	705	185	16	8	8	15	PAN	500-900	VIS-NIR	NASA
									30	1	450-515	VIS	
										2	525-605		
										3	639-690		
										4	750-900	NIR	
										5	1550-1750	SWIR	
										7	2090-2350		
									60	6	10400-12500	TIR	
LANDSAT 8	OLI (Operational Land Imager)	2013	98.2°	705	185	16	11	8	15	PAN	500-680	VIS	NASA
									30	1	435-450		
										2	450-510		
										3	530-590		
										4	640-670		
										5	850-880	NIR	
										CIRRUS	1360-1380		
										6	1570-1650	SWIR	
										7	2110-2290		
									100	10	10600-11190	TIR	
										11	11500-12150		
TERRA	ASTER	1999	98.3°	705	60	16	14	8	15	1	520-600	VIS	NASA-METI (Ministry of Economy Trade and Industry-Japan)
										2	630-690		
										3n	760-860	NIR	
										3b	760-860		
									30	4	1600-1700	SWIR	
										5	2145-2185		
										6	2185-2225		
										7	2235-2285		
										8	2295-2365		
										9	2360-2430		
								12	90	10	8125-8475	TIR	
										11	8475-8825		
										12	8925-9275		
										13	10250-10950		
										14	10950-11650		
SENTINEL-2	MSI	2013	98.62°	786	290	10 (combined 5)	13	12	10	2	490(±65 nm)	VIS	ESA
										3	560(±35 nm)		
										4	665(±30 nm)		
										8	842(±115 nm)	NIR	
									20	5	705(±15 nm)		
										6	740(±15 nm)		
										7	783(±20 nm)		
										8a	865(±20 nm)		
										11	1610(±90 nm)	SWIR	
										12	2190(±180nm)		
									60	1	443(±20 nm)	VIS	
										9	945(±20 nm)	NIR	
										10	1375(±30 nm)	SWIR	
EO-1	HYPERION	2000	98.7°	705	7.5	16	220	16	30	400-2500		VNIR-SWIR	NASA

Table 3.1- Technical information of the satellite imagery employed in the analysis

3.2. Field surface data-subsurface data and analyses

Among the traces highlighted by the RS analyses, those considered the most representative for the aims of the project were selected and qualitatively described on the field for the surface morphology and sedimentological characteristics (grain size, colors and accessory materials), then sampled (upper portion: 5-10 cm) for the spectral signatures analysis, and drilled for the shallow subsurface stratigraphy.

Laboratory spectral signatures on surface soil (upper 5cm) samples from the traces and their surroundings were extracted in the RS laboratory of the Earth Sciences Department, University of Florence using an Analytical Spectral Device (ASD) Field Spec Pro spectrometer which measures reflectance in 3-10 nm band widths over the 350-2500 nm range.

A dedicated Nadir viewing set-up, including two halogen tungsten lamps (24V; 70W) connected with a stabilized power supply device (TTi EX354D; Dual Output; 35V; 4A; 280W), was used to ensure minimum shadowing perturbation and to guarantee the control of the irradiance conditions. Lamps were located laterally with respect to the sample, at a distance of 60cm and inclined at 45°. The optic fiber was in the Nadir position at a height of 5-10 cm above the sample, resulting in a table-projected field of view diameter of 2-4.5 cm. All measurements were performed on the powdered samples (<2µm), using special care to level the powder to a uniform thickness.

For each sample surface, four averages of 100 reflectance measurements were acquired in different positions to reduce noise, while reference measurements on the Spectral on panel were averaged on the 100 spectra and repeated systematically every three samples.

The 11 mean spectra acquired in the different positions were averaged using the ASD ViewSpec Pro, and possible “steps” in the spectrum were eliminated using the “splice correction” function of this software. Normalization, and exclusion of noisy tales from spectra were obtained using a dedicated MATLAB script (The Matworks, Natick, MA) that transforms the entire spectral library into ASCII format.

Besides surface sample analyses, a total of 21 continuous cores (5 cores in the Pisa SR site and 16 in the MV), up to 10 m-long, were carried out using a percussion drilling technique (VibracorerAtlas Copco, Cobra model, equipped with Eijkelkamp samplers), which provides small diameter cores (diameter of 4 cm or 6 cm) qualitatively similar to the ones recovered by continuous core drills. Five shallower cores (2 m-long) were also drilled by a hand-auger in the SR site (fig.3.3).

The cores, which were positioned using GPS devices, were undertaken in areas with different reflectance response (dark *versus* bright portions in satellite images) and position with respect to the morphological features of the traces (e.g., meander point bar *versus* meander cut bank).

The cores were described in detail in terms of mean grain-size, consistency, sedimentary structures, color and presence/type of accessory materials, mainly including redoximorphic features, calcareous nodules, plant debris, wood/shells fragments, organic-matter and peaty layers, for the sedimentological characterization of individual facies associations.

Figure 3.3_Drilling methods used in the present work a) vibracore; and b) recovered cores; c) hand-auger for shallower drillings; and d) samples extracted.

In order to support and refine this interpretation, new cored successions (Cobra cores) were sampled for qualitative-semi quantitative benthic foraminifer/ostracod analyses (a total of 20and 42 samples for SR and MV cores respectively).

The sampling was performed in order to characterize the whole variety of lithofacies identified from visual cores inspection. The samples (ca. 50 g of sediments) were prepared following the standard procedures reported in Amorosi et al. (2013). The sediment fraction with granulometric size >125μm was analyzed under an optical microscope to describe the fossil assemblages mainly on the basis of autochthonous *versus* allochtohnous species and dominant *versus* secondary species.

According to previous works on the Po Plain (Bondesàn et al., 2006; Curzi et al., 2006), three main classes of relative abundance of species (abundant: >30%; common: 30-10% and rare: <10%) were used to identify different autochthonous associations.

Species identification and paleoenvironmental interpretations of mixed foraminifer-ostracod associations relied on key papers dealing with the spatial distribution patterns of modern Mediterranean and North Atlantic meiofauna (Albani et al., 1984, 2007; Athersuch et al., 1989; Albani and Serandrei Barbero, 1990; Henderson, 1990; Stoch, 1995; Montenegro and Pugliese, 1996; Ruiz et al., 2000; Murray, 2006; Melis and Covelli, 2013).

The chronological framework of the studied sedimentary successions was guaranteed by 12 new radiocarbon ages (3 and 9 ages from SR and MV, respectively) obtained from reference core samples (wood/plant fragments, peat, organic-rich clay and mollusk shells). The dating analyses were carried out at CIRCE Laboratory of Caserta (University of Naples) and KIGAM laboratory (Daejeon City, Korea).

Conventional ages were calibrated using specific programs (Calib 7.0.4 and OxCal 4.2 for SR and MV, respectively) and the INTCAL13 or MARINE13 calibration curves depending on the terrestrial or marine nature of the dating materials (Reimer et al., 2009). For mollusk shells, in order to compensate for the reservoir effect, an average value of Delta R was estimated from the dataset available online (http://calib.qub.ac.uk/marine/; 35±42 and 139±28 for the northern Tyrrhenian Sea and the northern Adriatic Sea, respectively). In this thesis, all the ages are reported as the highest probability range (cal yr BP) obtained using two standard deviations-2s.

Local stratigraphic sections intercepting the newly drilled cores were carried out and interpreted basing on lithofacies correlations and radiocarbon ages, in order to reconstruct the shallow subsurface (ca. uppermost 10 m) stratigraphy underneath selected reference traces.

Thus, the integration of RS and field data led to a high-resolution 3D paleoenvironmental reconstruction at the traces scale, that represented the base for a detailed reconstruction of the main paleoenvironmental evolution phases occurring in the study areas during the mid-late Holocene period (from lagoon basin to wave-dominated deltas; Anthony et al., 2014). To achieve this scope, further stratigraphic sections crossing the whole study areas and intercepting the highest quality data available from local geognostic databases were performed and interpreted with the support of additional radiocarbon ages, already reported in Amorosi et al. (2016; in press) and Bini et al. (2015).

References

Albani A.D., Favero V., Serandrei Barbero R., (1984). Benthonic foraminifera as indicators of intertidal environments. *Geo-Marine Letters* 4, 43–47.

Albani A. and Serandrei Barbero R., (1990). I Foraminiferi della Laguna e del Golfo di Venezia. Memorie Scienze Geologiche Padova 42, 271–341.

Albani A., Barbero R.S., Donnici S., (2007). Foraminifera as ecological indicators in the lagoon of Venice, Italy. Ecological Indicators 7: 239-253.

Athersuch J., Horne D.J., Whittaker J.E., (1989), Marine and brackish water ostracods, in KERMACK D.M., BARNES R.S.K. (eds.) *«Synopses of the British Fauna (New Series)»*, 43, Brill E.J., Leiden, 1-343.

Amorosi A. and Marchi N., (1999). High-resolution sequence stratigraphy from piezocone tests: An example from the Late Quaternary deposits of the southeastern Po Plain. SedimentaryGeology, 128(1–2), 67–81. http://doi.org/10.1016/S0037-0738(99)00062-7

Amorosi A., Rossi V., Sarti G., Mattei R., (2013). Coalescent valley fills from the late Quaternary record of Tuscany (Italy). Quaternary International, 288, 129–138. http://doi.org/10.1016/j.quaint.2011.10.015

Amorosi A., Antonioli F., Bertini A., Marabini S., Mastronuzzi G., Montagna, P., ..,Vai, G. B., (2014). The Middle-Upper Pleistocene Fronte Section (Taranto, Italy): An exceptionally preserved marine record of the Last Interglacial. Global and Planetary Change, 119, 23–38. http://doi.org/10.1016/j.gloplacha.2014.04.007

Amorosi A., Bruno L., Campo B., Morelli A., Rossi V., Scarponi D., Hong W., Bohacs K.M., Drexler T.M.(in press). Global sea-level control on local parasequence architecture from the Holocene record of the Po Plain,Italy submitted to Marine Geology, Marine Geology-submitted

Anthony E.J., Marriner N., Morhange C., (2014). Human influence and the changing geomorphology of Mediterranean delta sand coasts over the last 6000years:Fromprogradationtodestructionphase?, Earth-Science Reviews, 139, 336-361

Bini M., Rossi V., Amorosi A., Pappalardo M., Sarti G., Fabiani F, Gualandi L., Noti V., (2015). Palaeoenvironments and palaeotopography of a multilayered city at the Etruscan-Roman transition: early interaction of fluvial processes and urban growth at Pisa (Tuscany, Italy). Journal of Archaeological Science, 59 197–210.

Bondesan M., Cibin U., Colalongo M. L., Pugliese N., Stefani M., Tsakiridis E., Vaiani S.C., Vincenzi S., (2006). Benthic communities and sedimentary facies recording late Quaternary environmental fluctuations in a Po Delta subsurface succession (Northern Italy). In: Coccioni, R., Lirer, F. and Marsili, A., Eds., *Proceedings of the Second and Third Italian Meeting of Environmental Micropaleontology,* 21–31. Krakow: Grzybowski Foundation. Special Publication 11.

Curzi P.V., Dinelli E., Ricci Lucchi M., Vaiani S.C., (2006). Palaeoenvironmental control on sediment composition and provenance in the late Quaternary deltaic successions: a case study from the Po delta area (Northern Italy). Geological Journal, 41: 591–612.

Henderson P.A., (1990). Freshwater ostracods. In: Kermack DM, Barnes RSK (eds) Synopsis of the British fauna (New Series). Vol.42. *Universal Book Services,* Oegstgeest.

Hulley G.C., Hook S.J., Baldridge A.M., (2010). Investigating the effects of soil moisture on thermal infrared land surface temperature and emissivity using satellite retrievals and laboratory measurements, *Remote Sensing of Environment*, 114, 7, 1480-1493.

Krumbein W.C. and Sloss L.L., (1963). Stratigraphy and Sedimentation, San Francisco, W.H.

Lillesand T.M., Kiefer R.W., Chipman J.W., (2004). Remote sensing and image interpretation, – 5 th Edition. New York, Chichester, Brisbane, Toronto, Singapore.

Mallick K., Bhattacharya׳ B.K., Patel N.K., (2009). Estimating volumetric surface moisture content for cropped soils using a soil wetness index based on surface temperature and NDVI, *Agricultural and Forest Meteorology* 149,8,1327-1342.

Melis R. and Covelli S., (2013). Distribution and morphological abnormalities of recent foraminifera in the Marano and Grado Lagoon (North Adriatic Sea, Italy), *Mediterr. Mar. Sci.*, 14, 432–450,

Mira M., Valor E., Caselles V., Rubio E., Coll C., Galve J.M, Niclos R., Sanchez J.M., Boluda R., (2010). Soil Moisture Effect on Thermal Infrared (8-13 µm) Emissivity, IEEE transactions on Geoscience and Remote Sensing, v. 48, n. 5.

Montenegro M.E. and Pugliese N., (1996). Autecological remarks on the ostracod distribution in the Marano and Grado Lagoons (Northern Adriatic Sea Italy), in «Bollettino della Società Paleontologica Italiana», 3, 123-132.

Murray J.W., (2006). Ecology and applications of benthic foraminifera, Cambridge University Press, Cambridge, 426 pp.

Reimer P. J., Baillie M. G. L., Bard E., Bayliss A., Beck, J. W. Blackwell, P. G. Bronk Ramsey, C., Buck C. E., Burr G. S., Edwards R. L., Friedrich M., Grootes P. M., Guilderson T. P., Hajdas I., Heaton T. J., Hogg A. G., Hughen, K. A. Kaiser, K. F. Kromer, B. McCormac F. G., Manning S. W., Reimer R. W., Richards D. A., Southon, J. R. Talamo, S. Turney, C. S. M. van der Plicht, J. and Weyhenmeyer C. E., (2009). IntCal09 and Marine09 radiocarbon age calibration curves, 0-50,000 years cal BP. Radiocarbon, 51(4), 1111-1150.

Richards J.A., (1986). Remote Sensing Digital Image Analysis, Springer-Verlag.

Ruiz F., Gonzalez-Regalado M.L., Baceta J.I., Menegazzo-Vitturi L., Pistolato M., Rampazzo G., Molinaroli E., (2000). Los ostracodos actuales de la laguna de Venecia (NE de Italia). [Lesostracodesactuels de la lagune de Venise (NE Italie)] [Recentostracods from the Venicelagoon (NE Italy)], in *«Geobios»*, 33, 447-454.

Styllas M., (2014). A simple approach to define Holocene sequence stratigraphy using borehole and cone penetration test data. *Sedimentology* 61, 444–460.

Stoch F., (1994). Indagine ecologico-faunistica sui popolamenti entomostraci di alcuni stagni d’acqua salmastra dell’Isola della Cona (foce del Fiume Isonzo, Italia NordOrientale). Gortania Atti Museo Friuliano di Storia Naturale 16, 151–173.

Tou J.T. and Gonzalez R.C., (1974). Pattern Recognition Principles. Reading, MA: Addison-Wesley.

Zhang D. and Zhou G., (2016). Estimation of Soil Moisture from Optical and Thermal Remote Sensing: A Review- Sensors, ,16(8), 1308; doi:10.3390/s16081308.

CHAPTER 4_ PISA PLAIN (ARNO DELTA) RS-STRATIGRAPHIC RESULTS

The results derived from the integration of RS-stratigraphic data in the Pisa Plain and their local implications for mid-late Holocene paleoenvironmental reconstructions are presented in this chapter. Two different sections illustrate the results obtained from the urban (Pisa city site; 4.1) and extra-urban (Pisa S. Rossore-SR site; 4.2) settings respectively.

The Pisa Plain geomorphologic-stratigraphic framework is reported within the scientific paper, published in Palaeogeography, Palaeoclimatology, Palaeoecology in 2015, forming the core of section 4.1. The paper, titled "*Climatic signature of two mid–late Holocene fluvial incisions formed under sea-level highstand conditions (Pisa coastal plain, NW Tuscany,* Italy" (by Sarti G., Rossi V., Amorosi A., Bini M., Giacomelli S., Pappalardo M., Ribecai C., Ribolini A., Sammartino I.), focuses on the Pisa urban area and the study of the related mid-late Holocene paleodrainage system based on a multidisciplinary approach involving RS and stratigraphic data. As a co-author of the paper, I especially collaborated to the subsurface stratigraphic and paleogeographic reconstructions, while the RS data were analyzed by Dr. Monica Bini (airborne and satellite images) and Dr. Adriano Ribolini (2D Electrical Resistivity Tomography-ERT), both afferent to the Department of Geological Science of the University of Pisa. Since the employed satellite data and processing (SPOT, ALOS AVNIR-2 and TERRA ASTER) didn't include all those selected for this thesis, additional satellite imagery and analyses for the urban area were performed and reported at the end of section 4.1 and in Appendix A.

In particular, free-of-charge satellite images were studied through multitemporal and PCA analyses, in order to make the methodological approach followed in the urban setting be as much as possible consistent with the adopted method (see section 3.1).

In section 4.2 RS, reflectance and stratigraphic data collected in the croplands located between the city of Pisa and the outcropping beach-ridges (extra-urban area, SR site) are presented.

Then, in section 4.3 the results obtained in the SR-site from the application of the integrated methodology explained in Chapter 3 are shown.

SR data presentation can be considered on completion of the paleodrainage reconstruction achieved in the urban area of Pisa.

4.1. Pisa urban area

The article “Climatic signature of two mid–late Holocene fluvial incisions formed under sea-level highstand conditions (Pisa coastal plain, NW Tuscany, Italy)” by Sarti G., Rossi V., Amorosi A., Bini M., Giacomelli S., Pappalardo M., Ribecai C., Ribolini A., Sammartino I. (2015) is reported below.

In the paper, a high-resolution multidisciplinary study (stratigraphic, geomorphological, geophysical, palynological) proved to succeed in the identification and mapping of two paleochannel networks flowing in the Pisa urban area during the mid-late Holocene.

This paleoenvironmental-depositional reconstruction relied upon a grid of stratigraphic cross-sections and was refined through the cross-reference of subsurface stratigraphy with remote-sensed fluvial landforms/paleochannels traces, identified mainly on the basis of multitemporal aerial photographs analyses.

The reconstruction of Pisa proto-historic paleodrainages (active between ca. 4000-2500 cal yr BP) allowed a better understanding of river systems development and evolution in relation to natural and human-induced changes, occurred under highstand sea-level conditions.

Palaeogeography, Palaeoclimatology, Palaeoecology 424 (2015) 183–195

Contents lists available at ScienceDirect

Palaeogeography, Palaeoclimatology, Palaeoecology

journal homepage: www.elsevier.com/locate/palaeo

Climatic signature of two mid–late Holocene fluvial incisions formed under sea-level highstand conditions (Pisa coastal plain, NW Tuscany, Italy)

G. Sarti [a],*, V. Rossi [b], A. Amorosi [b], M. Bini [a], S. Giacomelli [a], M. Pappalardo [a], C. Ribecai [a], A. Ribolini [a], I. Sammartino [b]

[a] Department of Earth Science, University of Pisa, Pisa, Italy
[b] Department of Biological, Geological and Environmental Sciences, University of Bologna, Italy

ARTICLE INFO

Article history:
Received 17 September 2014
Received in revised form 4 February 2015
Accepted 8 February 2015
Available online 17 February 2015

Keywords:
Mid–late Holocene
Stratigraphic architecture
Channel incision
Pollen
Climate change
Pisa Plain

ABSTRACT

A multi-proxy (stratigraphic, geomorphological, palynological, geophysical) study of mid–late Holocene deltaic–alluvial deposits beneath the Pisa Plain (Tuscany, Italy) reveals short-term enhances of fluvial activity under relative sea-level highstand (HST) conditions (last ~7000 cal yr BP). Early HST delta progradation led to the progressive infill of a broad lagoon area (~5000 cal yr BP), followed by the development of a stable alluvial depositional environment (~4000 cal yr BP). The intense phase of alluvial aggradation was punctuated by two events of enhanced fluvial incision that cut down to 10 m the underlying lagoonal substrate. The two erosive events, which reflect centennial-scale changes in the aggradation/degradation ratio, are chronologically constrained to the Eneolithic–Bronze age transition (~3800 cal yr BP) and to the Bronze–Iron age transition (2900–2800 cal yr BP), respectively.

A detailed pollen profile highlights the correlation between these erosive events and two phases of increased humidity (*Abies* peaks 1 and 2) recorded in several sites of Europe. This correlation suggests a key-role of climate fluctuations in triggering channel incision. The peculiar high compressibility of the lagoonal substrate can also have acted as a factor able to foster the deepening of the channels. In contrast, the role of relative sea-level changes and human impact on the activation of the two erosive processes appears negligible.

1. Introduction

Under long-term highstand sea-level conditions, the majority of depositional models agree with the development of aggradational to progradational deltaic–alluvial sequences, in which isolated, high-sinuosity fluvial channels are cut through overbank fine-grained deposits (Posamentier et al., 1988; Catuneanu, 2006; Catuneanu et al., 2009). However, in Quaternary successions the complex interplay of regional (sea-level, climate), local (geological and tectonic setting, physiography) and human-induced forcing factors may strongly influence river activity on a sub-Milankovitch scale, inducing high-frequency changes in sedimentation patterns (Starkel, 1983, 2000; Maddy et al., 2001; Benito et al., 2003; Lewin et al., 2005; Jones et al., 2010; Macklin et al., 2012; Turner et al., 2013).

In this regard, the deltaic–alluvial successions formed during the mid–late Holocene period (ca. the last 8000–7000 cal yr BP) under decelerating sea-level rise (less than 1 mm yr^{-1}; Stanley and Warne, 1994; Lambeck et al., 2004) and increasing sediment supply due to both anthropogenic and climatic factors represent valuable sedimentary archives for a detailed comprehension of fluvial system dynamics and a pertinent evaluation of the main driving factors (Posamentier et al., 1988; Somoza et al., 1998; Catuneanu, 2006). Although generally weaker in amplitude and magnitude than Lateglacial (Heinrich stadial 1, BØlling–AllerØd interstadial and Younger Dryas) and last glacial (Dansgaard–Oeschger and Heinrich events) events (Alley et al., 2003; Hemming, 2004; Steffensen et al., 2008), the mid–late Holocene short-term climate oscillations (Mayewski et al., 2004; Wanner et al., 2008; Helama et al., 2010) are proven to leave identifiable traces in the fluvial record. Across western and central Europe, slack water flood deposits provide a centennial-scale record of flood frequency increase, potentially correlative to mid–late Holocene climatic changes (Macklin and Lewin, 2003; Lewin et al., 2005; Macklin et al., 2006; Starkel et al., 2006; Thorndycraft and Benito, 2006).

Valuable insights on high-frequency fluvial dynamics–climate–land use interactions can be inferred through a multiproxy, high-resolution examination of the mid–late Holocene stratigraphy recorded beneath the subsiding Mediterranean coastal plains. Here, the abundance of fine-grained deposits, where pollen and traces of human occupation are well preserved, and the good chronological control offered by

---

* Corresponding author. Tel.:+39 502215730.
E-mail addresses: sarti@dst.unipi.it (G. Sarti), veronica.rossi4@unibo.it (V. Rossi), alessandro.amorosi@unibo.it (A. Amorosi).

http://dx.doi.org/10.1016/j.palaeo.2015.02.020
0031-0182/

radiocarbon dates coupled with widespread archeological remains potentially make these highstand sedimentary wedges (Highstand Systems Tract-HST) a truly effective and powerful natural laboratory on which to infer the potential response of the coastal plain to future climatic variations due to both anthropogenic and natural causes.

In the Pisa coastal plain (NW Tuscany, Italy; Fig. 1A), located within the southern portion of the extensional Viareggio Basin (Malinverno and Ryan, 1986; Martini and Sagri, 1993; Patacca et al., 1993; Pascucci, 2005), the mid–late Holocene deltaic–alluvial succession is remarkably thick (10–15 m; Amorosi et al., 2013a) and rests on a laterally extensive stratigraphic marker, composed of homogeneous, soft lagoonal clays deposited during the late transgressive–early highstand phases (ca. 8000–5000 cal yr BP-Neolithic age in Table 1; Benvenuti et al., 2006; Rossi et al., 2011; Amorosi et al., 2013a). The prograding deltaic–alluvial wedge is made up of swamp soft clays, which in turn are overlain by poorly drained floodplain clays chronologically constrained to the proto-historic period (Table 1; Amorosi et al., 2013a). These fine-grained deposits are locally juxtaposed to crevasse splay/levee silty–sandy complex and fluvial sand bodies, deeply truncating the underlying succession (Sarti et al., 2012; Amorosi et al., 2013a) (Fig. 1).

Table 1
Archeological chronology for the Pisa Plain (slight modified from http://www.mappaproject.arch.unipi.it).

Age	Chronology	Time range (yr BC/AD)	Time range (cal yr BP)
Prehistoric	Neolithic	(5500–3300 BC)	ca. (7500–5300)
Proto-historic	Eneolithic	(3300–1900 BC)	ca. (5300–3800)
	Bronze age	(1900–901 BC)	ca. (3800–2850)
	Iron age	(900–721 BC)	ca. (2850–2700)
Historical	Early Etruscan period	(720–481 BC)	ca. (2700–2400)
	Late Etruscan period	(480–90 BC)	ca. (2400–2000)
	Early Roman period	(89 BC–192 AD)	ca. (2000–1750)
	Late Roman period	(193–600 AD)	ca. (1750–1350)
	Early middle ages	(601–1000 AD)	ca. (1350–950)
	Late middle ages	(1001–1491 AD)	ca. (950–450)
	Modern age	(1492–1814 A)	ca. (450–150)
	Contemporary age	(1815 AD–present)	ca. (150–present)

The overall vertical stacking pattern of facies in the Pisa Plain documents a typically progradational evolutionary trend that led to the formation of the modern deltaic and alluvial plains (Somoza et al.,

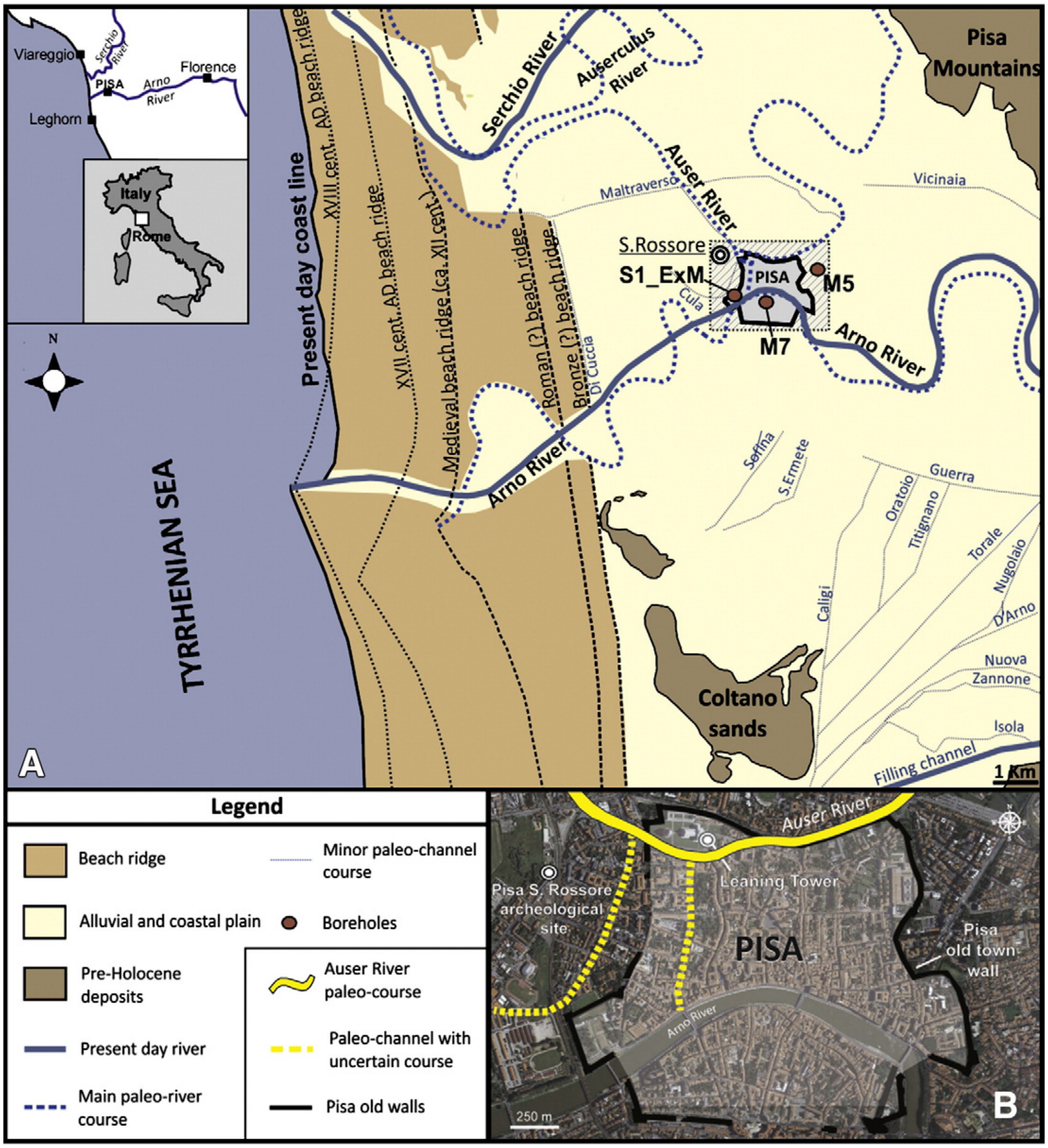

Fig. 1. A) Geological sketch map of the Pisa Plain with indication of the outcropping, juxtaposed coastal beach ridges and the *Auser* paleocourse hypothesized by Strabo (partially modified from Pranzini, 2001 and Sarti et al., 2010). The location of cores mentioned in text is also reported. B) Close-up of the study area corresponding to the Pisa urban and suburban zones. The Medieval city walls are shown with a bold line. The *Auser* paleocourse is also reported along with the location of the archeological site of Pisa S. Rossore.

1998; Amorosi and Milli, 2001; Vella et al., 2005; Fanget et al., 2014). In the Pisa urban area the establishment of a genuine alluvial depositional system was the result of the activity of the Arno River and a former branch of the Serchio River, known as *Auser*, flowing from the Pisa Mountains to the city (Fig. 1A–B). Up to the Etruscan age (ca. 2500–2000 cal yr BP; Table 1) these rivers were subjected to recurring processes of migration and avulsion favored by the very low gradients and high sinuosity (Amorosi et al., 2013a). This natural tendency was greatly thwarted by Roman waterworks and systematic land reclamation (Roman *Centuriatio*, starting from ca. 2000 cal yr BP), which led to the development of an extensive well-drained floodplain in the Pisa urban and suburban areas. Only during the Middle Ages (XI century; Bruni and Cosci, 2003) human intervention definitively forced the *Auser* outside the city walls.

This paper aims to improve our understanding of fluvial systems evolution in relation to natural and human-induced changes during the mid–late Holocene, a crucial period in the evolution of modern Mediterranean alluvial and coastal plains. Interpretation was strengthened by correlation of high-resolution stratigraphic, geomorphological and shallow geophysics data along with on-site pollen and archeological records.

Specifically, we focus on the role of two deep fluvial incisions occurred in the Pisa area under relative sea-level highstand conditions, during the Bronze–Iron ages (between ca. 4000 and 2500 cal yr BP; Table 1).

2. Materials and methods

2.1. Stratigraphic data and analysis

The stratigraphic architecture of the Pisa Plain prograding sedimentary wedge was investigated by means of a dense grid of cross-sections, following the paths of the highest quality core data stored into the georeferenced subsurface dataset (Amorosi et al., 2013b) with maximum spacing of ~500 m (Fig. 2). Detailed facies characterization of the mid–late Holocene succession was performed through integrated sedimentological, geochemical, micropaleontological and palynological analyses (Amorosi et al., 2013a) carried out on the reference cores (continuously cored boreholes and percussion drilling cores), recently drilled during the MAPPA Project coring campaign (http://www.mappaproject.arch.unipi.it) in the Pisa urban and suburban area (Fig. 2). This multidisciplinary approach allowed the identification of seven lithofacies associations, essential for high-resolution stratigraphic correlations and reconstruction of sedimentary evolution. The lithofacies, described in detail by Amorosi et al. (2013a), are here summarized in Table 2, along with the main diagnostic sedimentological and paleontological features.

2.2. Remote sensing analysis

In the study area the stratigraphic reconstruction was refined through identification of the past fluvial landforms by integrated techniques of remote sensing analysis (Bisson and Bini, 2012). Specifically, the analysis of multitemporal aerial photographs, ranging in age from 1943 to 2010, and multispectral images with medium–high resolution acquired from SPOT, ALOS AVNIR-2 and TERRA ASTER satellites allowed the identification of a series of prominent, shallow paleotraces (paleochannels) buried beneath the Pisa Plain.

In a key-portion of the study area, where the paleoArno and *Auser* merge as mentioned by Strabo (Fig. 1B), in order to reinforce the cross-reference between stratigraphic and morphological data a paleotrace was further investigated by 2D Electrical Resistivity Tomography (ERT) (Fig. 2). The ERT profile explored the uppermost 30 m from the ground level, adopting the roll-along acquisition technique,

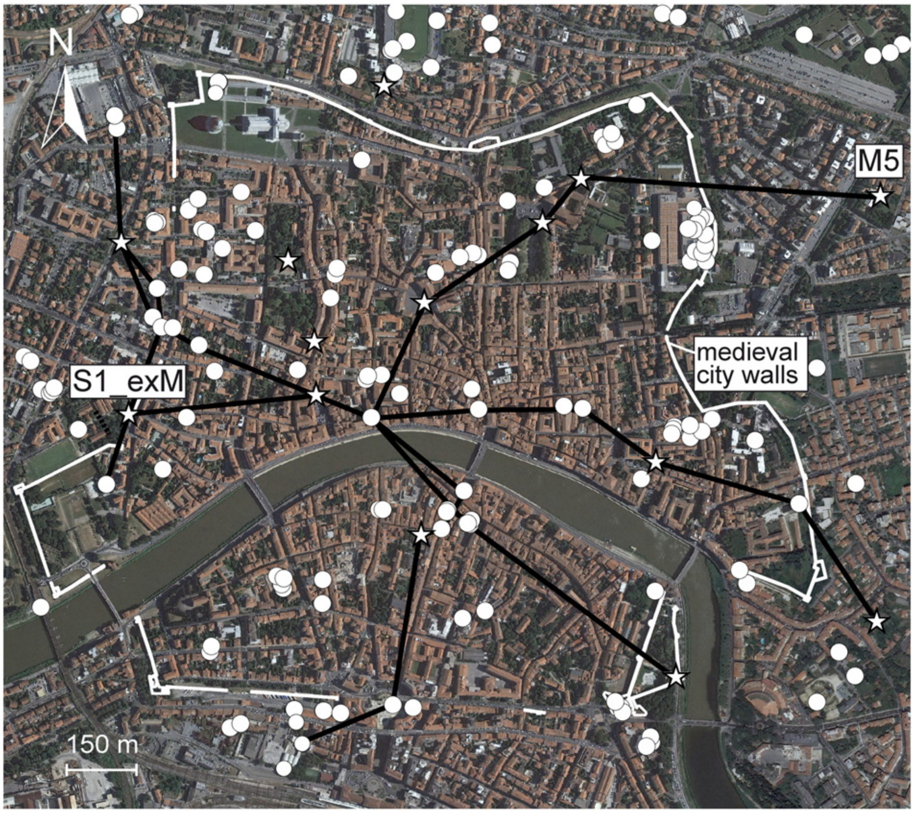

Fig. 2. Location map of the study area reporting the georeferenced subsurface dataset used for this work (from Amorosi et al., 2013b). The reference MAPPA cores are shown by white stars. The location of cores M5 and S1_exM, selected for palynological analysis and ERT calibration respectively, is highlighted. The bold lines and the dotted line indicate the cross-sections reported in Fig. 3 and the ERT profile of Fig. 4, respectively.

Table 2
Diagnostic sedimentological and paleontological features and interpretation of the main lithofacies associations from the mid–late Holocene subsurface succession of the Pisa Plain depicted in Fig. 3 (from Amorosi et al., 2013a).

Lithofacies	Sedimentological features	Micropaleontological content	Palynological content
Fluvial/distributary channel	Gray to yellow-brown, fine- to coarse-grained sand bodies with erosional lower boundary and distinctive fining-upward trend	Barren or poorly-preserved marine, brackish foraminifers and ostracods	No sampled
Crevasse splay, levee and subdelta	Silty sand and fine sand with characteristic coarsening-upward trend (crevasse splay and subdelta) or rhythmical sand–silt alternation (levee). Scattered plant remains, wood and small-sized, unidentifiable mollusc fragments are present, along with rare calcareous nodules and yellow-brown mottles	Barren or poorly-preserved marine, brackish foraminifers and ostracods	No sampled
Well-drained floodplain	Dry, stiff, light brown silty clay with low organic-matter content and evidence of subaerial exposure, including indurated horizons, calcareous nodules and yellow-brown mottles, due to iron and manganese oxides	Barren	Dark-brown to brown reworked phytoclasts and heterogeneous continental palynomorphs with many reworked specimens
Poorly-drained floodplain	Monotonous succession of light gray, soft clay and silty clay, with scarce organic matter and isolated, large (up to 3 cm) calcareous nodules. Sharp-based cm- to dm-thick sand and silt layers occur. Scattered plant remains were encountered along with few, thin-shelled mollusc fragments	Barren or few valves of *P. albicans* or *C. torosa*, the latter within organic-rich layers	Rounded, dark brown to black phytoclasts, homogeneous in size with AOM, the latter sporadically abundant within organic-rich layers. Many reworked specimens derived from either ancient sediments or adjacent lands
Lower/upper swamp	Dark soft clay and silty clay, with local presence of cm- to dm-thick sand layers. Wood fragments and peat layers are very abundant. Scattered fragments and shells of freshwater gastropods are also recorded	Scarce oligotypic ostracod fauna mainly composed of *Pseudocandona albicans* and accompanied by rare *Candona neglecta* and *Ilyocypris* species	Abundant, light orange to brown/black phytoclasts (majority > 100 μm). AOM abundant
Lagoon ("pancone")	Monotonous succession of soft blue-gray clay and silty clay with abundant shells of *Cerastoderma glaucum*. Cm-thick fine sand intercalations. Wood and plant fragments scattered	Moderately to highly marine-influenced brackish water meiofauna, dominated by *Ammonia tepida* and *A. parkinsoniana* and *Cyprideis torosa*	Orange-brown phytoclasts (<500 μm) and AOM — amorphous organic matter sporadically present, along with marine-related as dinocysts, foraminiferal linings and scolecodonts

with electrodes spacing of 2 m. A Schlumberger and Wenner configuration combined with dipole–dipole array was used. The 2D inversions of apparent resistivity were undertaken using the TomoLab software (www.geostudiastier.com).

2.3. Palynological analysis

Fifteen samples from clay and silt deposits of core M5 (Fig. 2 for location) were collected for palynological analysis. The presence of a thick, continuous fine-grained succession of lagoon, swamp and poorly-drained floodplain deposits (see Section 1), where pollen grains are expected to be well preserved, made M5 the reference core for the reconstruction of the pollen sequence. Within the lower portion of the core, between 10.5 and 6 m core depth, samples were taken at 20–40 cm intervals. Only two samples were collected from the uppermost part of the core, where pollen and spores are rare and badly preserved within crevasse splay sands and stiff, well-drained floodplain clays.

Standard palynological techniques (HCl, HF, chemical treatment) for mineral dissolution were applied on 10 g of each sample (Fægri and Iversen, 1989). In order to preserve all the organic components, neither oxidative nor alkali treatments were applied. The concentration of pollen, spores and other palynomorphs is estimated by adding a tablet containing a known amount of *Lycopodium* spores. At least 200 well-preserved pollen and non-pollen palynomorphs were counted per sample, and the relative abundance of each taxa was calculated. Pollen taxa were identified according to the literature (Reille, 1992, 1995, 1998 and online databases, http://www.europeanpollendatabase.net) and grouped on the basis of their ecological and climatic affinities, following the indications of previous works carried out in the Arno coastal plain (Aguzzi et al., 2007; Ricci Lucchi, 2008; Amorosi et al., 2009).

Among the non-pollen palynomorphs the marine-related elements, including dinocysts, foraminiferal linings and scolecodonts, and the pteridophyte spores were identified (Traverse, 1988) providing further paleoenvironmental information. In addition, reworked pre-Quaternary elements were counted to highlight phases of intense fluvial activity.

2.4. Chronology

The chronological framework of the studied succession benefited from 14 radiocarbon dates (Table 3) and scattered ceramic remains from the uppermost stratigraphic interval. AMS ^{14}C analyses were performed on wood fragments, organic matter and mollusc shells at CIRCE Laboratory of Caserta (Naples University). Conventional ages were calibrated using the CALIB5 program and the INTCAL09 or MARINE09 calibration curves (Reimer et al., 2009) for terrestrial and marine materials, respectively. In order to compensate for the reservoir effect, mollusc samples were calibrated using an average value of DeltaR (35 ± 42), estimated for the northern Tyrrhenian Sea from online databases (http://calib.qub.ac.uk/marine/). In this study, the ages are reported as the highest probability range (cal yr BP) obtained using two standard deviations-2σ (Table 3).

3. Mid–late Holocene deltaic–alluvial sedimentation and channel dynamics

3.1. Subsurface stratigraphic architecture

The mid–late Holocene deltaic–alluvial succession of the Pisa Plain records the gradual filling of a wide lagoon basin and the establishment around 5000 cal yr BP of a delta system that was replaced by an alluvial plain one thousand years later (Fig. 3A–D; Amorosi et al., 2013a). In terms of sequence stratigraphy, this prograding sedimentary wedge represents the HST of the late Quaternary depositional sequence and displays, as a whole, the distinctive sedimentary signature of a high-accommodation depositional setting (Miall, 1996; Catuneanu, 2006). Indeed, the occurrence of isolated to locally amalgamated channel deposits within a dominantly fine-grained succession (Fig. 3A–D) reflects the cumulative effect of highstand relative sea-level conditions and tectonic subsidence experienced by the study area during the Holocene (Lambeck et al., 2004; Pascucci, 2005).

According to previous work (Rossi et al., 2012; Amorosi et al., 2013a), the lower portion of the deltaic–alluvial succession is made up

Table 3
Radiocarbon chronology. List of the radiocarbon dates obtained from different core samples and discussed in this paper. Calibration has been performed using intcal09.14c (Reimer et al., 2009). Local reservoir correction DeltaR (35 ± 42) was applied to shell samples (*Cerastoderma glaucum* valves).

Code sample	Conventional age (^{14}C yr BP)	Calibrated age (^{14}C yr BP ±2σ)	Material
M9_5.35	2456 ± 41	2360–2618	Wood fragment
M9_2.75	827 ± 23	690–780	Wood fragment
M10_7.85	3613 ± 137	3572–4298	Organic clay
M10_5.30	2465 ± 27	2525 ± 94	Wood fragment
M4_8.15	3610 ± 24	3850–3978	Wood fragment
M4_3.80	1642 ± 26	1507–1613	Soil
M6_10.75	4915 ± 35	4990–5318	Mollusc shells
M6_8.70	4708 ± 47	4770–5133	Mollusc shells
M6_6.04	3395 ± 25	3576–3696	Organic clay
M7_11.40	2843 ± 23	2870–3005	Wood fragment
M7_8.77	2773 ± 23	2792–2929	Wood fragment
M7_7.10	2559 ± 28	2697–2752	Wood fragment
M5_8.76	3842 ± 24	4153–4300	Organic clay
M3_5.75	3496 ± 27	3694–3840	Wood fragments

of swamp clays, 1 to 3 m-thick, dated around 5000–4000 cal yr BP (Eneolithic age; Tables 1, 3). Up to 2 m-thick subdelta and distributary channel sand bodies, with top at ~6 mbsl, locally interrupt the lateral continuity of the swamp layers (cores S1_T, S1_6P and M19 in Fig. 3C–D). However, isolated to locally amalgamated channel bodies up to 5–4 m-thick and with top-of sand at ~5 mbsl locally truncate the underlying swamp and lagoon succession down to 10 mbsl (Fig. 3A–D). These channel sands grade upwards into poorly-drained floodplain clays or levee/crevasse sandy deposits (Fig. 3A–D). Facies architecture integrated with the available radiocarbon ages constrains the timing of fluvial incision to the Eneolithic–Bronze age transition (around 4000–3800 cal yr BP in Table 1). Upwards, poorly-drained floodplain clays, up to 4 m-thick, show vertical and lateral transition to crevasse splay/levee and fluvial channel sands, whose upper boundaries mainly cluster around 4 m and 1 mbsl (Fig. 3A–D). Channel deposits with top-of-sand at ~4 mbsl form remarkably thick (up to 5–6 m) sand bodies, which further erode the floodplain–swamp–lagoon succession down to 10 mbsl. Radiocarbon and archeological data constrain the activity of these channels to the Bronze–Iron transition (around 2900–2800 cal yr BP in Table 1).

In contrast, the channel bodies clustering at shallower depths (top-of-sand ~1 mbsl) are thinner (~2 m) and show lens-shaped geometries (core S5_SC in Fig. 3C). Upwards, around the present sea level, poorly-drained floodplain clays are overlain by well-drained floodplain silty clays dating back to the early Roman period (Fig. 3A–D and Table 1). Crevasse splay/levee deposits and isolated fluvial-channel bodies, with top-of sand around or above the present sea level, are mainly recorded beneath the modern Arno River course (Fig. 3A, C–D). A different stacking pattern of fine-grained lithofacies characterizes the historical Pisa city center, north of the modern Arno River course, where laterally

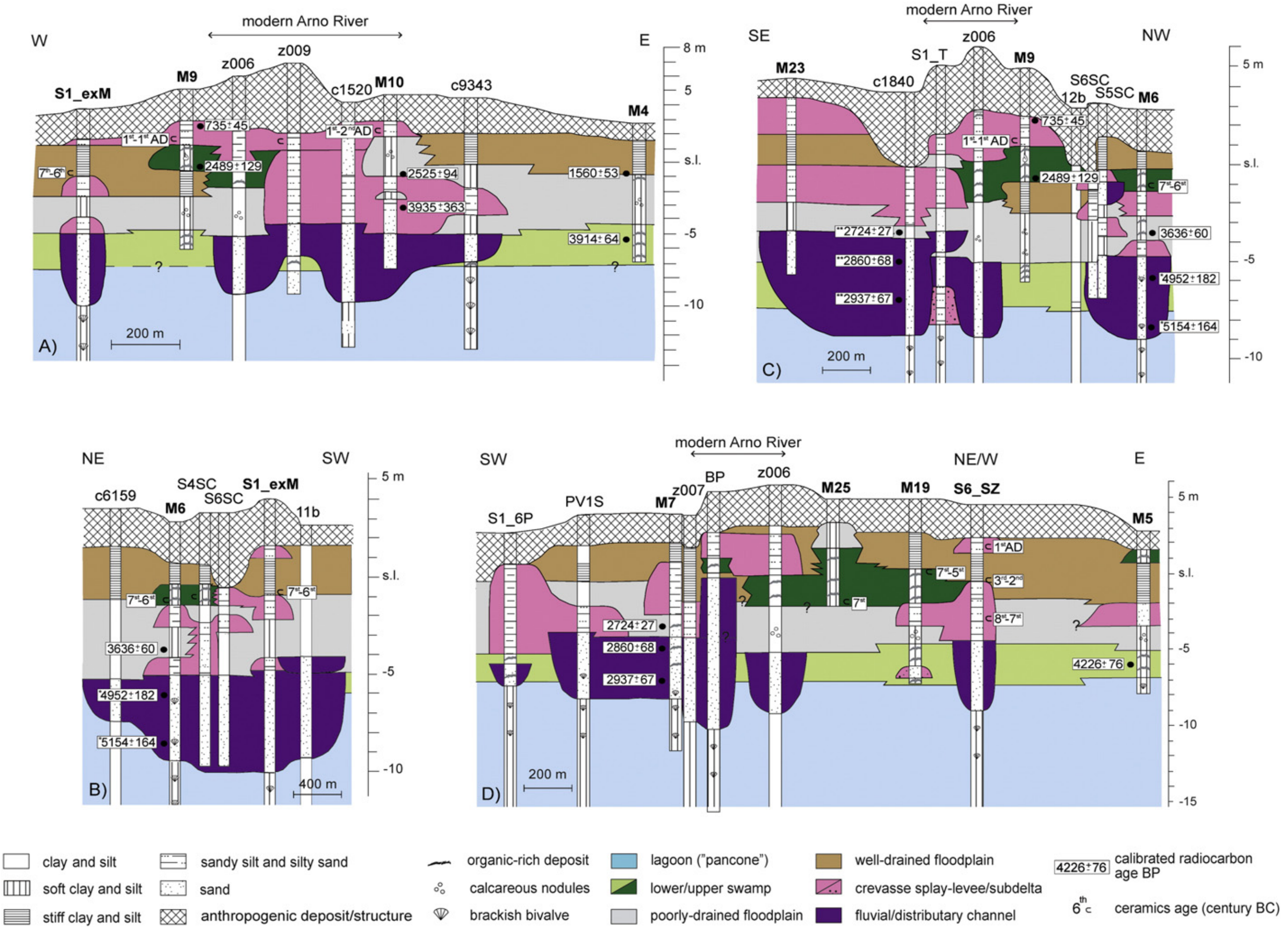

Fig. 3. Representative cross-sections depicting the mid–late Holocene lithofacies distribution and stratigraphic architecture of the deltaic–alluvial prograding wedge buried beneath the study area (section traces reported in Fig. 2). Reference MAPPA cores are in bold. Radiocarbon data are reported as calibrated yr BP (see Table 3), while the archeological data from Amorosi et al. (2013a) are reported in century BC/AD. Ages from reworked *Cardium* shells (asterisks) refer to lagoon environments pre-dating channel activity. Double asterisks indicate radiocarbon ages projected from core M7 (see Fig. 1 for location).

extensive clay deposits formed in ephemeral and shallow backswamps occur around 2 mbsl (Fig. 3A–D). Radiocarbon ages and several ceramic materials constrain the development of these low-lying wetlands to the late Iron–early Etruscan age (ca. 2500 cal yr BP/ca. 7th–5th century BC; Amorosi et al., 2013a). Anthropogenic structures, dated from the Roman period onwards, cut the alluvial succession at various stratigraphic levels.

3.2. Fluvial paleodrainage network

More than 10 distinct fluvial paleotraces were identified by remote sensing in the Pisa urban and suburban area (Fig. 4A), documenting the significant contribution of the fluvial network to the geomorphological evolution of the plain (Amorosi et al., 2013a).

Specifically, an east–west oriented paleochannel chronologically constrained to the Eneolithic–Bronze age transition (top-of-sand ~5 mbsl; Section 3.1. and Fig. 3A–D) was identified north of the modern Arno River (paleoArno; Fig. 4A). Consistent with Strabo's chronicles, a semi-coeval north–south oriented paleochannel flowing close to the west medieval city wall is referred to the *Auser* branch (paleoSerchio), which merged into the paleoArno close to the Arsenali area (Figs. 1 and 4A; Amorosi et al., 2013a). A further paleoachannel, active during the Eneolithic–Bronze age transition was identified in the eastern portion of the Pisa Plain with east–west flowing direction. On the basis of its position and orientation (see Figs. 1 and 4A), this paleochannel is interpreted as the *Auser* branch that flowed from the Pisa Mountains to the city area, running along the north medieval city wall before splitting into two or more branches as mentioned by the Greek geographer Strabo (chronicles, V, 2, 5, C 222). Neither stratigraphic nor morphological data allow to recognize the westward prolongation of this paleochannel, which was likely connected with the north–south *Auser* branch in the Arsenali area.

Concerning the drainage network active at the Bronze–Iron transition and related to the second phase of rapid channel incision and fill (top-of-sand ~4 mbsl; Fig. 3C–D), two paleotraces were identified immediately south of the modern Arno River (Fig. 4A). These traces document the abrupt southward shift of the paleoArno and two rapid phases of meander migration (Figs. 3C, D and 4A). In contrast, no paleotraces potentially pertaining to the *Auser* River course were identified (Fig. 4).

The ERT profile carried out along the north–south oriented *Auser* River paleotrace (Figs. 2 and 4A, B) reinforces our paleogeomorphological interpretation and traces out the geometry of the paleochannels involved in the first phase of rapid channel incision and fill.

Three sub-elliptical areas with high resistivity (300–1000 Ω m) are the most striking feature observed at 7–8 m depth (4–5 m ca. bsl) across the whole ERT section (4–5 m ca. asl, Fig. 4B). These areas show sharp contacts with the overlying low-resistivity layer and a progressive decrease in resistivity down to the lower limit of investigation (c.a. 14–15 m depth). Core S1_exM drilled nearby enabled lithofacies calibration of the electrical resistivity data (Fig. 4C). The rapid increase in resistivity at 7–8 m is coherent with the boundary between floodplain clays and the underlying thick succession of fluvial–channel sands. The contouring of these high-resistivity sands shows a sub-elliptical shape that can be related to a fluvial channel cross-section. Close to the lower limit of ERT resolution (c.a.12 m depth), the decrease of resistivity fits with the sharp transition to clayey lagoon sediments. In this respect, electrical resistivity data support the hypothesis that fluvial channels were carved into more conductive, fine-grained sediments.

4. Mid–late Holocene pollen record

Samples from core M5 contain a rich, autochthonous palynological association mainly composed of pollen grains and spores. Other palynomorphs (algae, dinoflagellates, scolecodonts and foraminiferal

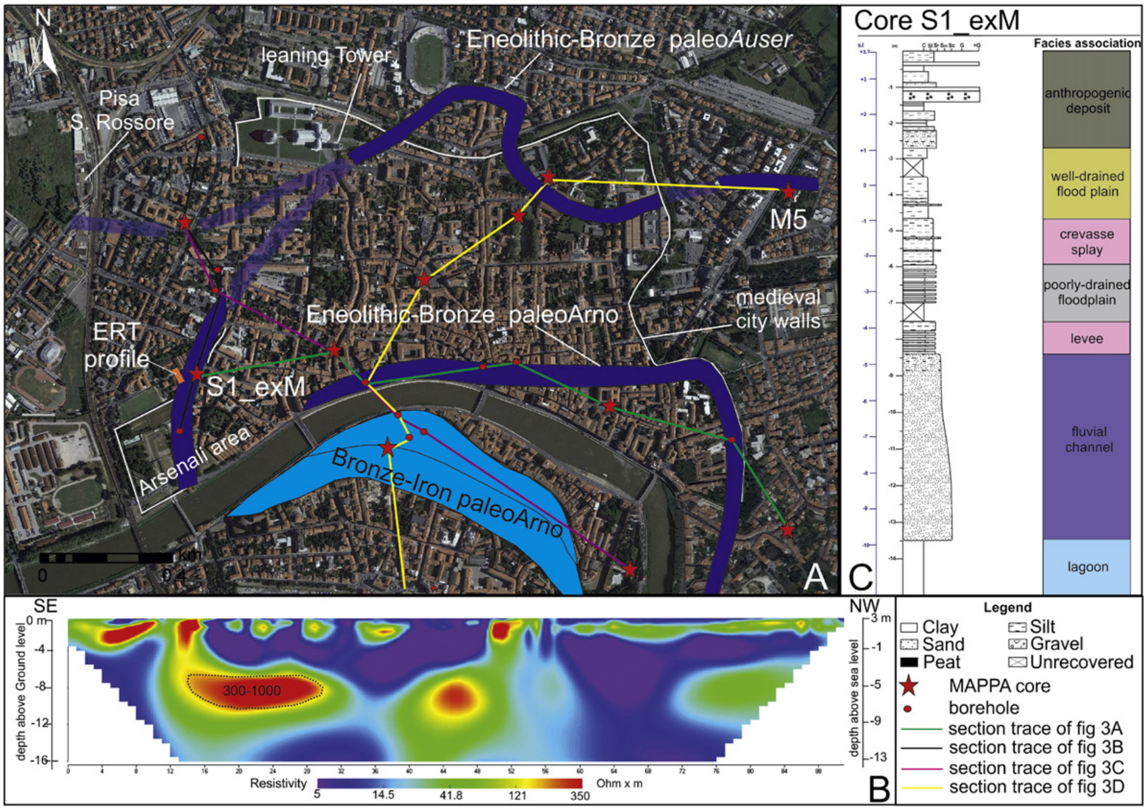

Fig. 4. A) Paleodrainage evolution of the Pisa Plain in proto-historic times (see Fig. 3A–D), reconstructed on the basis of integrated stratigraphic-remote sensing analyses. B) ERT profile and C) Core S1_exM stratigraphy are also shown.

linings) are recorded within lagoonal sediments in the lowermost part of the core. The state of preservation is generally good, with 3% indeterminable or unknown grains, while pollen concentration strongly fluctuates throughout the cored succession. Pollen concentration from lagoon sediments and the lowermost swamp succession varies from 13,434 to 16,126 grains/g. Within the overlying swamp clays, between 8.76 m and 8.60 m core–depth, the concentration abruptly drops to 4475 grains/g, and then further gradually decreases upwards. In contrast, pre-Quaternary palynomorphs generally exhibit an upward increasing trend in relative percentages with respect to the total autochthonous *plus* allochthonous assemblage.

Despite the overall dominance of arboreal pollen (AP), which is distinctive feature of the Holocene successions across the Mediterranean area (Bellini et al., 2009; Di Rita and Magri, 2012), high-frequency abundance changes of specific pollen groups (see Section 2.3) allow the distinction of four main pollen zones (1–4), corresponding to distinct vegetation phases (Fig. 5). These zones are described and interpreted in terms of past climatic conditions and environmental features, as follows (Fig. 5).

4.1. Zone 1: 10.50–9.60 m

4.1.1. Description

This zone is characterized by an autochthonous pollen association mainly composed of riparians (17–32%), almost entirely represented by *Alnus*, and deciduous/evergreen trees, such as *Quercus* and *Corylus* (~5–15% and 6–9.5%, respectively). Both groups show decreasing upward trends. Mountain and Mediterranean trees are also present with remarkable percentages (6–8% and 4–10.5%, respectively — Fig. 5).

The herbaceous taxa (NAP) are mainly represented by ubiquitous (up to ~31% at the top of the zone) and aquatic (~2–6%) plants.

Among non-pollen palynomorphs, pteridophyte spores are the most abundant (~10–12.5%), while marine-related elements (dinocysts, foraminiferal linings and scolecodonts) show low percentages. Reworked pre-Quaternary palynomorphs (pollen grains and dynocysts) are very scarce throughout this zone, peaking at ~4% close to its upper boundary (Fig. 5). The most common components of this group are species of *Corollina* genus, an extinct pollen taxon commonly found within lower Mesozoic sequences in both hemispheres (Traverse, 1988).

4.1.2. Interpretation

The high pollen concentration values and the scarce occurrence of reworked pre-Quaternary palynomorphs fit well with the development, in the Pisa Plain, of a wide lagoonal basin during the Neolithic age (Figs. 3 and 4), as recently documented by Amorosi et al. (2013a). The high abundance of *Alnus* and pteridophytes as well as the occurrence of marine-related palynomorphs are also consistent with this paleoenvironmental interpretation. Moreover, the presence of reworked *Corollina* specimens suggests sediment supplied by non-metamorphic Mesozoic sedimentary sequences cropping out north of Pisa.

The occurrence of mixed deciduous/evergreen oak forests, similar to those characterizing the west coasts of Italy between ca. 8000 and 5000 cal yr BP (Amorosi et al., 2009; Ribecai, 2011; Di Rita and Magri, 2012) indicates optimal warm and humid climate conditions.

4.2. Zone 2: 9.60–8.10 m

4.2.1. Description

This zone is characterized by a significant drop in pollen concentration (from 16,126 to 4475 grains/g), paralleled by the upward decrease of the AP/NAP ratio (~1) close to the upper boundary. The main character of the pollen association is the strong increase of riparians, mainly represented by *Alnus*, which peaks (~50%) close to the lower boundary of the zone and progressively decreases upwards (Fig. 5). Deciduous woody taxa (dominant *Ulmus* and subordinate *Quercus* and *Corylus*) are still present with considerable percentages (8–17%; Fig. 5). Mountain and Mediterranean trees invariably exhibit values lower than 5%.

Among the herbs, Poaceae display the highest percentages of the whole core (up to 25%; Fig. 5). The aquatic plants are abundant across the entire zone, with a distinct peak (~30.5%) close to its upper boundary, where pteridophytes also show very high percentages (~20%; Fig. 5).

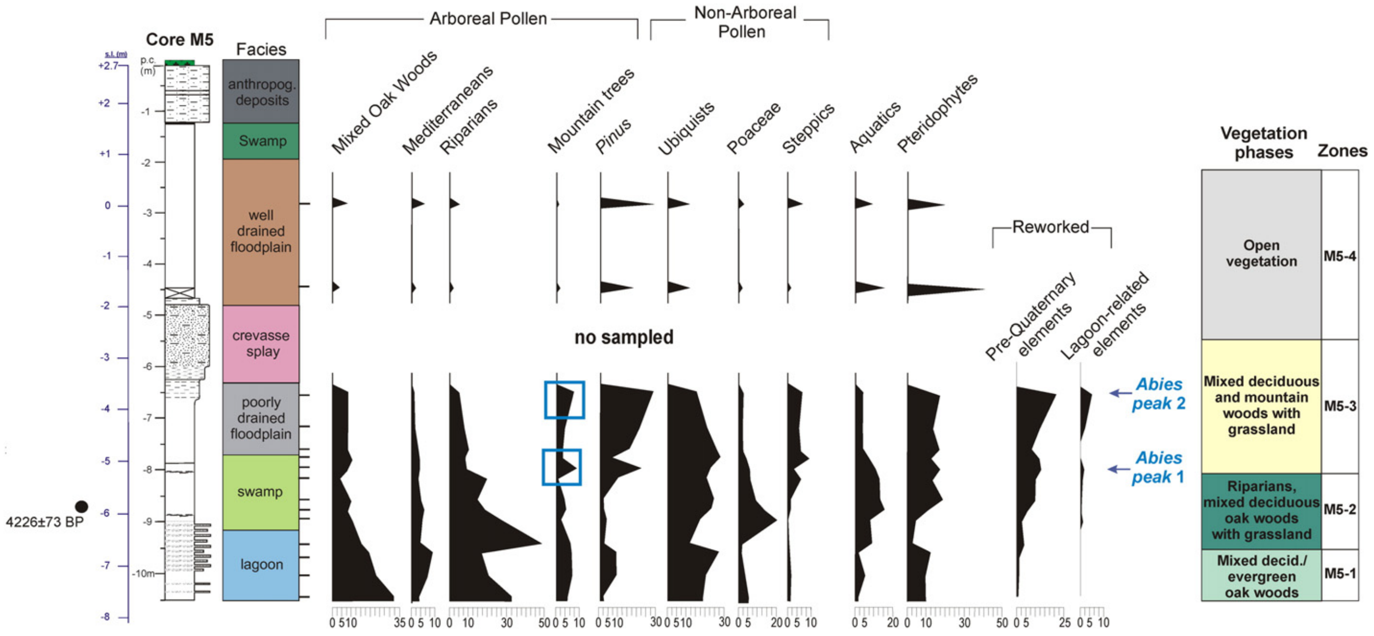

Fig. 5. Mid–late Holocene pollen record of core M5 (see Figs. 1 and 2 for location), with indication of the main vegetation phases/pollen zone (see Section 5 for more detailed information). The sandy interval (crevasse splay) is not sampled. Pollen taxa are grouped following Amorosi et al. (2009). Pollen concentration, AP/NAP ratio, pre-Quaternary and marine-related palynomorph percentages are also reported. Within zone M5-3, the *Abies* peaks 1 and 2 discussed in text are highlighted. Radiocarbon ages are reported as cal yr BP (see Table 3). For the lithological key of core M5 see Fig. 4. Lithofacies interpretation of core M5 is from Amorosi et al. (2013a); see Table 2 for more detailed facies information.

Reworked pre-Quaternary palynomorphs, mainly represented by *Corollina* spp., slightly increase in concentration relative to the underlying zone 1, with 10% relative abundance at the upper boundary (Fig. 5).

4.2.2. Interpretation

The rapid expansion of *Alnus*, a hygrophilous tree taxa requiring moist soils habitat (Di Rita and Magri, 2012) is consistent with the replacement of the lagoon by a vast wetland area around the Pisa city center at the transition to the Eneolithic age (around 5000 cal yr BP; Figs. 4 and 5; Amorosi et al., 2013a). The high percentages of both aquatic plants and pteridophytes in the uppermost portion of the pollen zone also testify to the progressive filling of the lagoon and to the establishment of distinct paludal conditions. Similarly, an upward increasing trend is shown by the reworked pre-Quaternary palynomorphs, reflecting the progressive influence of the drainage network at the core site area.

As a whole, the pollen association indicates the development of a marshland at the beginning of the Eneolithic age, rapidly followed by mixed woodlands and *Alnus* carrs, in accordance with other pollen records from the west coast of Italy (Di Rita and Magri, 2012). Interestingly, in the upper portion of the zone our data clearly indicate the partial replacement of deciduous-*Alnus* forests by grasslands, mainly composed of Poaceae, aquatics and ferns (pteridophytes), and a strong decrease of mountain trees (Fig. 5). These vegetation changes and the concomitant drop of both AP/NAP ratio and pollen concentration point to a phase of forest reduction around 4200–4000 cal yr BP (radiocarbon ages in Fig. 5), reasonably related to a short-term climatic perturbation towards drier conditions. A comparable and semi-coeval event of forest decline (ranging between 4500 and 3900 cal yr BP in Europe) has been recently reported from several coastal sites of central-southern Italy (Drescher-Schneider et al., 2007; Magri, 2007; Di Rita et al., 2010; Sadori et al., 2011; Di Rita and Magri, 2012) and related to the temporary latitudinal displacement of the inter-tropical convergence zone. This deterioration of climate conditions appears to be contemporary with a well-known, global climate event centered around 4200 cal yr BP, the so-called 4.2 ka event or event 3 of Bond et al. (1997, 2001), widely recorded by several proxies across the Mediterranean area (Magny et al., 2002, 2009; Mayewski et al., 2004; Piva et al., 2008; Bar-Matthews and Ayalon, 2011; Giraudi et al., 2011; Zanchetta et al., 2013).

These paleoclimatic records offer a complex picture of the 4.2 ka event with latitudinal and longitudinal contrasting humidity conditions (Magny et al., 2012a,b), probably due to the combined effect of cyclonic activity and seasonal, local patterns, and suggest for the central Mediterranean area a close succession of events (wet/dry/wet) between 4300 and 3800 cal yr BP (Magny et al., 2009; Zanchetta et al., 2013).

4.3. Zone 3: 8.10–6.50 m

4.3.1. Description

This zone is characterized by an abrupt decrease of the riparian trees (<10%) and aquatic plants. This trend is paralleled by a strong increase in *Pinus* (up to ~27.5%), which becomes the dominant arboreal taxon, and herbs, mainly represented by ubiquist and steppic taxa (Fig. 5). Mixed oak woods (*Quercus*, *Corylus*, *Ulmus* and *Tilia*) occur as secondary taxa with remarkable percentages (7–10%), while the Mediterranean and mountain trees are generally present at very low values (<4%; Fig. 5). Two anomalous samples close to the zone boundaries (~8 m and ~6.50 m core depth) show an increase of mountain trees (up to 10%), almost exclusively represented by *Abies* grains (*Abies* peaks 1 and 2 in Fig. 5). Reworked palynomorphs, derived from pre-Quaternary outcropping formations (*Corollina* spp., *Rhetipollis germanicus* and various Jurassic–Cretaceous dinoflagellates and spores) also peak within the same stratigraphic intervals, reaching the highest percentages of the whole cored succession (Fig. 5). Consistently, peaks of reworked dinocysts, foraminiferal linings and scolecodonts derived from the underlying lagoonal deposits cap the zone (~5%; Fig. 5).

4.3.2. Interpretation

The high amounts of *Pinus* grains, strongly resistant to mechanical stress, and the increasing abundance of the herbaceous taxa (Fig. 5) reflect the establishment of a genuine alluvial landscape (Amorosi et al., 2013a) with sparsely wooded grasslands during the Bronze–Iron ages (Figs. 3 and 5). On shorter timescales, two peaks of reworked palynomorphs (both pre-Quaternary and lagoon-derived) are recorded close to the lower and upper boundaries of this zone, recording rapid, high-energy flood events (Fig. 5). In the same stratigraphic intervals, two peaks of *Abies* (*Abies* peaks 1 and 2 in Fig. 5) reveal short-lived phases of increasing moistness. Indeed, *Abies* grows and spreads under high-humidity conditions only (Tinner and Lotter, 2006; Mariotti Lippi et al., 2007; Ricci Lucchi, 2008), and is currently found as scattered communities in the Tuscan Apennines at elevations higher than 1000 m.

To date, no comparable proto-historic events of *Abies* expansion have been recorded from other Italian coastal sites, possibly due to a combined effect of local climate and high human pressure (Tinner et al., 2013; Di Pasquale et al., 2014). Unique exception is the pollen record recovered from the near archeological site of Pisa S. Rossore (Fig. 1B), where remarkable percentages of drought-sensitive mountain trees (*Fagus* and *Abies*) have been encountered within the pre-Roman unit that overlies the Neolithic lagoon clays (Mariotti Lippi et al., 2007). Unfortunately, the available radiocarbon ages do not furnish a more precise chronological framework for this unit.

Nevertheless, our observations are in general agreement with the multi-proxy evidence of millennial to centennial-scale climate variability across the Mediterranean region during proto-historic times (Mayewski et al., 2004; Piva et al., 2008; Nieto-Moreno et al., 2011; Drake, 2012).

4.4. Zone 4: 4.5–2 m

4.4.1. Description

Similar to the upper part of the underlying zone M5-3, this zone exhibits low concentration values (from 840 to 1160 grains/g), and an autochthonous association dominated by *Pinus* and herbaceous taxa (Fig. 5).

4.4.2. Interpretation

With respect to the underlying zone 3, this pollen association indicates the development of a more open vegetation (grassland), with few oaks and Mediterranean trees. A similar vegetation cover has been widely reported from the west coasts of Italy during the last 2000 years (Di Rita and Magri, 2012).

5. Highstand sedimentation patterns, fluvial dynamics and vegetation landscapes

The mid–late Holocene stratigraphic architecture, combined with the network of paleochannels identified through remote sensing, geomorphological and geophysical analyses, documents a multifaceted depositional history of the Pisa Plain. Based on a multi-proxy record, changes in sedimentation patterns and paleodrainage system are framed in the local environmental–climate conditions deduced from the pollen record of core M5 (Fig. 5 and Section 5).

5.1. Pre-alluvial phase (Eneolithic age: ca. 5000–4000 cal yr BP)

If compared with the decelerating sea-level trend starting at ca. 7000 cal yr BP along the Italian coasts under highstand conditions (Lambeck et al., 2004, 2011), siltation of the wide lagoon basin originally developed in the Pisa area during the maximum marine transgression took place ca. 2000 years later (Fig. 3A–D). Around 5000 cal yr BP, at the beginning of the Eneolithic age (Fig. 3A–D and Table 1), the lagoon evolved into a vast marshland, crossed by distributary channels attributable to both Arno and Serchio rivers (Amorosi et al., 2013a). This phase was concomitant with a major change in vegetation cover (transition from pollen zones 1 to 2; Fig. 5). The replacement of mixed deciduous/evergreen oak forests by mixed woodlands and *Alnus* carrs with grasslands reflects the end of the Holocene climatic optimum (Fletcher and Sánchez Goñi, 2008; Combourieu Nebout et al., 2009) and the establishment of less humid conditions (Fig. 5). This long-term trend of increasing aridity/forest regression, extensively recorded across the West Mediterranean after 5000 cal yr BP (Jalut et al., 2000; Magny et al., 2002), reasonably promoted high sediment delivery, which, in turn, favored lagoon infilling and delta development.

The relationship between climatic aridification and coastal progradation appears to climax at the transition from deltaic to alluvial sedimentation. Indeed, alluvial plain development was preceded by a short-lived phase of pronounced forest reduction (AP/NAP ratio) and decline of drought-sensitive mountain trees, probably reflecting the arid episode of the well-known 4.2 ka event (Fig. 5).

5.2. Alluvial phase (Bronze age–Present: ca. last 4000 cal yr BP)

5.2.1. Bronze–Iron age (ca. 4000–2500 cal yr BP)

Following the characteristic mid–late Holocene progradation trend, shared by all major Mediterranean delta systems (Somoza et al., 1998; Bellotti et al., 2004; Aguzzi et al., 2005; Vella et al., 2005; Amorosi et al., 2008, 2013b; Milli et al., 2013), the marshlands emerged and abruptly turned into floodplain areas at the transition with the Bronze age, around 3800 cal yr BP (Fig. 3A–D). The establishment of an alluvial plain subject to recurring flooding events is testified by poorly-drained floodplain conditions and by the widespread occurrence of thick, coarse-grained overbank successions (Fig. 3A–D). These depositional features along with the rapidly changing drainage configuration (Fig. 4A) point to a Bronze–Iron phase of intense fluvial activity, high runoff rates and floodplain sedimentation, reasonably promoted by a dense channel network (Fig. 4A) and the progressive reduction of forests (sparsely wooded grasslands of pollen zone 3; Fig. 5). A semi-coeval phase of alluvial plain overflow has been inferred by Marra et al. (2013) for the Tiber Plain during the last 3500 cal yr BP. Consistent with our paleohydrographic reconstructions (Fig. 4A), Benvenuti et al. (2006) documented at the nearby Pisa San Rossore archeological site (Fig. 1) a pre-Roman channel-fill, truncated by Roman fluvial sands, and a genetically-related overbank succession, whose upper portion is dated to the Iron age.

However, two events of rapid channel incision and fill abruptly interrupted this phase of intense alluvial aggradation, as clearly documented by stratigraphic and ERT data (Figs. 3, 4C). The sudden occurrence of high-energy, erosional phases is also recorded by the two concomitant peaks in reworked pollen grains and lagoon-derived marine palynomorphs from the floodplain succession of core M5 (Fig. 5).

Across the study area, the first erosive phase produced a 4–5 m-deep incision within the underlying lagoon–paludal succession (Figs. 3B, 4C). Subsurface stratigraphy and the available radiocarbon ages constrain chronologically this event to the Eneolithic–Bronze transition, between ca. 3800 and 3600 cal yr BP, i.e. shortly after alluvial plain development (Fig. 3).

The timing of the second incision-fill event is more accurately constrained by a series of radiocarbon ages available from the fluvial–channel succession recovered at core M7 (Fig. 3D). Fluvial incision occurred at the Bronze–Iron transition, cutting the underlying lagoon–paludal–floodplain clays down to ~5–6 m (Fig. 3C, D). In less than 200 years the river channel was filled (Fig. 3D), and alluvial aggradation persisted up to the beginning of the Etruscan age (ca. 2500 cal yr BP). In conjunction with this high-energy fluvial event, the paleoArno River abruptly changed its position and for the first time shifted south of its modern course (Fig. 4A).

Interestingly, two short-lived (centennial-scale) climatic events of increased humidity are recorded within the Bronze–Iron floodplain succession of core M5 (*Abies* peaks 1 and 2; Fig. 5), at stratigraphic intervals correlative with the top-of-channel bodies formed during the rapid incision-fill phases (see Figs. 3D and 5).

The integration of stratigraphic, geomorphological, geophysical and palynological data documents good synchronicity of highstand sedimentation patterns, fluvial dynamics (aggradation/degradation ratio) and local climate changes, on a variety of time scales. In contrast, no direct (archeological) or indirect (palynological) evidence of strong human frequentation and impact on the Pisa Plain landscape has been recovered for the Bronze–Iron period, to date (Ribecai, 2011; Di Rita and Magri, 2012; Amorosi et al., 2013a).

5.2.2. Etruscan age to Present (ca. 2500 cal yr BP–Present)

The beginning of the Etruscan age was characterized by the development of a complex alluvial setting under uninterrupted aggradational conditions. Low-lying backswamps, which became progressively inhabited, were formed north of the modern Arno River, between the proto-historic fluvial–channel systems (Amorosi et al., 2013a; Figs. 3, 4).

The transition to the Roman age (ca. 2000 cal yr BP) marked the early stage of the development of the modern Pisa Plain. This phase was characterized by the extensive growth of a well-drained alluvial plain, with widespread development of indurate horizons and grasslands (Figs. 3, 5). The natural tendency of both paleoArno and paleoSerchio branches to change their courses was radically reduced by numerous waterworks (Martini et al., 2011), and wetland areas were partially reclaimed (Sarti et al., 2010). Since the Middle Ages onwards (ca. 1300–1400 cal yr BP; Table 1), an anthropogenic stratification occurred, revealing the progressive urbanization of the study area.

6. Discussion

The two events of channel incision and infill detected beneath the Pisa Plain at the transition between the Eneolithic–Bronze ages and the Bronze–Iron ages (~3800 cal yr BP and 2900–2800 cal yr BP; Figs. 3, 5) indicate the occurrence of high-frequency (centennial-scale), prominent changes in the aggradation/degradation ratio during the mid–late Holocene sea-level highstand.

In particular, increased fluvial activity:

a) could be related to rapid (centennial-scale) climatic changes towards more humid conditions;
b) could be the result of small amplitude relative sea-level changes (i.e. base-level changes);
c) could represent the effect of human impact.

6.1. Climate

As widely documented in the literature (Ashley and Hamilton, 1993; Blum and Törnqvist, 2000; Lewis et al., 2001; Macklin et al., 2002; Straffin and Blum, 2002; Vandenberghe, 2003; Döll and Schmied, 2012), climate fluctuations at regional/sub-regional or global scale can induce significant changes in both discharge regime and sediment production and delivery to downstream locations. In the Pisa Plain, two (centennial-scale) climatic events of increased humidity occurred during the Eneolithic–Iron age, interrupting the long-term mid–late Holocene aridification trend (*Abies* peaks 1 and 2; Fig. 5). Radiocarbon and archeological dates (Fig. 3) allow to assign the two peaks of *Abies* to the Eneolithic–Bronze and Bronze–Iron transitions, around ~3800 cal yr BP and 2900–2800 cal yr BP, respectively (Fig. 5).

Within comparable time windows (Table 4), a number of multiproxy Mediterranean records provide evidence for two centennial-scale climatic events with similar characteristics (Nieto-Moreno et al., 2011; Roberts et al., 2011; Magny et al., 2012a,b; Fletcher and Zielhofer, 2013; Benito et al., 2015). The older one falls within the chronological interval of the well-known 4.2 ka event (Bond et al., 1997; Mayewski et al., 2004; Finné et al., 2011), which apparently shows a tripartite humidity oscillation between ~4300 and 3800 cal yr BP in the central-western Mediterranean area (Magny et al., 2009). In this regard, the first *Abies* peak recorded in core M5 might correspond to the wet phase closing the 4.2 ka event (Fig. 5).

Similarly, the youngest *Abies* peak recognized in core M5 (Fig. 5) resembles the new increase in humidity condition documented around 2800 cal yr BP from the western Mediterranean (Biserni and van Geel, 2005; Magny et al., 2007; Giraudi et al., 2011) and from west-central Europe (Magny, 2004) by high lake levels and pollen data.

As a whole, our data suggests i) the regional or supra-regional character of the two humidity peaks documented in this paper and ii) the close relationships between high-frequency climatic fluctuations and stratigraphic architecture, as shown by the strict correspondence between pollen signature and phases of fluvial erosion paralleled by an increase in reworked palynomorphs.

These data point towards the role played by climate fluctuations in triggering channel incision.

6.2. Relative sea-level changes

Relative sea-level (RSL) changes result from the interaction between global (eustatism) and local factors (i.e. hydrostasia, tectonic and sediment compaction), and produce a re-adjustment of the river longitudinal profile to the new base-level position. Specifically, fluvial incision can be triggered by RSL fall, although a direct, simple cause–effect relationship cannot be stated a priori (Schumm, 1993; Legarreta and Uliana, 1998).

Since the pioneering work of Pirazzoli (1976), the Holocene RSL history of the central Mediterranean basin has been investigated using different types of markers. The two most recent and reliable models (Spada and Stocchi, 2007; Lambeck et al., 2011) have been worked out cross-checking predictions with field data. Nevertheless, the two models misfit. Although the amount of available index points concerning the Holocene sea level in this area is remarkable and constantly increasing, there is still a certain amount of uncertainty on sea-level elevation even during the late Holocene (Morhange et al., 2001, 2006, 2013; Antonioli et al., 2007, 2009; Furlani et al., 2011; Primavera et al., 2011; Spampinato et al., 2011; Bini et al., 2012; Evelpidou et al., 2012; Amato et al., 2013).

Small-amplitude sea-level lowering along the Tyrrhenian coastline during the late Holocene has been hypothesized by Benvenuti et al. (2006) and Marra et al. (2013). However, clear evidence of proto-historic eustatic fall episodes has not been reported, to date. In contrast, all most detailed RSL predicted curves (Lambeck et al., 2004, 2011; Spada and Stocchi, 2007) match on a progressive rising trend since about 6000 cal yr BP. Moreover, the extensional tectonic context of the Pisa Plain, placed within the subsiding Viareggio Basin (Mariani and Prato, 1988; Argnani et al., 1997; Pascucci, 2005) and land subsidence induced by high compressible fine-grained deposits compaction (Rossi et al., 2011; Sarti et al., 2012) have enhanced this RSL rising trendthrough the addition of new accommodation space (Posamentier et al., 1988; Catuneanu, 2006; Hu and Plint, 2009).

Based on these data, there is currently no evidence of a link between RSL and the triggering of the two erosive processes. Conversely, the peculiar geotechnical features (high compressibility and plasticity) of the lagoon clays beneath the city of Pisa (Ministero dei Lavori Pubblici, 1971; Callisto and Calbresi, 1998; Sarti et al., 2012) could have enhanced to some degree the rate and the value of channel incisions, as documented by experimental data achieved in the Venice lagoon deposits (Amos et al., 2010).

6.3. Human impact

An intensive human frequentation of the Pisa Plain area started off during the Iron–Etruscan transition (around 2500 cal yr BP), about three centuries later than the most recent proto-historic channel incision (Benvenuti et al., 2006; Mariotti Lippi et al., 2007; Bellini et al., 2009; Ribecai, 2011; Di Rita and Magri, 2012; Amorosi et al., 2013a). Only sporadic human settlements dated to the proto-historic period are documented on the surrounding highlands (Bagnone, 1982; Pasquinucci, 1994; Grifoni Cremonesi, 2006). In this respect, changes in land use patterns or any other type of human influence appear to be unrelated to the onset and/or amplification of the two events of fluvial incision.

7. Conclusions

A multi-proxy study of the mid–late Holocene deltaic–alluvial succession in the Pisa Plain reveals short-term fluvial evolution and changes in sedimentation patterns under relative sea-level highstand conditions (last ~7000 cal yr BP). The integration of high-resolution stratigraphic and paleohydrographic reconstructions with pollen data provides valued information about the relationships between fluvial dynamics and local paleoenvironmental–paleoclimate conditions.

The major outcomes of this study can be summarized as follows:

(i) deltaic progradation took place with a long-term mid–late Holocene aridification. The transition to a genuine alluvial plain was immediately predated by a short-lived phase of pronounced forest reduction around 4200 cal yr BP;

(ii) stratigraphic and paleohydrographic features reveal a Bronze–Iron age phase of high fluvial activity, increased runoff and floodplain sedimentation promoted by a dense channel network, involving Arno and *Auser* river courses, in an open vegetation landscape (sparsely wooded grasslands);

(iii) the proto-historic phase of intense alluvial aggradation was punctuated by two rapid events of enhanced fluvial incision that cut down to 10 m the underlying lagoonal substrate. Radiocarbon and archeological data constrain these events to the Eneolithic–Bronze age and Bronze–Iron age transitions (~3800 cal yr BP and 2900–2800 cal yr BP, respectively);

Table 4

Bronze–Iron age centennial flooding events in the Mediterranean regions based on ^{14}C-dated Holocene fluvial deposits (modified after Benito et al., 2014).

Central Italy (this study)	Southern Italy (cal yr BP)	E-Iberian Peninsula (cal yr BP)	Southern France (cal yr BP)	Tunisia (cal yr BP)	Eastern Mediterranean (cal yr BP)
≈3800	4200–4100				
				4100–3700	4100–3700
	3450–3000				
≈2900–2800			3000–2750	3300–3000	3400–3200
		2850–2700		2850–2350	
	2350–1850	2450–2150	2300–1750		

(iii) the correlation between these events and two phases of increased humidity (*Abies* peaks 1 and 2) suggests that climate played a role in triggering channels incision;
(iv) relative sea-level changes did not played a significant role in the activation of fluvial incision, while the substrate nature (highly compressible lagoon clays) may have fostered the deepening of the channels;
(vi) mid–late Holocene (HST) coastal plain deposits formed in subsiding basin settings are excellent archive to elaborate high-resolution depositional models, and may represent reliable past analogues on which to infer the potential response of modern environments to future climatic variations.

Acknowledgments

We thank the archeological staff of the MAPPA project for its support and suggestions. We are also grateful to Prof. Thierry Corrège and the reviewers for their useful comments.

References

Aguzzi, M., Amorosi, A., Sarti, G., 2005. Stratigraphic architecture of Late Quaternary deposits in the lower Arno Plain (Tuscany, Italy). Geol. Romana 38, 1–10.

Aguzzi, M., Amorosi, A., Colalongo, M.L., Ricci Lucchi, M., Rossi, V., Sarti, G., Vaiani, S.C., 2007. Late Quaternary climatic evolution of the Arno coastal plain (Western Tuscany, Italy) from subsurface data. Sediment. Geol. 202, 211–229.

Alley, R.B., Marotzke, J., Nordhaus, W.D., Overpeck, J.T., Peteet, D.M., Pielke, R.A., Wallace, J.M., 2003. Abrupt climate change. Science 299 (5615), 2005–2010.

Amato, V., Aucelli, P.P.C., Ciampo, G., Cinque, A., Di Donato, V., Pappone, G., Petrosino, P., Romano, P., Rosskopf, C.M., Russo Ermolli, E., 2013. Relative sea level changes and paleogeographical evolution of the southern Sele plain (Italy) during the Holocene. Quat. Int. 288, 112–128.

Amorosi, A., Milli, S., 2001. Late Quaternary depositional architecture of Po and Tevere river deltas (Italy) and worldwide comparison with coeval deltaic successions. Sediment. Geol. 144 (3), 357–375.

Amorosi, A., Dinelli, E., Rossi, V., Vaiani, S.C., Sacchetto, M., 2008. Late Quaternary palaeoenvironmental evolution of the Adriatic coastal plain and the onset of Po River Delta. Palaeogeogr. Palaeoclimatol. Palaeoecol. 268 (1–2), 80–90.

Amorosi, A., Ricci Lucchi, M., Rossi, V., Sarti, G., 2009. Climate change signature of small-scale parasequences from Lateglacial–Holocene transgressive deposits of the Arno valley fill. Palaeogeogr. Palaeoclimatol. Palaeoecol. 273, 142–152.

Amorosi, A., Rossi, V., Sarti, G., Mattei, R., 2013a. Coalescent valley fills from the late Quaternary record of Tuscany (Italy). Quat. Int. 288, 129–138.

Amorosi, A., Bini, M., Giacomelli, S., Pappalardo, M., Ribecai, C., Rossi, V., Sammartino, I., Sarti, G., 2013b. Middle to late Holocene environmental evolution of the Pisa coastal plain (Tuscany, Italy) and early human settlements. Quat. Int. 303, 93–106.

Amos, C.L., Umgiesser, G., Ferrarin, C., Thompson, C.E.L., Whitehouse, R.J.S., Sutherland, T.F., Bergamasco, A., 2010. The erosion rates of cohesive sediments in Venice lagoon. Cont. Shelf Res. 30, 859,870.

Antonioli, F., Anzidei, M., Lambeck, K., Auriemma, R., Gaddi, D., Furlani, S., Orrù, P., Solinas, E., Gaspari, A., Karinja, S., Kovačić, V., Surace, L., 2007. Sea-level change during the Holocene in Sardinia and in the northeastern Adriatic (central Mediterranean Sea) from archaeological and geomorphological data. Quat. Sci. Rev. 26 (19–21), 2463–2486.

Antonioli, F., Ferranti, L., Fontana, A., Amorosi, A., Bondesan, A., Braitenberg, C., Dutton, A., Fontolan, G., Furlani, S., Lambeck, K., Mastronuzzi, G., Monaco, C., Spada, G., Stocchi, P., 2009. Holocene relative sea-level changes and vertical movements along the Italian and Istrian coastlines. Quat. Int. 206 (1–2), 102–133.

Argnani, A., Bernini, M., Di Dio, G.M., Papani, G., Rogledi, S., 1997. Stratigraphic record of crustal scale tectonics in the Quaternary of the Northern Apennines (Italy). Il Quaderno 10, 595–602.

Ashley, G.M., Hamilton, T.D., 1993. Fluvial response to late Quaternary climatic fluctuations, central Kobuk Valley, northwestern Alaska. J. Sediment. Res. 63 (5).

Bagnone, D., 1982. L'insediamento neolitico e dell'inizio dell'età dei metalli di Poggio di Mezzo (San Rossore, Pisa). Atti Soc. Toscana Sci. Nat. Resid. Pisa Mem. Ser. A 89, 61–82.

Bar-Matthews, M., Ayalon, A., 2011. Mid-Holocene climate variations revealed by high-resolution speleothem records from Soreq Cave, Israel and their correlation with cultural changes. The Holocene 21 (1), 163–171.

Bellini, C., Mariotti Lippi, M., Montanari, C., 2009. The Holocene landscape history of the NW Italian coasts. The Holocene 19 (8), 1161–1172.

Bellotti, P., Caputo, C., Davoli, L., Evangelista, S., Garzanti, E., Pugliese, F., Valeri, P., 2004. Morpho-sedimentary characteristics and Holocene evolution of the emergent part of the Ombrone River delta (southern Tuscany). Geomorphology 61 (1), 71–90.

Benito, G., Sopeña, A., Sánchez-Moya, Y., Machado, M.J., Pérez-González, A., 2003. Palaeoflood record of the Tagus River (Central Spain) during the Late Pleistocene and Holocene. Quat. Sci. Rev. 22 (15–17), 1737–1756.

Benito, G., Macklin, M.G., Zielhofer, C., Jones, A.F., Machado, M.J., 2014. Holocene flooding and climate change in the Mediterranean. Catena http://dx.doi.org/10.1016/j.catena.2014.11.014.

Benito, G., Macklin, M.G., Cohen, K.M., Herget, J., 2015. Past hydrological extreme events in a changing climate. Catena http://dx.doi.org/10.1016/j.catena.2014.12.001.

Benvenuti, M., Mariotti Lippi, M., Pallecchi, P., Sagri, M., 2006. Late-Holocene catastrophic floods in the terminal Arno River (Pisa, Central Italy) from the history of a Roman riverine harbor. The Holocene 16 (6), 863–876.

Bini, M., Brückner, H., Chelli, A., Pappalardo, M., Da Prato, S., Gervasini, L., 2012. Palaeogeographies of the Magra Valley coastal plain to constrain the location of the Roman harbour of Lunae (NW Italy). Palaeogeogr. Palaeoclimatol. Palaeoecol. 337, 37–51.

Biserni, G., Van Geel, B., 2005. Reconstruction of Holocene palaeoenvironment and sedimentation history of the Ombrone alluvial plain (South Tuscany, Italy). Rev. Palaeobot. Palynol. 136 (1), 16–28.

Bisson, M., Bini, M., 2012. A multidisciplinary approach to reveal palaeohydrographic features: the case study of Luna archaeological site surroundings. Int. J. Geogr. Inf. Sci. 26, 327–343.

Blum, M.D., Törnqvist, T.E., 2000. Fluvial responses to climate and sea-level change: a review and look forward. Sedimentology 47 (1), 2–48.

Bond, G., Showers, W., Cheseby, M., Lotti, R., Almasi, P., DeMenocal, P., Priore, P., Cullen, H., Hajdas, I., Bonani, G., 1997. A pervasive millennial-scale cycle in North Atlantic Holocene and glacial climates. Science 278 (5341), 1257–1266.

Bond, G., Kromer, B., Beer, J., Muscheler, R., Evans, M.N., Showers, W., Hoffmann, S., Lotti-Bond, R., Hajdas, I., Bonani, G., 2001. Persistent solar influence on North Atlantic climate during the Holocene. Science 294 (5549), 2130–2136.

Bruni, S., Cosci, M., 2003. Alpheae veterem contemptlor originis urbem, quam cingunt geminis Arnus et Ausur aquis. Il paesaggio di Pisa etrusca e romana: materiali e problemi. In: Bruni, S. (Ed.), Il porto urbano di Pisa. La fase etrusca. Il contesto e il relitto ellenistico, Pisa, pp. 29–43.

Callisto, L., Calbresi, G., 1998. Mechanical behavior of natural soft clay. Geotechnique 48, 495–513.

Catuneanu, O., 2006. Principles of Sequence Stratigraphy. Elsevier, Amsterdam, p. 375.

Catuneanu, O., Abreu, V., Bhattacharya, J.P., Blum, M.D., Dalrymple, R.W., Eriksson, P.G., Fielding, C.R., Fisher, W.L., Galloway, W.E., Gibling, M.R., Giles, K.A., Holbrook, J.M., Jordan, R., Kendall, C.G.St.C., Macurda, B., Martinsen, O.J., Miall, A.D., Neal, J.E., Nummedal, D., Pomar, L., Posamentier, H.W., Pratt, B.R., Sarg, J.F., Shanley, K.W., Steel, R.J., Strasser, A., Tucker, M.E., Winker, C., 2009. Towards the standardization of sequence stratigraphy. Earth Sci. Rev. 92 (1), 1–33.

Combourieu Nebout, N., Peyron, O., Dormoy, I., Desprat, S., Beaudouin, C., Kotthoff, U., Marret, F., 2009. Rapid climatic variability in the west Mediterranean during the last 25,000 years from high-resolution pollen. Clim. Past 5 (3), 503–521.

Di Pasquale, G., Allevato, E., Cocchiararo, A., Moser, D., Pacciarelli, M., Saracino, A., 2014. Late Holocene persistence of *Abies alba* in low–mid altitude deciduous forests of central and southern Italy: new perspectives from charcoal data. J. Veg. Sci. 25 (5), 1299–1310.

Di Rita, F., Magri, D., 2012. An overview of the Holocene vegetation history from the central Mediterranean coasts. J. Mediterr. Earth Sci. 4, 35–52.

Di Rita, F., Celant, A., Magri, D., 2010. Holocene environmental instability in the wetland north of the Tiber delta (Rome, Italy): sea–lake–man interactions. J. Paleolimnol. 44 (1), 51–67.

Döll, P., Schmied, H.M., 2012. How is the impact of climate change on river flow regimes related to the impact on mean annual runoff? A global-scale analysis. Environ. Res. Lett. 7 (1), 014037.

Drake, B.L., 2012. The influence of climatic change on the Late Bronze Age Collapse and the Greek Dark Ages. J. Archaeol. Sci. 39, 1862–1870.

Drescher-Schneider, R., De Beaulieu, J.-L., Magny, M., Walter-Simonnet, A.-V., Bossuet, G., Millet, L., Brugiapaglia, E., Drescher, A., 2007. Vegetation history, climate and human impact over the last 15,000 years at Lago dell'Accesa (Tuscany, Central Italy). Veg. Hist. Archaeobot. 16 (4), 279–299.

Evelpidou, N., Pirazzoli, P., Vassilopoulos, A., Spada, G., Ruggieri, G., Tomasin, A., 2012. Late Holocene sea level reconstructions based on observations of roman fish tanks, Tyrrhenian coast of Italy. Geoarchaeology 27 (3), 259–277.

Fægri, K., Iversen, J., 1989. In: Fægri, K., Kaland, P., Krzywinski, K. (Eds.), Textbook of Pollen Analysis, fourth ed. Wiley, Chichester.

Fanget, A.S., Berné, S., Jouet, G., Bassetti, M.A., Dennielou, B., Maillet, G.M., Tondut, M., 2014. Impact of relative sea level and rapid climate changes on the architecture and lithofacies of the Holocene Rhone subaqueous delta (Western Mediterranean Sea). Sediment. Geol. 305, 35–53.

Finné, M., Holmgren, K., Sundqvist, H.S., Weiberg, E., Lindblom, M., 2011. Climate in the eastern Mediterranean, and adjacent regions, during the past 6000 years. A review. J. Archaeol. Sci. 38 (12), 3153–3173.

Fletcher, W.J., Sánchez Goñi, M.F., 2008. Orbital- and sub-orbital-scale climate impacts on vegetation of the western Mediterranean basin over the last 48,000 yr. Quat. Res. 70, 451–464.

Fletcher, W.J., Zielhofer, C., 2013. Fragility of Western Mediterranean landscapes during Holocene rapid climate changes. Catena 103, 16–29.

Furlani, S., Biolchi, S., Cucchi, F., Antonioli, F., Busetti, M., Melis, R., 2011. Tectonic effects on Late Holocene sea level changes in the Gulf of Trieste (NE Adriatic Sea, Italy). Quat. Int. 232 (1–2), 144–157.

Giraudi, C., Magny, M., Zanchetta, G., Drysdale, R.N., 2011. The Holocene climatic evolution of Mediterranean Italy: a review of the continental geological data. The Holocene 21 (1), 105–115.

Grifoni Cremonesi, R., 2006. Il neolitico e l'età dei metalli in Toscana: sviluppi culturali e strategie insediative. In: Peruzzi, A. (Ed.), Pianeta Galileo, pp. 199–211 (Firenze).

Helama, S., Fauria, M.M., Mielikäinen, K., Timonen, M., Eronen, M., 2010. Sub-Milankovitch solar forcing of past climates: mid and late Holocene perspectives. Geol. Soc. Am. Bull. 122 (11–12), 1981–1988.

Hemming, S.R., 2004. Heinrich events: massive late Pleistocene detritus layers of the North Atlantic and their global climate imprint. Rev. Geophys. 42 (1), RG1005. http://dx.doi.org/10.1029/2003RG000128.

Hu, Y.G., Plint, A.G., 2009. An allostratigraphic correlation of a mudstone-dominated, syntectonic wedge: the Puskwaskau Formation (Santonian–Campanian) in outcrop and subsurface, Western Canada Foreland Basin. Bull. Can. Petrol. Geol. 57 (1), 1–33.

Jalut, G., Esteban Amat, A., Bonnet, L., Gauquelin, T., Fontugne, M., 2000. Holocene climatic changes in the Western Mediterranean, from southeast France to south-east Spain. Palaeogeogr. Palaeoclimatol. Palaeoecol. 160 (3–4), 255–290.

Jones, A.F., Macklin, M.G., Lewin, J., 2010. Flood series data for the later Holocene: available approaches, potential and limitations from UK alluvial sediments. The Holocene 20, 1123–1135.

Lambeck, K., Antonioli, F., Purcell, A., Silenzi, S., 2004. Sea-level change along the Italian coast for the past 10,000 yr. Quat. Sci. Rev. 23 (14), 1567–1598.

Lambeck, K., Antonioli, F., Anzidei, M., Ferranti, L., Leoni, G., Scicchitano, G., Silenzi, S., 2011. Sea level change along the Italian coast during the Holocene and projections for the future. Quat. Int. 232 (1–2), 250–257.

Legarreta, L., Uliana, M.A., 1998. Anatomy of hinterland depositional sequences: Upper Cretaceous fluvial strata, Neuquen Basin, West-Central Argentina. In: Shanley, K.W., McCabe, P.J. (Eds.), Relative Role of Eustasy, Climate, and Tectonism in Continental Rocks. Spec. Publ. Soc. Econ. Paleont. Miner. 59, pp. 83–92.

Lewin, J., Macklin, M.G., Johnstone, E., 2005. Interpreting alluvial archives: sedimentological factors in the British Holocene fluvial record. Quat. Sci. Rev. 24, 1873–1889.

Lewis, S.G., Maddy, D., Scaife, R.G., 2001. The fluvial system response to abrupt climate change during the last cold stage: the Upper Pleistocene River Thames fluvial succession at Ashton Keynes, UK. Glob. Planet. Chang. 28 (1), 341–359.

Macklin, M.G., Lewin, J., 2003. River sediments, great floods and centennial-scale Holocene climate change. J. Quat. Sci. 18 (2), 101–105.

Macklin, M.G., Fuller, I.C., Lewin, J., Maas, G.S., Passmore, D.G., Rose, J., Woodward, J.C., Black, S., Hamblin, R.H.B., Rowan, J.S., 2002. Correlation of fluvial sequences in the Mediterranean basin over the last 200 ka and their relationship to climate change. Quat. Sci. Rev. 21, 1633–1641.

Macklin, M.G., Benito, G., Gregory, K.J., Johnstone, E., Lewin, J., Michczyńska, D.J., Soja, R., Starkel, L., Thorndycraft, V.R., 2006. Past hydrological events reflected in the Holocene fluvial record of Europe. Catena 66 (1), 145–154.

Macklin, M.G., Lewin, J., Woodward, J.C., 2012. The fluvial record of climate change. Philosophical Transactions of the Royal Society A: mathematical. Phys. Eng. Sci. 370 (1966), 2143–2172.

Maddy, D., Bridgland, D., Westaway, R., 2001. Uplift-driven valley incision and climate-controlled river terrace development in the Thames Valley, UK. Quat. Int. 79 (1), 23–36.

Magny, M., 2004. Holocene climatic variability as reflected by mid-European lake-level fluctuations, and its probable impact on prehistoric human settlements. Quat. Int. 113, 65–79.

Magny, M., Miramont, C., Sivan, O., 2002. Assessment of the impact of climate and anthropogenic factors on Holocene Mediterranean vegetation in Europe on the basis of palaeohydrological records. Palaeogeogr. Palaeoclimatol. Palaeoecol. 186, 47–59.

Magny, M., de Beaulieu, J.-L., Bégeot, C., Heiri, O., Millet, L., Peyron, O., Walter-Simonnet, A.V., 2007. Holocene climate changes in the central Mediterranean as recorded by lake-level fluctuations at Lake Accesa (Tuscany, Italy). Quat. Sci. Rev. 26 (13), 1736–1758.

Magny, M., Vannière, B., Zanchetta, G., Fouache, E., Touchais, G., Petrika, L., Coussot, C., Walter-Simonnet, A.-V., Arnaud, F., 2009. Possible complexity of the climatic event around 4300–3800 cal. BP in the central and western Mediterranean. The Holocene 19 (6), 823–833.

Magny, M., Peyron, O., Sadori, L., Ortu, E., Zanchetta, G., Vannière, B., Tinner, W., 2012a. Contrasting patterns of precipitation seasonality during the Holocene in the south and north-central Mediterranean. J. Quat. Sci. 27 (3), 290–296.

Magny, M., Arnaud, F., Billaud, Y., Marguet, A., 2012b. Lake-level fluctuations at Lake Bourget (eastern France) around 4500–3500 cal. a BP and their palaeoclimatic and archaeological implications. J. Quat. Sci. 27 (5), 494–502.

Magri, D., 2007. Advances in Italian palynological studies: late Pleistocene and Holocene records. GFF 129 (4), 337–344.

Malinverno, A., Ryan, W.B., 1986. Extension in the Tyrrhenian Sea and shortening in the Apennines as result of arc migration driven by sinking of the lithosphere. Tectonics 5 (2), 227–245.

Mariani, M., Prato, R., 1988. I bacini neogenici costieri del margine tirrenico: approccio sismico stratigrafico. Geol. Ital. Mem. 41, 519–531.

Mariotti Lippi, M.M., Bellini, C., Trinci, C., Benvenuti, M., Pallecchi, P., Sagri, M., 2007. Pollen analysis of the ship site of Pisa San Rossore, Tuscany, Italy: the implications for catastrophic hydrological events and climatic change during the late Holocene. Veg. Hist. Archaeobot. 16 (6), 453–465.

Marra, F., Bozzano, F., Cinti, F.R., 2013. Chronostratigraphic and lithologic features of the Tiber River sediments (Rome, Italy): implications on the post-glacial sea-level rise and Holocene climate. Glob. Planet. Chang. 107, 157–176.

Martini, I.P., Sagri, M., 1993. Tectono-sedimentary characteristics of Late Miocene–Quaternary extensional basins of the Northern Apennines, Italy. Earth Sci. Rev. 34 (3), 197–233.

Martini, I.P., Sarti, G., Pallecchi, P., Costantini, A., 2011. Landscape influences on the development of the Medieval–Early Renaissance city-states of Pisa, Florence, and Siena, Italy. Landscapes and Societies (pp. 203–221). Springer, Netherlands, p. 467.

Mayewski, P.A., Rohling, E.E., Stager, J.C., Karlen, W., Maasch, K.A., Meeker, L.D., Meyerson, E.A., Gasse, F., van Kreveld, S., Holmgren, K., Lee-Thorp, J., Rosqvist, G., Rack, F., Staubwasser, M., Schneider, R.R., Steig, E.J., 2004. Holocene climate variability. Quat. Res. 62, 243–255.

Miall, A.D., 1996. The Geology of Fluvial Deposits. Springer-Verlag, p. 582.

Milli, S., D'Ambrogi, C., Bellotti, P., Calderoni, G., Carboni, M.G., Celant, A., Di Bella, L., Di Rita, F., Frezza, V., Magri, D., Pichezzi, R.M., Ricci, V., 2013. The transition from wave-dominated estuary to wave-dominated delta: the Late Quaternary stratigraphic architecture of Tiber River deltaic succession (Italy). Sediment. Geol. 284–285, 159–180.

Ministero dei Lavori Pubblici, 1971. Ricerche e studi sulla Torre pendente di Pisa e I fenomeni connessi alle condizioni d'ambiente. Istituto Geografico Militare, Firenze (I, II, II).

Morhange, C., Laborel, J., Hesnard, A., 2001. Changes of relative sea level during the past 5000 years in the ancient harbor of Marseilles, Southern France. Palaeogeogr. Palaeoclimatol. Palaeoecol. 166 (3–4), 319–329.

Morhange, C., Pirazzoli, P.A., Marriner, N., Montaggioni, L.F., Nammour, T., 2006. Late Holocene relative sea-level changes in Lebanon, Eastern Mediterranean. Mar. Geol. 230 (1–2), 99–114.

Morhange, C., Marriner, N., Excoffon, P., Bonnet, S., Flaux, C., Zibrowius, H., Goiran, J.P., Amouri, M.E., 2013. Relative sea-level changes during Roman Times in the Northwest Mediterranean: the 1st century A.D. Fish tank of Forum Julii, Fréjus, France. Geoarchaeology 28 (4), 363–372.

Nieto-Moreno, V., Martínez-Ruiz, F., Giralt, S., Jiménez-Espejo, F., Gallego-Torres, D., Rodrigo-Gámiz, M., García-Orellana, J., Ortega-Huertas, M., De Lange, G.J., 2011. Tracking climate variability in the western Mediterranean during the Late Holocene: a multiproxy approach. Clim. Past 7 (4), 1395–1414.

Pascucci, V., 2005. Neogene evolution of the Viareggio Basin, northern Tuscany (Italy). Geol. Acta 4, 123–138.

Pasquinucci, 1994. Il popolamento dall'età del Ferro al Tardo Antico. In: Mazzanti, R. (Ed.), La pianura di Pisa ed i rilievi contermini.

Patacca, E., Sartori, P., Scandone, P., 1993. Tyrrhenian basin and Apennines. Kinematic evolution and related dynamic constraints. In: Boschi, E., Mantovani, E., Morelli, A. (Eds.), Recent Evolution and Seismicity of the Mediterranean Region. Kluwer Academic Publishers, Dordrecht, Netherlands, pp. 161–171.

Pirazzoli, P.A., 1976. Sea level variations in the northwest Mediterranean during Roman times. Science 194 (4264), 519–521.

Piva, A., Asioli, A., Trincardi, F., Schneider, R.R., Vigliotti, L., 2008. Late-Holocene climate variability in the Adriatic sea (Central Mediterranean). The Holocene 18 (1), 153–167.

Posamentier, H.W., Jervey, M.T., Vail, P.R., 1988. Eustatic controls on clastic deposition I — conceptual framework. In: Wilgus, C.K., Hastings, B.S., C. G. St, Kendall, C., Posamentier, H.W., Ross, C.A., Van Wagoner, J.C. (Eds.), Sea Level Change: An Integrated Approach. SEPM Special Publication 42, pp. 110–124.

Pranzini, E., 2001. Updrift river mouth migration on cuspate deltas: two examples from the coast of Tuscany (Italy). Geomorphology 38 (1–2), 125–132.

Primavera, M., Simone, O., Fiorentino, G., Caldara, M., 2011. The palaeoenvironmental study of the Alimini Piccolo lake enables a reconstruction of Holocene sea-level changes in southeast Italy. The Holocene 21 (4), 553–563.

Reille, M., 1992–98. Pollen et spores d'Europe et d'Afrique du Nord. Laboratoire de botanique historique et palynologie, Marseille.

Reimer, P.J., Baillie, M.G.L., Bard, E., Bayliss, A., Beck, J.W., Blackwell, P.G., Bronk Ramsey, C., Buck, C.E., Burr, G.S., Edwards, R.L., Friedrich, M., Grootes, P.M., Guilderson, T.P., Hajdas, I., Heaton, T.J., Hogg, A.G., Hughen, K.A., Kaiser, K.F., Kromer, B., McCormac, F.G., Manning, S.W., Reimer, R.W., Richards, D.A., Southon, J.R., Talamo, S., Turney, C.S.M., van der Plicht, J., Weyhenmeyer, C.E., 2009. INTCAL 09 and MARINE09 radiocarbon age calibration curves, 0, 50,000 years Cal BP. Radiocarbon 51, 1111–1150.

Ribecai, C., 2011. Synthesis of Late Quaternary palynological studies in the Arno coastal plain and surroundings: toward a comprehensive Late Quaternary palaeovegetational hystory. Atti Soc. Toscana Sci. Nat. Mem. Ser. A 116, 163–170.

Ricci Lucchi, M., 2008. Vegetation dynamics during the last interglacialeglacial cycle in the Arno coastal plain (Tuscany, western Italy): location of a new tree refuge. Quat. Sci. Rev. 27, 2456–2466.

Roberts, N., Eastwood, W.J., Kuzucuo lu, C., Fiorentino, G., Caracuta, V., 2011. Climatic, vegetation and cultural change in the eastern Mediterranean during the mid-Holocene environmental transition. The Holocene 21 (1), 147–162.

Rossi, V., Amorosi, A., Sarti, G., Potenza, M., 2011. Influence of inherited topography on the Holocene sedimentary evolution of coastal systems: an example from Arno coastal plain (Tuscany, Italy). Geomorphology 135 (1), 117–128.

Rossi, V., Amorosi, A., Sarti, G., Romagnoli, R., 2012. New stratigraphie evidence for the mid–late Holocene fluvial evolution of the Arno coastal plain (Tuscany, Italy) [Données stratigraphiques nouvelles concernant l'évolution fluviale de la plaine côtière de Arno (Toscane, Italie) à l'Holocène moyen-supérieur]. Geomorphol. Relief Process. Environ. 2, 201–214.

Sadori, L., Jahns, S., Peyron, O., 2011. Mid-Holocene vegetation history of the central Mediterranean. The Holocene 21 (1), 117–129.

Sarti, G., Bini, M., Serena, G., 2010. The growth and the decline of Pisa (Tuscany, Italy) up to the Middle Ages: correlations with landscape and geology. In: geological setting and urban development of selected Italian towns up to the Middle Ages and legacies of ancient problems throughout the ages. Il Quaderno dell'Ostetrica Ital. J. Quat. Sci. 23 (2bis), 311–322.

Sarti, G., Rossi, V., Amorosi, A., 2012. Influence of Holocene stratigraphic architecture on ground surface settlements: a case study from the City of Pisa (Tuscany, Italy). Sediment. Geol. 281, 75–87.

Schumm, S.A., 1993. River response to base level change: implications for sequence stratigraphy. J. Geol. 101, 279–294.

Somoza, L., Barnolas, A., Arasa, A., Maestro, A., Rees, J.G., Hernández-Molina, F.J., 1998. Architectural stacking patterns of the Ebro delta controlled by Holocene high-frequency eustatic fluctuations, delta-lobe switching and subsidence processes. Sediment. Geol. 117 (1), 11–32.

Spada, G., Stocchi, P., 2007. SELEN: a Fortran 90 program for solving the "sea-level equation". Comput. Geosci. 33 (4), 538–562.

Spampinato, C.R., Costa, B., Di Stefano, A., Monaco, C., Scicchitano, G., 2011. The contribution of tectonics to relative sea-level change during the Holocene in coastal south-eastern Sicily: new data from boreholes. Quat. Int. 232 (1–2), 214–227.

Stanley, D.J., Warne, A.G., 1994. Worldwide initiation of Holocene marine deltas by deceleration of sea-level rise. Science 265 (5169), 228–231.

Starkel, L., 1983. The reflection of hydrologic changes in the fluvial environment of the temperate zone during the last 15,000 years. Background to Palaeohydrologypp. 213–235.

Starkel, L., 2000. Heavy Rains and Floods in Europe During Last Millennium. Reconstructions of Climate and Its Modeling, Prace geograficzne, l07. Institute of Geography of the Jagiellonian University, Cracow, pp. 55–62.

Starkel, L., Soja, R., Michczyńska, D.J., 2006. Past hydrological events reflected in Holocene history of Polish rivers. Catena 66 (1), 24–33.

Steffensen, J.P., Andersen, K.K., Bigler, M., Clausen, H.B., Dahl-Jensen, D., Fischer, H., Goto-Azuma, K., Hansson, M., Johnsen, S.J., Jouzel, J., Masson-Delmotte, V., Popp, T., Rasmussen, S.O., Röthlisberger, R., Ruth, U., Stauffer, B., Siggaard-Andersen, M.L., Sveinbjörnsdóttir, Á.E., Svensson, A., White, J.W.C., 2008. High-resolution Greenland ice core data show abrupt climate change happens in few years. Science 321 (5889), 680–684.

Straffin, E.C., Blum, M.D., 2002. Holocene fluvial response to climate change and human activities; Burgundy, France. Neth. J. Geosci. Geol. Mijnb 81 (3), 417–430.

Thorndycraft, V.R., Benito, G., 2006. Late Holocene fluvial chronology of Spain: the role of climatic variability and human impact. Catena 66 (1), 34–41.

Tinner, W., Lotter, A.F., 2006. Holocene expansions of *Fagus sylvatica* and *Abies alba* in Central Europe: where are we after eight decades of debate? Quat. Sci. Rev. 25 (5–6), 526–549.

Tinner, W., Colombaroli, D., Heiri, O., Henne, P.D., Steinacher, M., Untenecker, J., Vescovi, E., Allen, J.R.M., Carraro, G., Conedera, M., Joos, F., Lotter, A.F., Luterbacher, J., Samartin, S., Valsecchi, V., 2013. The past ecology of *Abies alba* provides new perspectives on future responses of silver fir forests to global warming. Ecol. Monogr. 83 (4), 419–439.

Traverse, A., 1988. Plant evolution dances to a different beat: plant and animal evolutionary mechanisms compared. Hist. Biol. 1 (4), 277–301.

Turner, F., Tolksdorf, J.F., Viehberg, F., Schwalb, A., Kaiser, K., Bittmann, F., von Bramann, U., Pott, R., Staesche, U., Breest, K., Veil, S., 2013. Lateglacial/early Holocene fluvial reactions of the Jeetzel River (Elbe valley, northern Germany) to abrupt climatic and environmental changes. Quat. Sci. Rev. 60, 91–109.

Vandenberghe, J., 2003. Climate forcing of fluvial system development: an evolution of ideas. Quat. Sci. Rev. 22 (20), 2053–2060.

Vella, C., Fleury, T.J., Raccasi, G., Provansal, M., Sabatier, F., Bourcier, M., 2005. Evolution of the Rhône delta plain in the Holocene. Mar. Geol. 222, 235–265.

Wanner, H., Beer Wanner, H., Beer, J., Bütikofer, J., Crowley, T.J., Cubasch, U., Flückiger, J., Goosse, H., Grosjean, M., Joos, F., Kaplan, J.O., Küttel, M., Müller, S.A., Prentice, I.C., Solomina, O., Stocker, T.F., Tarasov, P., Wagner, M., Widmann, M., 2008. Mid- to Late Holocene climate change: an overview. Quat. Sci. Rev. 27 (19), 1791–1828.

Zanchetta, G., Bini, M., Cremaschi, M., Magny, M., Sadori, L., 2013. The transition from natural to anthropogenic-dominated environmental change in Italy and the surrounding regions since the Neolithic: an introduction. Quat. Int. 303, 1–9.

4.1.1 Additional remote sensing data (Landsat and Sentinel 2a satellite imagery) for the urban area

The multitemporal analyses performed on multispectral satellite images (Tab. 4.1) selected from the optical sensors Landsat 7 ETM+, Landsat 8 OLI, Sentinel 2a, ASTER, despite the use of the combinations of different EM bands aimed to enhance the images and favor the identification of features inside the scenes, attested that no evident geological traces are visible by photo-interpretation, reasonably due to prominent urban structures (fig. 4.1).

In addition to the visual interpretation, a semi-automatic processing (PCA) was also performed on the scenes without furnishing any interesting results in the detection of traces, suggesting the unsuccessful application of these RS data and techniques for mapping paleochannels and/or paludal areas in long-settled city areas.

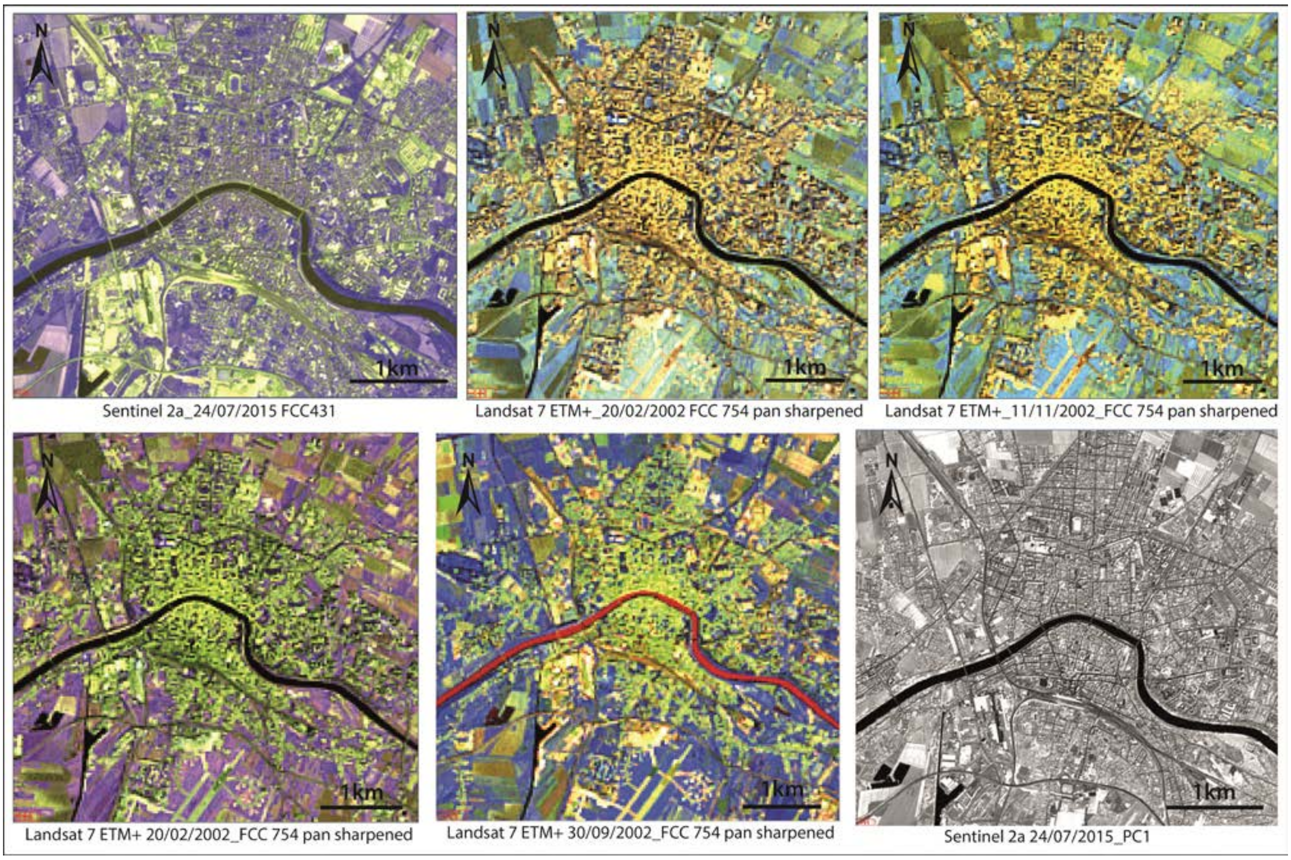

Sentinel 2a_24/07/2015 FCC431

Landsat 7 ETM+_20/02/2002 FCC 754 pan sharpened

Landsat 7 ETM+_11/11/2002_FCC 754 pan sharpened

Landsat 7 ETM+ 20/02/2002_FCC 754 pan sharpened

Landsat 7 ETM+ 30/09/2002_FCC 754 pan sharpened

Sentinel 2a 24/07/2015_PC1

Figure 4.1_Some of the processed satellite images (False Color Composite-FCC and Principal Component Analysis-PCA) clipped for the urban area of Pisa. Scenes are from different sensors (Landsat 7 ETM+ and Sentinel 2a) and acquired in different seasons (see the reported below each image).

4.2 Pisa extra-urban area (SR site)

4.2.1 The acquired dataset

The RS, surface and subsurface data selected for the analysis and involved in the workflow illustrated in Chapter 3 are listed in detail below:

- **RS data**

The detailed photointerpretation of the study site was carried out employing 11 multispectral satellite images from different optical sensors, including Landsat 7 ETM+, Landsat 8 OLI, ASTER and Sentinel 2A optical sensors (see Chapter 3 and Tab. 3.1 a for technical characteristics and Tab. 4.1 for images date details), together with Google Earth imagery.

Satellite imagery	Acquisition date
Landsat 7 ETM+	11 November 2000
	15 February 2001
	02 February 2002
	30 September 2002
Landsat 8 OLI	10 September 2015
TERRA-ASTER	19 September 2004
	21 September 2008
	08 August 2012
	06 August 2011
SENTINEL2-MSI	24 July 2015
	13 January 2016

Tab. 4.1_ List of the optical multispectral satellite images used in the present work

The traces identified on the imagery and from LiDAR DTM were digitalized and mapped in a GIS environment and georeferenced in UTM-WGS 84 projection system.

- **Surface spectral data**

Laboratory analyses aimed to investigate the spectral signatures of surface deposits were carried out on 5 soil samples (uppermost 5 cm) collected in correspondence with selected areas (fig. 4.2), involving the identified traces and their surroundings, showing persistently different reflectance values from various satellite sensors observations.

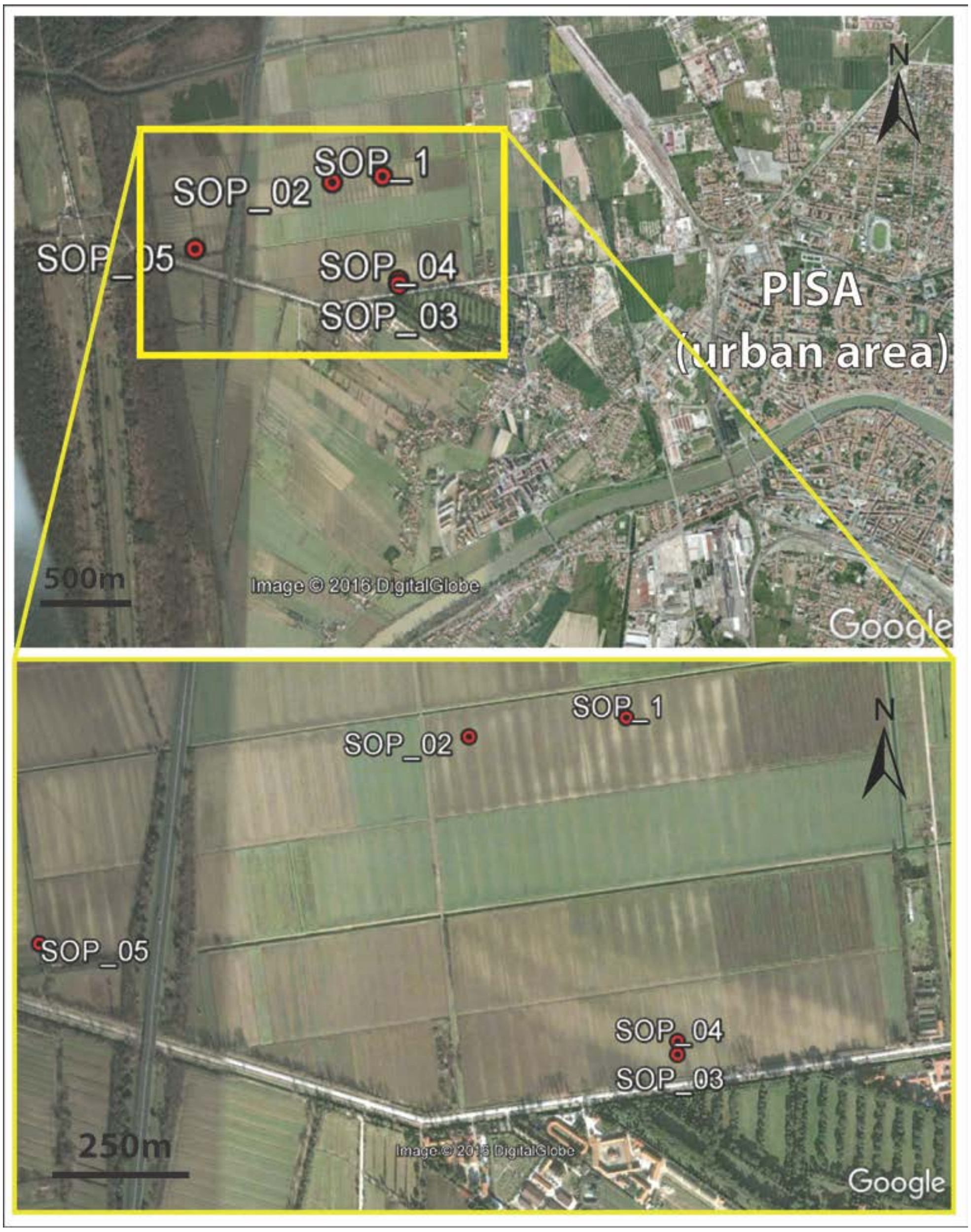

Figure 4.2_Images from Google Earth displaying the location (red circles)of the soil samples (SOP1-SOP5) collected in the San Rossore site for the laboratory spectral signature extraction.

- **Subsurface sedimentologic and stratigraphic data**

Five boreholes (labelled from TSP1 to TSP5), up to 10 m long, were drilled using Cobra vibracorer in key areas, selected following the same criteria used for soil sampling (figs. 4.2., 4.3), in order to study the subsurface stratigraphic succession occurring underneath the remote-sensed bright and dark traces/areas.

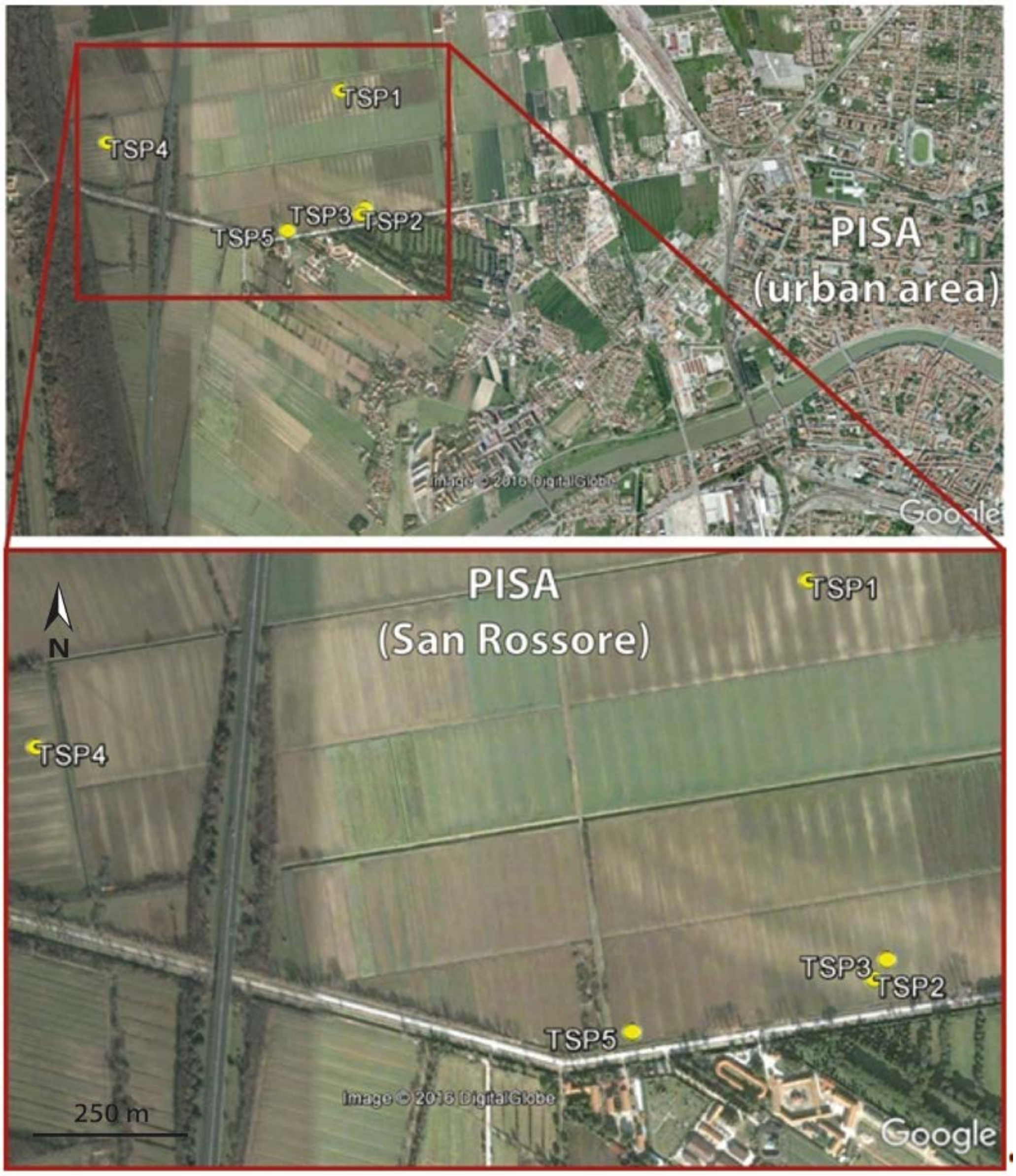

Figure 4.3_Image from Google Earth displaying the locations (yellow circles) of new cores (TSP1-TSP5) drilled (vibracores up to 10 m long) in the San Rossore (SR) site.

Detailed facies analyses of the cored successions were performed based on high-resolution sedimentologic descriptions, supported and refined by the meiofauna content (benthic foraminifers and ostracods) determination.

Twenty samples were collected for micropaleontological analyses from 3 reference cores (TSP3, TSP4 and TSP5) recording all the spectrum of lithofacies recognized from the visual inspection.

Additional 5 shallow cores (labelled from TM1 to TM5), up to 2 m long and drilled using an hand-auger (see Chapter 3, fig. 3.2), were undertaken to further support the stratigraphic analysis of the remote-sensed traces (fig. 4.4).

Finally, small-scale cross-sections were carried out to reconstruct the subsurface stratigraphic architecture of the study site and to match it with the most prominent remote-sensed landforms identified combining satellite imagery and DTM (see figs. 4.12 and 4.13).

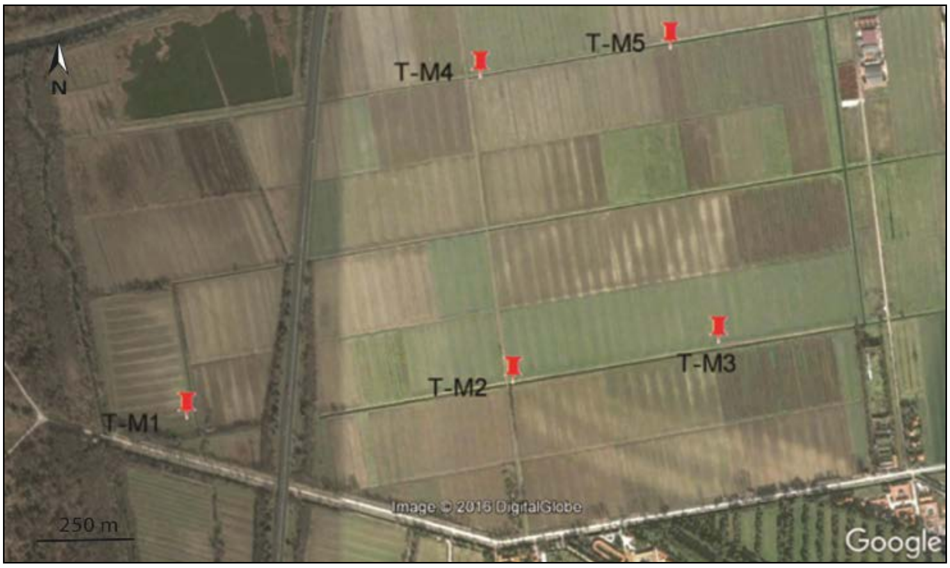

Figure 4.4- Image from Google Earth displaying the location (red symbols) of hand-auger cores 2 m long (TM1-TM5) drilled in the San Rossore (SR) site.

The chronological framework was guaranteed by 3 new radiocarbon ages (Tab. 4.2)

.Sample core_ID	Core depth (m)	Material	Conventional age (yr BP)	Calibration dataset	2_sigma calibrated age range (cal yr BP)
TSP4_D	2.95-3.00	peat	2637±30	IntCal13	2732-2791 (99%)
TSP4_F	5.65-5.75	shell	4939±64	Mixed Marine NoHem	5319-5587 (100%)
TSP4_E	7.80-7.90	shell	5592±89	Mixed Marine NoHem	5940-6342 (100%)

Table 4.2_ List of the new radiocarbon dating. Local reservoir correction DeltaR (35±42) was applied to shell samples. Percentages associated to the calibrated age values represent the related area under probability distribution using two standard deviations-2s.

4.2.2 Data presentation

4.2.2.1 RS-detected landforms

The analyses performed on satellite images, integrated with the LiDAR DTM, led to map in the SR site two main traces interpreted as past landforms (A and B in fig. 4.5). Specifically, the plan-view arrangement of pixels with contrasting brightness (spectral reflectance behaviour of the surface) on the scene and the topographic profiles carried out on DTM LiDAR outline morphological features attributable to fluvial landforms (paleochannels).

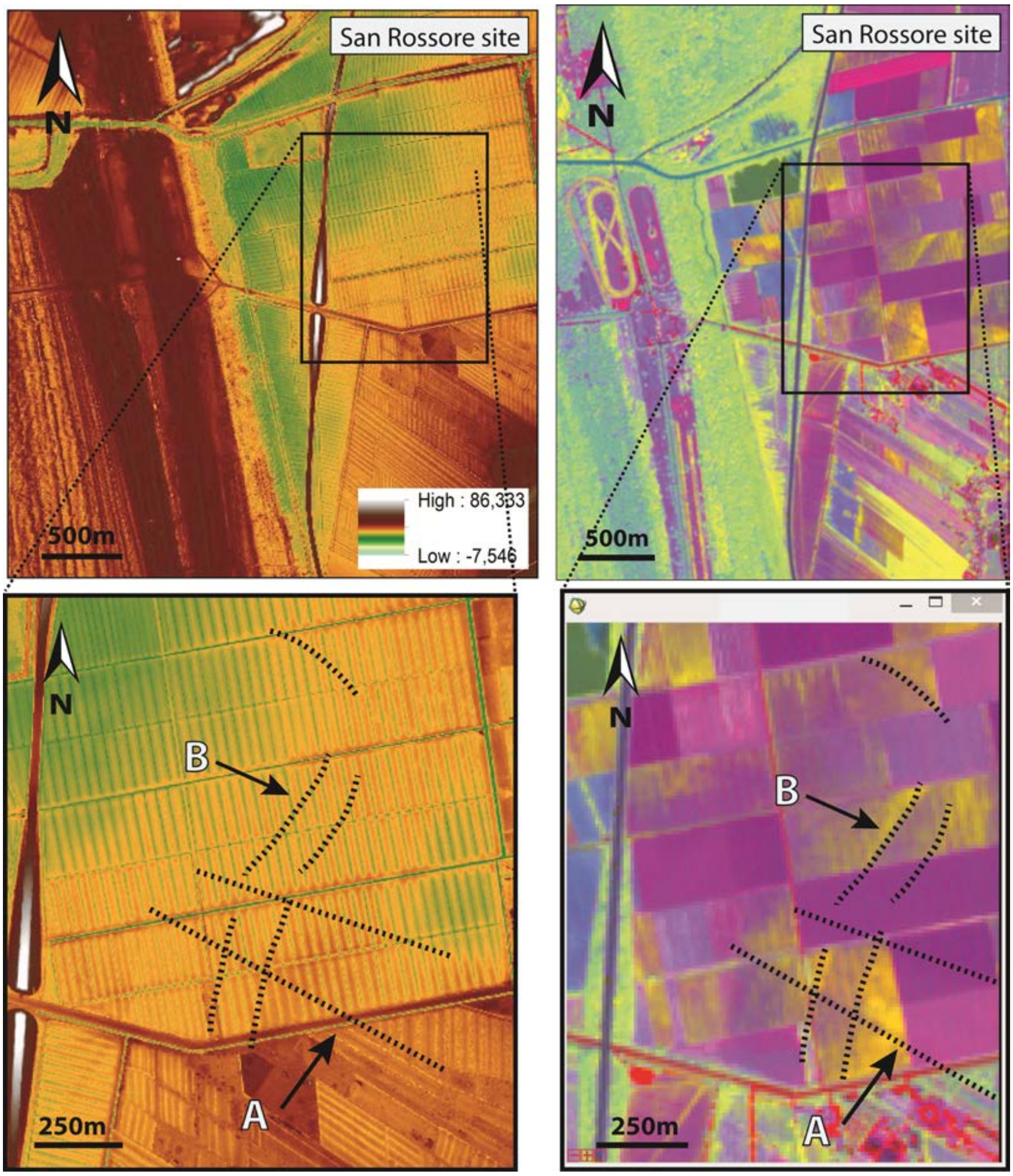

Figure 4.5_ Clipping from DTM LiDAR (on the left) and Sentinel2a-24 July 2015- Principal Component 123 (on the right) of the San Rossore site. The two main different traces recognizable on the figures are highlighted with a black dotted line and labelled with A and B.

Trace A is characterized by bright pixels (i.e., high reflectance values) arranged to form a ca. 1 km-long, wide, rather regualr straight band with a distinct NW-SE orientation. The trace, that doesn’t display a costant width becoming gradually narrower moving westwards (from ca. 250 m at the SE edge to ca. 150 m at the NW edge), is longitudinally marked by the occurrence of a thin, central strip of dark pixels (i.e., low reflectance values; fig. 4.6 a,b). The topographic profile performed across the trace (fig. 4.6) doesn’y dispaly any peculiar trend but documents a quite regular slight decrease in elevation from SW (ca. 1,5-1 m above sea level-a.s.l.) to NE (ca. 1-0,5 m a.s.l.).

These morphologic characteristics (plan-view pattern and elevation distribution) point to an anthropic rather than natural origin for trace A, likely connected to an artificial ditch used to drain waters or an irrigation canal. According to this interpretation, the orientation of the trace seems to follow the *decumani* axis of the agrarian system known as *Centuratio*, created during the Roman period and used until the Medieval ages. The *Centuratio* traces of Pisa Plain, still partially visible from Google Earth, have been highlighted in detail by Cosci (1990) and Bini et al. (2012a) on the basis of aerial photos interpretation.

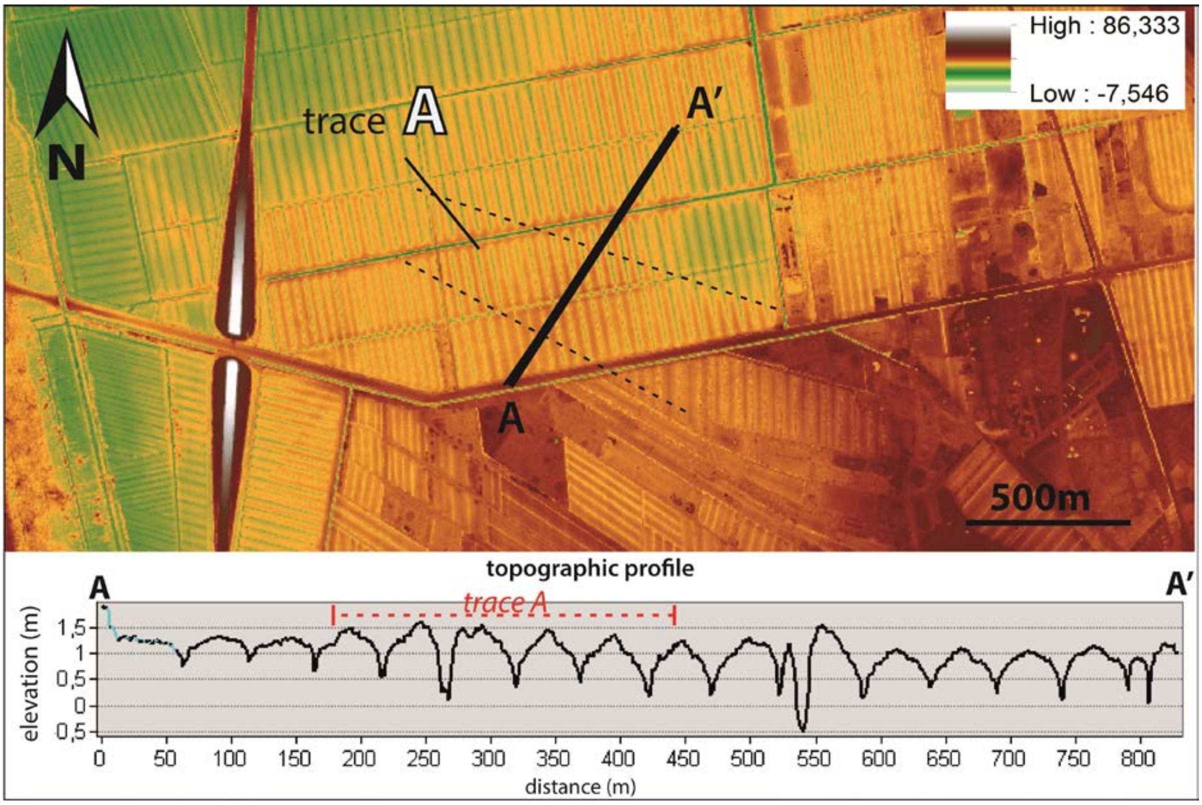

Figure 4.6_ Short topographic profile across trace A based on LiDAR DTM data. From A to A’ a slight decrease in elevation is documented.

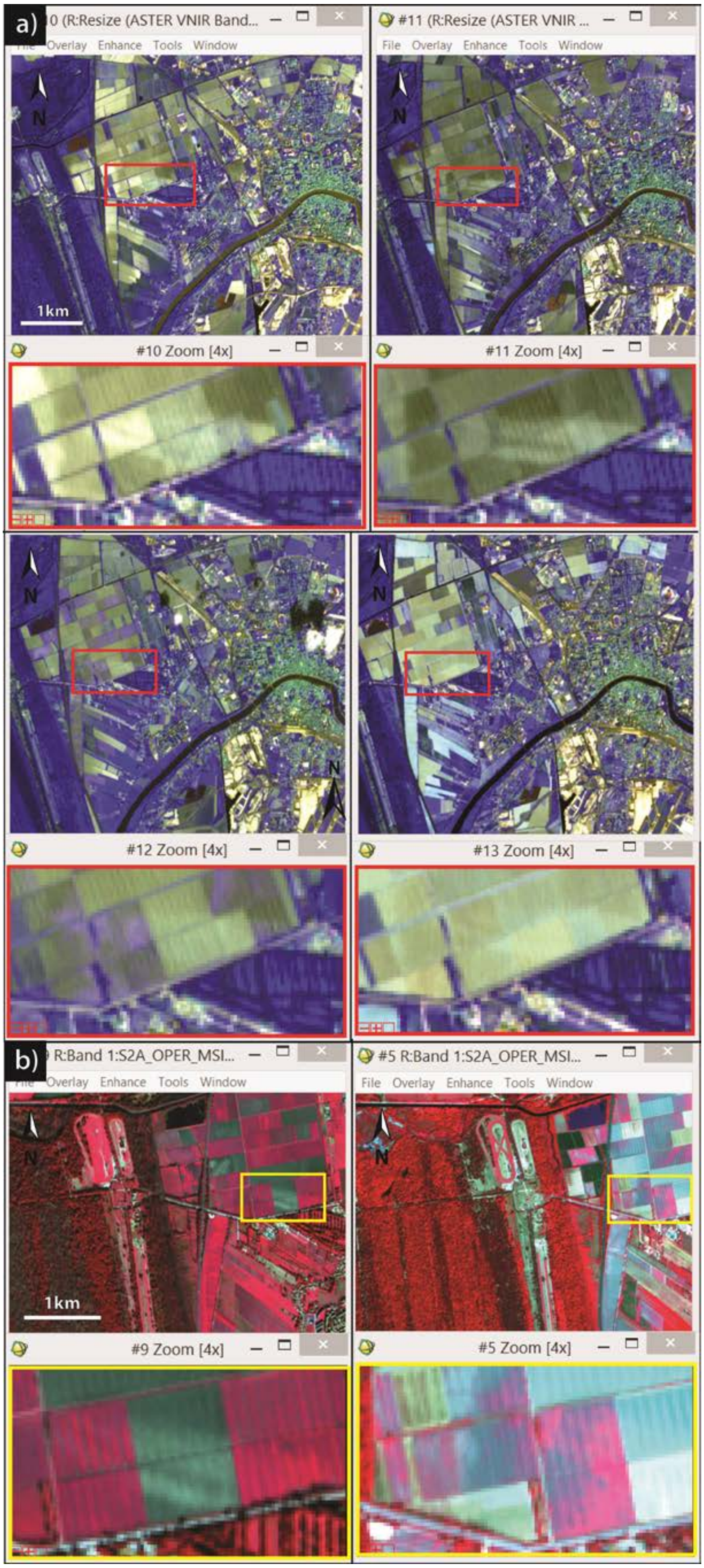

Figure 4.7_ a) 3N21 False Color Composite (FCC) of ASTER (scenes from different seasons of different years, see tab. 4.1); b) FCC 842, of Sentinel 2a (scene from different seasons of the year, see tab.4.1). Paleotrace A, differently from B, even though variably visible over time, is always identifiable.

Trace A crosses and apparently overlies another trace (labelled with B) characterized by opposite orientation (ca. NNE-SSW orientation; fig. 4.5).

In contrast to trace A, that is always detectable on satellite images even though with a different degree of visibility over time, trace B results scarcely identifiable or even "invisible" in several scenes as documented by the multitemporal analysis (fig. 4.7 a, b). Despite this, a little portion of trace B results visible from a set of Google Earth scenes (fig. 4.4), already partially highlighted by previous works dealing with airborne and satellite photos (Bini et al., 2012 a, b) and classified as "terrain anomaly".

Among all the available scenes, only that recorded by Sentinel 2a in 24 July 2015 once processed results suitable to clearly identify and map trace B (fig. 4.5) thanks to EM spectral bands combination involving, in particular, the ones from the NIR spectral regions. Indeed, this combination allows for the first time to highlight alternating bright-dark-bright pixels arranged in a ca. 1.5 km long continuous sinuous trace with a rather constant width of ca. 80 m (fig. 4.5).

Despite the absence of any diagnostic morphologic trends recognizable from DTM profiles (i.e., convexity) as documented by the topographic section performed across trace B (fig. 4.8), it is possible to associate the trace with a portion of the SR site that displays elevations slightly higher with respect to the surroundings, rising up ca. 1 m (figs. 4.5, 4.8). These morphologic characteristics, revealed by the employed remote-sensed data, allow to reasonably attribute trace B to a sinuous paleochannel branch.

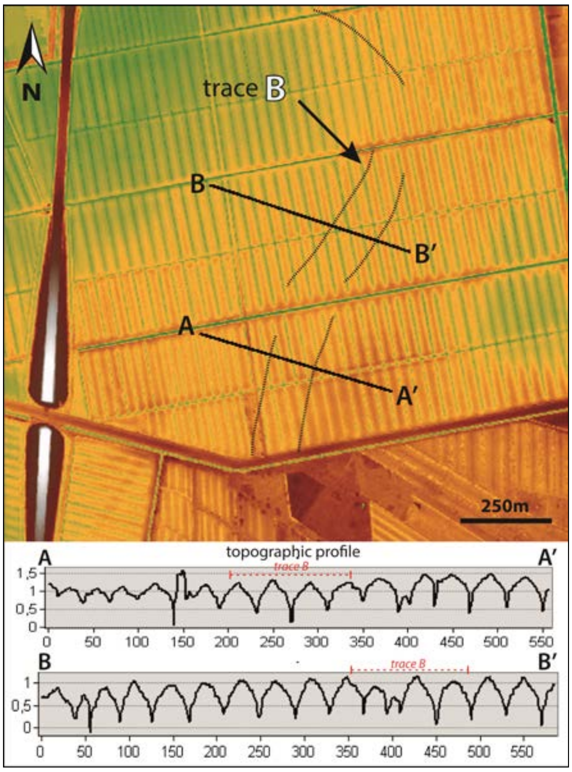

Figure 4.8_ Two short topographic profiles carried out across trace B based on DTM LiDAR data. A quite constant flat morphology characterize both the profiles.

4.2.2.2 Soil spectral signatures

Laboratory reflectance spectra of soil samples collected from both on-traces (bright and dark portions) and out-of-traces dark areas (see fig. 4.2 for samples location) are reported in Figure 4.9.

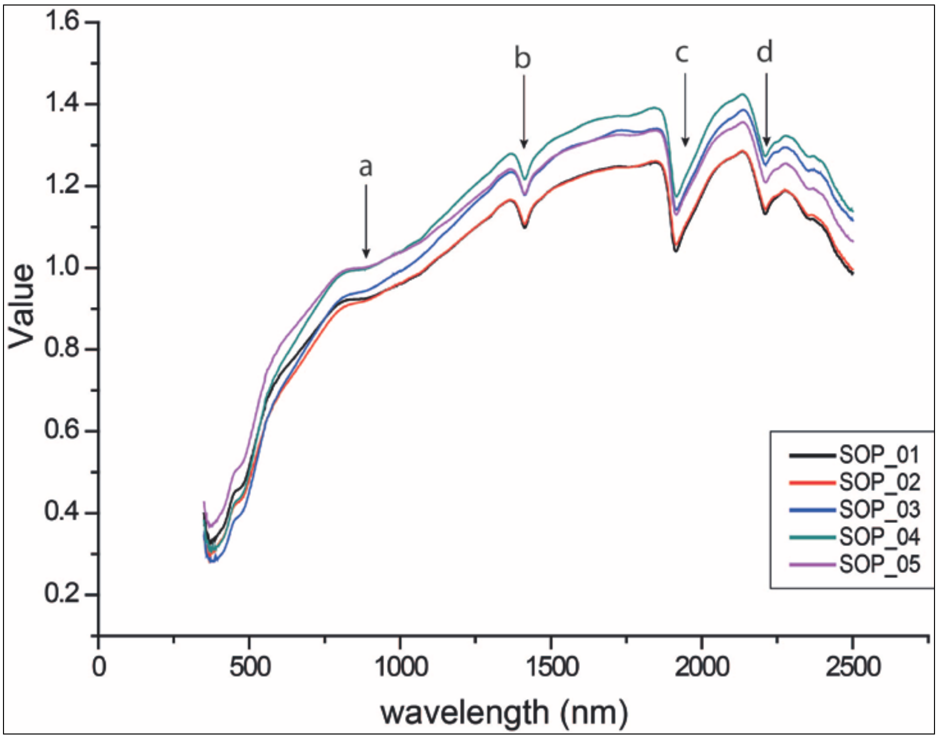

Figure 4.9_ Spectral signatures of San Rossore site soil samples (SOP_01 and SOP_03 collected from bright portion of traces A and B; SOP_04 from dark portion within trace A; SOP_02 and SOP_05 are out-of-traces, see fig. 4.2 section 4.2.1 for the location).

It is worthy to note that all the samples display very similar spectral signatures, typical of bare soils (Stoner and Baumgardner, 1981; Baumgardner et al., 1985), in which reflectance values increase with the increase of the wavelength, and in which water adsorption bands at around 1400 nm and 1900 nm occur (b and c in fig. 4.9). An absorption band around 2200 nm in all the spectra (d in fig. 4.9) is also present, likely associated to the occurrence of Al-OH features typical of clay-minerals. Moreover, all the extracted spectra are characterized by another, less pronounced, absorption band located at around 900 nm and attributable to the occurrence of Iron-oxides (Hunt and Salisbury, 1970; Hunt, 1989; Baumgardner et al. 1985; Burns, 1993; Ellis and Mellor, 1995), consistently with the sedimentological observation undertaken on surface desposits during the field survey.

Thus, the soils spectra testify the occurrence of clayey deposits on the surface, irrespective of the samples location respect with the occurence of the traces, i.e., both within (bright or dark portions) and out of RS-detected traces.

4.2.2.3 Subsurface core stratigraphy

4.2.2.3.1. Cobra core data

The description of the stratigraphy and the vertical stacking pattern of facies recovered by Cobra cores are briefly reported below, following a remote sensed-geomorphological criterion, i.e., on-trace cores *versus* out-of-trace cores (see fig. 4.3), to support data integration presented in the subsequent section 4.3.

The subsurface facies associations reported here have been defined on the basis of the deposits sedimentologic characteristics and the microfossils content, as described in detail in the following section 4.2.2.4 where all the facies are listed. Stratigraphic logs with photographic report of each core are also included in the Appenidx B.

- On-traces (bright and dark portions) TSP1, TSP2, TSP3, TSP5 cores (fig. 4.10)
- Out-of-trace (dark areas) TSP4 core (fig.4.10)

The uppermost 30-70 cm of the cored succession is invariably composed of unstructured brown clays and silty clays, usually containing root remains and vegetal fragments, indicative of regular interference by agriculture activities (cropland-C). At distal locations (core TSP4 in fig. 4.3) cropland sediments overlie ca. 50 cm of reclaimed deposits.

- **On-trace cores**

TSP1 (7 m long)

Location: on-trace B, bright area

Stratigraphy: at the base TSP1 shows ca. 1 m of flood-tidal delta deposits composed of grey coarse-to-medium sands with abundant mollusk shell fragments, locally interrupted by grey clayey cm-thick layers. These deposits are overlain by ca. 1 m-thick swamp clays displaying in the upper portion a set of mm-thick sandy layers indicative of recurring flood events. Upwards, around 4.5 m b.g.l., a 2.5 m-thick overbank succession composed of silty sands-sandy silts, hosting small (Ø mm) scattered Fe-Mn oxides, occur. The presence of two small-scale fining-upward sequences, the lowermost more evident, possibly document two main phases of overbank aggradation. Mottled floodplain stiff clays cap the cored succession.

TSP2 (9 m long)

Location: on-trace A, bright area

Stratigraphy: a lagoon succession, stratigraphically correlative to the lagoon deposits recorded underneath the Pisa city area and locally known as “pancone” (Sarti et al., 2015; section 4.1), forms the basal portion of core TSP2. These clayey deposits gradually passes, around 8 m b.g.l., to 1.5 m-thick, coarsening-upward flood-tidal sands, which are in turn overlain by a m-thick (ca. 3 m) monotonous succession of organic-rich, dark grey swampy clays. Upcore, homogeneous light grey clays hosting scattered small (Ø < 1cm) calcareous nodules occur, recording the development of a poorly-drained floodplain at the core site. Poorly-drained deposits are replaced around 3 m b.g.l. by 1 meter of swampy clays, that abruptly passes upwards to stiff floodplain deposits. The floodplain succession, which characterized the uppermost portion of the core, is abruptly interrupted around 1.4 m b.g.l. by less than 1 m of massive overbank sandy silts.

TSP3 (9 m long)

Location: on-trace A, dark strip

Stratigraphy: the TSP3 cored sequence displays a vertical stacking pattern of facies almost identical respect to that recorded at the close TSP2. A back-barrier succession composed of lagoon and flood-tidal delta deposits forms the basal portion of the core. Upwards, around 6.8 m b.g.l., a m-thick succession of swamp-poorly floodplain-swamp clays occurs. Around 2 m b.g.l. the uppermost swamp deposits abruptly turn into brown stiff floodplain clays. Thus, in contrast to TSP2, no overbank deposits are recorded within the uppermost portion. However, around 1 m b.g.l. a thin (less than 50 cm) but distinct fining-upward succession formed by silty sands-sandy silts-silts occurs.

TSP5 (8 m long)

Location: on-trace B, dark area

Stratigraphy: ca. 4 m-thick channel-fill sands, eroding the underlying lagoon deposits, form the lower portion of core TSP5. This succession, composed of fine-to-medium grey sands organized in fining upward successions, is abruptly overlain by 1 m of alternating clay and silt-sandy silt layers interpreted as an abandoned channel deposit. A ca. 3 m-thick succession of floodplain clays, formed under poorly-drained and then well-drained conditions, composes the upper portion of the core. This succession is interrupted around 2 m b.g.l. by a thin (ca. 40 cm-thick) interval of paludal deposits containing several charcoals.

- **Out-of-traces core**

TSP4 (10 m long)

Location**:** out of traces

Stratigraphy: the lower portion of the core TSP4 consists of a m-thick lagoon fine-grained succession containing a highly diversified meiofauna, indicative of a strong marine influence (low confined/outer lagoon in front of an inlet), and overlain around 7.5 m b.g.l. by flood-tidal delta sands and silts. These deposits, ca. 1.5 m-thick and displaying a brackish meiofauna accompanied by poorly-preserved shallow marine species, are chronologically constrained by radiocarbon dating (see Tab. 4.2) between ca. 6150 cal yr BP and 5450 cal yr BP.

Upwards a renewed phase of low-energy, back-barrier deposition is recorded by ca. 2 m of lagoonal clays, characterized by subtle but significant changes in the meiofauna content. Indeed, the abrupt upward decrease in species diversity, paralleled by an increasing dominance of the euryhaline species *C. torosa*, and the occurrence within the uppermost portion (around 4.5 m b.g.l.) of the freshwater-oligohaline ostracod *Darwinulina stevensoni* point to a marked increase in degree of confinement in the lagoon basin (Amorosi et al., 2014). Around 4 m b.g.l. washover sand-silt deposits abruptly overlain the lagoon succession recording a high-energy, storm event in the back-barrier basin. Upwards, the superposition of soft clays containing an oligotypic euryhaline ostracodfauna, exclusively composed of *C. torosa* valves, documents the establishment around 2750 cal yr BP (fig. 4.10; Tab. 4.2) of a highly confined, possibly barred, brackish basin as a coastal wetland/ lake. The progressive emersion of the basin is testified by the superposition of organic-rich swamp clays capping the cored succession.

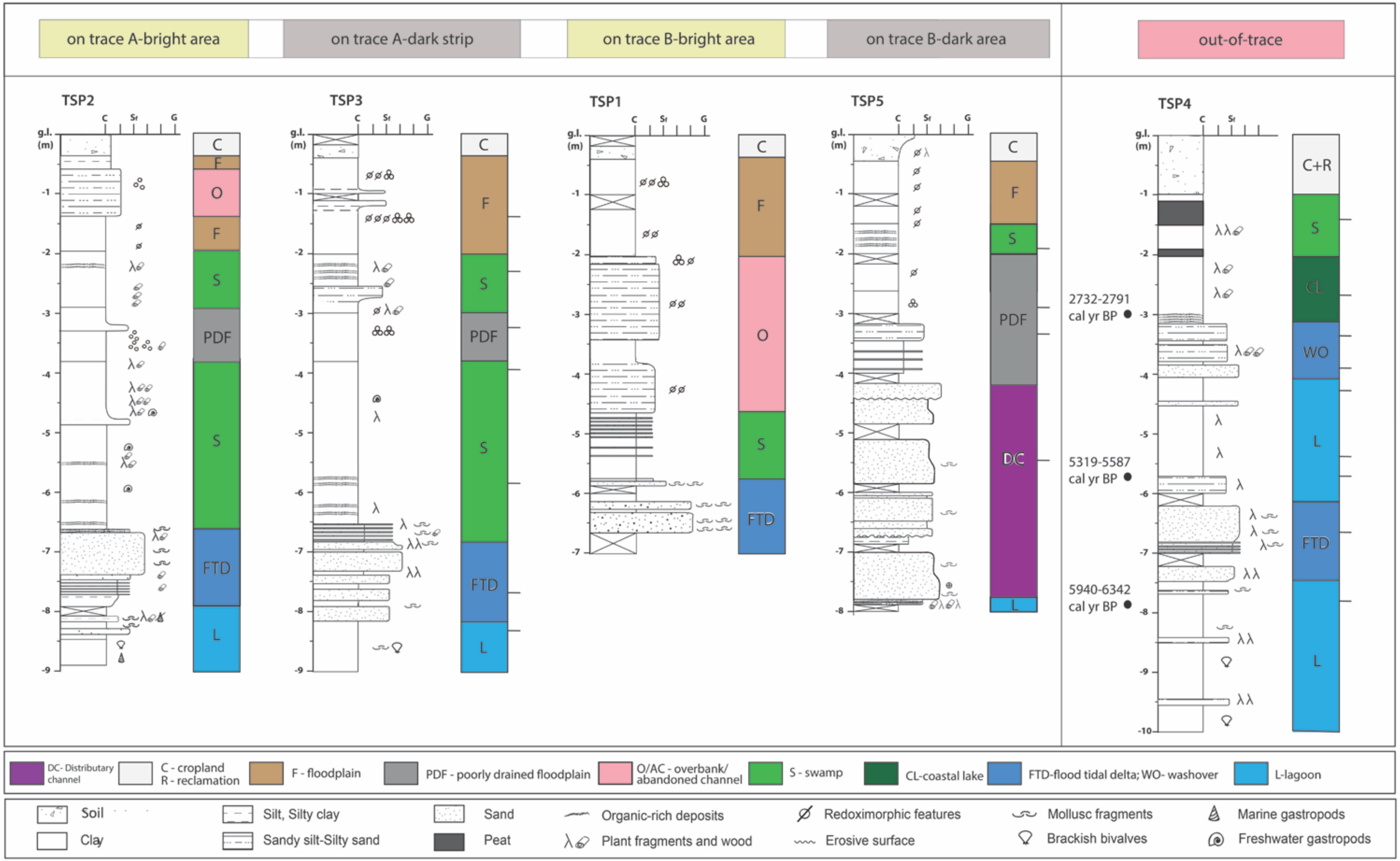

Figure 4.10_Stratigraphic logs and facies analysis carried out on the cores drilled in the San Rossore site (Pisa Plain). Radiocarbon dates performed on core samples are reported with black circles on the log. The location of the cores with respect of the remote-sensed traces (i.e. on-trace bright-dark portions/out-of-trace) is reported on the top of each stratigraphic log.

4.2.2.3.2 Additional shallow cores data (hand-auger drilling)

Detailed sedimentological descriptions of the five hand-auger cores, ca. 2 m long, drilled in distinct areas of the SR site (fig. 4.4) and used to test the subsurface stratigraphic expression of the RS-detected traces A and B (see section 4.3), are presented below. In this section, each core is described following a descending order, from the top to the bottom.

TM1 (fig. 4.11 a): from the ground level (0,55 m a.s.l.) unstructured brown clays occur, turning at around 50 cm b.g.l. into stiff brown clays with red and dark-grey mottles visible from ca. 70 cm b.g.l. downwards and connected to the presence of small (Ø mm) Fe-Mn oxides. Around 1,3 m b.g.l., a clayey succession composed of grey clays, progressively less mottled, and then, around 1,4 m b.g.l., black organic enriched clays occurs down to 2 m b.g.l.

TM2 (fig. 4.11 b): from the ground level (1,07 m a.s.l.) unstructured light-brown silty clays including roots fragments occur. Red and dark-grey mottles are encountered between ca. 40 cm and 80 cm b.g.l., due to the presence of small (Ø mm) Fe-Mn oxides. Downwards, light-brown clays with red and dark-grey mottles occur showing a high accumulation of Fe-Mn oxides, between ca. 1,4 m and 1,6 m b.g.l., accompanied by the occurrence of small (Ø mm) calcareous nodules. Between 1,6 m and 1,65 m b.g.l. these clays turn the color from mottled brown to dark-grey up to 1,9 m b.g.l., where pass to brown dark-grey mottled silty clays.

TM3 (fig. 4.11 c): from the ground level (0,75 m a.s.l.) unstructured dark-brown silty clays with fragments roots occur down to 30 cm b.g.l., where brown clays, locally mottled due to the presence of Fe-Mn oxides and hosting small (Ø mm) calcareous nodules, occur. Between 1,2 m and 1,6 m b.g.l. these clays turn into homogeneous dark-grey clays that pass downwards to greyish-brownish silty clays and silts with abundant red and dark grey mottles (Fe-Mn oxides) up to the bottom of the core.

TM4 (fig. 4.11 d): from the ground level (0,22 m a.s.l.) unstructured brown clays/silty clays with fragments roots and rare scattered Fe-Mn oxides, responsible for red and dark-grey, occur. They pass around 75 cm b.g.l. to brown clays including scattered Fe-Mn oxides and small (Ø mm) calcareous nodules. Around 1,45 m b.g.l. the mottled clays pass to organic-rich dark-grey clays, including two thin peat layers (at ca. 1,7 m and 1,9 m b.g.l.), up to the bottom of the core.

TM5 (fig. 4.11 e): from the ground level (0,9 m a.s.l.) unstructured homogeneous brown clays occur down to ca. 1,4 m b.g.l., where a 5 cm-thick dark-grey clayey layer turns into clays with sparse red and dark-grey mottles. From 1,4 m b.g.l. to the bottom of the core, silty clays hosting scattered small (Ø mm) Fe-Mn oxides and calcareous nodules are encountered.

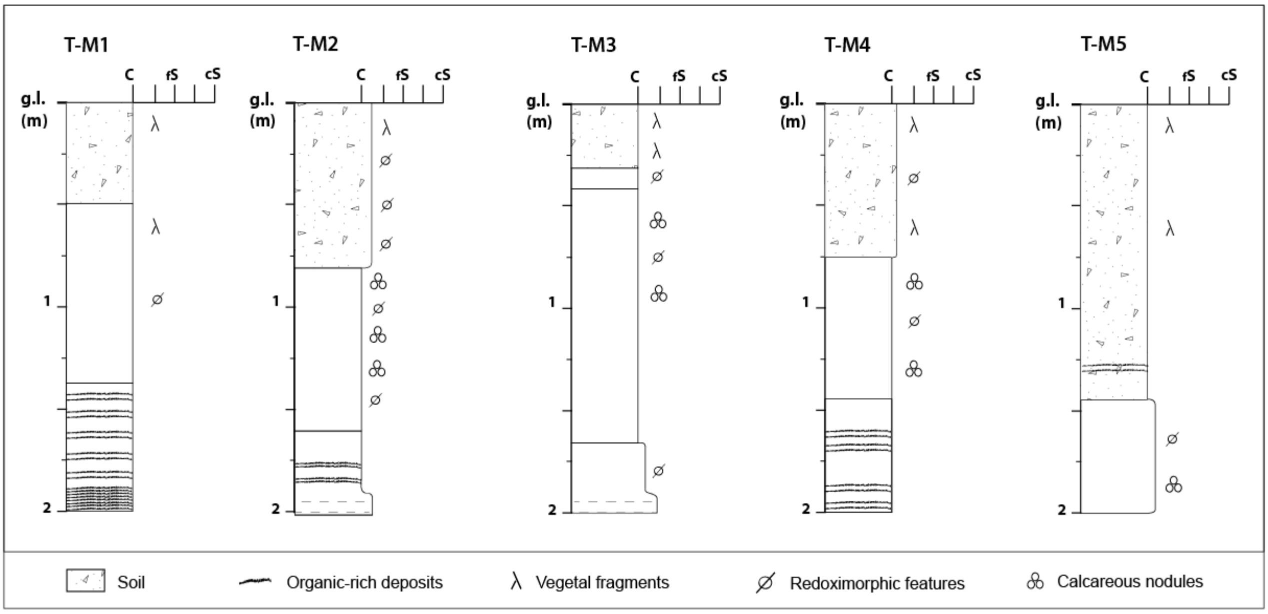

Figure 4.11_ Stratigraphic logs of the shallow cores drilled from the San Rossore (SR) site

As documented by the previous descriptions, all the shallow hand-auger cores confirm the widespread occurrence of fine-grained deposits within the uppermost 2 m of the subsurface succession, invariably in correspondence of both the white/dark portions of trace B and the dark strip of trace A (figs. 4.4, 4.5).

4.2.2.3.3_Subsurface facies associations

Eight main facies associations were recognized for the mid-late Holocene succession buried beneath the SR site, considering the sedimentologic features previously described (see section 4.2.2.1), the meiofauna content and the depositional vertical-lateral relationships recorded by cores.

Detailed facies descriptions and interpretations in terms of depositional environments are reported below following an overall ascending order:

- ***Lagoon (L)***

  Description: this facies association, characterizing the lowest portion of the drilled succession, is composed of extremely soft grey-blue grey clays and silty clays locally containing mm- to cm-thick (commonly less than 10 cm) silty-sandy layers. Mollusk fragments and shells, mainly represented by disarticulated valves of the typical coastal-lagoon species *Cerastoderma glaucum*, are encountered along with plant debris. Rare wood fragments can be also found close to facies upper boundary. An abundant well-preserved meiofauna dominated by opportunistic and euryhaline species as

Cyprideis torosa and *Ammonia tepida-A. parkinsoniana* characterizes this facies association. Locally, brackish-marine ostracods, including *Loxoconcha* and *Leptocythere* species (*Loxoconcha elliptica*, *Loxoconcha stellifera*, *Leptocythere bacescoi* and *Leptocythere ramosa*), are encountered as secondary taxa along with *Haynesina germanica*, *Aubygnina perlucida* and several species of Miliolids, mainly belonging to *Miliolinella* and *Pseudotriloculina* genera. At distal locations (core TSP4; fig. 4.3) in correspondence of the uppermost portion of this facies a peculiar oligotypic meiofauna, exclusively composed of valves of *C. torosa* (dominant species) and, as secondary species, *Darwinulina stevensoni* a freshwater-low brackish species (Henderson, 1990), is found.

Interpretation: sedimentological features indicate a low-energy depositional setting characterized by dominant settling processes, occasionally replaced by higher-energy traction processes (silty-sandy layers). The meiofauna content, dominated by *Cyprideis torosa* and *Ammonia tepida-A. parkinsoniana*, is considered indicative of a semi-protected brackish basin subject to salinity oscillations (Athersuch et al., 1989; Murray 2006) as a lagoon. The alternative occurrence, as secondary species, of brackish-marine or freshwater-low brackish ostracods indicates an high or low marine influence, respectively. This interpretation is also supported by the presence of an highly diversified foraminiferal assemblage, including shallow marine miliods, encountered with the brackish-marine ostracodfauna.

- ***Washover (WO)/Flood tidal delta (FTD)***

Description: this facies association, which invariably shows vertical relationships with lagoon deposits, is less than 2 m thick and is either made up of *(i)* light grey fine-medium sands, locally interrupted by cm-thick clay-silt layers, commonly showing a general coarsening-upward trend or *(ii)* dm-thick sandy layer overlaid by a rhythmical alternation of silt-clay layers. The latter are exclusively recorded at distal locations (core TSP4; fig. 4.3). Scattered vegetal and mollusk shell fragments are recorded, along with local enrichment of organic matter within the fine-grained layers. A scarce, poorly-preserved meiofauna composed of euryhaline (*C. torosa*) and shallow marine (*Loxoconcha rhomboidea*, *Aurila* sp., *Cytheridea neapolitana*, *Urocythereis* sp.) ostracods, mainly accompanied by *Ammonia* (*A. tepida* and *A. beccarii*) and Miliolid species is found.

Interpretation: the sedimentological and micropaleontological (mixed brackish-shallow marine poorly-preserved meiofauna) features along with the stratigraphic position of these deposits point to a back-barrier/lagoon high-energy depositional setting subject to marine currents/waves. Specifically, the CU sandy-dominated successions are interpreted as a flood tidal delta, formed in the outer/low-confined portion of the lagoon in direct connection with the sea through an inlet. The sandy-silty deposits recorded at distal locations at the top of the lagoon succession (see core

TSP4; fig. 4.9) are interpreted as a washover fan taking into account also the geomorphologic context (core TSP4 located immediately behind the first outcropping beach-ridge; fig. 4.3).

- ***Wetland (WT)***

  Description: this facies association, ca. 1 m-thick, is exclusively recorded within the upper portion of the distal core TSP4 (figs. 4.3, 4.10) and is composed of soft, light grey clays containing vegetal fragments and local accumulation of decomposed organic matter. An abundant autochthonous ostracodfauna exclusively composed of valves of *C. torosa* characterizes this facies.

  Interpretation: the sedimentologic characteristics point to a quiet deposition governed by decantation. The occurrence of an oligotypic euryhaline ostracodfauna is indicative of a highly-confined, slightly brackish coastal basin as a wetland, or at least a coastal lake. This interpretation is also supported by the stratigraphic position of this facies at the top of the lagoon succession at distal locations behind the outcropping beach-ridges.

- ***Swamp (S)***

  Description: this facies association, ranging in thickness between ca. 3-0.5 m and occurring at different stratigraphic levels within the studied succession, is represented by soft, dark-grey clays and silty clays. Abundant wood fragments, decomposed organic matter, locally forming thin organic-rich layers, and few freshwater gastropods (mainly *Planorbis*) are encountered. At distal locations (core TSP4; figs. 4.3, 4.10) cm- to dm-thick peaty layers also occur. An abundant, autochthonous ostracodfauna composed of freshwater-low brackish ostracods (*Pseudocandona albicans* and *Ilyocypris* species) is found, with the exception of samples collected from organic-rich/peaty layers deposits that are barren of microfossils.

  Interpretation: the distinctive sedimentological features (dark color, soft consistency and abundance of decomposed organic matter and wood fragments) and the fossil content are indicative of a wet, low-energy environment rich in woody vegetation as a swamp. The presence of an ostracodfauna dominated by limnetic to mesohaline species preferring slow-flowing waters (Henderson 1990; Meisch 2000) suggests the development of slightly brackish, stagnant conditions. In this context, low levels of oxygenation, typical of organic-rich substrata, is likely the reason of the absence of ostracods within organic-rich, peaty layers (Horne and Boomer, 2000; Frenzel and Boomer, 2005).

- ***Distributary channel (DC)***

  Description: this facies association, which is exclusively recorded in the lower portion of core TSP5 (figs. 4.3, 4.10), consists of grey medium-to-fine silty sands with an overall thickness of ca. 3 m, FU internal trends and basal erosive boundaries. Wood and vegetal remains together with mollusk fragments are locally present. Scattered coral fragments are also present at the base of the sandy succession. No microfossils are recorded.

Interpretation: this m-thick sandy succession is interpreted as a channel-filling. Specifically, the occurrence of mollusk fragments and coral fragments, the latter at the bottom, along with the latero-vertical stratigraphic relationships with the other facies suggest that these deposits represent the filling of a distributary channel.

- ***Poorly-drained floodplain (PDF)***

Description: this facies association, up to 0.5 m-thick, occurs within the upper portion of the studied succession. It is composed of rather soft, light grey clay and silty clay, with low organic-matter content and scattered calcareous nodules. Small-sized vegetal fragments are locally present, while no microfossils are found.

Interpretation: the fine-grained granulometry, the soft consistency, the absence of meiofauna and the occurrence of calcareous nodules suggest a low-energy, alluvial depositional setting subjected to short-lived phases of subaerial exposure as a poorly-drained floodplain. These peculiar poorly-drained conditions are likely due to a combination of high groundwater table and frequent fine-grained sediment floods that prevented a prolonged subaerial exposition.

- ***Floodplain (F)***

Description: this facies association, up to 2 m-thick, represents the uppermost portion of the studied succession. It is composed of dry, stiff brown clays and silty clays with evidences of subaerial exposure, including indurated horizons and redoximorphic features (i.e., Fe-Mn oxides and calcareous nodules). A dm-thick silty-sandy layer is found within core TSP3. Scattered vegetal fragments and thin layers of charcoals and small brick fragments are locally present. No microfossils are found.

Interpretation: the sedimentological features and the absence of meiofauna indicate a low-energy, alluvial depositional setting subject to subaerial exposure. The presence of layers enriched in charcoals and bricks fragments suggest human frequentation of the plain.

- ***Overbank (O)/Abandoned Channel (AC)***

Description: this facies association occurs at different stratigraphic levels and displays thickness ranging from 1 m to 2.5 m. It is either made up of a massive or fining upward succession of fine silty sands-sandy silts, or an alternation of sand-clay cm to dm-thick layers overlying channel-fill sands. Scattered small (Ø mm) Fe-Mn oxides, responsible for the reddish and dark-greyish mottles, and calcareous nodules are also found. No microfossils are observed.

Interpretation: lithology, grain-size trends and facies vertical relationships point to a channel-related depositional setting. Specifically, the silty sand-sandy silt successions are generally interpreted as overbank deposits, while the sand-clay alternation occurring onto channel-fill sands is interpreted as an abandoned channel deposit.

4.3. RS-stratigraphic data integration

Based on both subsurface facies and RS analyses, two small-scale stratigraphic sections involving the new drilled cores and crossing traces A (yellow line section fig. 4.11) and B (black line section fig. 4.11), respectively, were carried out to clarify the relationship between the RS-detected traces, visible from the surface, and the SR site depositional architecture. Indeed, the evident mismatching existing between the high-energy depositional processes connected to the formation of landforms, especially for the paleochannel B, and the clayey lithology of the soil samples (section 4.2.2.2) suggests that the stratigraphic expression of the traces should to be searched beneath the surface (i.e., beneath the uppermost 50 cm).

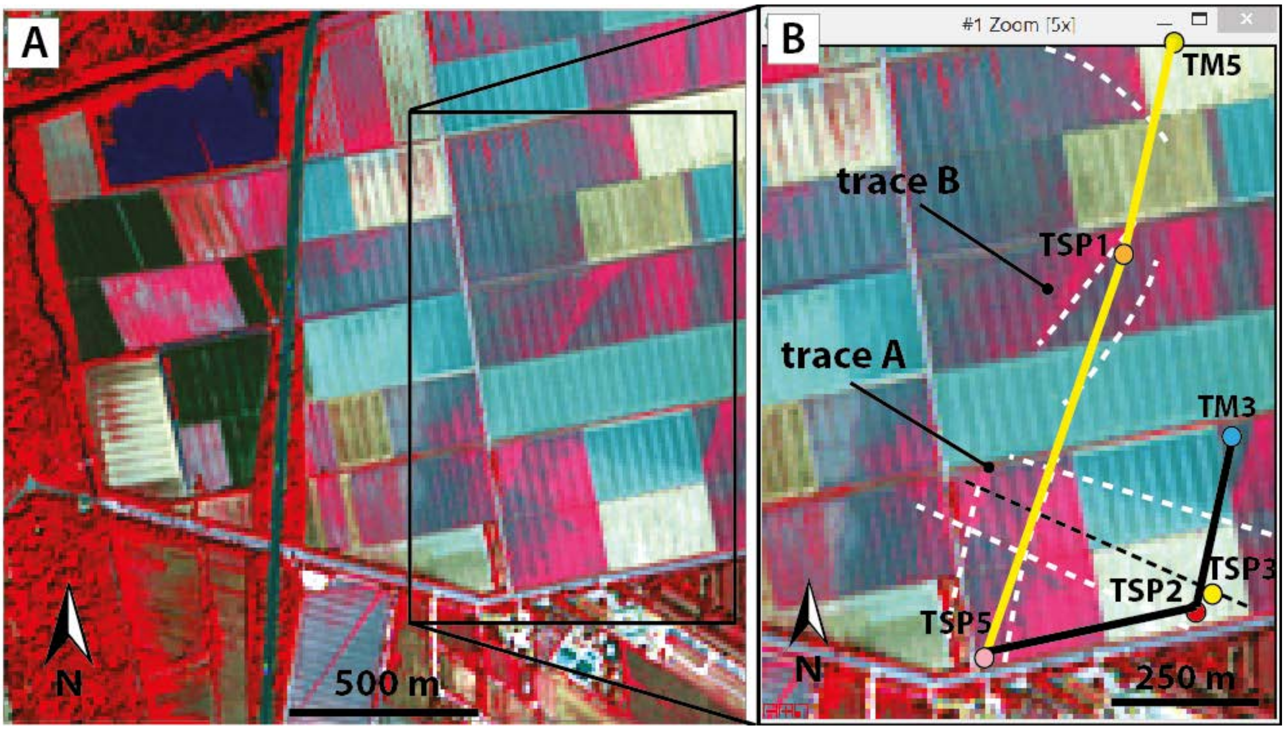

Figure 4.11_ a) False Color Composite (FCC) 843 from Sentinel 2a (scene 24 July 2015); b) zoom-in of the remote-sensed traces (white and black dotted lines); yellow line=trace of cross-section reported in fig. 4.12a, black line=trace of cross section reported in fig.4.12b)

As shown in Figure 4.12 a,b, cores TSP2 and TSP3, both located on trace A (figs. 4.3, 4.11) and drilled respectively on its bright portion and dark longitudinal strip (fig. 4.3), intercept a similar vertical stacking pattern of facies, mainly consisting of fine-grained deposits.

The bottom of the cores shows a readily identifiable stratigraphic marker for the mid-late Holocene succession of the Pisa Plain: the lagoon clayey unit known as “pancone” (Rossi et al., 2011).

This marker can be identified and tracked from proximal (Pisa city area) to distal (SR site) areas owing to its peculiar sedimentological and micropaleontological characteristics (very soft gray an homogeneous clays containing *C. torosa+A. tepida-A. parkinsoniana* assemblage), testifying the development of a wide lagoon basin since ca. 8000 cal yr BP (Amorosi et al., 2013).

The upwards occurrence of a flood-tidal delta sandy deposits documents a phase of low degree of confinement for the SR lagoon area that abruptly turns into a swampland attested between ca. 6-3 m b.s.l.

The uppermost portion of the succession corresponding with trace A is mainly composed of alluvial clays-silts recording the establishment of an alluvial landscape, characterized by a progressive subaerial emersion of the plain (poorly-drained floodplain are replaced by well-drained floodplain).

This floodplain succession is temporary interrupted by a renewed phase of swamp development, recorded by organic-rich deposits between ca. 2-1 m b.s.l. (fig. 4.12a).

The most significant stratigraphic difference between cores TSP2 and TSP3 is the occurrence within TSP2, which is located on the bright portion of landform A, of a 0.8 m-thick overbank sandy deposit interrupting between ca. 0.6 m and 1.4 m b.g.l. the homogeneous clayey floodplain succession (figs. 4.9, 4.12b).

This overbank sedimentation fits with the bright portion of trace A and its anthropic origin, previously hypothesized on the basis of morphological evidences (i.e., landform A in section 4.2.2.1).

Indeed, such relatively thin, shallow overbank succession, lacking of a corresponding channel-fill sandy deposit in the nearby core TSP3, is consistent with the peculiar dynamics of an anthropic canal (i.e., historical ditch draining the plain-Pisa *Centuratio*; section 4.2.2.1).

The clay-dominated succession occurs at correlative stratigraphic depths within core TSP3 reasonably corresponds to the clay plug that commonly caps an artificial channel, according to the position of the core drilled in correspondence of the “thalweg” detected by satellite sensors as a longitudinal dark strip (figs. 4.3, 4.11, 4.12b).

The occurrence of a distinct sandy-silty layer, less than 50 cm thick, around the s.l. within the clayey succession (figs. 4.9; 4.12b) indicates a temporary high-energy event recorded within the canal.

On the opposite sides of trace A (out-of-trace areas) no overbank silty-sandy layers are recorded within the uppermost 2 m of deposits recovered by the hand-auger core TM3 and the vibracore TSP5 (figs. 4.12a, b). In particular, TSP5 shows a quite different stratigraphic motif above the lagoon succession (i.e., stratigraphic marker), consistent with the succession recorded by core TSP1 as showed in section a) of figure 4.12. Both of cores are, in fact, drilled on trace B even if in slightly different positions (figs. 4.11, 4.12a) respect to the thalweg location of trace B.

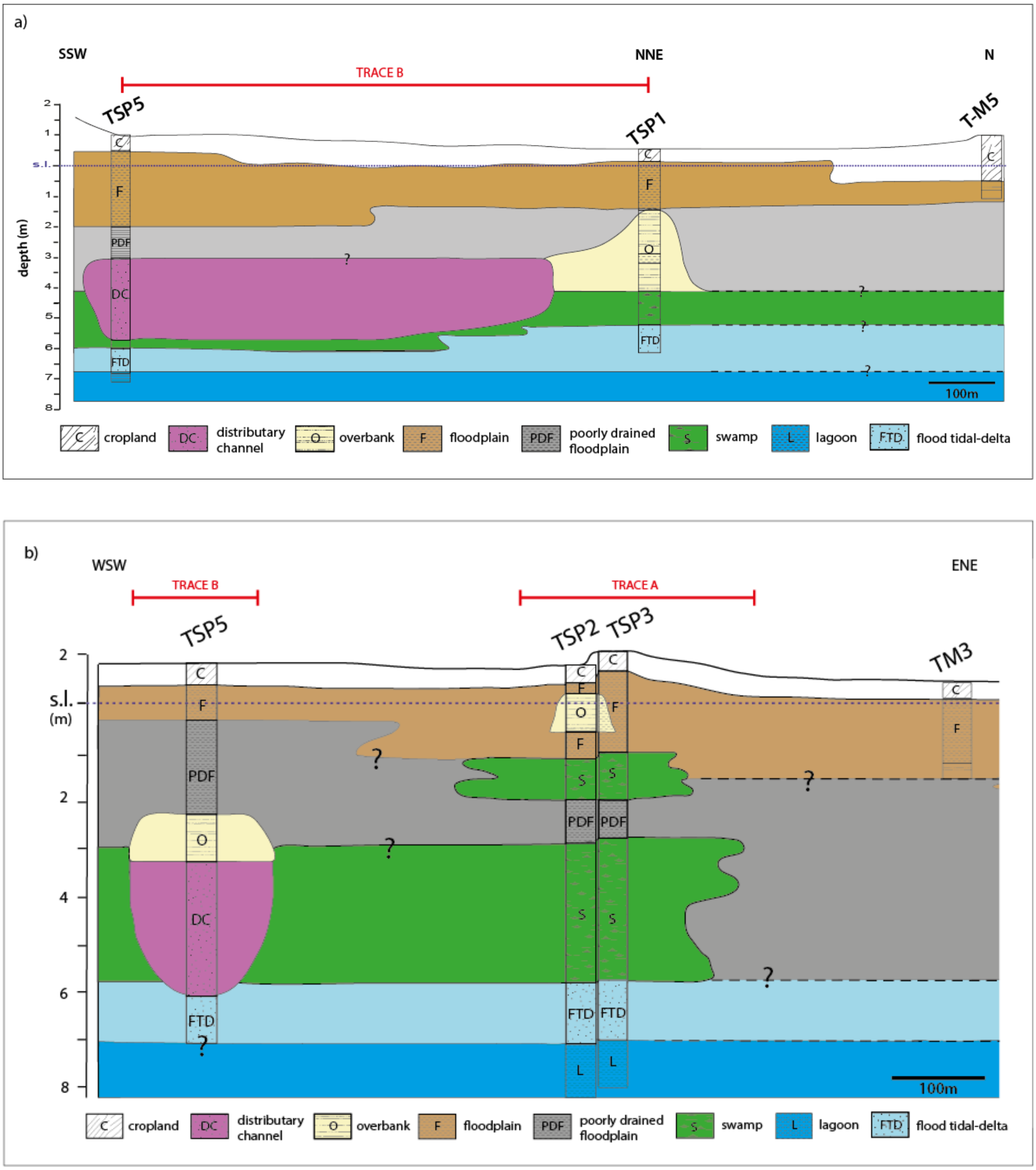

Figure 4.12_Interpreted stratigraphic sections across the identified traces (a-traces A; b-trace B and A) and facies correlations.

In detail, core TSP5 displays a m-thick channel-fill body, with top-of-sand at ca. 4 m b.g.l., eroding the underlying lagoon deposits and passing upwards to a clayey alluvial succession.

On the basis of the sedimentologic characteristics and the latero-vertical stratigraphic relationships (the channel-fill body passes laterally to swamps; see section a in fig. 4.12b), these channel-fill sands are interpreted as a distributary-channel deposit well compatible with the depocentral (thalweg) position of core TSP5 respect to trace B (dark portion in fig. 4.12b).

Thus, the sedimentary body associated to the physical depositonal processes that formed the remotely-sensed landform B (sinuous paleochannel) is recorded at ca. 4 m b.g.l.

Similarly, core TSP1 shows above a back-barrier (flood-tidal delta sands)-swamp succession a m-thick overbank sandy-silty deposit stratigraphically correlated with the distributary channel sands in core TSP5 (figs. 4.10, 4.12b). This interpretation is consistent with the location of core TSP1 on the bright portion of trace B, lateral to the dark depocentral portion and interpretable as an overbank area (figs 4.3, 4.12 a,b).

Westward to traces A and B, in a distal position, out-of-traces and close to the innermost outcropping beach-ridges located ca. westwards, core TSP4 intercepts a stratigraphic succession devoid of any alluvial/fluvial deposits and recording the progressive natural filling of the lagoon up to recent reclamation works (fig. 4.9).

Thus, the stratigraphic correlation carried out among TSP4-TSP5-TSP2 (W-E oriented section in fig. 4.13) together with radiocarbon data allows to set landforms A and B, identified on a plan-view by RS and physically connected to buried depositional bodies by stratigraphic data, into a comprehensive depositional-paleoenvironmental framework of this portion of the plain.

The distributary channel (landform B) has been active during the proto-historic (between ca. 5300-2700 cal yr BP) phase of Pisa Plain progradation, when a wide swampland suddenly developed across the SR site likely in response to the closing of the inlet through which flood-tidal delta sands extensively entered the lagoon basin around 6100-5400 cal yr BP (fig. 4.13).

The progressive closing of the lagoon is well recorded in core TSP4 by the ostracodfauna (increasing dominance of the euryhaline species *C. torosa* and appearance of the freshwater-oligohaline species *D. Stevensoni)*, and likely reflects the progradation of the laterally continuous set of the innermost outcropping beach-ridges, antecedent those archeologically dated to the II-I century BC and located ca. 170 m from core TSP4 (Pranzini, 2007).

During Etruscan times (since ca. 2700 cal yr BP), the lagoon turned into a calm and stagnant wetland then replaced by a swampy area according to the general prograding trend of the Arno delta system, recorded by the set of beach-ridges archeologically dated to II-I century BC onwards and located more than 800 m westwards (Pranzini, 2007).

Landward, a progressively well-drained alluvial plain developed (shift from poorly-drained floodplain to floodplain in core TSP2, TSP3 and TSP5 in figs., 4.9, 4.12 a,b, 4.13), recording in its upper portion the presence of a canal (landform A in cores TSP2 and TSP3; fig. 4.12b).

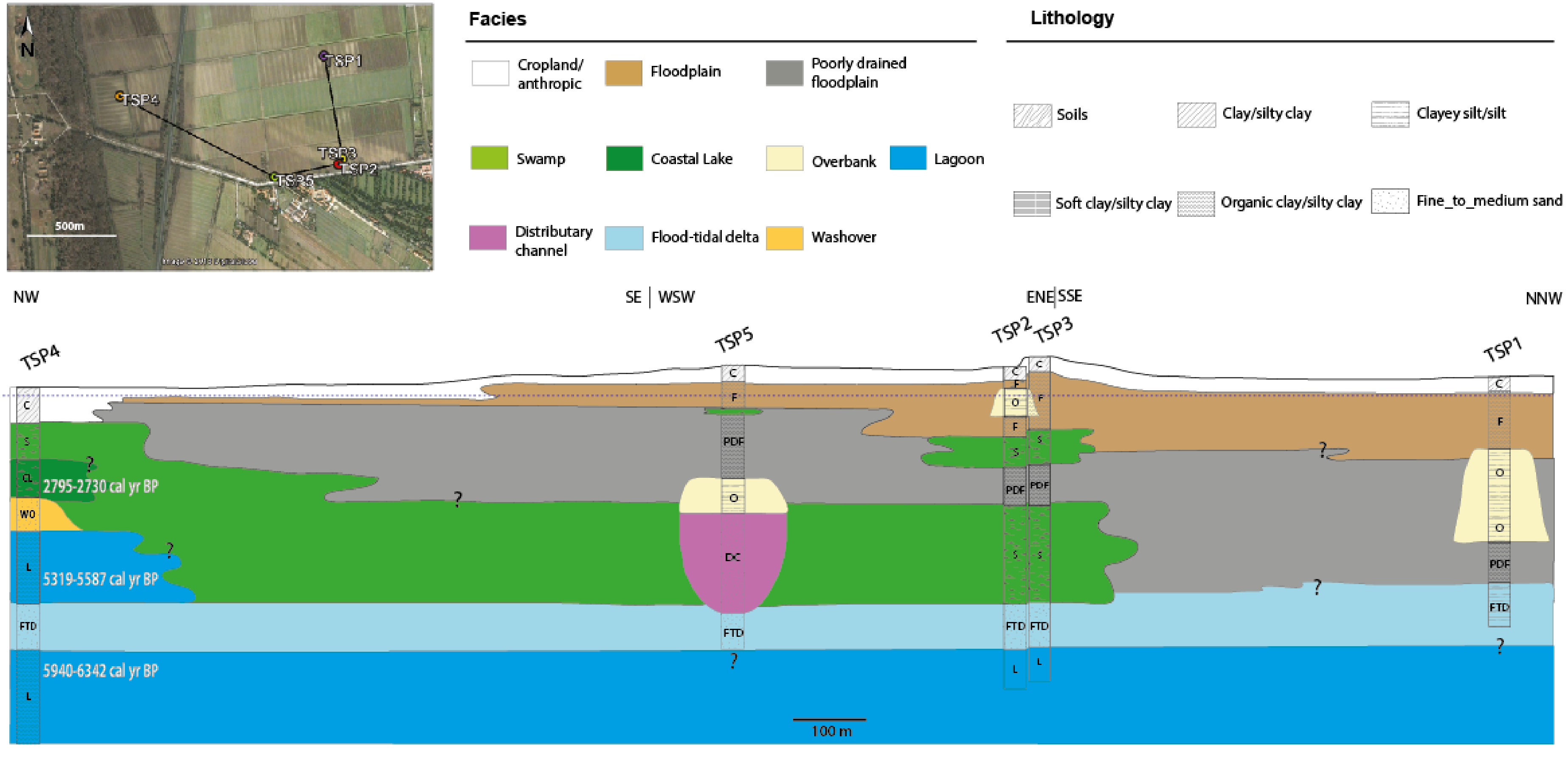

Figure 4.13_ Trace of the stratigraphic section based on deep cores data (TSP1-TSP5), stratigraphic section and facies correlations (C: cropland, F: floodplain, O: overbank, S: swamp; PDF: poorly drained floodplain; DC: distributary channel; FTD: flood tidal delta;WO: waskover; CL: coastal lake; L: lagoon)

References

Amorosi A., Rossi V., Sarti G., Mattei R., (2013). Coalescent valley fills from the late Quaternary record of Tuscany (Italy). *Quaternary International*, *288*, 129–138. http://doi.org/10.1016/j.quaint.2011.10.015.

Athersuch J., Horne D.J., Whittaker J.E., (1989). Marine and brackish water ostracods, in KERMACK D.M., BARNES R.S.K. (eds.) «Synopses of the British Fauna (New Series)», 43, Brill E.J., Leiden, 1-343.

Baumgardner M.F., Silva L.F., Biehl L.L. and Stoner E.R., (1985). Reflectance properties of soils. Adv. Agron. 38 1–44.

Baumgardner M.E and Stoner R., (1982) .Soil mineralogical studies by remote sensing. Trans. Int. Congr. Soil Sci. 12th,New Debli 5,419-441.

Bini M., Kukavicic M., Pappalardo M., (2012a). Remote sensing study on the Pisa plain, MapPapers 5en-II, 2012, 201-211.

Bruni S. and Cosci M., (2003). Alpheae veterem contemplor originis urbem quam cingunt Arnus et Ausur aquis. Il paesaggio di Pisa etrusca e romana: materiali e problemi, in Il porto urbano di Pisa antica, Pisa.

Burns R., (1993). Mineralogical Applications of Crystal Field Theory, Second Edition, Cambridge University Press, Cambridge, 551p.

Cosci M., (1990). Il contributo della fotografia aerea all'indagine archeologica, in VAGGIOLI M.A., San Giuliano Terme. La storia, il territorio, Pisa, 181-183.

Ellis S. and Mellor A., (1995). Soils and Environment, London: Routledge. A modern text with many examples and illustrations of soil profiles, soil transects and soil distributions.

Henderson P.A., (1990). Freshwater ostracods. In: Kermack DM, Barnes RSK (eds) Synopsis of the British fauna (New Series). Vol42. Universal Book Services, Oegstgeest.

Hunt G.R., Salisbury J.W., (1970). Visible and near infrared spectra of minerals and rocks. I. Silicate minerals. Modern Geology, 1, 283-300.

Hunt G.R., (1989). Spectroscopic properties of rocks and minerals, in Practical Handbook of Physical Properties of Rocks and Minerals (ed. Carmichael, R. C.), Boca Raton, Florida: C.R.C. Press Inc., 599-669.

Meisch C., (2000). Freshwater Ostracoda of Western and Central Europe. Spektrum Academischer, Heidelberg, Berlin.

Pranzini E., (2007). Airborne LiDAR survey applied to the analysis of historical evolution at the Arno River delta (Italy) in «Journal of Coastal Research» SI 50 (Proceedings of the 9th International Coastal Symposium), 400 – 409 http://www.griffith.edu.au/conference/ics2007/pdf/ICS078.pdf.

Rossi V., Amorosi A., Sarti G., Potenza M., (2011). Influence of inherited topography on the Holocene sedimentary evolution of coastal systems: an example from Arno coastal plain (Tuscany, Italy). Geomorphology 135 (1), 117–128.

CHAPTER 5_MEZZANO VALLEY (PO DELTA PLAIN) RS-STRATIGRAPHIC RESULTS

The present chapter illustrates the results obtained from the integration of the RS and subsurface data in the reconstruction of mid-late Holocene depositional evolution of the Mezzano Valley (MV), following a subdivision into two sections that refers to the regions in which the study area can be splitted (west and east portions) on the basis of the different patterns dispalyed by the remote-sensed traces. In fact, to the west the MV is characterized of features basically connected with the occurrence a paleo-drainage system, while to the east the MV is marked by the presence of outcropping/sub-outcropping beach-ridges.

Following this subdivision, section 5.1 concerns with the RS-stratigraphic investigation on the paleo-drainage and it is structured in a paper object of a forthcoming publication. It presents the application of the integrated methodological approach and the results obtained, and it is followed by a short paragraph reporting additional subsurface data (shallow vibracores) collected in the area and not included in the paper.

Section 5.2, presents surface and subsurface data dealing with beach-ridges remote-sensed traces, not involved in the publication.

The mentioned sections are followed by a detailed description (section 5.3) of the facies associations identified in the MV subsurface succession on the basis of the sedimentological characteristics and the meiofauna content cited inside the sections 5.1 and 5.2.

5.1. Paleodrainage RS-detected traces (MV west area)

5.1.1 Paper object of forthcoming publications

A mid-late Holocene tidally-influenced drainage system reconstructed by integrated remote sensing, sedimentological and stratigraphic analysis (Po Plain, Italy)

Authors

S. Giacomelli[1,2], V. Rossi[1], A. Amorosi[1], L. Bruno[1], B. Campo[1], A. Ciampalini [4], A. Civa[2], M. Sgavetti[2], R.C. Souza Filho[3]

[1]Department of Biological, Geological and Environmental Sciences, University of Bologna, Via Zamboni 67, 40127 Bologna, Italy. serena.giacomelli3@unibo.it

[2]Department of Chemistry, Life Sciences and Environmental Sustainability, University of Parma, Parco Area delle Scienze, 11/a, 43124 Parma, Italy. serena.giacomelli@unipr.it

[3]Instituto de Geociências - Universidade Estadual de Campinas - UNICAMP

[4]Department of Earth Sciences, University of Firenze, Via La Pira 4, 50121 Firenze, Italy

Abstract

The growing availability of open-access (RS) data and the rapid improvements in technology have encouraged an increasing use of the Remote Sensing (RS) satellite imagery in geomorphologic studies aimed to reconstruct past landscapes and drainage systems of modern alluvial-coastal plains. However, the stratigraphic interpretation of RS-derived traces, in terms of both facies and depth of burial, is still an open issue as well as the relationship between traces visualization and subsurface stratigraphy. Through an example from the southern portion of Po coastal plain (N Adriatic Sea, Italy) we show to what extent mid-late Holocene depositional architecture may influence surface identification of paleotraces in lowland areas, furnishing new insights into the RS application in Quaternary Geology.

A multivariate analysis, including free-of-charge optical images from different satellites, Digital Terrain Model (DTM) from LiDAR, soil reflectance spectra and cores facies stratigraphy, based on lithological and micropaleontological (benthic foraminifers and ostracods) features, has been performed on a wide (200 sq km) Po Plain wetland known as Mezzano Valley (MV) that hosted a lagoon basin at the peak of Holocene transgression. The integration of images visual interpretation (high reflectance/bright pixels *versus* low reflectance/dark pixels), and DTM analyses allowed the 3D-mapping of numerous and persistent bright traces rising up to ca. 1 m above the surrounding dark areas. These narrow, meandering paleotraces show hierarchical organization, in terms of meander sinuosity and width, from distal to proximal locations forming a dense dendritic paleodrainage network typical of a tidally-influenced system. Sedimentological (soil spectra) and stratigraphic (cores lithofacies and stratigraphic sections) calibration of two selected meanders (M1 and M2) reveals that paleochannel morphologies detected by RS data not only represent the surface expression of buried sandy channel bodies but also guide the spatial distribution of peaty lithofacies up to the surface. Indeed, on-trace areas invariably lack peaty deposits within the uppermost 6-7 m and record the occurrence of m-thick channel-fill sands with the top around 2-4 m below the ground level. In contrast, out-of-trace areas are characterized by organic-rich soils and a m-thick subsurface succession composed of intertidal-supratidal peaty deposits (mud flat, salt marsh and/or swamp lithofacies) recording the progressive isolation of the MV lagoon from the sea. The resulting spatial distribution patterns of organic-rich deposits, and hence of moisture, induce the sharp reflectance contrasts (traces) detected by satellite sensors.

Thus, the fully integration of surface and subsurface data reveals the occurrence of a tidally-influenced lagoon system beneath the microtidal Po Delta and allows a high-resolution plan-view mapping of a buried paleodrainage system. This tidally-influenced phase is radiocarbon dated to the early phases of Holocene sea-level highstand (ca. 6000-2500 cal yr BP) and was reasonably promoted by a combination of autogenic factors, including the low topographic gradient and the delta progradation far from the study area.

These finding hold promise for a successful application of a free-of-charge RS-stratigraphic approach to improve the reconstruction of past paleogeographic scenarios for coastal-deltaic lowlands shedding new light on their geomorphic evolution.

Keywords: satellite images, DTM-LiDAR, paleodrainage, facies architecture, mid-late Holocene, Po Delta

1. Introduction

Over the past decades, an increasing employment of remote sensing (RS) data in geomorphologic-geologic studies in response to the growing availability of open-access databases and the continuous improvement in the RS technology (Smith and Pain, 2009; Oguchi et al., 2013) has verified. It is known that airborne and spaceborne data, besides their widespread use in geological mapping, environmental monitoring and land-use studies (Bakker et al., 2009), can provide specific information on the distribution and morphologies of landforms.

Free-of-charge satellite imagery (e.g., Landsat and ASTER) is considered a powerful tool for the identification and mapping of past drainages and wetlands in alluvial-coastal plains, despite lower geometric resolution (e.g., 30 m and 15 m in visible-near infrared electromagnetic region-VNIR for Landsat and ASTER, respectively) than high-priced, airborne photographs. The key advantages of such satellite images are the production of different combinations of spectral bands (electromagnetic spectrum) and the capability to perform multitemporal analysis at low cost. Specifically, the creation of false color composite (FCC) images permits to depict subtle changes in soil moisture that result in the visualization on scenes of bright *versus* dark traces (i.e., high *versus* low reflectance values detected by satellites) over wide areas. Bright colors are interpreted to reflect well-drained conditions, and are commonly associated with fluvial-channel sands, whereas dark colors indicate wet/saturated conditions typical of fine-grained organic-rich sediments, such as those that characterize wetlands (Sgavetti, 1974; Sgavetti and Ferrari, 1988; Bisson and Bini, 2011; Bini et al., 2012).

Recently, a combined RS approach, based on satellite images and Digital Elevation Models (DEMs) derived from LiDAR (Light Detection And Ranging), has been increasingly and successfully adopted in the paleohydrographic reconstruction of wide portions of alluvial-delta plains (e.g., Ghilardi et al., 2008; Piovan et al., 2010; Ravazzi et al., 2013): especially in geoarcheological contexts (e.g., Fouache et al., 2005; Vött, 2007; Mozzi et al., 2010; Furlani et al., 2012) and in areas where dense vegetation cover makes the acquisition of field data extremely difficult (Rossetti et al., 2008, 2015; Mantelli et al., 2009; Andrades-Filho et al., 2014). However, the stratigraphic interpretation of RS-derived traces, in terms of both facies and depth of burial is still unclear. Reflectance is considered to be controlled by the upper few microns of the surface (Smith and Pain, 2009), but the extent to which subsurface stratigraphy may influence traces visualization is unknown.

In order to contribute to the above-mentioned issues and test the potentiality of satellite imagery as a tool for a plan-view identification of buried sedimentary bodies in coastal plains, a multidisciplinary approach integrating RS with field surface and subsurface data was applied to the Mezzano Valley, a wide lowland located south of the modern Po Delta (Fig. 1), in northern Italy. In this area, previous RS works (Sgavetti, 1974; Sgavetti and Ferrari, 1988) highlighted the presence of a dense network of narrow, meandering bright traces (paleochannels) of still unknown stratigraphic significance and age in the context of the Po Delta evolution.

Specific aims of this study are to *(i)* evaluate the effectiveness of a fully integrated RS-stratigraphic approach in the reconstruction of paleodrainage systems buried beneath modern coastal/delta plain areas; (*ii*) assess the influence of subsurface stratigraphy in the visualization and mapping of paleotraces to the surface, and (*iii*) complement conventional geomorphologic analysis in reconstructing the recent evolution of the Po Delta.

2. Geomorphological and stratigraphic setting

The Mezzano Valley (MV) is a ca. 200 sq km lowland belonging to an abandoned Po Delta lobe, south of the modern Po Delta (Fig. 1). A brackish lacustrine environment, known as “Valli di Comacchio”, which survived the extensive reclamation works carried out since the second half of the XIX century (Bondesan, 1990), separates the MV from the Modern-Contemporary Age beach-ridges and back-barrier humid areas. Recent reclamation works led the MV to emerge in the ‘60s.

Well-developed sets of juxtaposed beach-ridges, identified by Sgavetti and Ferrari (1988) in the eastern portion of the MV, testify several phases of shoreline progradation during the mid-late Holocene, under wave-dominated conditions (Fig. 1; Ciabatti, 1966; Sgavetti and Ferrari, 1988; Bondesan et al, 1990; 1995; Amorosi et al., 2003, 2005; Stefani and Vincenzi, 2005). Cuspate beach-ridges in the easternmost portion of the study area and in the contiguous Comacchio lake can be seen as evidence of ancient delta lobes (Sgavetti and Ferrari, 1988; Amorosi et al., 2003; Stefani and Vincenzi, 2005) fed by distinct Po paleo-branches (Po di Spina, Po di Primaro). Archeological data constrain delta activity in this area to the Etruscan time, up to the XII century, when the major avulsion known as “Rotta di Ficarolo” forced the entire Po River system to migrate northwards, marking the beginning of the modern delta (Ciabatti, 1990; Bondesan, 2000; Bondesan et al., 2001; Stefani and Vincenzi, 2005; Amorosi et al., 2008; Rossi and Vaiani, 2008).

As a part of the modern Po Delta, the MV belongs to the wider Po Plain system that constitutes the uppermost portion of an elongated foredeep basin delimited by the Alps to the north and the Apennines to the south. This basin was filled during the Pliocene and the Quaternary by a thick (> 7km) shallowing-upward succession of deep-marine to alluvial sediments (Pieri and Groppi, 1981; Ricci Lucchi, 1982, 1986).

The Middle Pleistocene–Holocene subsurface succession consists of vertically stacked transgressive-regressive (T-R) cycles, with alternating marine and alluvial deposits that reflect a glacioeustatic control in the Milankovitch (100 kyr) band (Amorosi et al., 2004, 2008).

High-resolution stratigraphic studies of Holocene deposits (Amorosi et al, 2005; Amorosi et al., in press; Stefani and Vincenzi, 2005) identified the formation of a lagoon basin in the early stages of transgression (ca. 11000–9000 cal yr BP), and its widespread development in the study area at peak transgression (around 7000 cal yr BP). Short-term paleoenvironmental changes occurred during the Holocene, as documented by the vertical stacking of m-thick parasequences within the ca. 30 m-thick T-R depositional wedge (Amorosi et al. 2005, in press). Specifically, the retrogradational stacking of parasequences in the early Holocene (Fig. 2) reflects the stepped, post-glacial eustatic sea-level rise (Bard et al., 1990; Liu et al., 2004). On the other hand, mid-late Holocene parasequences are interpreted to reflect the evolution of the prograding Po Delta system under sea-level highstand conditions (Lambeck et al., 2011; Vacchi et al., 2016), as revealed by the complex prograding pattern of outcropping and sub-outcropping beach ridges (Stefani and Vincenzi, 2005).

3. Material and methods

Different surface (satellite images, DTM LiDAR, soil features) and subsurface (core) data from the MV were analyzed in a GIS (Geographic Information System) environment. We focused on the uppermost 10 m, which record the highstand depositional evolution of the southern Po delta plain during the last ca. 6000 years (Amorosi et al., in press). The MV paleodrainage network reported for the first time in Sgavetti and Ferrari (1988) was studied in detail through a fully integrated RS-stratigraphic approach. Among all the paleodrainage traces that were mapped combining satellite and LiDAR data, two prominent meandering traces located in key (proximal *versus* distal) portions of the study area were selected for the acquisition of field data (soil and core samples).

3.1 RS-data and processing

The RS dataset consisted of multispectral and hyperspectral satellite optical images (sensor wavelengths ranging between 0.5-3 µm; Tab. 1a) and LiDAR elevation values.

Fiftheen images from Landsat 7 ETM+ (Enhanced Thematic Mapper Plus), Landsat 8 OLI (Operational Land Imager), Sentinel-2 MSI (Multispectral Instruments), ASTER (Advanced Spaceborne Thermal Emission and Reflection Radiometer) and Hyperion satellites were collected from the NASA Land Processes Distributed Active Archive Center (LP DAAC), USGS (United States Geological Survey) and the Scientific Hub ESA (European Space Agency)-Copernicus on-line databases (http://earthexplorer.usgs.gov/; https://scihub.copernicus.eu/dhus/#/home), along with Google Earth imagery. Since clouds and vegetation canopy represent obstacles for the effectiveness of image analysis for geologic purposes, only scenes recording bare soils under fair atmospheric conditions were selected (Tab. 1b).

In order to extract information about the pixels' spectral signature and to compare reflectance data among different images, the multispectral and hyperspectral scenes were pre-processed for the atmospheric correction. This process allowed the extraction of the Top of Atmosphere (ToA) reflectance (corresponding to the percent of energy reflected from the surface with respect to the incident energy) from the total radiance, that represents the energy recorded by the sensor for each pixel of the scene.

The Hyperion data were also adjusted for the bad bands. In contrast, no pre-processing was needed for the Sentinel-2 MSI imagery, as the level-1C type data directly furnish information about the ToA reflectance. The images were just converted to GeoTIFF format using SNAP (Sentinel Application Platform) by ESA online toolbox. This procedure led to combine reflectance with other types of data in a GIS environment.

Images were radiometrically and geometrically enhanced using ENVI software to recognize different elements that constitute the scenes on the basis of pixels' brightness contrast (i.e., reflectance values). A better identification of these elements was obtained through appropriate false color composites (FCC) in red-green-blue (RGB) visualization. In particular, the combination of sunlight spectral bands mostly sensitive to lithology and moisture, such as those from NIR (Near Infrared) and MIR-SWIR (Mid-Short Wave Infrared) regions, resulted to be particularly fruitful (Fig. 3). Despite the large use of TIR (Thermal Infrared) bands to estimate soil moisture (Pratt et al., 1979; Carlson, 1986; Jackson et al., 2004), these bands were excluded due to their low spatial resolution (Tab. 1) with respect to the investigated targets (generally less than 150 m wide).

The visual interpretation of the images was supported by a semi-automatic processing which includes the unsupervised digital image classification with the ISODATA-Iterative Self-Organizing Data Analysis Technique algorithm, and the Principal Component Analysis-PCA. The former groups pixels in classes based on their reflectance affinity, while the latter maximizes the spectral differences.

Multitemporal analysis of Landsat imagery (Tab. 1b) was also performed to study and compare over time the spectral response of the identified traces under different atmospheric conditions (Fig. 4).

All traces attributable to drainage networks or to beach-ridge complexes on the basis of their plain view geometry (Sgavetti and Ferrari, 1988) were mapped in a GIS environment and georeferenced in the UTM-WGS84 projection system.

The satellite image traces were matched with a 1 m-ground resolution DTM obtained from the aerial laser-scanning survey, commissioned in 2008 by MATTM (*Ministero dell'Ambiente e della Tutela del Territorio e del Mare*), in order to improve the geomorphological characterization of the study site. Elevation data were acquired by ALTM 3100AE Gemini laser-scanner (Tab. 3), recording data at a flight altitude between 1050 m and 1300 m from the ground level, with average acquisition density of 0.8 and 1.5 points/m^2 for coastal and inland zones, respectively (http://ambiente.regione.emilia-romagna.it/geologia/temi/costa/il-rilievo-lidar). This high-resolution DTM allowed to produce altimetric profiles across the traces identified by image analysis. All the microreliefs recorded within the MV area, were then mapped with planimetric and altimetric precisions of 1 m and ca. 0.15 m, respectively.

3.2 *Field data and analyses*

Sedimentological and stratigraphic studies were performed in correspondence with two selected paleomeanders, M1 and M2 in Figures 5a,b, located in the northern (proximal) and southern (distal) portions of the MV (Fig. 5a). Based on RS data, these paleomeanders apparently belong to two distinct channel network ramifications.

A campaign of soil sampling and coring was carried out at M1 and M2 sites, after a field survey aimed to the description of local morphological and sedimentological characteristics (grain-size, colors, and accessory materials).

Field data acquisition was performed primarily on the dark and bright portions characterizing the meander loop (i.e. meander trace, out-of-meander concave and convex banks; Fig. 5b).

Laboratory spectral signature analyses were carried out on eleven soil samples, from both RS-detected traces and adjacent areas (SOC in Fig. 5b), at the Remote Sensing laboratory of the Earth Sciences Department, University of Florence. An Analyical Spectral Device (ASD) Field Spec Pro spectrometer, which measures reflectance in 3-10 nm bandwidths over the 350-2500 nm range, was used. A dedicated Nadir viewing set-up, including two halogen tungsten lamps (24 V; 70 W) connected with a stabilized power supply device (TTi EX354D; Dual Output; 35V; 4A; 280W) was used to ensure minimum shadowing perturbation and guarantee the control of the irradiance conditions. Lamps were placed lateral to the sample, at a distance of 60 cm and inclined at 45°. The optic fiber was in the Nadir position at a height of 5-10 cm above the sample, resulting in a table-projected field of view diameter of 2-4.5 cm. All measurements were performed on powdered samples (<2 µm), using special care to level the powder to a uniform thickness. For each sample, four averages of 100 reflectance measurements were acquired in different positions to reduce noise, while reference measurements on the Spectralon panel were averaged on the 100 spectra and repeated systematically every three samples. The 11 mean spectra acquired in the different positions were averaged using the ASD ViewSpec Pro, and possible “steps” in the spectrum were eliminated using the “splice correction” function of this software. Normalization and exclusion of noisy tales from spectra were obtained using a dedicated Matlabscript (The Matworks, Natick, MA) that transforms the entire spectral library into ASCII format (Garfagnoli et al., 2013; Ciampalini et al., 2015). Moving to the subsurface, 6 cores (3 cores for each meander; Fig. 5b) up to 7 m-long were recovered to reconstruct the vertical stacking pattern of facies underneath the paleomeanders. A vibracoring device (Atlas Copco, Cobra model, equipped with Eijkelkamp samplers), which provides cores with small diameter (ca. 6 cm) but very high quality, was used.

For each meander (M1 and M2), the bright (TSC1 and TSC3) and dark portions observed along the concave banks were drilled (TSC5 and TSC4). One borehole (TSC2) was also located on the dark area along the convex bank of meander M1, and another one (TSC6) on the dark stripe identified within meander M2. All cores were positioned using a Global Positioning System (GPS) device. Each core was described in detail in terms of mean grain size, consistency, color and accessory materials, including calcareous nodules, redoximorphic features, plant debris/wood, peaty layers, and shells. To refine lithofacies interpretation, cores were sampled for benthic foraminifers/ostracods (42 samples), which are known to be excellent paleoenvironmental proxies in coastal settings, especially if jointly considered (Amorosi et al., 2014). Samples were prepared following the standard procedures reported in Amorosi et al. (2013). Each sample containing well-preserved, autochthonous meiofauna was dry-sieved through sieves of 125 microns. The fraction >125 micron was semi-quantitatively analyzed, according to the methodology adopted by Bondesàn et al. (2006) and Curzi et al. (2006) for other cores drilled in the Po Plain. Three main classes of species relative abundance (abundant: >30%; common: 30-10% and rare: <10%) were used to identify different autochthonous associations. Allochthonous associations, composed of scarce, poorly-preserved specimens, were also considered and qualitatively described in terms of taxa occurrence. Species identification and paleoenvironmental interpretations of mixed foraminifer-ostracod associations were based on several key papers dealing with the spatial distribution patterns of modern meiofauna in Mediterranean and North Atlantic coastal areas (Albani et al., 1984, 2007; Athersuch et al., 1989; Albani and Serandrei Barbero, 1990; Henderson, 1990; Stoch, 1995; Montenegro and Pugliese, 1996; Ruiz et al., 2000; Murray, 2006; Melis and Covelli, 2013).

In order to reconstruct sediment body geometries beneath areas with contrasting reflectance values, stratigraphic correlation was carried out between cores along short transects transversal to the meandering traces (M1 and M2).

The chronological framework was guaranteed by 9 radiocarbon ages (Tab. 4) performed on wood fragments, peaty layers, organic clays and mollusk shells at CIRCE Laboratory of Caserta (Naples University) and KIGAM laboratory (Daejeon City, Korea). Conventional ages were calibrated using Oxcal 4.2 (Bronk Ramsey and Lee, 2013) and the IntCal13 and Marine13 calibration curves for terrestrial and marine materials, respectively (Reimer et al., 2013). In order to compensate for the reservoir effect, mollusk samples were calibrated using an average value of DeltaR (35±42), estimated for the northern Adriatic Sea and available online (http://calib.qub.ac.uk/marine/). In this study, all ages are reported as the highest probability range (cal. years BP) obtained using two standard deviations-2σ (Tab. 4).

4 Results

4.1 Morphologic features of the paleodrainage system

As shown by the DTM, the MV is mostly located below the present sea level.Its margins are physically marked by canalized Po River paleobranches, ca. 0.5-1 m above sea level-a.s.l. (Po di Primaro and Po di Spina; Bondesan, 1990; Ciabatti, 1990; Bondesan, 2001). The MV has depressions in the middle, where minimum quotes occur down to ca. 4/5m m b.s.l. (Fig. 6). This topographic trend is even more obvious behind the outcropping beach-ridge complexes, locally partially flattened by agriculture activities.

Within the concave-up configuration of the western sector, the integration of different RS techniques (multi- and hyper-spectral, multitemporal satellite image analyses and LiDAR profiles) led to detailed 3D-mapping of a complex paleodrainage system, composed of numerous and persistent bright traces rising up to ca. 1 m above the surrounding dark areas (Fig. 8 a, b).

Most of the RS-detected, meandering traces display clear convex-up topographic profiles from one bank to the opposite side. Micro-morphologies related to the convex and concave banks are also observed (Fig. 8b), except for areas strongly reworked or flattened by agriculture activities. In this case, bright traces often show a longitudinal, narrow dark strip in central position, interpreted as the thalweg brought to light by the anthropic removal of surface deposits that cap the channel body (Fig. 8c). The DTM profiles performed across the bright traces also furnish information about river evolution. In areas poorly affected by human activities, meander topographic profiles exhibit a convex side and a cut bank concave side, that point to the lateral migration of point bar.

The RS-derived traces are arranged into a dense and dendritic–paleodrainage system (Fig. 7) made up of narrow, meandering channels (Hughes, 2012). A hierarchical organization, in terms of meander sinuosity and width, from distal (eastern) to proximal (western) locations (branching pattern of Van Veen, 1950) was observed. Close to the outcropping beach-ridges, the channels are tens-m wide and display a low degree of sinuosity that progressively increases in back-barrier position, where channels are more numerous, very narrow and with smaller radius of curvature (Fig. 7, Fig. 8a).

These morphological features point to a paleodrainage influenced by tidal currents and characterized by tidal channels, from which originates a progressively smaller and more sinuous pattern of tidal creeks, consistent with the landward dissipation of marine energy (Dalrymple et al., 2012). The clustering of ribbon-shaped channels in the southern MV, immediately behind the barriers, reflects the decrease in flow velocity in highly protected areas developed lateral to the main inlet. This interpretation is consistent with the general stratigraphic framework of the study area, which documents the prolonged persistence of a wide back-barrier lagoon system during the mid-late Holocene (Fig. 2, section 2).

Despite the complexity of the MV paleodrainage, the tidal inlet was identified in the area presently occupied by the canalized Po di Spina paleobranch. From this area, two main tidally-influenced channel networks, identified by satellite images PCA and DTM analysis, seem to diverge following slightly different flow directions (Fig. 7). The meanders M1 and M2 (Fig. 5 a,b, section 3.2) that we selected for sedimentological and stratigraphic analyses belong to these two distinct, and possibly non-coeval networks.

4.2. Sedimentological and stratigraphic calibration of remotely-sensed paleomeanders

4.2.1. *Surface characterization*

The field survey across the M1 and M2 traces identified the widespread presence of clay and silt deposits, generally hosting plant roots and, at places, shell fragments. Consistent with field analysis, Hyperion spectral data assign both bright and dark features to the silty loam textural class (ENVI spectral library, John Hopkins University).

The geometric resolution of the analyzed images (pixel size is 30mX30m) prevents determination of a precise spectral signature for the bright (paleochannel traces) and dark areas. For this reason, we checked through laboratory reflectance spectra on soil samples. Surface (5 cm) sediment layers on and around the meandering traces (Fig. 5b, section 3.2) display the typical bare soil signature (Stoner and Baumgardner, 1981; Baumgardner et al. 1985), in which reflectance increases with the wavelengths and water absorption bands are observed around 1400 nm and 1900 nm. Samples from the bright areas (paleomeander traces) show high values of reflectance and an evident adsorption band in the VIS-NIR region, around 800 nm (Fig. 9), due to the presence of Fe-oxides (Hunt and Salisbury, 1970; Hunt, 1977; Baumgardner et al. 1985; Burns, 1993, Ellis and Mellor, 1995). In contrast, samples from the dark areas (outside the meander loops), invariably show spectra with lower reflectance values and lack of absorption bands with flattening in the VIS-NIR region, which is indicative of the presence of organic matter (Stoner and Baumagardner, 1981; Burns, 1993).

4.2.2. Subsurface stratigraphy

Integrated sedimentological and micropaleontological analyses on the mid-late Holocene succession drilled in the study area led to characterize the lithofacies described in Table 4. Facies analysis on cores TSC1-TSC6 documents distinct vertical stacking patterns of lithofacies in areas characterized by different reflectance values and position relative to the meander loops (Figs. 5, 10). The stratigraphy is described below, following a mixed, RS-geomorphological (on-trace *versus* out-of-trace; convex bank *versus* concave bank of the meander) criterium. On-trace cores invariably lack peaty facies and document the top of tidally-influenced channel sands 2-4 m below the ground level. In contrast, cores drilled out of the paleodrainage traces show thick successions of salt marsh and/or swamp deposits. The uppermost part of all cores (40-50 cm) consists of anthropogenic deposits related to agricultural activities.

On-trace stratigraphy

The lower parts of the 7 m-deep cores drilled on the bright paleochannel traces (TSC1 and TSC3; Fig. 5b, section 3.2) invariably consist of > 3 m-thick medium sands including small-sized, scattered vegetal/wood fragments, organic-rich layers and, occasionally, few poorly-preserved valves of *Cyprideis torosa*. At TSC3 core site (meander M2; Fig.5b, section 3.2), the sandy succession overlies lagoonal clays through a prominent erosional discontinuity, marked by a 1 m-thick lag deposit rich in shell fragments of brackish (i.e., *Abra segmentum* and *Cerastoderma glaucum*) and marine (i.e., *Cerithium submamillatum*) mollusks. These features point to channel deposits strongly influenced by marine currents, consistent with the morphological interpretation of the RS paleodrainage (i.e., tidally-influenced channel network; section 4.1. and Figs. 8, 9a).

Overbank deposits of variable thickness occur above the channel-top-sand in M1 and M2, at different depths (Fig. 10). They consist of silt-sand alternations, a few cm- to dm-thick, containing vegetal/wood remains and, at distal locations (M2), a poorly-preserved meiofauna composed of species typical of intertidal mud flats (dominant *Ammonia tepida* and *Haynesina germanica* with the subordinate occurrence of *Trochammina inflata*; Horton and Edwards, 2006).

Paludal clays and silts, < 1 m thick, containing an oligotypic ostracofauna dominated by species preferring slightly brackish, slow-moving waters (*Pseudocandona albicans*), cap the cored successions.

Underneath the dark strip within the M2 paleotrace (core TSC6; Fig. 5, section 3.2), a thin (< 50 cm-thick) succession of abandoned-channel sediments rich in organic matter and mollusk fragments is recorded above channel sands. This facies is overlain by mud flat clays, with a brackish foraminiferal fauna indicative of highly-restricted conditions (*Ammonia tepida* and *Haynesina germanica* as dominant species; Debenay et al., 2000; Debenay and Guillou, 2002; Tab. 4). Upwards, peaty swamp clays occur.

Out-of-trace stratigraphy

A similar succession of fine-grained, back-barrier lithofacies, including subtidal, intertidal and supratidal deposits (Tab.4), is recorded by cores TSC4 and TSC5, which were recovered 100-200 m far from M1 and M2 channel axes (Fig. 5b, section 3.2). In the distal core (M2-TSC4 in Fig. 5b, section 3.2), 4.5 m-thick lagoonal deposits are abruptly overlain by swamp peaty clays, whereas a gradual, shallowing-upward trend is recorded at proximal locations (M1-TSC5 in Fig. 5b, section 3.2) by the transition from lagoonal to mud flat, salt marsh and peaty swamp deposits. Silt-sand alternations, a few cm thick, containing a scarce poorly-preserved brackish meiofauna (mainly *A. tepida-A. parkinsoniana*, *H. germanica*) are interpreted to reflect overbank deposition of tidal-channel suspended sediment (M1 meander in Fig. 5b, section 3.2).
Underneath the M1 convex bank, the lower part of core TSC2 shows a 2 m-thick tidally-influenced channel sand body that erodes the underlying lagoonal deposits. Upwards, salt-marsh deposits overlain by peaty swamp clays cap the core succession.

5. Discussion

<u>5.1. Factors controlling the surface identification of paleodrainage traces</u>

Satellite images, sometimes used in conjunction with DTM-LiDAR, are commonly used to depict recent changes in the alluvial plain drainage systems and to delineate past morphological features, such as paleochannels, in coastal-deltaic areas (Cohen et al. 2014; Mozzi et al., 2010; Piovan et al., 2010, 2012). The visualization of paleochannels in coastal plain areas is generally favored by contrasting soil features (texture, lithology, moisture content), which influence the reflectance values recorded by satellite sensors under bare conditions (Salter et al., 1966; Smith and Pain, 2009). It is widely accepted that the RS identification of landforms is strictly related to the juxtaposition of distinct lithofacies, such as channel-fill sands, overbank sand-silt alternations, and floodplain/delta plain silts and clays. The creation of multispectral composite images aimed at enhancing differences in soil lithology and moisture has improved the visualization of paleochannels in several Mediterranean alluvial-delta plains (Bini et al., 2012), including the MV (sub-section 3; Sgavetti and Ferrari, 1988).

In the MV, the cross-reference of RS-derived, paleomeander traces with soil data highlights compositional differences that fit well with the spatial distribution of bright traces and surrounding dark areas. The former in general correspond to Fe oxide-rich soils, whereas the latter are characteristic of organic-rich soils. Contrasting values of organic matter content can, in fact, explain differences in soil reflectance, as organic-rich soils are known to be responsible, besides moisture, for the decrease in the whole reflectance values (resulting in dark colors), especially in the VIS region (organic matter fraction >2% in Baumgardner et al., 1970).

The absence of surficial channel-related deposits, along with the persistence across different seasons and physical conditions (vegetation cover and human land use) of the remote-sensed traces detected by multitemporal satellite images suggest a subsurface stratigraphic influence in the surface visibility (bright and dark areas) of the paleochannels traces.

Core facies analysis and stratigraphic cross-sections across paleomeanders M1 and M2 show that the tidally-influenced channel sand bodies physically associated to the bright traces occur at depths > 2-4 m below the ground level (Fig. 11). The spatial distribution of these sandy bodies in the subsurface, in turn, conditions the spatial distribution of the overlying lithofacies, producing on the surface the recorded differences in soil optical behaviors between on-trace and out-of-trace areas.

The development of tidally-influenced, branching paleo-networks within a semi-protected embayment determined a characteristic depositional architecture in the subsurface of the MV basin, with sand bodies encasedinto lagoonal (mud flat and salt marsh) fine-grained deposits, evolving into peaty swamps (Fig. 11). The lateral migration and filling of these meandering channels produced well-defined convex micro-morphologies rising above the low-lying MV basin, depicted by LiDAR and assigned to the channel-levee complex (sub-paragraph 4.2.1.; Fig. 8a). On these micro-reliefs, paludal clayey silts were subject to incipient pedogenesis, as documented by the formation of Fe oxides. Whereas, in adjacent, naturally depressed out-of-trace areas, thick successions of peaty clays accumulated, recording the progressive isolation of the basin from the sea (transition from salt-marsh to swamp clays; Fig. 11).

Similarly, channel abandonment and the widespread establishment of stagnant waters favored the deposition of organic-rich/peaty lithofacies within channels (i.e., thalweg), resulting in the RS-detected dark strip inside the trace (M2 trace in Fig. 5b, section 3.2).

The paleochannel morphologies detected by RS data, thus, represent the surface expression of buried sandy channel bodies, and reflect the spatial distribution of the overlying lithofacies, in particular of peaty (mud flat, salt marsh and swamp) deposits. The different organic matter content influences the deposits capacity to retain moisture, resulting in the sharp contrasts in reflectance values detected on the surface by satellite sensors. Thick packages of near-surface, organic-matter-rich layers may decrease reflectance values, preventing the RS detection of underlying sand bodies, as recorded by core TSC2, where the buried channel sands are overlain by a 4 m-thick succession of salt marsh and swamp layers (Fig. 11).

A close relationship therefore links the shallow (6-7 m) subsurface stratigraphy and the remotely sensed paleodrainage system of the MV.

5.2. *Development of a tidally-influenced system in the microtidal Po Delta*

The combination of RS data (multi and hyperspectralsatellite image analyses and DTM LiDAR) with high-resolution surface and subsurface sedimentological and stratigraphic data proved to be a powerful tool to reconstruct in detail past coastal drainage networks. This approach also allowed for the first time to define the relationships between remote-sensed paleochannel traces and corresponding lithofacies, leading to the reconstruction of a tidally-influenced depositional network developed during the mid-late Holocene.

In the low-lying coastal setting of the MV, processing of satellite images and LiDAR data showed great efficacy for unravelling two main tidally-influenced systems (Fig. 7), whose facies characteristics were examined by core analysis. Stratigraphic correlation beneath two key paleomeanders and radiocarbon dating and document that these channel systems, geomorphologically comparable in terms of pattern, size and hierarchization, developed in two distinct periods between ca. 6000-2500 cal yrs BP, when the MV was a wide, sheltered mud-rich interdistributary area of the Po Delta system (Amorosi et al., in press).

This embayment was partially enclosed by a set of prograding beach-ridges, archeologically dated to the pre-Etruscan period (older than ca. 2700 cal yr BP; Bondesan et al., 1995; Stefani and Vincenzi, 2005), behind which the tidally-influenced drainage developed. A tidal inlet interrupted the sandy barriers at the northeastern edge of the study area, where the two tidally-influenced networks diverge landwards (Fig. 7, section 4.1).

The channel sand bodies are encased within a clay succession made upof lagoon/subtidal deposits and intertidal (mud flat and salt marsh) facies. The record of mud flat and salt marsh deposits, mainly identified on the basis of meiofauna analysis, supports the subaqueous nature of channels and the strong influence of tides in the MV during the early phases of sea-level highstand.

This tidally-influenced depositional system likely developed in response to a variety of factors that favored the local and temporarily amplification of tidal currents. According to previous works (Longhitano et al., 2010, 2012a, b and references herein) on the Quaternary record of tidal deposits in the Mediterranean, microtidal area (tidal range <2 m; Dean and Dalrymple, 2004), specific morphologies of the coastline (straits, confined gulfs or embayment) and general basin characteristics (width and bathymetry) can induce significant tidal amplification, together with local, –wind-induced effects on tides. Indeed, it is widely accepted that tidal processes can be significant, especially during transgressive periods, when estuaries and embayment are commonly diffuse along the coastlines.

The co-occurrence of an embayment in the MV and of a very shallow-flat shelf in the northernmost Adriatic sector could reasonably have amplified the tidal currents effects.

Po delta dynamics may have favored the tidal-influence during the sea-level highstand. During the earliest phases of Po Delta construction, between ca. 7000-2500 cal yr BP, the MV was far from the Po delta direct influence, and only in Etruscan times, a delta lobe developed in front of the MV (Po di Spina delta lobe; Bondesan et al., 1995; Stefani and Vincenzi, 2005; Amorosi et al., in press).

The switch from a tidally-influenced embayment to a barred-paludal basin is stratigraphically recorded by the transition from intertidal to swamp deposits, the latter radiocarbon dated from ca. 2700 cal yr BP onwards (Fig. 11). From that time, a complex pattern of prograding delta lobes is recorded in front of the MV, up to ca. 800 cal yr BP, when a major fluvial avulsion (i.e., Rotta di Ficarolo, in 1152) forced the entire Po River system to migrate northwards, marking the onset of the modern Po Delta (Stefani and Vincenzi, 2005; Amorosi et al., 2008; Rossi and Vaiani, 2008).

Due to the lack of direct fluvial sediment supply, the MV remained an interdistributary area over time, as testified by the radiocarbon age of ca. 2200 cal yr BP obtained 50 cm below the ground level in TSC2 (Fig. 11).

Conclusions

The integration of RS data with detailed sedimentological and stratigraphic analysis revealed the presence of a buried, tidally-influenced paleodrainage system below the Mezzano Valley, south of the present Po Delta. The combination of free-of-charge multispectral and hyperspectral satellite optical images, LiDAR DTM, soil spectral analyses and high-resolution core facies data showed the effectiveness of RS data and techniques in reconstructing buried landscapes and provides valued information about the mid-late Holocene sedimentary dynamics.

The major outcomes of this study can be summarized as follows:

- satellite imagery processing and analysis (e.g., FCC RGB visualization, multitemporal analysis and PCA), combined with DTM LiDAR, allowed the identification and detailed mapping of meandering paleochannels, whose associated deposits are buried at > 2 m below the ground level;
- paleochannels are highlighted by the arrangement of pixels with contrasting brightness (spectral reflectance variable values on the surface) and by distinct topographic profiles, if not flattened by anthropic activities. The brightness (i.e., reflectance values) variability of is guided by the spatial

distribution of surface moisture, which mainly depends on the spatial distribution of organic-rich/peat deposits;

- the spatial distribution of meandering paleochannels, with well-defined micro-morphologies, influences the distribution of organic-rich deposits, which tend to accumulate in low-lying areas lateral to the channels;
- free-of-charge satellite images combined with DTM LiDAR data represent a suitable tool for high-resolution paleoenvironmental-paleodrainage reconstructions of coastal plains. The RS paleochannels represent the surface expression of buried sandy bodies, whose formation and activity can be dated back up to the early highstand phases;
- the approach adopted in this work could be particularly effective in depositional settings similar to the MV, where isolated coarse-grained sediment bodies are encased into fine-grained organic-rich deposits;
- the identification of a tidally-influenced lagoon system within the microtidal Po Delta during the mid-late Holocene sea-level highstand can furnish new insights for high-resolution depositional models and paleogeographic reconstructions of other Mediterranean delta areas.
- the tidally-influenced depositional phase, dated between ca. 6000-2500 cal yr BP, was reasonably promoted by a combination of autogenic factors, including the low topographic gradient of the coastal area and delta progradation far from the study area.

Acknowledgements

We gratefully thank Giovanni Sarti, Monica Bini, and Marta Pappalardo for providing core drilling device and the useful scientific discussions. We also thank Mirko Carlini, Giovanna Serventi and Teresa Trua for stimulating discussion and for the constructive comments and advices. We are also grateful to Dilce Fatima Rossetti and to Roberto Tinterri for their helpful suggestions, and to Francesco Rinaldi and Michele Triggia for the precious technical support.

We thank the owners of Comacchio croplands for their willingness, and in particular, Corrado Noventa for the precious logistic support.

Figure and Table captions

Figure 1_Study area location

Figure 2_ Stratigraphic section across the north margin of the study area (modified from Amorosi et al., in press): high resolution (parasequences) depositional architecture of the Holocene transgressive-regressive wedge

Figure 3_ Examples of satellite images processing: A) False Color Composition (FCC) 432 ASTER; B) FCC 754_Landsat 7 ETM+; C) Unsupervised classification; D) Principal Component Analysis (PCA) Landsat 7 ETM+

Figure 4_ Multitemporal analysis from different Landsat 7 ETM+ and Landsat 8 OLI scenes. Suitable False Color Composite (732 for Landsat 7 ETM+; 743 for Landsat 8 OLI) are used here to enhance the contrast between bright and dark areas, highlightening paleochannels traces.

Figure 5_ A) Location of the two meandering RS-detected traces investigated; B) location of the core drillings (labelled with “TSC” associated with drop symbols) and soil samples survey (labelled with “SOC” and associated with pin symbols).

Figure 6_ Vibracore drillings operation on the field and details of the recovered cores.

Figure 7_ Clip on the Mezzano Valley area from the DTM LiDAR from MATTM (Ministero dell'Ambiente e della Tutela del Territorio e del Mare) 2008 survey. Scale colors display elevation values in meters.

Figure 8_ Paleotraces drainage network highlighted and mapped by means the satellite image analysis (e.g. PCA ASTER) and DTM LiDAR integration.

Figure 9_ Examples of plain view and topographic profiles of some mapped meandering traces; B) high resolution topographic profile across an identify meander on DTM LiDAR (convex-concave up banks); C) bright traces displaying a central narrow longitudinal black strip.

Figure 10_ Portion of a False Color Composite (FCC) Hyperion scene with a RS-detected meandering trace highlighted and reflectance spectra from bright and dark pixels belonging to the trace.

Figure 11_ A, B) Location of soil samples collected from the two meanders analyzed (M1 and M2) for reflectance signatures extraction and C) laboratory spectra extracted.

Figure 12_ Stratigraphic logs and lithofacies analysis of the six cores drilled from the two meanders selected (M1 and M2).

Figure 13_Interpreted short stratigraphic sections across the two traces selected (M1 and M2, Fig. 5b), involving the vibracores cores drilled, reconstructing the depositional architecture underneath the RS-detected meanders.

Table 1_ Technical characteristics of optical satellite imagery used for the RS analyses.

Table 2a_ List of the optical satellite multispectral and hyperspectral imagery analyzed (* - imagery listed in detail in Table 2b).

Table 2b_ Attribute values of Landsat 7 ETM+ and Landsat 8 OLI imagery involved in the multitemporal images analysis

Table 3_ ALTM Gemini laser-scanner technical specifications (modified after Pirotti et al, 2013).

Table 4_List of the main lithofacies associations interpreted from the mid–late Holocene subsurface succession of the Mezzano Valley (Po delta plain), with the decription of the related diagnostic sedimentological and paleontological features.

Table 5_List of the radiocarbon dates reported in this paper. Local reservoir correction DeltaR (139±28) was applied to shell samples. Percentages associated to the calibrated age values represent the related area under probability distribution using two standard deviations-2s.

References

Albani, A. and Serandrei Barbero, R., (1990). I Foraminiferi della Laguna e del Golfo di Venezia. Memorie Scienze Geologiche Padova 42, 271–341.

Albani, A.D., Favero V., Serandrei Barbero, R., (1984). Benthonic foraminifera as indicators of intertidal environments. Geo-Marine Letters 4, 43–47.

Albani, A., Barbero, R.S., Donnici, S. (2007). Foraminifera as ecological indicators in the lagoon of Venice, Italy. Ecological Indicators 7: 239-253.

Amorosi, A., Centineo, M.C., Colalongo, M.L., Pasini, G., Sarti, G., Vaiani, S.C. (2003). Facies architecture and Latest Pleistocene–Holocene depositional history of the Po Delta (Comacchio area), Italy. J. Geol. 111, 39–56.

Amorosi, A., Colalongo, M.L., Fiorini, F., Fusco, F., Pasini, G.,Vaiani, S.C., Sarti, G. (2004). Palaeogeographic and palaeoclimatic evolution of the Po Plain from 150-ky core records. Glob.Planet. Change 40, 55– 78.

Amorosi, A., Centineo, M. C., Colalongo, M. L., & Fiorini, F. (2005). Millennial-scale depositional cycles from the Holocene of the Po Plain, Italy. Marine Geology, 222–223 (1–4), 7–18.

Amorosi, A., Dinelli, E., Rossi, V., Vaiani, S. C., & Sacchetto, M. (2008). Late Quaternary palaeoenvironmental evolution of the Adriatic coastal plain and the onset of Po River Delta. Palaeogeography, Palaeoclimatology, Palaeoecology, 268 (1–2), 80–90.

Amorosi, A., Pavesi, M., Ricci Lucchi, M., Sarti, G., & Piccin, A. (2008). Climatic signature of cyclic fluvial architecture from the Quaternary of the central Po Plain, Italy. Sedimentary Geology, 209(1–4), 58–68.

Amorosi, A., Bini, M., Giacomelli, S., Pappalardo, M., Ribecai, C., Rossi, V., Sammartino, I., Sarti, G. (2013). Middle to late Holocene environmental evolution of the Pisa coastal plain (Tuscany, Italy) and early human settlements. Quaternary International 303, 93–106.

Amorosi, A., Antonioli, F., Bertini, A., Marabini, S., Mastronuzzi, G., Montagna, P., Negri, A., Rossi V., Scarponi D., Taviani, M., Angeletti L., Piva A., Vai, G. B., (2014). The Middle-Upper Pleistocene Fronte Section (Taranto, Italy): An exceptionally preserved marine record of the Last Interglacial. Global and Planetary Change, 119, 23–38.

Amorosi A., Bruno L., Campo B., Morelli A., Rossi V., Scarponi D., Hong W., Bohacs K. M., Drexler T.M.(in press). Global sea-level control on local parasequence architecture from the Holocene record of the Po Plain,Italy, Marine and Petroleum Geology.

Andrades-Filho, C. de O., Rossetti, D. de F., Bezerra, F. H. R., Medeiros, W. E., Valeriano, M. de M., Cremon, É. H., & Oliveira, R. G. de. (2014). Mapping Neogene and Quaternary sedimentary deposits in northeastern Brazil by integrating geophysics, remote sensing and geological field data. Journal of South American Earth Sciences, 56 (January 2016), 316–327.

Athersuch, J., Horne, D.J., Whittaker, J.E., (1989). Marine and brackish water ostracods, in KERMACK D.M., BARNES R.S.K. (eds.) «Synopses of the British Fauna (New Series)», 43, Brill E.J., Leiden, pp. 1-343.

Bard, E., Hamelin, B., Fairbanks, R.G., Zindler, A., (1990). Calibration of the 14C timescale over the past 30,000 years using mass spectrometric U–Th ages from Barbados corals. Nature 345, 405–410.

Baumgardner M. F., Kristof S. J., Johannsen C. J. and Zachary, A. L. (1970). Effects of organic matter on multispectral properties of soils. Proc. Indian Acad. Sci. 79: 413–422.

Baumgardner M.F., Silvia L.F. Biehl L.L. and Stoner E.R. (1985). Reflectance properties of soil. Adv. Agro.38, 1-43.

Bini, M., Kukavicic, M., &Pappalardo, M. (2012). Interpretazione di Pianura di Pisa, 212–222.

Bondesan , M. (1990). Le zone umide salmastre dell'Emilia Romagna: aspetti geografici e geomorfologici. In: Aspetti naturalistici delle zone umide salmastre dell'Emilia Romagna, pp.23-56. Regione Emilia-Romagna

Bondesan, M., Favero, V., &Vinals, M. J. (1995). New evidence on the evolution of the Po delta coastal plain during the Holocene. Quaternary International, 29/30 (95), 105–110.

Bondesan , M. (2001). L'evoluzione idrogrfica e ambientale della pianura ferrarese negli ultimi 3000 anni. In: Broglio A., Bondesan M. (a cura di), Storia di Ferrara, I. Territorio e preistoria, Ferrara (2001), pp. 228-263.

Bondesàn, M., Cibin, U., Colalongo, M.L., Pugliese, N., Stefani, M., Tsakiridis, E., Vaiani, S.C.and Vicenzi, S., (2006).Benthic communities and sedimentary facies recording late Quaternary environmental fluctuations in a Po Delta subsurface succession (Northern Italy). In: Coccioni, R., Lirer, F. and Marsili, A., Eds., Proceedings of the Second and Third Italian Meeting of Environmental Micropaleontology, 21–31. Krakow: Grzybowski Foundation. Special Publication 11.

Bronk Ramsey, C., and Lee, S., (2013). Recent and Planned Developments of the Program OxCal. Radiocarbon, 55(2-3), 720-730.

Burns, R., (1993). Mineralogical Applications of Crystal Field Theory, Second Edition, Cambridge University Press, Cambridge, 551p.

Carlson, T.N., (1986). Regional scale estimations of surface moisture availability and thermal inertia using remote sensing measurements, Remote Sensing, Reviews 1 (2) 197–247.

Ciabatti, M., (1966). Ricerche sull'evoluzione del Delta Padano. Giornale di Geologia, 34-2, 381-410.

Ciabatti, M, (1990). Geomorfologia ed evoluzione del Delta Padano. In: Il Mondo della Natura in Emilia-Romagna: la Pianura e la Costa. Federazione Cassae Risparmio e banche del Monte dell'Emilia-Romagna, Milano, 57-76.

Ciampalini, A., Raspini, F., Bianchini, S., Frodella, W., Bardi, F., Lagomarsino, D., Di Traglia, F., Moretti, S., Proietti, C., Pagliara, P., Onori, R., Corazza, A., Duro, A., Basile, G., Casagli, N., (2015). Remote sensinga stool for development of landslide databases: The case of the Messina Province (Italy) geodatabase Geomorphology 249 (2015) 103–118

Cohen, M.C.L., França, M.C., Rossetti, D.F., Pessenda, L.C.R., Giannini, P.C.F., Lorente, F.L., Buso Jr., A.A., Castro, D.,Macario, K., (2014). Landscape evolution duringthelateQuaternaryat the Doce River mouth, Espírito Santo State, Southeastern Brazil. Palaeogeogr.Palaeoclimatol. Palaeoecol. 415, 48–58.

Curzi, P. V., Dinelli, E., Ricchi Lucchi, M., and Vaiani, S.C., (2006). Paleoenvrinomental control on sediment composition and provenance in the late Quaternary deltaic successions: a case study from the Po delta area (Northern Italy). Geological Journal, 41, 591-612

Dalrymple, R.W., Mackay, D.A., Ichaso, A.A., and Choi, K.S., (2012). Processes, morphodynamics, and facies of tide-dominated estuaries, in Davis, Jr., R.A., and Dalrymple, R.W. (eds.), Principles of Tidal Sedimentology: New York, Springer Science and Business Media, p. 79-108.

Dean, R.G., Dalrymple, R.A., (2004). Coastal processes with engineering applications. Cambridge University Press, pp. 476.

Debenay J-P, Guillou J-J, (2002) Ecological transitions indicated by foraminiferal 414 assemblages in paralic environments. Estuaries 25: 1107-1120 Ellis, S. and Mellor, A. (1995). Soils and Environment, London: Routledge. A modern text with many examples and illustrations of soil profiles, soil transects and soil distributions.

Fouache É., Dalongeville R., Kunesch S., Suc J. P., Subally D., Prieur A., Lozoue P., (2005).The environmental setting of the harbor of the classical site of Oeniades on the Acheloos delta, Greece. *Geoarchaeology*, 20, 3, 285-302.

Furlani S., Antoniolic F., Biolchia S., Gambine T., Gaucie R.,LoPrestig V., Anzideih M., Devotod S., Palomboi M., Sullig A., (2012). Holocene sea-level change in Malta. *Quatenary International*, 288, 146-157.

Garfagnoli, F., Martelloni, G., Ciampalini, A., Innocenti, L., Moretti, S., (2013). Two GUIsbased analysis tool for spectroradiometer data pre-processing. Earth Sci. Inf. 6 (4), 227–240.

Ghilardi M., Kunesch S., Styllas M., Fouache E., (2008). Reconstruction of Mid-Holocene sedimentary environments in the central part of the Thessaloniki Plain (Greece), based on microfaunal identification, magnetic susceptibility and grain-size analyses. *Geomorphology*, 97, 3-4, 617-630.

Henderson, P.A., (1990). Freshwater ostracods. In: Kermack DM, Barnes RSK (eds) Synopsis of the British fauna (New Series). Vol 42. Universal Book Services,Oegstgeest.

Horton, B.P. and Edwards, R.J., (2006). Quantifying Holocene sea level change using intertidalforaminifera: lessons from the British Isles. Cushman Foundation for ForaminiferalResearch Special Publication 40

Hughes, Z.J., (2012). Tidal channels on tidal flats and marshes, in Davis, Jr., R.A., and Dalrymple, R.W. (eds.), Principles of Tidal Sedimentology: New York, Springer Science and Business Media, p. 269-301.

Hunt, G.R., (1977). Spectral signatures of particulate minerals, in the visible and near-infrared, Geophysics, 42, 501-513.

Hunt, G.R., and Salisbury, J.W., (1970). Visible and near infrared spectra of minerals and rocks. I. Silicate minerals, Mod. Geology 1, 83-300 Hunt and Salisbury.

Jackson, J.T., Chen, D., Cosh, M. et al., (2004). Vegetation water content mapping using Landsat data derived normalized difference water index for corn and soybeans, Remote Sensing of Environment 92 (4) 475–482.

Lambeck, K., Antonioli, F., Anzidei, M., Ferranti, L., Leoni, G., Scicchitano, G., Silenzi, S., (2011). Sea level change along the Italian coast during the Holocene and projections for the future. Quaternary International 232, 250–257.

Liu, J.P., Milliman, J.D., Gao, S., Cheng, P., (2004). Holocene development of the Yellow River’s subaqueous delta, North Yellow Sea. Marine Geology 209, 45–67.

Longhitano, S.G., Sabato, L., Tropeano, M. and Gallicchio, S., (2010). A Mixed Bioclastic–Siliciclastic Flood-Tidal Delta in a Micro Tidal Setting: Depositional Architectures and Hierarchical Internal Organization (Pliocene, Southern Apennine, Italy), Journal of Sedimentary Research, 80, 1, 36-53.

Longhitano, S. G, Mellere, D., Steel, R. J., Ainsworth, R. B., (2012a). Tidal depositional systems in the rock record: A review and new insights, Sedimentary Geology, 279, 2-22.

Longhitano, S.G., Chiarella, D., Di Stefano, A., Messina, C., Sabato, L., Tropeano, M., (2012b). Tidal signatures in Neogene to Quaternary mixed deposits of southern Italy straits and bays. In: Longhitano, S.G., Mellere, D., Ainsworth, R.B. (Eds.), Modern and ancient depositional systems: perspectives, models and signatures.SedimentaryGeology, 279, 74–96.

Mantelli L.R., Rossetti D. F., Albuquerque P. G., Valeriano M.M., (2009). Applying SRTM digital elevation model to unravel Quaternary drainage in forested areas of Northeastern Amazonia, Computers and *Geoscience*, 35, 12, 2331-2337.

Melis, R. and Covelli, S., (2013). Distribution and morphological abnormalities of recent foraminifera in the Marano and Grado Lagoon (North Adriatic Sea, Italy), Mediterr. Mar. Sci., 14, 432–450.

Montenegro, M.E. and Pugliese, N., (1996). Autecological remarks on the ostracod distribution in the Marano and Grado Lagoons (Northern Adriatic Sea Italy), in «Bollettino della Società Paleontologica Italiana», 3, pp. 123-132.

Mozzi, P., Piovan, S., Rossato, S., Cucato, M., Abbà, T., Fontana, A., (2010). Paleohydrography and early settlements in Padua (Italy). Il Quaternario, Italian Journal of Quaternary Sciences, 23(2bis), 387-400vol.spec.

Murray, J. W., (2006): Ecology and applications of benthic foraminifera, Cambridge University Press, Cambridge, 426 .

Oguchi, T.,Wasklewicz, T.,Hayakawa, Y.S.,(2013). Remote data in fluvial geomorphology:characteristics and applications. In: Shroder,J.(Editorin Chief), Wohl,E.(Ed.),Treatise on Geomorphology. Academic Press, San Diego, CA,vol.9, Fluvial Geomorphology, pp.711–729.

Pethick, J. (2001). Coastal management and sea-level rise. Catena, 42(2–4), 307–322.

Pieri, M., and Groppi, G., (1981). Subsurface geological structure of the Po Plain, Italy. Progetto FinalizzatoGeodinamica, CNR Pubbl. 414, 23 p.

Piovan, S., Mozzi, P., Stefani, C., (2010). Bronze age paleohydrography of the southern Venetian Plain. Geoarchaeology, 25(1), 6–35.

Piovan, S., Mozzi, P., Zecchin, M., (2012). The interplay between adjacent Adige and Po alluvial systems and deltas in the lateHolocene (NorthernItaly). Geomorphology, 18, 4- pp. 427-440

Pratt, A., and Ellyett, C.D., (1979). The thermal inertia approach to mapping of soil moisture and geology, Remote Sensing of Environment, 8 (2) 151–168.

Ravazzi C., Marchetti M., Zanon M., Perego R., Quirino T., Deaddis M., De Amicis M., Margaritora D., (2013). Lake evolution and landscape history in the lower Mincio River valley, unravelling drainage changes in the central Po Plain (N-Italy) since the Bronze Age. *Quaternary International*, 288, 195-205.

Reimer PJ, Bard E, Bayliss A, Beck JW, Blackwell PG, Bronk Ramsey C, Buck CE, Cheng H, Edwards RL, Friedrich M, Grootes PM, Guilderson TP, Haflidason H, Hajdas I, Hatté C, Heaton TJ, Hoffmann DL, Hogg AG, Hughen KA, Kaiser KF, Kromer B, Manning SW, Niu M, Reimer RW, Richards DA, Scott EM, Southon JR, Staff RA, Turney CSM, van der Plicht J., (2013). IntCal13 and Marine13 radiocarbon age calibration curves 0–50,000 years cal BP. Radiocarbon 55(4):1869–1887.

Ricci Lucchi, F.,Colalongo, M. L., Cremonini, G., Gasperi, G.,Iaccarino, S., Papani, G., Raffi, I., and Rio, D., (1982). Evoluzione sedimentaria e paleogeografica del margine appenninico. In Cremonini, G., and RicciLucchi, F., eds. Guida alla geologia del margine appenninico-padano. Guide Geologiche Regionali

Ricci Lucchi F., (1986). Foreland basin system of the Northern Apennines and related clastic wedges: a preliminary outline.Giorn.Geol., 48-1/2, 165-186.Soc.Geol. Ital., p. 17–46.

Rossetti, D. F., and Goes, A. M., (2008). Late Quaternary drainage dynamics in northern Brazil based on the study of a large paleochannel from southwestern Marajo Island. Anais Da Academia Brasileira De Ciencias, 80(3), 579–593.

Rossi, V. and Vaiani, S.C., (2008). Benthic foraminiferal evidence of sediment supply changes and fluvial drainage reorganization in Holocene deposits of the Po Delta, Italy, «MARINE MICROPALEONTOLOGY»,69, 106-118

Rossi, V., Sammartino, I., Amorosi, A., Sarti, G., De Luca, S., Lena, A., Morhange, C. (2014). New insights into the palaeoenvironmental evolution of Magdala ancient harbour (Sea of Galilee, Israel) from ostracod assemblages, geochemistry and sedimentology. Journal of Archaeological Science.

Ruiz F., Gonzalez-Regalado M.L., Baceta J.I., Menegazzo-Vitturi L., Pistolato M., Rampazzo G., Molinaroli E., (2000). Los ostracodosactuales de la laguna de Venecia (NE de Italia). [Lesostracodesactuels de la lagune de Venise (NE Italie)] [Recentostracods from the Venicelagoon (NE Italy)], in «Geobios», 33, 447-454.

Salter P.J., Berry G., Williams J.B.,(1966). The influence of texture on the moisture characteristic of soil. III Quantitative relationship between particle size, composition and available water capacity. J. Soil Sci. 17, 93-98.

Sgavetti, M., (1974). Le caratteristiche di riflettività spettrale di una zona della pianura Padana su immagini ERTS-1, Anno XXXII-Bollettino di Geologia e Scienze Affini, n.3.

Sgavetti M. and Ferrari C., (1988). The use of TM data for the study of a modern deltaic depositional system. Int. J. Remote Sensing, 9, nos. 10 and 11, 1613-1627

Shafian, S. and Maas, S. J., (2015). Index of soil moisture using raw Landsat image digital count data in Texas High Plains. Remote Sensing, 7(3), 2352–2372.

Smith, M.J. and Pain, C.F., (2009). Applications of remote sensing in geomorphology. Progress in Physical Geography (33), 568-582.

Stefani, M. and Vincenzi, S., (2005). The interplay of eustasy, climate and human activity in the late Quaternary depositional evolution and sedimentary architecture of the Po Delta system. Marine Geology, 222–223(1–4), 19–48.

Stoch, F., (1995). Indagine ecologico-faunistica sui popolamenti entomostraci di alcuni stagni d’acqua salmastra dell’Isola della Cona (foce del Fiume Isonzo, Italia Nord Orientale). Gortania Atti Museo Friuliano di Storia Naturale 16, 151–173.

Stoner, E. and Baumgardner, M. F., (1981). Characteristics variations in reflectance of surface soils. Soil Sci. Soc.Am. J. 45, 1161-1165.

Vacchi, M., Marriner, N., Morhange, C., Spada, G., Fontana, A., Rovere, A., (2016). Multiproxy assessment of Holocene relative sea-level changes in the western Mediterranenan: Sea-level variability and improvements in the definition of the isostatic signal. Earth-Science Reviews 155, 172–197.

van Veen, J., (1950). Ebb and Flood-Channel Systems in the Netherlands Tidal Waters (in Dutch with English summary), KNAG 2e Ser., part 67, Delft Univ. of Technol., Netherlands.

Vött A., Schriever A., Handl M., Brückner H., (2007). Holocene palaeogeographies of the central Acheloos River delta (NW Greece) in the vicinity of the ancient seaport Oiniadai. *Geodinamica Acta* 20/4, 241–256.

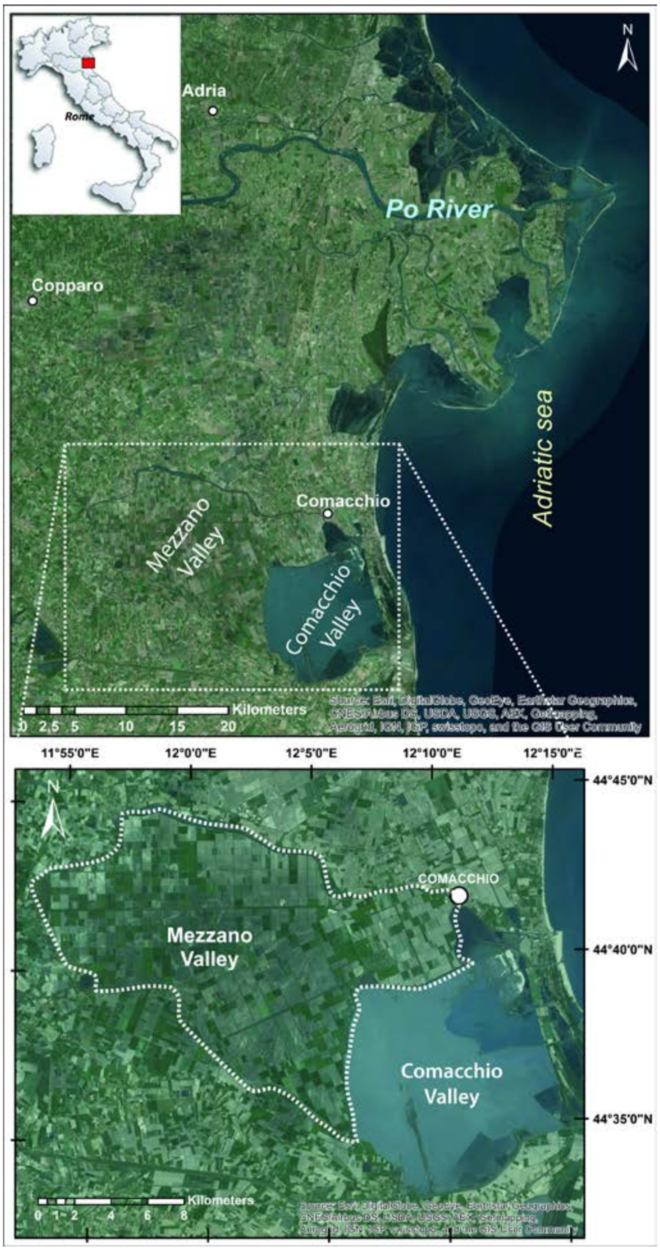

Source: Esri, DigitalGlobe, GeoEye, Earthstar Geographics, CNES/Airbus DS, USDA, USGS, AEX, Getmapping, Aerogrid, IGN, IGP, swisstopo, and the GIS User Community

Figure 1

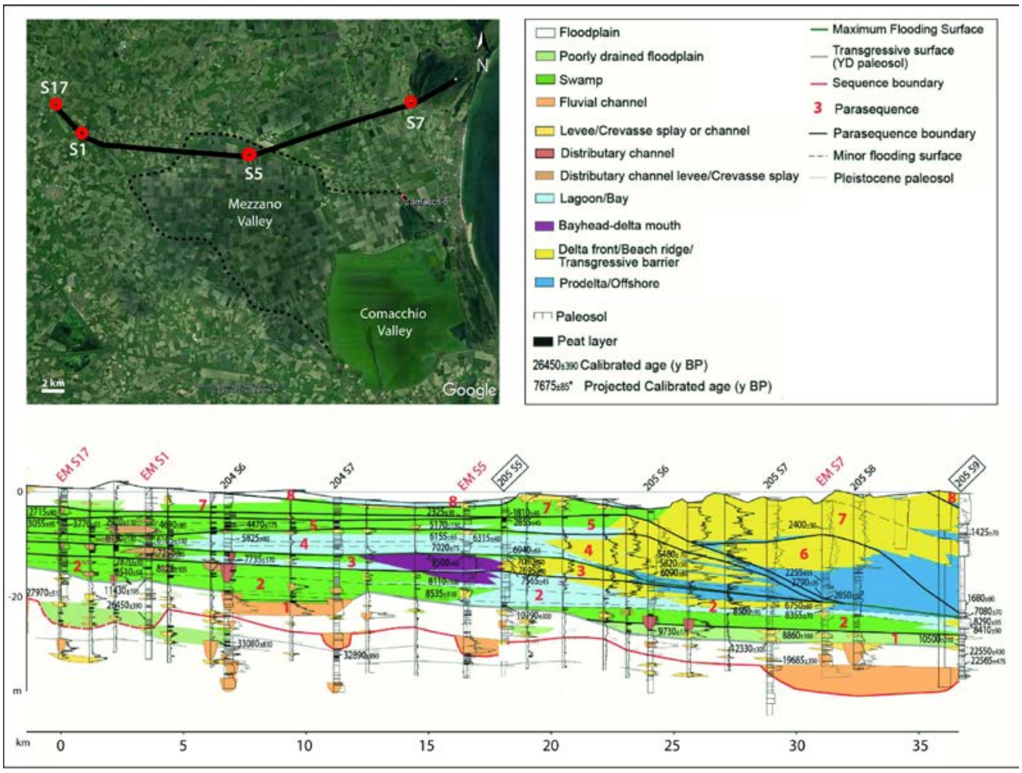
S17
S1
S5
S7
N
Mezzano Valley
Comacchio Valley
2 km
Google
Floodplain
Poorly drained floodplain
Swamp
Fluvial channel
Levee/Crevasse splay or channel
Distributary channel
Distributary channel levee/Crevasse splay
Lagoon/Bay
Bayhead-delta mouth
Delta front/Beach ridge/ Transgressive barrier
Prodelta/Offshore
Paleosol
Peat layer
26450±390 Calibrated age (y BP)
7675±85* Projected Calibrated age (y BP)
Maximum Flooding Surface
Transgressive surface (YD paleosol)
Sequence boundary
3 Parasequence
Parasequence boundary
Minor flooding surface
Pleistocene paleosol
EM S17
EM S1
204 S6
204 S7
EM S5
205 S5
205 S6
205 S7
EM S7
205 S8
205 S9
0
-20
m
km
0
5
10
15
20
25
30
35

Figure 2

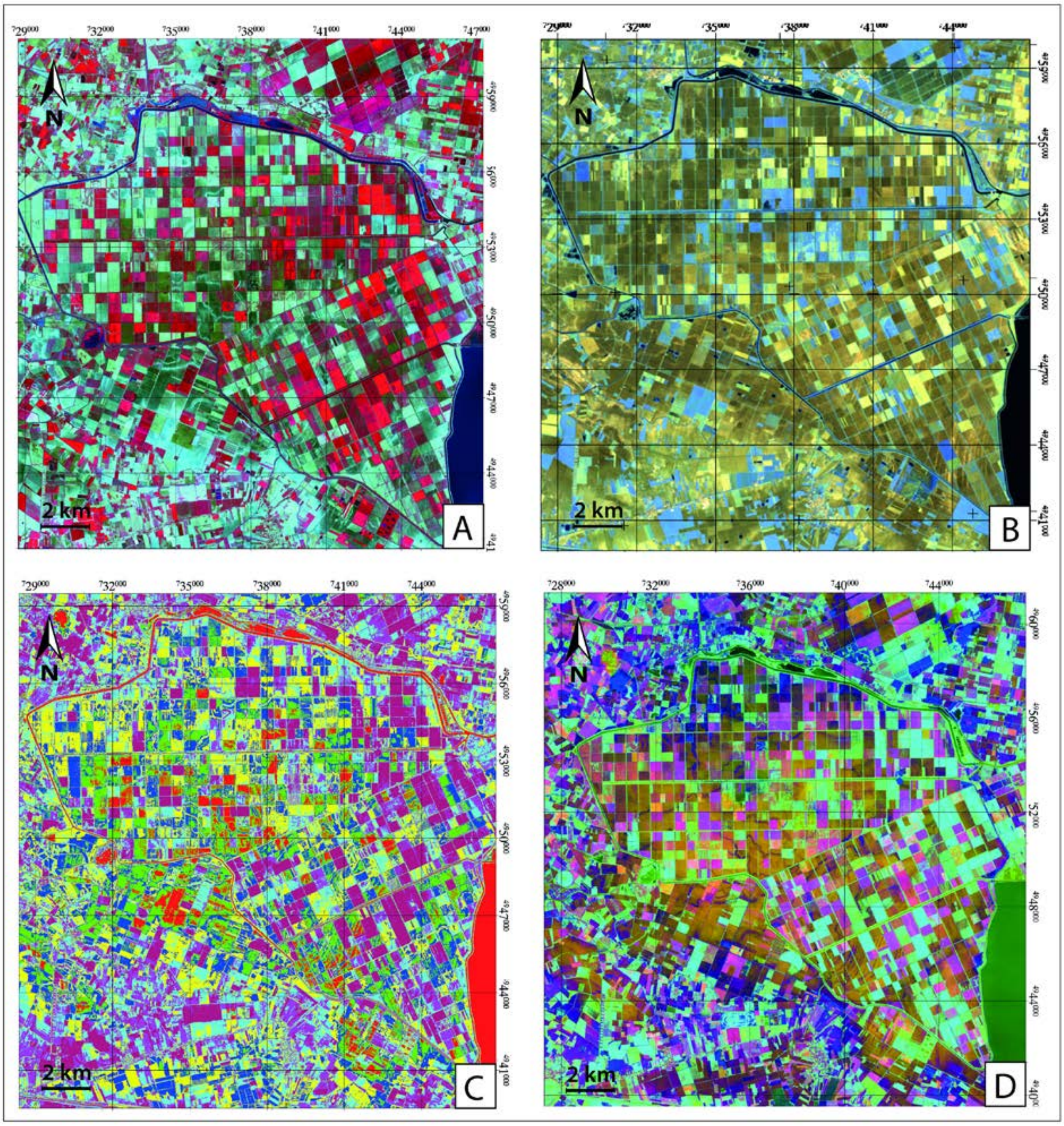
729000
732000
735000
738000
741000
744000
747000
N
2 km
A
B
C
D
728000
736000
740000

Figure 3

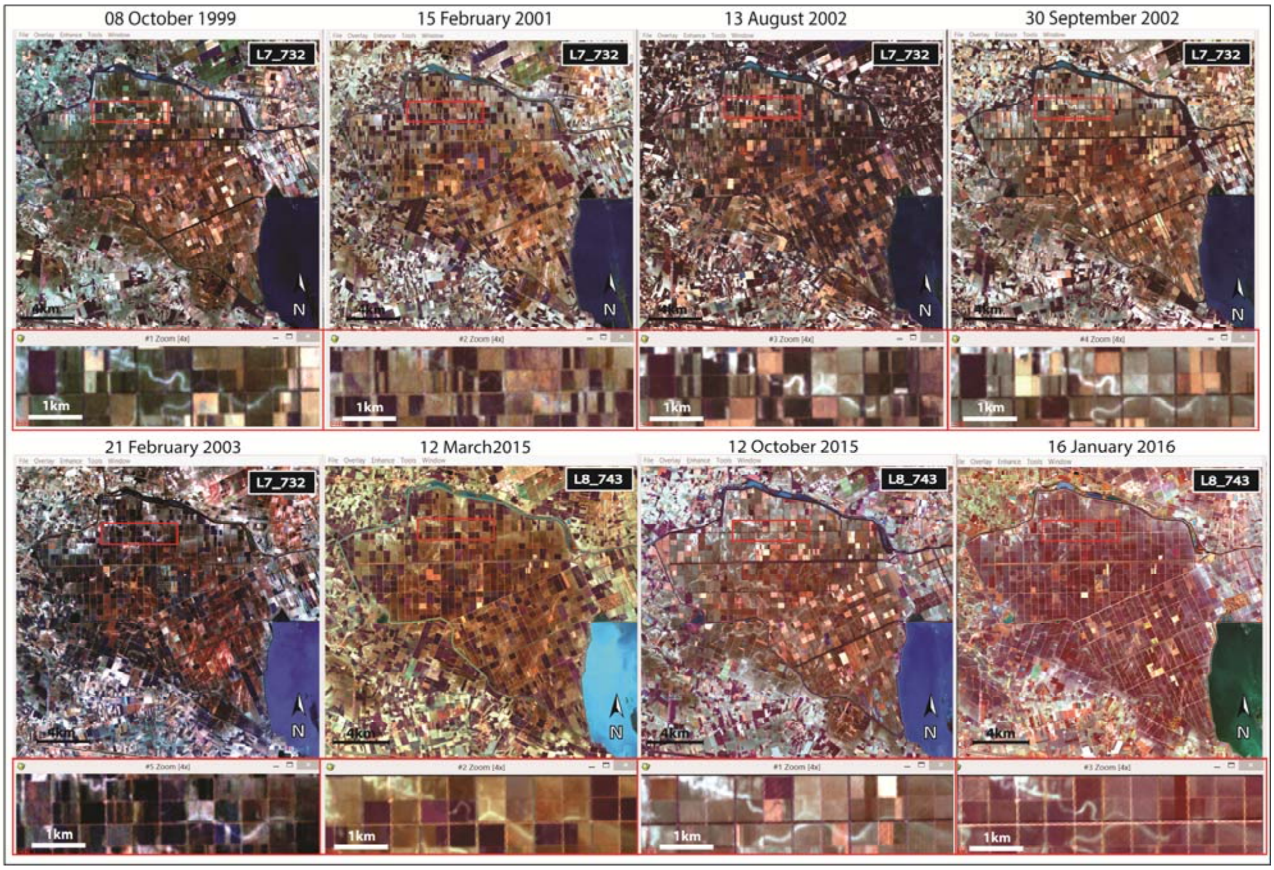
08 October 1999
L7_732
4km
N
#1 Zoom [4x]
1km
15 February 2001
L7_732
4km
N
#2 Zoom [4x]
1km
13 August 2002
L7_732
4km
N
#3 Zoom [4x]
1km
30 September 2002
L7_732
4km
N
#4 Zoom [4x]
1km
21 February 2003
L7_732
4km
N
#5 Zoom [4x]
1km
12 March2015
L8_743
4km
N
#2 Zoom [4x]
1km
12 October 2015
L8_743
4km
N
#1 Zoom [4x]
1km
16 January 2016
L8_743
4km
N
#3 Zoom [4x]
1km

Figure 4

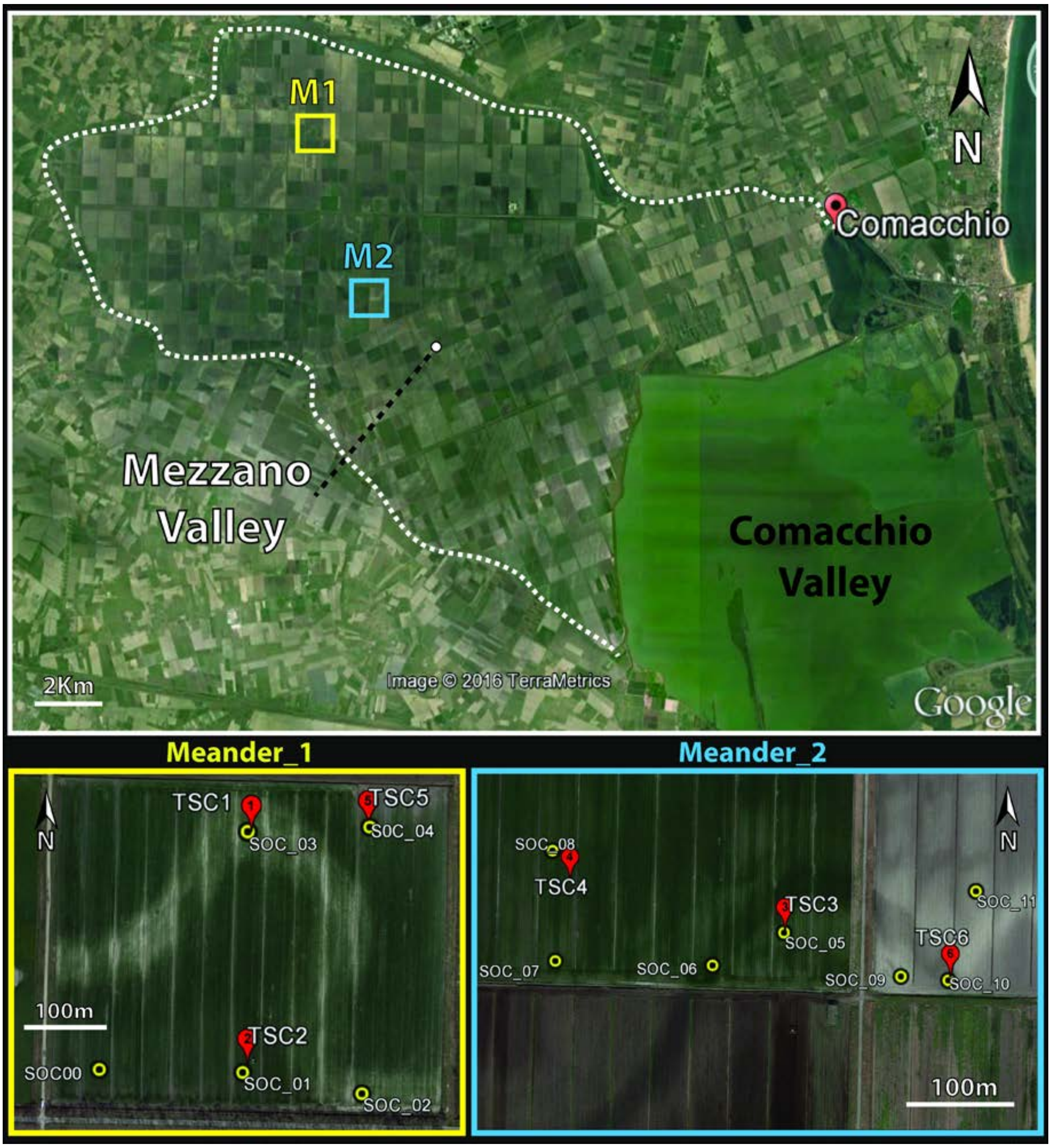
M1
M2
N
Comacchio
Mezzano Valley
Comacchio Valley
2Km
Image © 2016 TerraMetrics
Google
Meander_1
Meander_2
N
TSC1
TSC5
SOC_03
SOC_04
100m
TSC2
SOC00
SOC_01
SOC_02
SOC_08
TSC4
TSC3
SOC_05
SOC_11
TSC6
SOC_07
SOC_06
SOC_09
SOC_10
N
100m

Figure 5

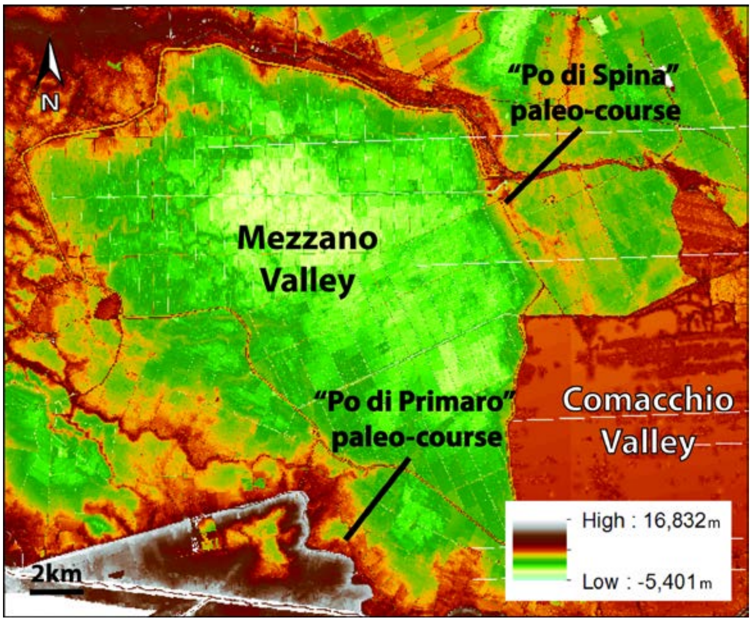
N
"Po di Spina"
paleo-course
Mezzano
Valley
"Po di Primaro"
paleo-course
Comacchio
Valley
High : 16,832m
Low : -5,401m
2km

Figure 6

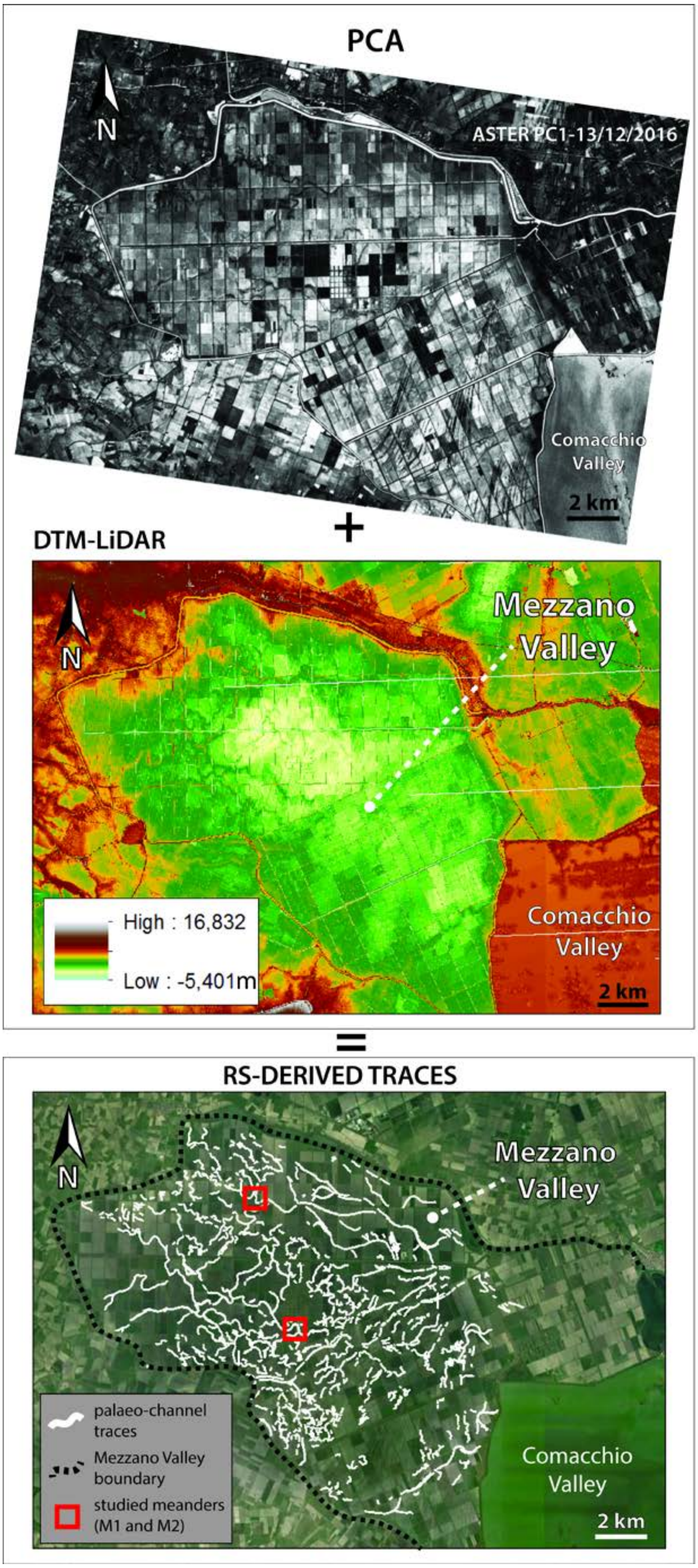
PCA
N
ASTER PC1-13/12/2016
Comacchio Valley
2 km
+
DTM-LiDAR
N
Mezzano Valley
High : 16,832
Low : -5,401m
Comacchio Valley
2 km
=
RS-DERIVED TRACES
N
Mezzano Valley
palaeo-channel traces
Mezzano Valley boundary
studied meanders (M1 and M2)
Comacchio Valley
2 km

Figure 7

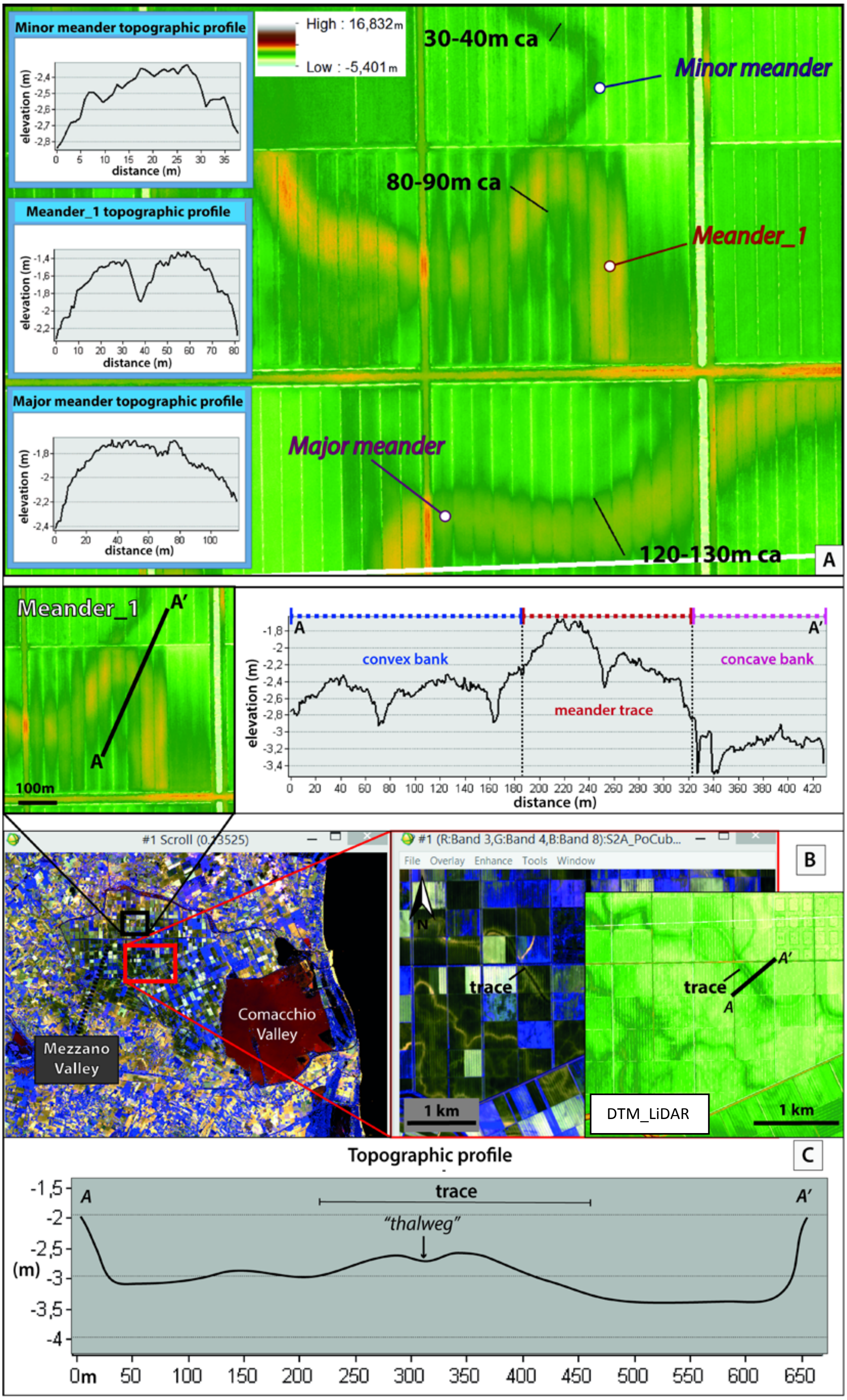
Minor meander topographic profile
elevation (m)
-2,4
-2,5
-2,6
-2,7
-2,8
0 5 10 15 20 25 30 35
distance (m)
Meander_1 topographic profile
-1,4
-1,6
-1,8
-2
-2,2
0 10 20 30 40 50 60 70 80
Major meander topographic profile
-1,8
-2
-2,2
-2,4
0 20 40 60 80 100
High : 16,832m
Low : -5,401m
30-40m ca
Minor meander
80-90m ca
Meander_1
Major meander
120-130m ca
A
Meander_1
A'
A
100m
convex bank
meander trace
concave bank
-1,8
-2
-2,2
-2,4
-2,6
-2,8
-3
-3,2
-3,4
0 20 40 60 80 100 120 140 160 180 200 220 240 260 280 300 320 340 360 380 400 420
#1 Scroll (0,13525)
#1 (R:Band 3,G:Band 4,B:Band 8):S2A_PoCub...
File Overlay Enhance Tools Window
B
N
trace
1 km
DTM_LiDAR
Comacchio Valley
Mezzano Valley
Topographic profile
C
trace
"thalweg"
-1,5
-2
-2,5
(m) -3
-3,5
-4
0m 50 100 150 200 250 300 350 400 450 500 550 600 650

Figure 8

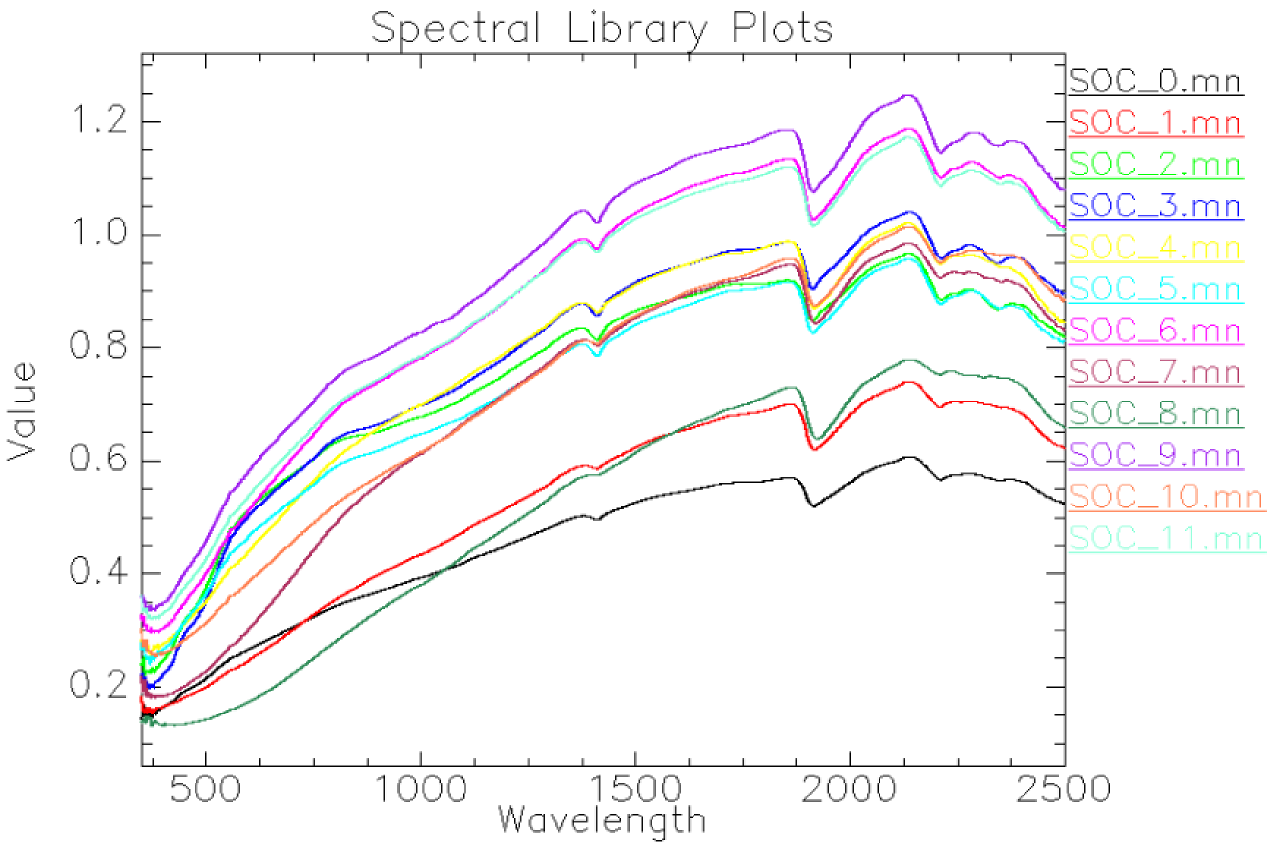
Spectral Library Plots
Value
Wavelength
1.2
1.0
0.8
0.6
0.4
0.2
500
1000
1500
2000
2500
SOC_0.mn
SOC_1.mn
SOC_2.mn
SOC_3.mn
SOC_4.mn
SOC_5.mn
SOC_6.mn
SOC_7.mn
SOC_8.mn
SOC_9.mn
SOC_10.mn
SOC_11.mn

Figure9

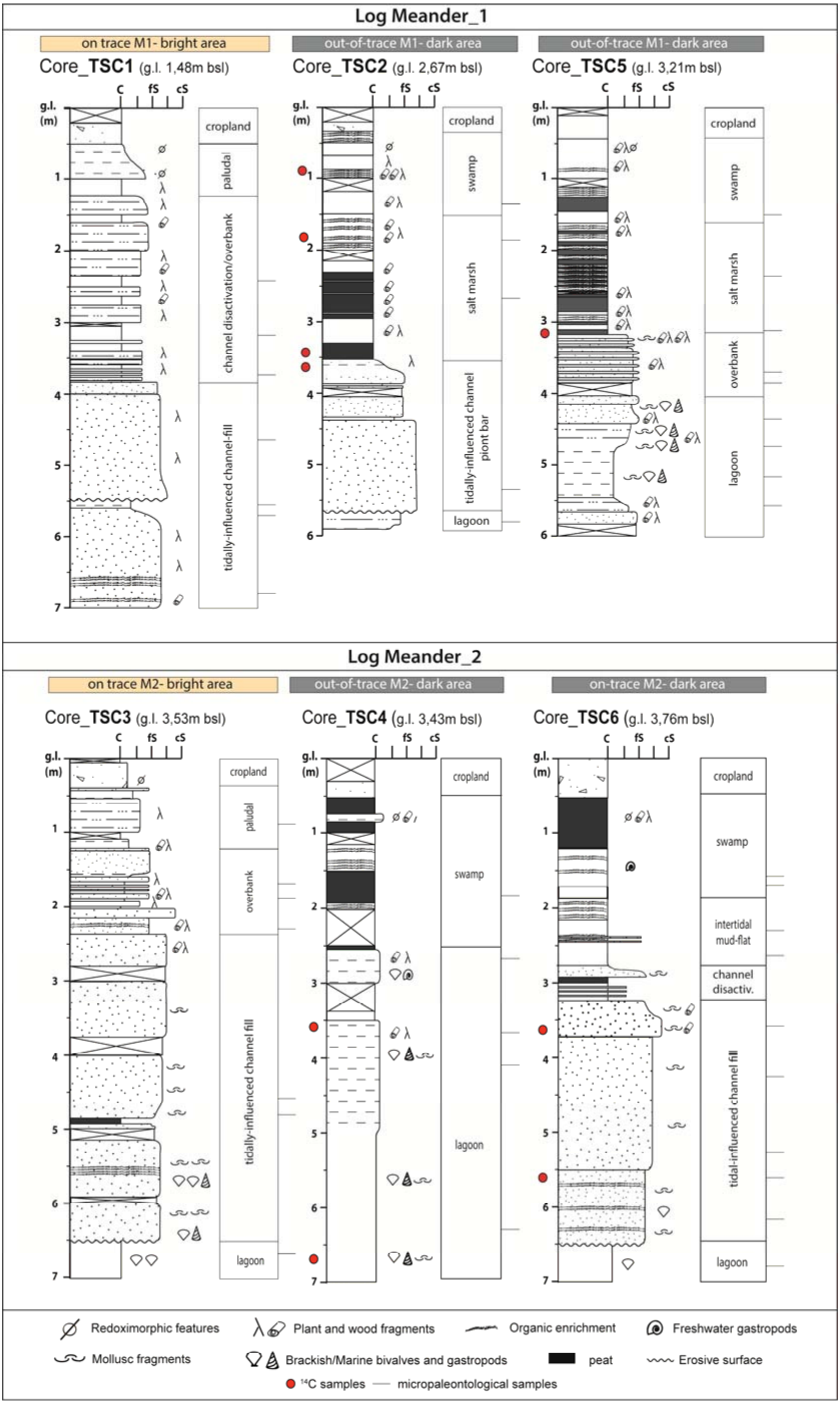
Log Meander_1
on trace M1- bright area
out-of-trace M1- dark area
out-of-trace M1- dark area
Core_TSC1 (g.l. 1,48m bsl)
Core_TSC2 (g.l. 2,67m bsl)
Core_TSC5 (g.l. 3,21m bsl)
C fS cS
g.l. (m)
1
2
3
4
5
6
7
cropland
paludal
channel disactivation/overbank
tidally-influenced channel-fill
swamp
salt marsh
tidally-influenced channel piont bar
lagoon
overbank
Log Meander_2
on trace M2- bright area
out-of-trace M2- dark area
on-trace M2- dark area
Core_TSC3 (g.l. 3,53m bsl)
Core_TSC4 (g.l. 3,43m bsl)
Core_TSC6 (g.l. 3,76m bsl)
tidally-influenced channel fill
intertidal mud-flat
channel disactiv.
tidal-influenced channel fill
Redoximorphic features
Plant and wood fragments
Organic enrichment
Freshwater gastropods
Mollusc fragments
Brackish/Marine bivalves and gastropods
peat
Erosive surface
^{14}C samples
micropaleontological samples

Figure 10

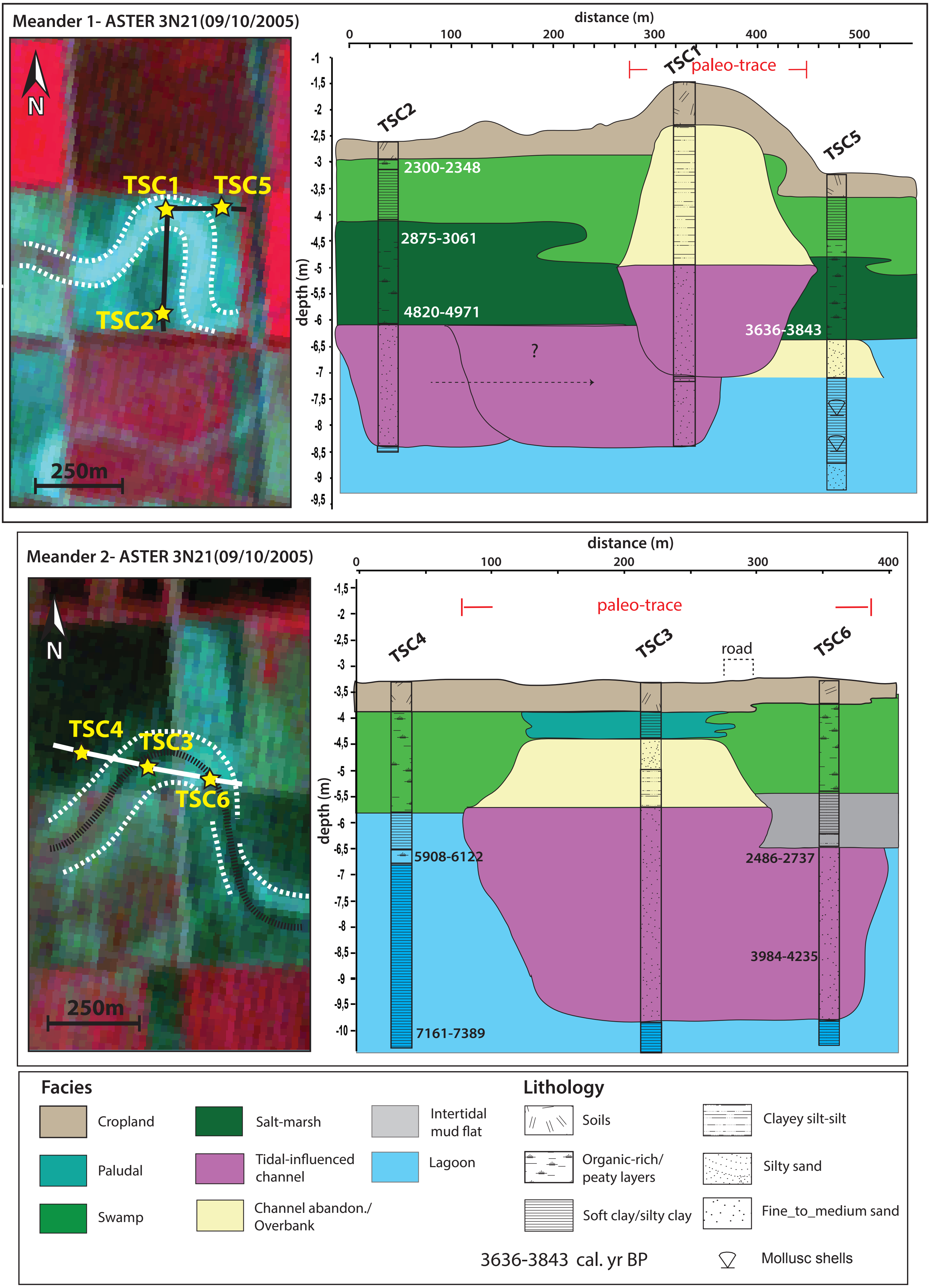
Meander 1- ASTER 3N21(09/10/2005)
N
TSC1
TSC5
TSC2
250m
distance (m)
0
100
200
300
400
500
-1
-1,5
-2
-2,5
-3
-3,5
-4
-4,5
-5
-5,5
-6
-6,5
-7
-7,5
-8
-8,5
-9
-9,5
depth (m)
TSC2
TSC1
paleo-trace
TSC5
2300-2348
2875-3061
4820-4971
3636-3843
?
Meander 2- ASTER 3N21(09/10/2005)
N
TSC4
TSC3
TSC6
250m
distance (m)
0
100
200
300
400
-1,5
-2
-2,5
-3
-3,5
-4
-4,5
-5
-5,5
-6
-6,5
-7
-7,5
-8
-8,5
-9
-9,5
-10
depth (m)
paleo-trace
TSC4
TSC3
road
TSC6
5908-6122
2486-2737
3984-4235
7161-7389
Facies
Cropland
Salt-marsh
Intertidal mud flat
Paludal
Tidal-influenced channel
Lagoon
Swamp
Channel abandon./ Overbank
Lithology
Soils
Clayey silt-silt
Organic-rich/ peaty layers
Silty sand
Soft clay/silty clay
Fine_to_medium sand
3636-3843 cal. yr BP
Mollusc shells

Figure 11

Satellite	Sensor	Swath width (km)	Revisit time (days)	Number of spectral bands	Spectral resolution (bits)	Spatial resolution (m)	Bands and wavelength ranges (nm)		Description
LANDSAT 7	ETM+ (Enhanced Thematic Mapper Plus)	185	16	8	8	15	PAN	500-900	VIS-NIR
						30	1	450-515	VIS
							2	525-605	
							3	639-690	
							4	750-900	NIR
							5	1550-1750	SWIR
							7	2090-2350	
						60	6	10400-12500	TIR
LANDSAT 8	OLI (Operational Land Imager)	185	16	11	8	15	PAN	500-680	VIS
						30	1	435-450	
							2	450-510	
							3	530-590	
							4	640-670	
							5	850-880	NIR
							CIRRUS	1360-1380	
							6	1570-1650	SWIR
							7	2110-2290	
						100	10	10600-11190	TIR
							11	11500-12150	
TERRA	ASTER	60	16	14	8	15	1	520-600	VIS
							2	630-690	
							3n	760-860	NIR
							3b	760-860	
						30	4	1600-1700	SWIR
							5	2145-2185	
							6	2185-2225	
							7	2235-2285	
							8	2295-2365	
							9	2360-2430	
					12	90	10	8125-8475	TIR
							11	8475-8825	
							12	8925-9275	
							13	10250-10950	
							14	10950-11650	
SENTINEL-2	MSI	290	10 (combined 5)	13	12	10	2	490(±65 nm)	VIS
							3	560(±35 nm)	
							4	665(±30 nm)	
							8	842(±115 nm)	NIR
						20	5	705(±15 nm)	
							6	740(±15 nm)	
							7	783(±20 nm)	
							8a	865(±20 nm)	
							11	1610(±90 nm)	SWIR
							12	2190(±180nm)	
						60	1	443(±20 nm)	VIS
							9	945(±20 nm)	NIR
							10	1375(±30 nm)	SWIR
EO-1	HYPERION	7.5	16	220	16	30	400-2500		VNIR-SWIR

Table 1a

Satellite imagery	Acquisition date
TERRA-ASTER	13 October 2001
	10 October 2007
SENTINEL2-MSI	18 June 2015
	13 August 2015
	12 September 2015
EO1-HYPERION	07 June 2001
	07 January 2006
*LANDSAT 7 ETM+	
*LANDSAT 8 OLI	

Satellite imagery	Acquisition date	Acquisition time	Scene cloud cover (%)
*Landsat 7 ETM+	08 October 1999	09:51:35-09:52:02 a.m.	0.02
	15 February 2001	09:48:58-09:49:25 a.m.	0.16
	13 August 2002	09:46:43-09:47:10 a.m.	1.22
	30 September 2002	09:46:16-09:46:43 a.m.	21.34
	21 February 2003	09:47:12-09:47:39 a.m.	0.15
*Landsat 8 OLI	18 March 2015	09:58:05-09.58:37 a.m.	34.42
	12 October 2015	09:58:31-09:59:31 a.m.	20.05
	16 January 2016	09:58:35-09:59:06 a.m.	10.01

Table 1b

Sensor	**Laser properties**								**Precision and resolution**	
Model and Company	Wavelenght (µm)	Pulse length (ns)	Beam divergence (mrad)	Scan frequency (Hz)	Pulse frequency-min-Max (kHz)	Max.scan angle -FOV (deg)	Pulse sampling freqency	Horizontal (m 1σ)	Vertical (m 1σ)
ALTM Gemini - Optech	1064	7	0,8/0,25 I/e	70 (oscillating mirror)	167	50	<2.0 m	1/5500 x altitude	< 35cm

Table 2

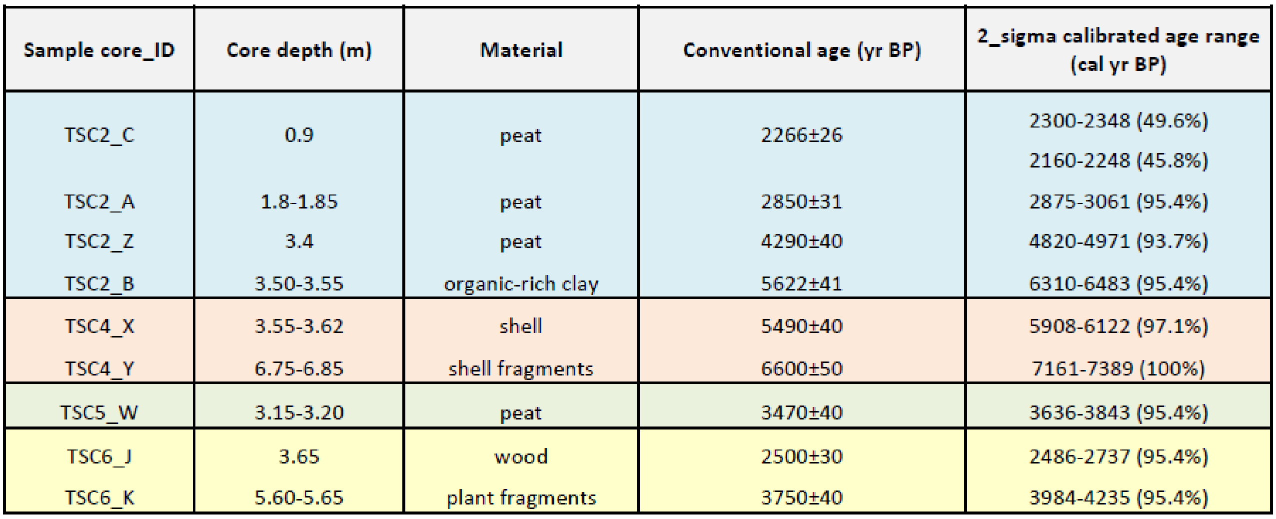

Sample core_ID	Core depth (m)	Material	Conventional age (yr BP)	2_sigma calibrated age range (cal yr BP)
TSC2_C	0.9	peat	2266±26	2300-2348 (49.6%) 2160-2248 (45.8%)
TSC2_A	1.8-1.85	peat	2850±31	2875-3061 (95.4%)
TSC2_Z	3.4	peat	4290±40	4820-4971 (93.7%)
TSC2_B	3.50-3.55	organic-rich clay	5622±41	6310-6483 (95.4%)
TSC4_X	3.55-3.62	shell	5490±40	5908-6122 (97.1%)
TSC4_Y	6.75-6.85	shell fragments	6600±50	7161-7389 (100%)
TSC5_W	3.15-3.20	peat	3470±40	3636-3843 (95.4%)
TSC6_J	3.65	wood	2500±30	2486-2737 (95.4%)
TSC6_K	5.60-5.65	plant fragments	3750±40	3984-4235 (95.4%)

Table 3

Depositional setting	Lithofacies	Sedimentological features	Micropaleontological content
Supratidal	Overbank/channel abandonement sands and silts	Centimetric to decimetric alternation of *(i)* gray silty sands and sandy silts or *(ii)* soft light gray silty clays and sandy silts. Vegetal debris are commonly encountered.	Scarce meiofauna composed of both well-preserved and poorly preserved specimens of highly confined, brackish foraminifers, as *Ammonia tepida, Haynesina germanica* and *Trochammina inflata*, occur within the sandy-silty deposits. Scattered valves of the low brackish ostracods *Pseudocandona albicans* are found within the silty clay-sandy silt alternations.
	Paludal clays and silts	Monotonous succession of light gray-light brown silts and clayey silts, with reddish mottled due to the presence of slightly altered vegetal fragments.	Olygotypic ostracod fauna dominated by *Pseudocandona albicans*, a mesohaline species preferring stagnant conditions and slow-moving waters.
	Swamp peaty clays	Dark gray soft clays with abundant vegetal and wood fragments. Cm-thick peaty layers and small gastropod shells are also encountered.	Abundant meiofauna exclusively composed of valves of *Pseudocandona albicans*, a mesohaline ostracod species preferring stagnant conditions and slow-moving waters. Peaty layers are barren in microfossils.
Intertidal	Saltmarsh peaty clays	Centimetric alternation of dark gray-black organic-rich soft clays with abundant wood fragments and black peaty layers.	Barren of microfossils or few specimens of the agglutinated foraminifer *Trochammina inflata*, tolerant to highly restricted brackish conditions and ample oscillations of the water table.
	Mud-flat clays and silts	Light gray clays and silty clays, hosting scattered vegetal fragments (reed) and organic-rich/peaty layers. Thin layers of medium-to-fine sands locally occur. Small, thin-shelled mollusk fragments are also encountered.	Olygotypic meiofauna mainly composed of highly-confined foraminiferal species (*Haynesina germanica* and *Ammonia tepida*) tolerant to stagnant, organic-rich environmental conditions. The agglutinated foraminifer*Trochammina inflata* locally occurs as rare taxon. Ostracods are absent.
Subtidal	Tidally-influenced channel sands	Metric-thick, fining-upward succession of light gray fine-to-medium sands, with abundant micas and scattered plant and mollusk shells fragments. Abundant shells of *Cerastoderma* commonly occur at the basal portion of the sandy succession (channel lag), marked by an erosional surface.	Barren of microfossils. One samples collected from channel-lag sands contains few abraded valves of the euryhaline ostracod *Cyprideis torosa*.
	Lagoon clays and silts	Homogeneous succession of soft light-gray clays, silty clays and clayey silts with abundant entire shells of mollusks, especially *Cerastoderma glaucum,* and small scattered vegetal debris. Cm-thick fine sand intercalations are locally recorded.	Abundant meiofauna dominated by the euryhaline species *Cyprideis torosa* and *Ammonia tepida* (both >30%). The brackish-marine ostracods *Loxoconcha elliptica* and *Leptocythere bacescoi* occur as common species, along with highly-confined (*Haynesina germanica*) and low-confined (*Aubygnyna perlucida*, *Cribroelphidium* spp.) foraminiferal species.

Table 4

5.1.2 Additional subsurface data concerning with paleodrainge traces: shallow cores (2 m long)

Following the spatial distribution of the traces identified through RS data, further six cores 2m-long were drilled around the MV (fig. 5.1), to furtherly assess/test the possible presence of sandy deposits connected to the paleochannels traces occurring on the surface.

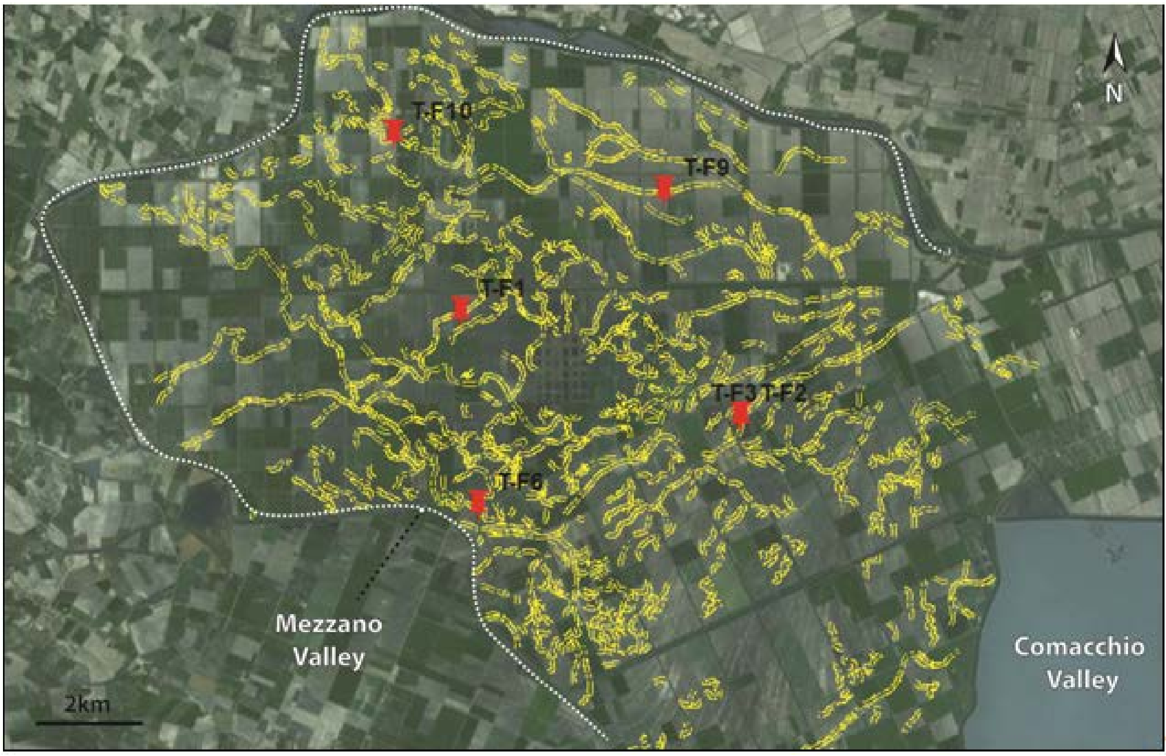

Figure 5.1_ Image from Google Earth reporting the RS-detected traces mapped (yellow lines), connected with the paleodrainage system and the location of the shallow cores (2m-long) drilled (red symbols).

All the shallow cores were drilled on-trace, and in particular five drillings were carried out on the bright portions (TC-F1, TC-F2, TC-F6, TC-F9, TC-F10) and one on the black portion (TC-F3) of the RS-detected traces.

As shown in fig. 5.2 the cores don’t record in any case the occurrence of sandy deposits on the surface. In detail, the cores located on the bright portion recorded at the base of the recovered succession the occurrence of fine-sand bodies, with FU trends, and top attesting at different depths, ranging between 80 cm b.g.l. and 1.8 m b.g.l., consistent on the basis of the sedimentologic and morphologic traces characteristics with tidally-influenced channel deposits.

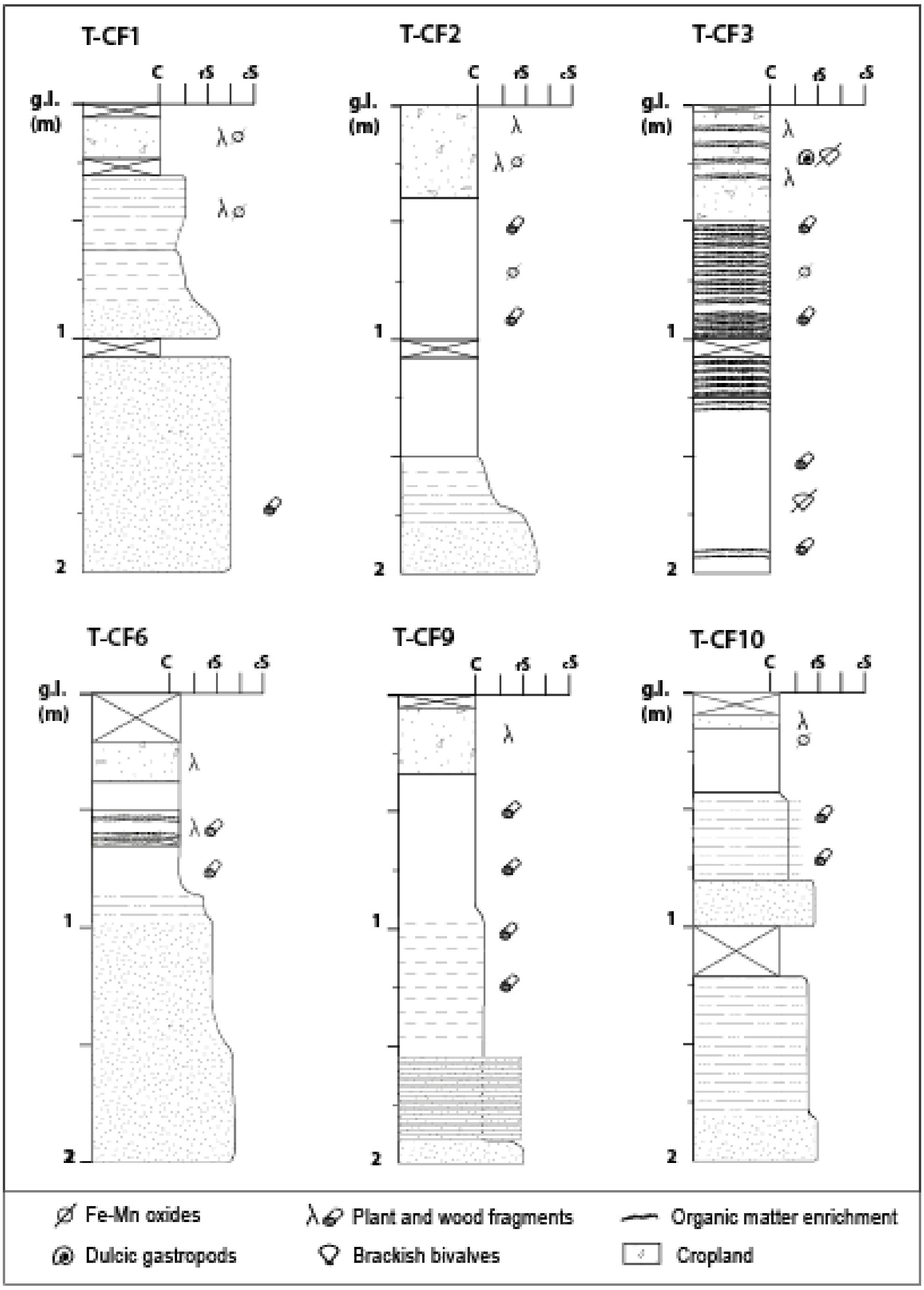

Figure 5.2_Stratigraphic logs of the drilled shallow cores (2m-long) on the RS-detected traces in the Mezzano Valley (MV) site.

Above, sandy bodies are generally overlaid by greyish, at time greyish-brownish, clays and silty clays, with abundant roots and vegetal fragments locally slightly altered (scattered reddish mottles) and rare thin organic layers consistent with wetland deposits.

In core T-CF9, a 40 cm-thick alternation of centimetric layers of clays and fine sands document an overbank deposit occurring above a decimetric channel sand layer.

Core located on the dark portion of the remote-sensed trace record from the base (2m b.g.l.) an invariably clay succession. From the bottom, grey clays with scattered vegetal fragments and rare small (millimeter) thin-shell fragments pass upwards at around 1m b.g.l.to dark organic-rich clays, hosting abundant vegetal fragments and, locally, peat reaching the surface.

At around 45 cm b.g.l. bioturbation traces and abundant roots occur into the clays, that upward turn into clayey croplands. These deposits are consistent with backswamp settings developed in a morphologic low (possible thalweg position) likely left from the channel abandonment activity.

- 5.2 Beach-ridges RS-detected traces (MV east area)

5.2.1 RS-derived geomorphological features

The satellite images analysis integrated with DTM LiDAR data allowed to map the detailed 3D expression of numerous bright and dark linear juxtaposed features (respectively high and low reflectance values) occurring on areas charaterized by bare soils (black and bright strips respectively in fig. 5.3) already partially investigated by Sgavetti (1974) and Bondesan et al. (1995) and attributed to outcropping/sub-outcropping beach-ridges.

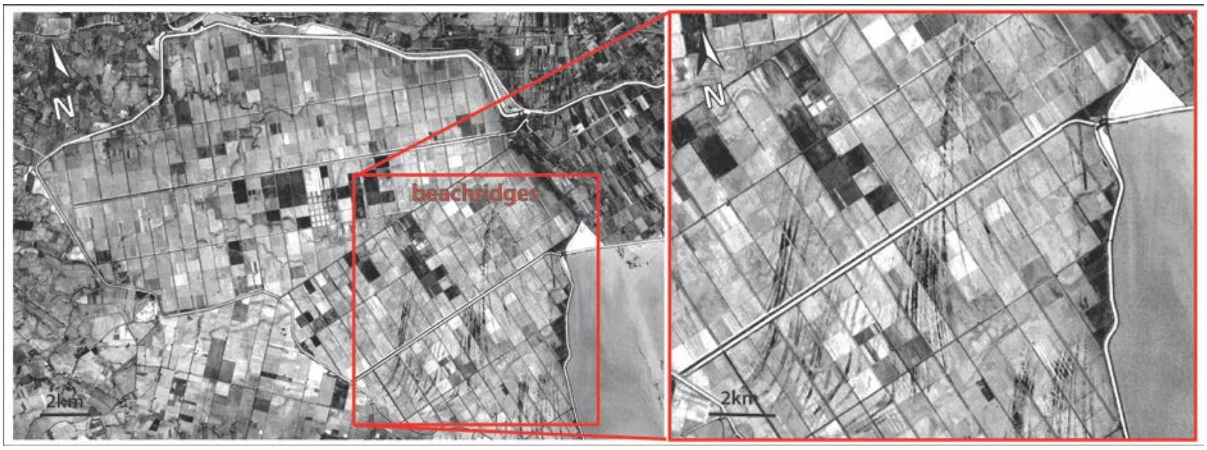

Figure 5.3_ Principal Component 1 (PC1) of ASTER (visible-near ifrared) VNIR bands; zoom in: highlighted traces (beachridges) as alternation of dark and bright strips of pixels.

The alternation of bright and dark features (groups of pixels) outline a series of mainly continuous straight-slightly curved traces, with an overall SW-NE orientation, covering an area of ca. 45 km^2. The traces display regular widths, very similar to each other, of tens-meters (fig. 5.4).

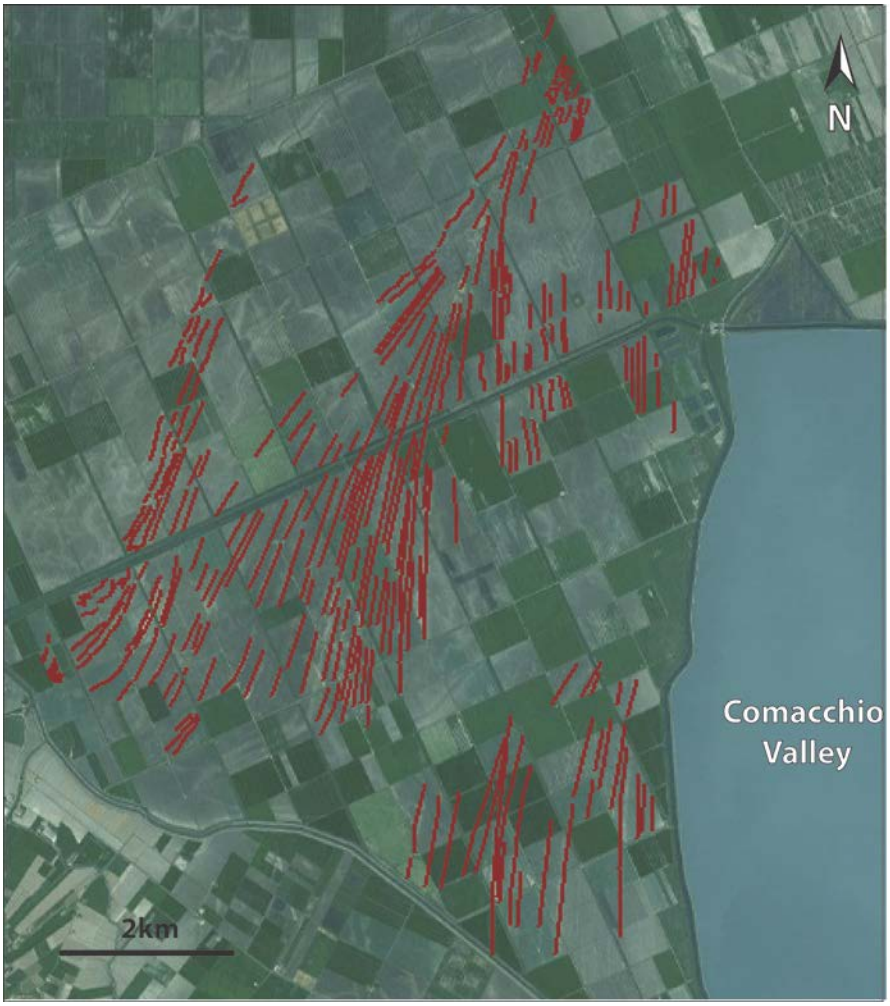

Figure 5.4_Image from Gooogle Earth with mapped traces (red lines) of the remote-sensed beach-ridges.

Despite the presence of the beach-ridges, the ground elevation extracted by the DTM LiDAR display values that maintain always under the sea level (fig. 5.5). Topographic profiles carried out across (NW-SE) the traces, reveal a softly wavy topographic profile, with elevation excursions that range between ca. 50 cm-1 m a.s.l.

The plain spatial arrangement together with the morphologic characteristics (hook-shaped, curved, straight) of the traces allow to divide them almost in 4 distinct groups (fig. 5.6).

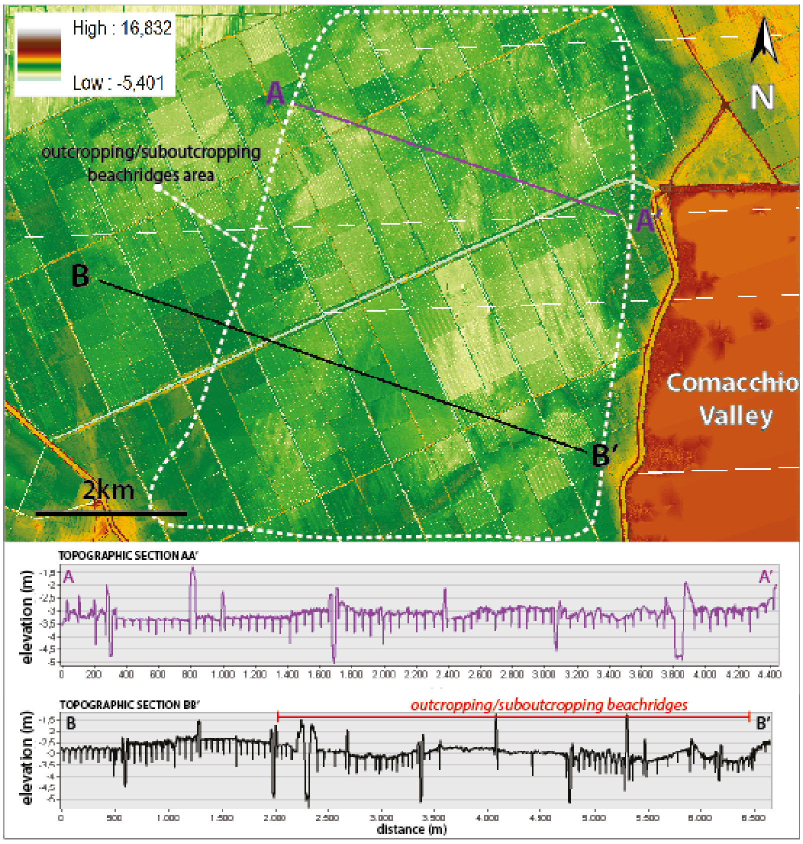

Figure 5.5_Extract from DTM LiDAR of the beach-ridges area, reporting the traces of the topographic sections, AA' and BB', crossing the beachridges from NW to SE.

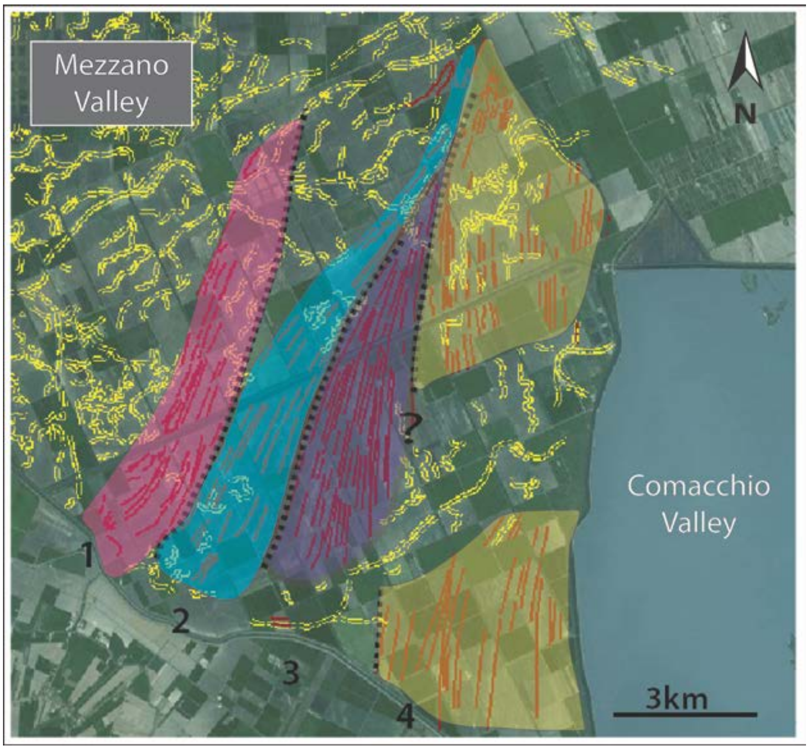

Figure 5.6_ Possible grouping of the remote-sensed traces on the basis of the their geometric patterns.

The innermost group (1 in fig.5.6) displays an overall straight SW-NE orientation, with a regular, parallel and close juxtaposition of the traces, that southwards show a delimited hook-shaped bending.

Moving seawards, within the second group, the traces, even though maintaining the general SW-NE orientation, turn into slight S-shape bends (2 in fig 5.6) juxtaposed features.

The consecutive group, differently, displays slightly curved traces, with an evident converging trend from S to N (3 in fig. 5.6).

The outermost group instead consists of locally interrupted traces, with a slightly curved shape, specular and symmetric respect to the main interruption (4 in fig. 5.6).

The morphologic differences among groups of traces likely reflect different stages of the shoreline progradation, marked by variable environmental conditions and different depositional processes occurring over time, e.g. an early development of discontinuous beach-barrier with spits (1) evolving in well-developed beach-barriers (2) mainly related to dominant longshore current sediment distribution, that turn in beach-ridges and then strandplain beach-riges (3-4) connected to the onset of river delta lobes and fluvial sediment supply.

5.2.2 Subsurfaces data: shallow cores (2m-long)

Following the distribution of the highlighted RS traces, four cores 2m-long were drilled to collect surface and shallow-subsurface lithologic and stratigraphic data.

All the shallow cores were drilled on trace, 2 on both bright (TF-5, TF-8) and black (TF-4, TF-7) ones (fig. 5.7).

Logs of the shallow cores recovered from the drillings are reported in the following Figure 5.8.

As shown in fig. 5.8 cores TF-5 and TF-8, located on the bright traces, recorded from the bottom to the top, light-grey well-sorted medium-to-fine sands passing at around 60 cm b.g.l. respectively to brown fine silty sands, with small (ϕ mm) scattered Fe-Mn oxides and to grey silty clays with altered vegetal debris.

Cores TF-4 and TF-7, located on the adjacent dark traces, recorded similar deposits at the bottom, made of respectively, medium-to-fine light-grey sands and fine-sands with scattered vegetal fragments that pass upwards, around 70 cm b.g.l., to light-grey clays and silty clays with frequent vegetal fragments. In the case of core TF-4, an organic matter enrichment occurred in the uppermost 30 cm b.g.l.

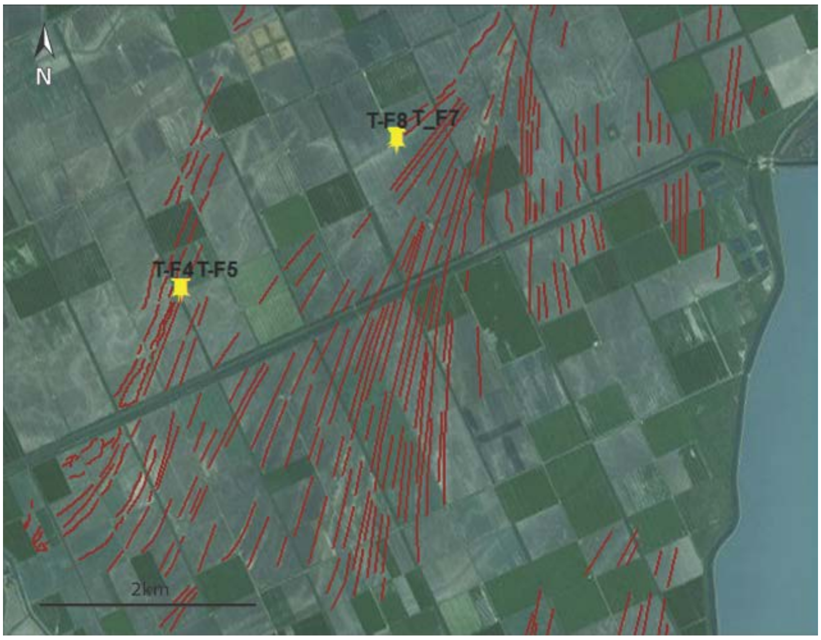

Figure 5.7_ Image from Google Earth with location of the shallow cores (2m long) drillings (yellow symbols) and the mapped beachridges (red lines).

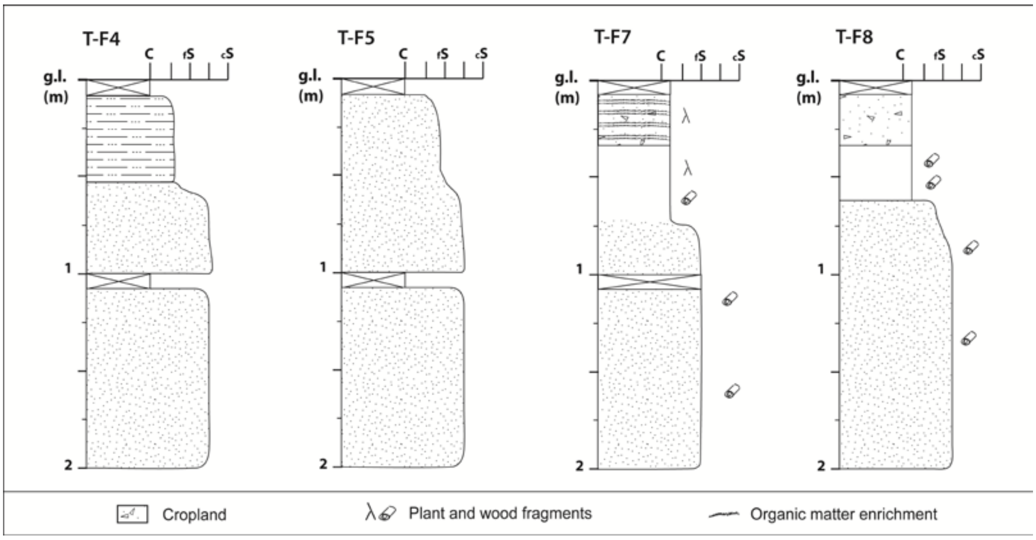

Figure 5.8_ Stratigraphic logs of the drilled shallow cores in the beachridges area.

Thus, the drillings revealed the occurrence, both on the surface and in the shallow subsurface, of sands and sandy silt deposits in correspondence of the bright traces.

Conversely, clayey deposits with different degree of organic matter enrichment, topping towards the surface the sandy bodies invariably occurring in the shallow subsurface, marked the dark traces on the surface.

5.3 Facies associations

Ten main facies associations (almost mentioned in section 5.1) were recognized for the mid-late Holocene succession buried beneath the MV site, considering the sedimentologic features, the meiofauna content and the depositional vertical-lateral relationships recorded by cores.

Detailed facies descriptions and interpretations in terms of depositional environments are reported below. The uppermost 30-50 cm of the cored succession is invariably composed of unstructured brown, dark-brown clays and silty clays, locally organic, with possible scattered shell fragment and vegetal-roots remains and interpreted as a cropland (C).

- ***Paludal (P)***

  Description: this facies, which is exclusively recorded within the uppermost portion of the studied succession, shows a thickness of ca. 1 m and is composed of soft grey homogeneous silts and clayey silts, with reddish mottled due to the presence of local, scattered slightly altered vegetal fragments. Few valves of *Pseudocandona albicans*, a mesohaline ostracod species preferring slow-moving waters (Henderson, 1990), can be locally encountered.

  Interpretation: the sedimentological features together with the local occurrence of a scarce freshwater-low brackish ostracodfauna preferring stagnant conditions point to a low-energy, coastal environment occasionally subject to brief period of subaerial exposure, such as a wetland.

- ***Swamp (S)***

  Description: this facies, which is recorded within the upper portion of the drilled succession, is composed of dark-grey, soft clays hosting abundant vegetal and wood fragments, black peat and/or organic-rich layers, with an overall thickness ranging between 1-2 m. Locally rare small (Ø mm) gastropod shells are encountered. An abundant ostracodfauna dominated by *P. albicans* occurs, except for organic-rich/peaty layers that commonly result barren of microfossils.

  Interpretation: the peculiar sedimentological features (dark color, soft consistency, abundance of vegetal/wood debris and peat and/or organic-rich layers) and the presence of a typical stagnant freshwater-low brackish ostracod species (*P. albicans*; Henderson, 1990) indicate for this facies a low-energy depositional environment with abundant vegetation occurring, such as a paludal setting. The absence of meiofauna within organic-rich/peaty layers is probably due to depleted oxygen conditions (Horne an Boomer, 2000; Frenzel and Boomer, 2005).

- ***Salt-marsh (SM)***

  Description: this facies, which is exclusively recorded within cores drilled at proximal locations, is characterized by an alternation of centimetric soft dark-grey, organic-rich clays hosting abundant vegetal/wood fragments and black peat layers, with an overall thickness of ca. 1.5 m. This facies differs from the swamp facies association for a general higher concentration of peat (the mineralogic component is very reduced) and the sporadic occurrence of the agglutinated foraminifer *Trochammina inflata*.

  Interpretation: sedimentological characteristics and the scattered occurrence of a typical salt-marsh foraminifer (Horton and Edwards, 2006) point to a salt-marsh environment.

- ***Intertidal mud-flat (IMF)***

  Description: light-grey clays and silty clays, hosting scattered vegetal fragments (reed) slightly altered, and, locally, organic-rich clays or thin layers of medium-to-fine sands compose this facies association. Scattered small (millimetric) thin-shells of mollusks occur. The meiofauna is exclusively composed of foraminiferal species typical of relatively highly-confined brackish environments (Debenay and Guillou 2002) as *Haynesina germanica* and *Ammonia tepida*.

  Interpretation: the sedimentological features together with the occurrence of an oligotypic foraminiferal calcareous fauna indicative of highly-confined coastal settings, subject to stressed conditions and typically found in modern intertidal environments (Horton and Edwards, 2006; Leorri and Cearreta, 2009), allow to interpret these deposits as an intertidal mud-flat.

- ***Lagoon (L)***

  Description: this facies association marks the lower portion of the investigated sedimentary succession. It consists of light-grey homogeneous soft clays, silty clays and clayey silts with abundant entire shells of mollusks, especially *Cerastoderma glaucum*, and locally small scattered vegetal debris. An abundant meiofauna, dominated by the euryhaline species *C. torosa* and *Ammonia tepida-A. parkinsoniana* is recorded. As secondary species, foraminiferal taxa commonly found into lagoon basins (Albani and Serandrei Barbero, 1990), *H. germanica*, *Aubygnyna perlucida*, *Cribroelphidium* (*C. granosum*) species, and brackish-marine ostracods (*Loxoconcha elliptica*, *Leptocythere bacescoi*) are encountered.

  Interpretation: the sedimentological features and the peculiar fossil content, composed of euryhaline and brackish-marine species, lead to interpret this unit as formed in a low-energy setting partially barred to the sea and subject to remarkable marine influence, such as a brackish lagoon.

- ***Tidally-influenced channel fill (TC)/ Tidally-influenced channel point bar (TCP)***

  Description: this facies association is either made up of *(i)* light-grey, medium-to-fine "quartzy" sands 1-2 m thick and hosting abundant up-to-centimetric mollusk shells (especially *Cardium*) in the lower portion marked by a basal erosive surface. Scattered vegetal fragments and locally centimetric-thick, grey-dark grey silty-sandy layers with abundant small vegetal debris occur; and *(ii)* light-grey sands, with a thickness of 2 m, characterized by a basal erosive boundary and a fining-upward (FU) trend, from fine silty sands to clayey silt. Locally scattered small shell fragments occur.

  Samples collected from this facies are commonly barren of microfossils, or at least contain few fragments of unidentifiable ostracods. Only one sample collected from the lowermost portion (channel lag) of the sandy succession cored at distal location show few abraded valves of the euryhaline ostracod *C. torosa* (Athersuch et al., 1989).

  This facies association occurs at different stratigraphic levels and displays thickness ranging from 1 m to 2.5 m.

  Interpretation: the sedimentological features point to a high-energy channelized depositional setting. The fossil content, when is present, together with the latero-vertical stratigraphic relationships with intertidal-subtidal facies allow to interpret these deposits as *(i)* a tidally-influenced channel-fill succession and *(ii)* a point bar of a migrating tidally-influenced channel .

- ***Overbank (O)/ Channel abandonment (CA)***

  Description: this facies association is either made up of *(i)* centimetric to decimetric alternation of grey fine silty sands-sandy silts and silts with slightly altered vegetal debris, few specimens of *A. tepida-A. parkinsoniana*, *H. germanica* and *T. Inflata* and a total thickness of ca. 1 m, and *(ii)* centimetric to decimetric alternation of soft light-grey clays-silty clays and light-grey silts-sandy silts, containing slightly altered vegetal debris and scattered valves of *P. albicans*, with a total thickness of ranging between ca. 0.5-1.5 m. Locally thin sandy layers can occur.

  Interpretation: the sedimentological features, reflecting the occurrence of alternating high to low energy pulsations, together with the latero-vertical relationships with the other facies, especially TC/TCP, allow to interpret this facies strictly connected with the activity of tidal-influenced channels. Specifically, the centimetric to decimetric alternation of sandy-silty deposits containing few, likely displaced, typical brackish-intertidal foraminifers *(i)* is interpreted as an overbank deposits, while the centimetric to decimetric clay-silt alternation *(ii)* invariably recorded at the top of TC are interpreted as representative of the channel deactivation.

- ***Beach-ridge (BR)***

Description: this outcropping/sub-outcropping facies, reaching the depth of ca. 2 m, consists of light-grey medium-to-fine sands, with scattered reddish mottles due to the presence of slightly altered small vegetal debris. No occurrence of shells or shell fragments is recorded. Locally these deposits pass upwards to dark-brown organic silts-sandy silts with small and scattered Fe-Mn oxides. Plant fragments and roots also occur. No samples have been collected for micropaleontological analyses.

Interpretation: based on the sedimentological features this unit is interpreted as a beach-ridges facies, including the “dune” (sandy deposits) and “interdune” (sandy deposits with silty-sandy top) sub-units.

References

Albani A. & Serandrei Barbero R., (1990). I Foraminiferi della Laguna e del Golfo di Venezia. Memorie Scienze Geologiche Padova 42, 271–341.

Athersuch J., Horne D.J., Whittaker J.E., (1989). Marine and brackish water ostracods, in KERMACK D.M., BARNES R.S.K. (eds.) «Synopses of the British Fauna (New Series)», 43, Brill E.J., Leiden, pp. 1-343.

Bondesan M., Favero V., Vinals M. J. (1995). New evidence on the evolution of the Po delta coastal plain during the Holocene. *Quaternary International*, *29/30*(95), 105–110.

Debenay J.-P. and Guillou J. J., (2002). Ecological transitions indicatedby foraminiferal assemblages in paralic environments. Estuaries25, 1107–1120.

Frenzel P. and Boomer I., (2005). The use of ostracods from marginal marine, brackish waters as bioindicators of modern and Quaternary environmental change, Palaeogeography, Palaeoclimatology, Palaeoecology, 225, 68-92.

Henderson P.A., (1990) Freshwater ostracods. In: Kermack DM, Barnes RSK (eds) Synopsis of the British fauna (New Series). Vol,42. *Universal Book Services,* Oegstgeest.

Horne D.J. and Boomer I., (2000).The role of Ostracoda in saltmarsh meiofaunal communities. In: Sherwood, B.R., Gardiner, B.G. & Harris, T. (eds) British Saltmarshes. Forrest Text, Cardigan, for the Linnean Society of London,182–202.

Horton B.P. and Edwards R.J., (2006). Quantifying Holocene sea level change using intertidalforaminifera: lessons from the British Isles. Cushman Foundation for ForaminiferalResearch Special Publication 40

Leorri E. and Cearreta A., (2009). Quantitative assessment of the salinity gradient within the estuarine systems in the southern Bay of Biscay using benthic foraminifera.Continental Shelf Research 29, 1226–1239.

Sgavetti M., (1974). Le caratteristiche di riflettività spettrale di una zona della pianura Padana su immagini ERTS-1, Anno XXXII-Bollettino di Geologia e Scienze Affini, n.3.

CHAPTER 6_ DISCUSSION AND CONCLUSIONS

In this chapter the results obtained through the application of the proposed integrated RS-stratigraphic approach for each study area (Pisa Plain and Mezzano Valley) are compared and discussed.

In detail, the discussion concerns with two different but complementary aspects that represent the two main purposes of the present work: *(i)* to evaluate the effectiveness and the potentiality of free-of-charge RS data analysis (optical multispectral/hyperspectral satellite images), combined with DTM LiDAR, in the identification of buried landforms in coastal-delta plain settings and analyze the stratigraphic factors influencing RS detected traces surface visibility, and *(ii)* to furnish new insights into the sedimentary evolution of the two selected coastal areas during the highstand phase (ca. 7000 cal. yr BP onwards).

Thus, the two topics are discussed into separate sections, as follows.

6.1_ The effectiveness of RS data and analyses in reconstructing Holocene landscapes buried beneath modern coastal-delta plains

The present work results a successful case of application of free-of-charge satellite optical images and DTM LiDAR in delineating past buried drainage morphologies in different extra-urban coastal-delta plain settings: active wave-dominated delta plain-Pisa Plain (SR site) *versus* abandoned wave-dominated delta plain-Mezzano Valley (MV). In contrast, unsuccessful employment of these RS data and analysis for mapping paleochannels in the Pisa urban area confirms the necessity to use and apply other passive and/or active RS data and analyses (airborne photo-interpretation, ERT) in long-settled city areas.

The comparison of the results obtained from the two extra-urban study sites, i.e. the San Rossore site and the Mezzano Valley, through the integration of RS-stratigraphic data allows to improve our knowledge about the relationship existing between RS-detected traces and shallow subsurface stratigraphy.

The main aspects regarding the effectiveness of RS data (satellite imagery and DTM LiDAR) as a tool for a plan-view identification of buried sedimentary bodies in coastal areas are listed as follows:

1) in croplands, appropriate satellite imagery processing and analysis (in particular false color composition, multitemporal analysis and PCA), combined with DTM LiDAR, allow the identification and detailed mapping on the surface of buried landforms (paleochannels) and their morphological features. These landforms are highlighted by the arrangement of pixels with contrasting brightness (spectral reflectance behaviour of the surface) and, possibly, (micro) topographic variations detected on the surface;

2) the arrangement of pixels with contrasting brightness (bright-high reflectance values *versus* dark-low reflectance values) depends on the spatial distribution patterns of surface moisture that, in turn, is influenced by the superficial distribution of organic-rich deposits and/or by the shallow subsurface stratigraphic architecture;
3) in the Mezzano Valley, and potentially in similar interdistributary wetlands, the superficial spatial distribution of lithofacies with different organic-matter content, and then with different capacity to retain moisture, is guided by the stratigraphic architecture of the uppermost ca. 6-7 m. Indeed, the development, lateral migration and filling of numerous but isolated meandering paleochannels induced recurrent well-defined micro-morphologies, still detected by LiDAR, that favored the deposition of organic-rich clays (salt marsh and then swamp) in correspondence of low-lying areas lateral to the meanders;
4) in the Pisa Plain, as in other prograding delta plains where an alluvial phase occurred during the last millennia, the brightness contrast patterns induced by the spatial distribution of surface moisture are less evident and more discontinuous than in the MV. The occurence of facies heteropies in the shallow subsurface (at least uppermost 2m) alluvial succession (channel fill/overbank *versus* floodplain or clayey plug/abandoned channel facies, i.e., granular *versus* cohesive deposits) favor the development of irregular surface moisture patterns;
5) the degree of visibility of RS-detected traces in deltaic-alluvial contexts as that of Pisa Plain, characterized by limited occurrence of organic-rich deposits and frequent and alluvial facies heteropies over short distances, can be very low for landforms buried more than 1 m below the ground level. Only in few scenes those landforms can be detected as evident and continuous traces, when the lateral transition between fine-grained and granular deposits is highlighted by evident moisture variations;
6) the RS approach results to be particularly effective in depositional context characterized by the formation of isolated coarse-grained sedimentary bodies encased in homogeneous and widespread fine-grained organic-rich deposits. This depositional architecture, encountered in the subsurface of the MV site, documents to favor clear reflectance contrasts.

Thus, free-of-charge satellite images combined with DTM LiDAR data represent an easily available, convenient tool that can be suitable for the reconstruction of paleodrainage morphologies and deposits buried at depths more than 2-3 m below the ground level. The RS-detected paleochannels can be considered the surface geomorphological expression of buried sandy bodies, whose formation and activity can be dated back up to the early highstand phases.

Also considering the limitations in alluvial-deltaic contexts (see point 5), optical satellite images and DTM LiDAR can be a powerful tool for wide-scale paleoenvironmental reconstructions in coastal areas, in addition to the common employment in restricted sites (e.g., archeological sites) and in substitution of high-resolution RS data with limited access or paid (e.g., aerial photo).

6.2_Holocene sedimentary evolution phases of lagoon system as revealed integrating RS and stratigraphic data

The fully integration of RS data and analyses with subsurface stratigraphic data has allowed to reconstruct with a good degree of detail the three-dimensional depositional/sedimentary evolution of the study sites during the last 7000 cal yr BP.

The identification of buried landforms and their stratigraphic placement and age, thanks to the integration of high-resolution stratigraphic data (cores) and spatial continuous surface information (RS-detected traces), helps to better understand the environmental changes occurred in the study areas over the mid-late Holocene period.

Stratigraphic sections across each study area, intercepting the main RS-detected landforms and involving both new and already available stratigraphic data (Arno and Po geognostic databases) are presented in Figures 6.1 and 6.2.

They represent the base to compare and discuss the mid-late Holocene sedimentary evolution of two microtidal lagoons, formed during the peak of marine transgression (8000-7000 calibrated yr BP; Fairbanks, 1989; Bardet al., 1996) and progressively filled.

Specifically, Figure 6.1 shows a W-E (sea-to-land) oriented section, carried out from the extra-urban Pisa Plain (including the innermost outcropping beach-ridge and the SR croplands) to the urban area of Pisa.

The section passes through all the main RS-detected traces identified for the Pisa Plain, in this thesis and in previously published works, and the highest quality core data including the new drilled cores and three mappa cores (mappa2-M2, mappa7-M7 and mappa26-M26) derived from the “MappaProject” research which I belonged to.

Figure 6.2 shows three SW-NE oriented stratigraphic sections (A, B,C, respectively west to east) carried out in the Mezzano Valley study area intercepting, among others, the RS-detected traces selected for this study (meanders M1 and M2 in Chapter 5, section 5.2)

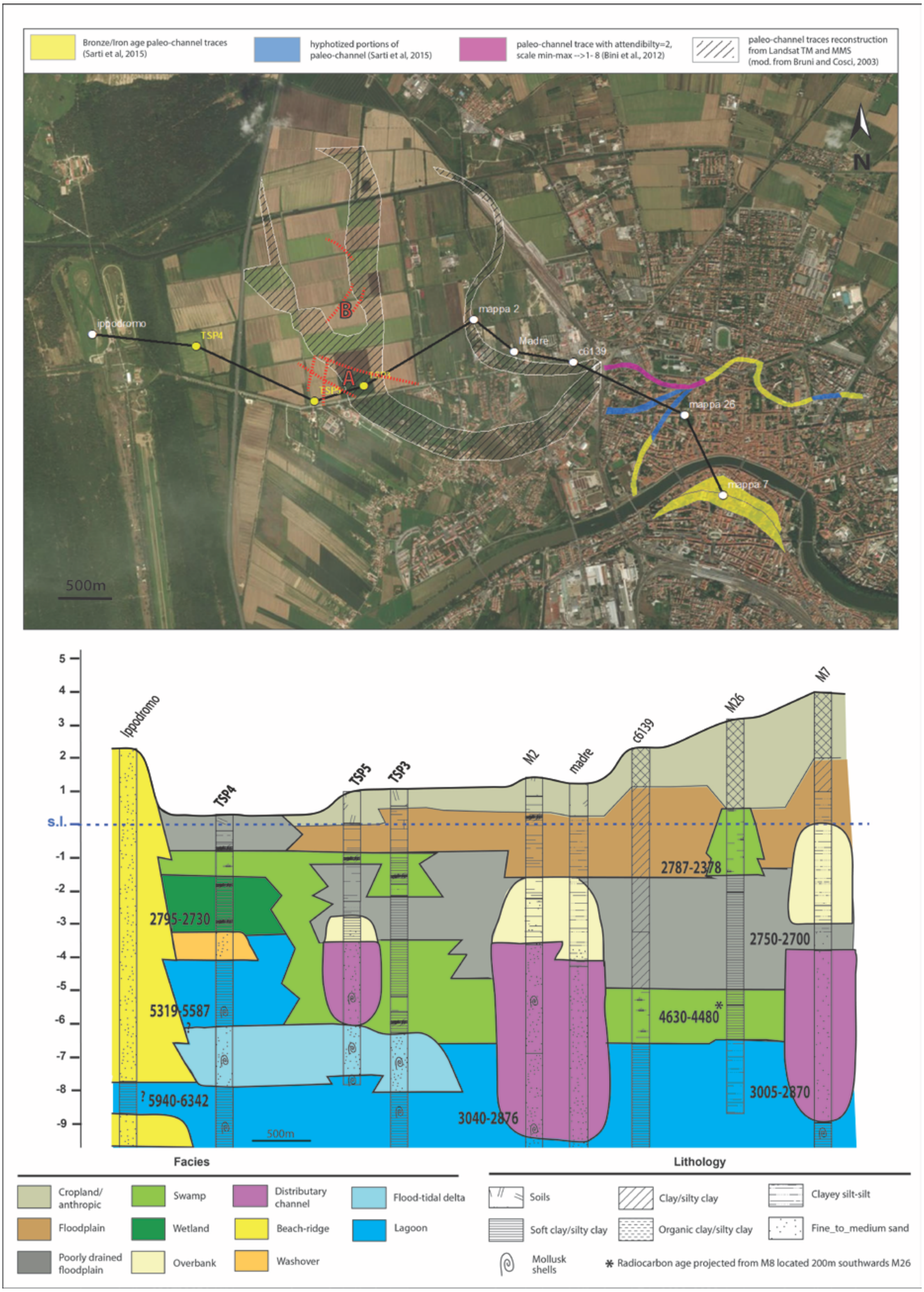

Figure 6.1_Interpreted stratigraphic section across the San Rossore (Pisa) study area.

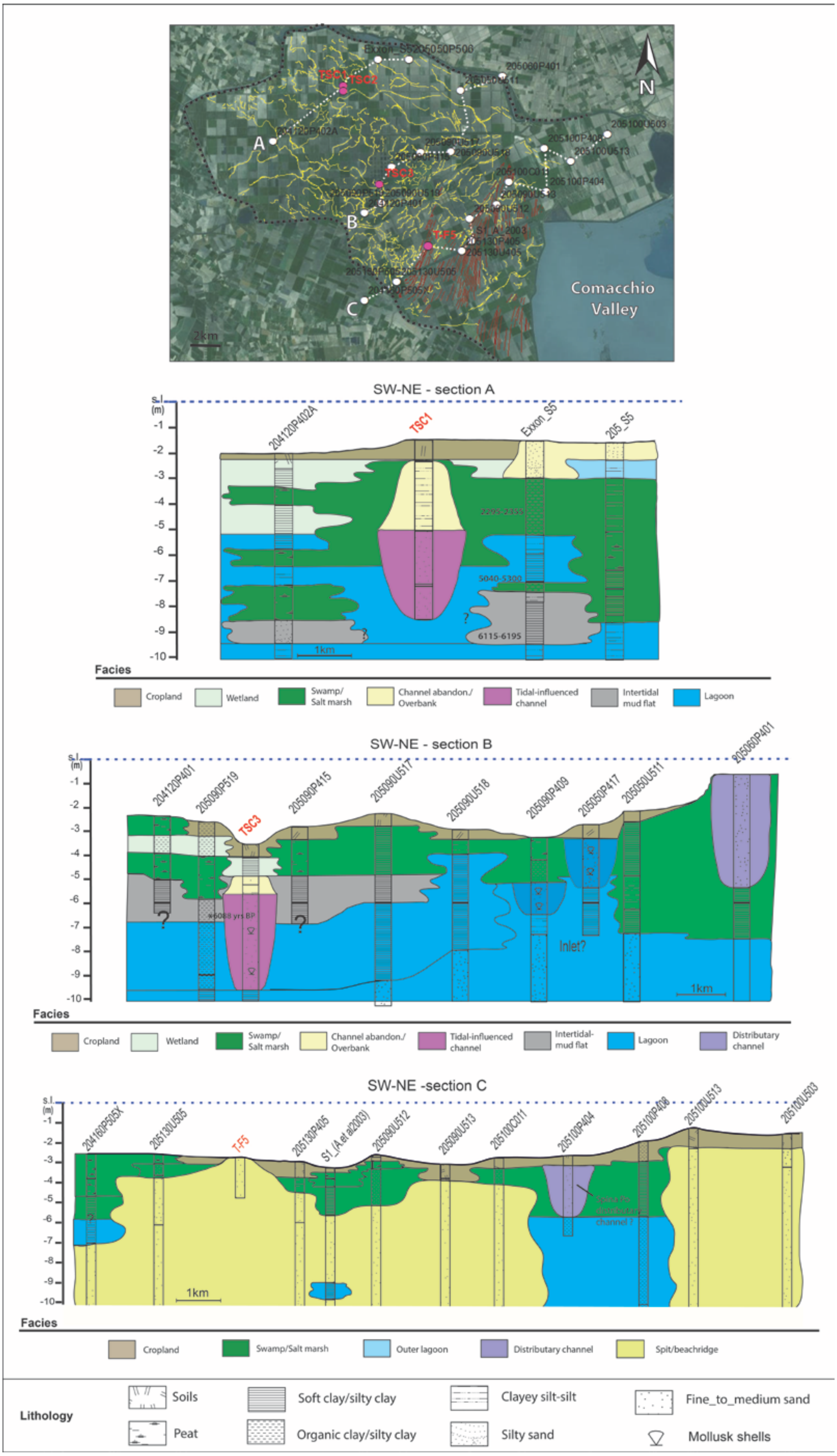

Figure 6.2_Stratigraphic sections across the Mezzano Valley study area.

As shown in Figures 6.1 and 6.2 and according to Amorosi et al. (2003, 2013), a wide lagoon system invariably occupied both the study areas during the earliest stages of sea-level highstand between ca. 7000-5000 cal yr BP. However, different evolutionary steps leading to the lagoon siltation can be defined for the Pisa Plain and the Mezzano Valley.

In detail, as shown in Figure 6.1 and Figure 6.3, the lagoon occurring in Pisa started to undergo enclosed/confined environmental conditions passing from an early “leaky” stage with early barriers wide-opened to the sea, which favored a high marine influence up to relatively internal positions, as testified by the extensive record of flood-tidal delta deposits, to a progressively more restricted stage (Kjerfve & Magill, 1989) since around 5000 cal yr BP.

A strong decrease in marine influence is recorded between ca. 5000-2700 cal yr BP either at distal (SR site) and proximal (Pisa city area) locations by peculiar vertical stacking patterns of facies, and likely connected to the development of the first sets of more laterally-continuous beach-ridges.

At distal locations, the meiofauna content found within the lagoon succession overlying the flood-tidal delta deposits testifies a rapid increase in degree of confinement until the transformation of the lagoon into a brackish lake environment, almost totally barred to the sea and only occasionally reached by sea currents during storm events (washover fan in TSP4).

Consistently, at proximal locations the lagoon abruptly turned into a paludal environment (swamp) and then into a poorly-drained floodplain crossed by channels, as those mapped mainly using airborne photos and discussed in Sarti et al. (2015). Other channel-bodies (cores TSP5, M2 and Madre), showing a similar top-of-sand depth and likely active before the Etruscan period (ca. 2700 cal yr BP), crossed the Pisa Plain forming a complex proto-historic paleodrainage that distributed sediments from the alluvial-delta plain to the sea.

All of them are connected to two sinuous branches, identified on the basis of RS analyses (fig. 6.1) and pointing to a main river mouth at the northern edge of the SR site.

Since the Etruscan period, an alluvial depositional phase progressively dominated by few river branches and well-drained conditions (Bini et al., 2015; Amorosi et al., 2013) characterized the Pisa Plain even if locally brief phases of renewed swamp development occurred over time (backswamps within a floodplain context; see Amorosi et al., 2013).

At the same time, at distal position (TSP4), this progradational trend is recorded by the development of confined swamps reclaimed in recent times. Here the morphologic setting, i.e. back-barrier location (morphologic low), has locally prevented the development of well-drained conditions over time.

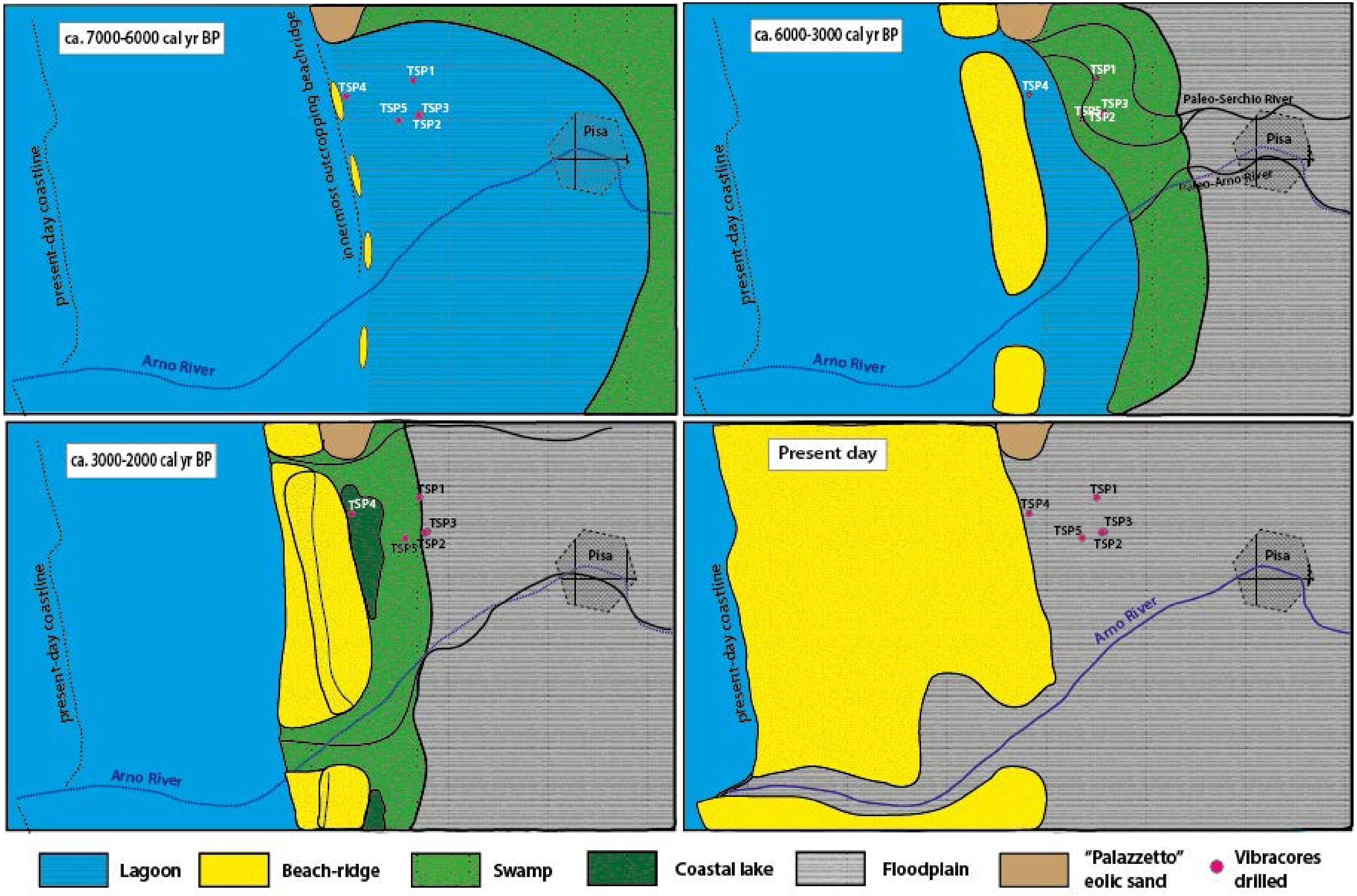

Figure 6.3_Interpretative sketch of the depositional evolutionary phases of thePisa lagoon.

On the other side, in the Mezzano Valley, as shown in Figure 6.2a and Figure 6.4, a tidally-influenced phase started to affect the lagoon since ca. 6000 cal yr BP with the development of mud-flat/salt-marsh environments crossed by a dense and articulated drainage system, made of narrow meandering channels whose traces are visible on satellite images. The RS-stratigraphic data integration documented two main paleodrainage networks, active at different time between ca. 6000 cal yr BP and 2500 cal yr BP as documented by the results obtained from the two investigated meanders (see Chapter 5, section 5.2). The development of this drainage system in the mentioned time interval seems to be related with the development of more continuous beach-barriers enclosing the MV over time, as shown in Figure 5.5 of section 5.3.1, that likely favored together with the gentle topographic gradient marking the Northern Adriatic Sea, the amplification of the tidal influence inside the lagoon through narrow inlets.

After 2400 cal yr BP, widespread swamp and brakish paludal environments developed in the area and the tidally-influenced channels underwent a progressive “siltation”, as documented by the thick overbank deposits occurring in TSC1.

The development of paludal environmental conditions and the “siltation” of the channels are consistent with the activation of the Po di Spina delta lobe in front of the study area (around 2700 yr BP; Bondesan, 1995; Stefani and Vincenzi, 2005) that prevented the sediment supply from the sea. From this time onward the Mezzano Valley environmental conditions “freezed” (as testify by the dating in TSC2), as this area continued to be by-passed by the sediment supply carried toward the sea by the Po fluvial branches (Po di Volano and Po di Spina). These branches were responsible for the construction of various delta lobes, until the major avulsion, known as Rotta di Ficarolo (in 1152), that forced the entire Po River system to migrate northward (modern Po Delta; Stefani & Vincenzi, 2005; Amorosi et al., 2008).

Thus, the integration of RS-detected traces and subsurface data, supported by the information furnished by the outcropping/sub-outcropping beach-ridges, that represent remarkable geomorphological elements of the lagoon systems, highlights different mechanisms controlling the lagoon infilling in the two study areas:

i) in Pisa, the infilling of the lagoon is connected to both the growth of well-developed, continuous beach-ridges barring the lagoon from the sea, forcing it to evolve towards a paludal environment, and the activity of distributary channels linked to an early articulated drainage system composed of Arno and Serchio paleobranches. These conditions led to the development of a lagoon delta that with the progressive progradation of the alluvial system, evolved at around 3000-2000 yr cal BP in a wave-dominated delta system, responsible for the burial of the paludal environments and the alluvial delta plain growth;

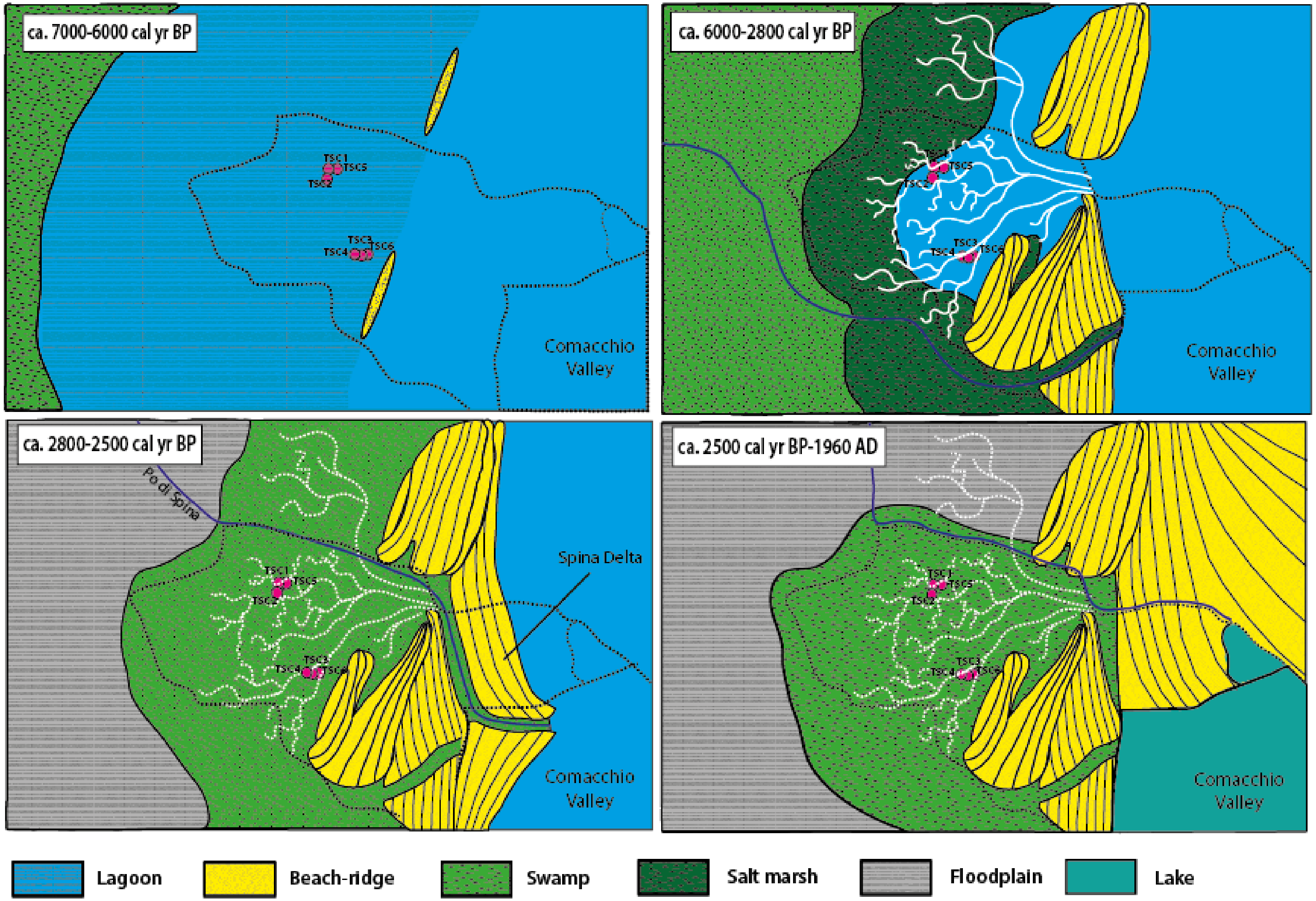

Figure 6.4_Interpretative sketch of the depositional evolutionary phases of the Mezzano Valley lagoon.

ii) in the Mezzano Valley, the low topographic gradient and the northern position of the Po River paleobranches (Piovan et al., 2010; 2012) promoted the development of an interdistributary bay hosting a lagoon during. This lagoon enclosed from the growth of continuous beach-ridges supplied mainly by longshore currents experienced a tidally-influenced phase, during which the development of a tidally-influenced channels network was favored.

The following onset in the area of Po river branches (Spina and Volano) that regularly by-passed the interdistributary bay, to construct different delta lobes seawards, caused the development of a confined paludal environment up to the present time (1964 Mantello land reclamation works, Bondesan, 1990), characterized by negligible sediment supply over time, neither from the sea nor from the rivers.

References

Amorosi A., Centineo M.C., Colalongo M.L., Pasini G., Sarti G., Vaiani S.C., (2003). Facies architecture and Latest Pleistocene–Holocene depositional history of the Po Delta (Comacchio area), *Italy. J. Geol.* 111, 39–56.

Amorosi A., Pavesi M., Ricci Lucchi M., Sarti G., Piccin A., (2008). Climatic signature of cyclic fluvial architecture from the Quaternary of the central Po Plain, Italy. *Sedimentary Geology*, *209* (1–4), 58–68. http://doi.org/10.1016/j.sedgeo.2008.06.010

Amorosi A., Rossi V., Sarti G., Mattei R., (2013). Coalescent valley fills from the late Quaternary record of Tuscany (Italy). *Quaternary International*, *288*, 129–138. http://doi.org/10.1016/j.quaint.2011.10.015

Bard E., Hamelin B., Arnold M., Montaggioni L.F., Cabioch G., Faure G., Rougerie F., (1996). Deglacial sea level record from Tahiti corals and the timing of global meltwater discharge. Nature 382, 241–244.

Bini M., Rossi V., Amorosi A., Pappalardo M., Sarti G., Fabiani F, Gualandi L., Noti V., (2015). Palaeoenvironments and palaeotopography of a multilayered city at the Etruscan-Roman transition: early interaction of fluvial processes and urban growth at Pisa (Tuscany, Italy). Journal of Archaeological Science 59 197–210.

Bondesan M., (1990). Le zone umide salmastre dell’Emilia Romagna: aspetti geografici e geomorfologici. In: *Aspetti naturalistici delle zone umide salmastre dell’Emilia Romagn*a, pp.23-56. Regione Emilia-Romagna

Bondesan M., Favero V., Vinals M. J., (1995). New evidence on the evolution of the Po delta coastal plain during the Holocene. *Quaternary International*, *29/30*(95), 105–110.

Fairbanks R.G., (1989). A 17,000-year glacio-eustatic sea level record: influence of glacial melting rates on the Younger Dryas event and deep-ocean circulation. Nature 342, 637–642.

Kjerfve B. & Magill K.E., (1989). Geographic and hydrographic characteristic of shallow coastal lagoon, *Marine Geology*, 88, 187-199

Piovan S., Mozzi P., Stefani C., (2010). Bronze age paleohydrography of the southern Venetian Plain. *Geoarchaeology*, *25*(1), 6–35. http://doi.org/10.1002/gea.20300

Piovan S., Mozzi P., Zecchin M. (2012). The interplay between adjacent Adige and Po alluvial systems and deltas in the late Holocene (Northern Italy). *Geomorphology*, 18, 4- pp. 427-440

Sarti G., Rossi V., Amorosi A., Bini M., Giacomelli S., Pappalardo M., Ribecai C., Ribolini A., Sammartino I., (2015). Climatic signature of two mid-late holocene fluvial incisions formed under sea-level highstand conditions (Pisa coastal plain, NW Tuscany, Italy). *Palaeogeography, Palaeoclimatology, Palaeoecology,* 424, 183-195.

Stefani M. & Vincenzi S., (2005). The interplay of eustasy, climate and human activity in the late Quaternary depositional evolution and sedimentary architecture of the Po Delta system. *Marine Geology*, *222–223*(1–4), 19–48. http://doi.org/10.1016/j.margeo.2005.06.029

APPENDIX A

SATELLITE IMAGES: PCA and FCC examples
(Pisa Plain and Mezzano Valley study areas)

Acknowledgement:

Data available from the U.S. Geological Survey.

Acknowledgement:

Data distributed by the Land Processes Distributed Active Archive Center (LP DAAC), located at USGS/EROS, Sioux Falls, SD. http://lpdaac.usgs.gov

PC1_Pisa_L7_11November2000

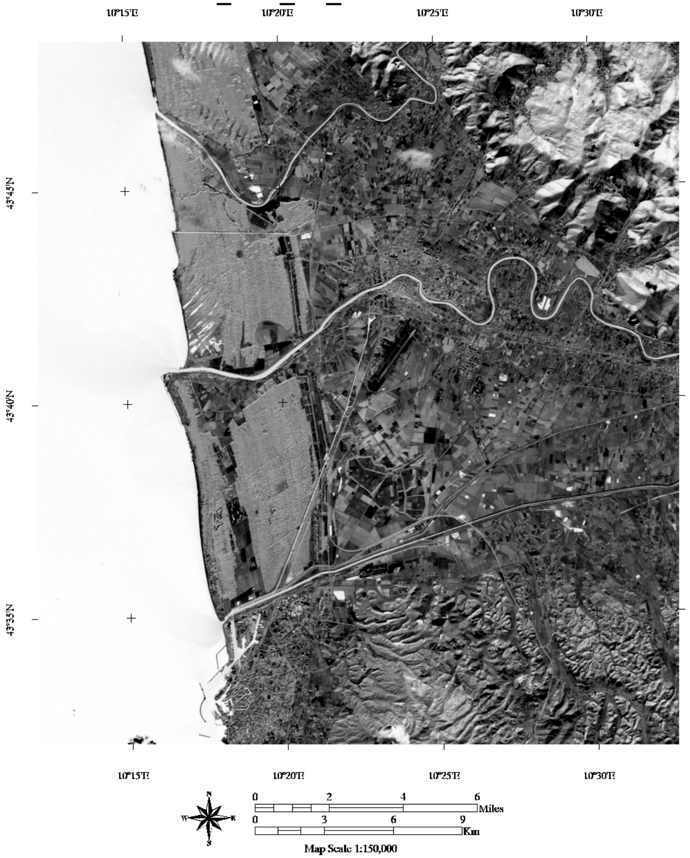

PC2_Pisa_L7_11November2000

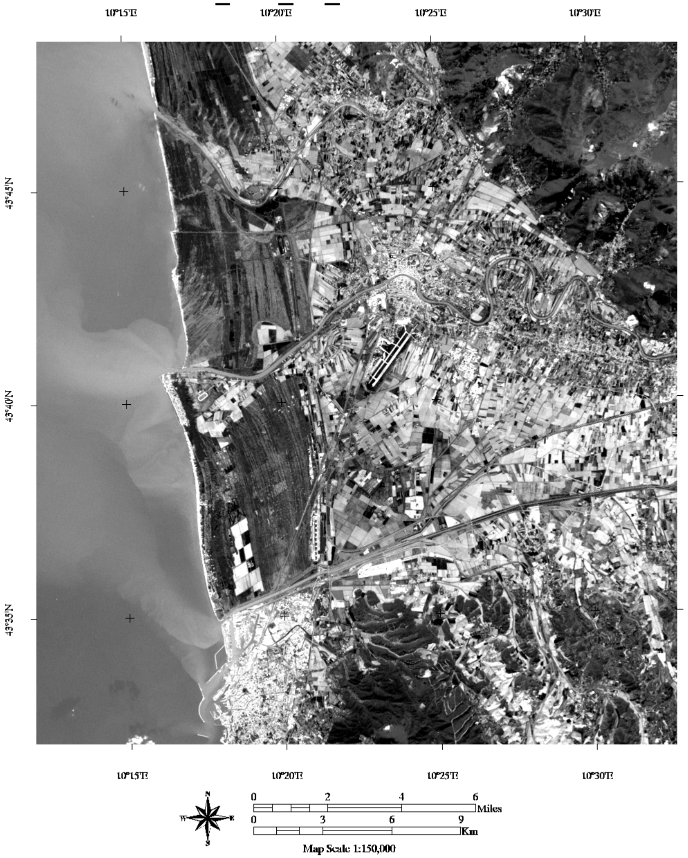

PC3_Pisa_L7_11November2000

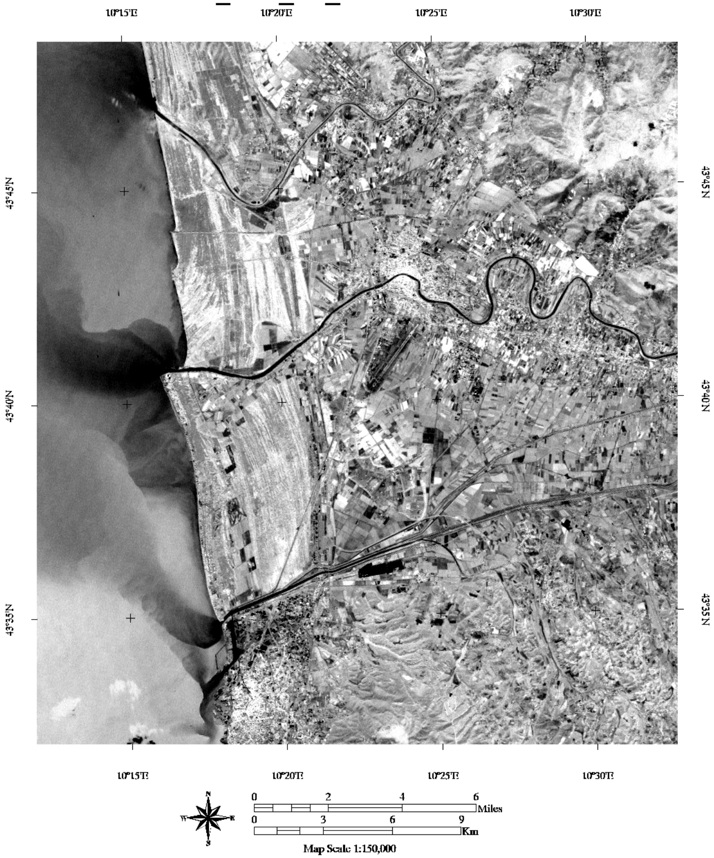

PC1_Pisa_L7_15February2001

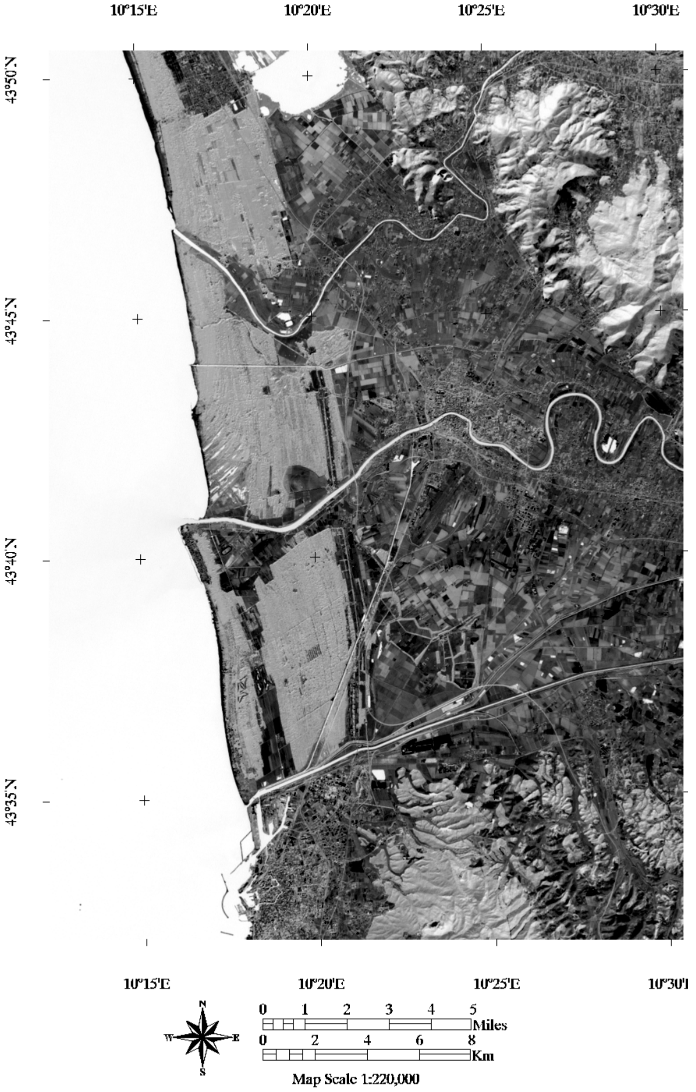

PC2_Pisa_L7_15February2001

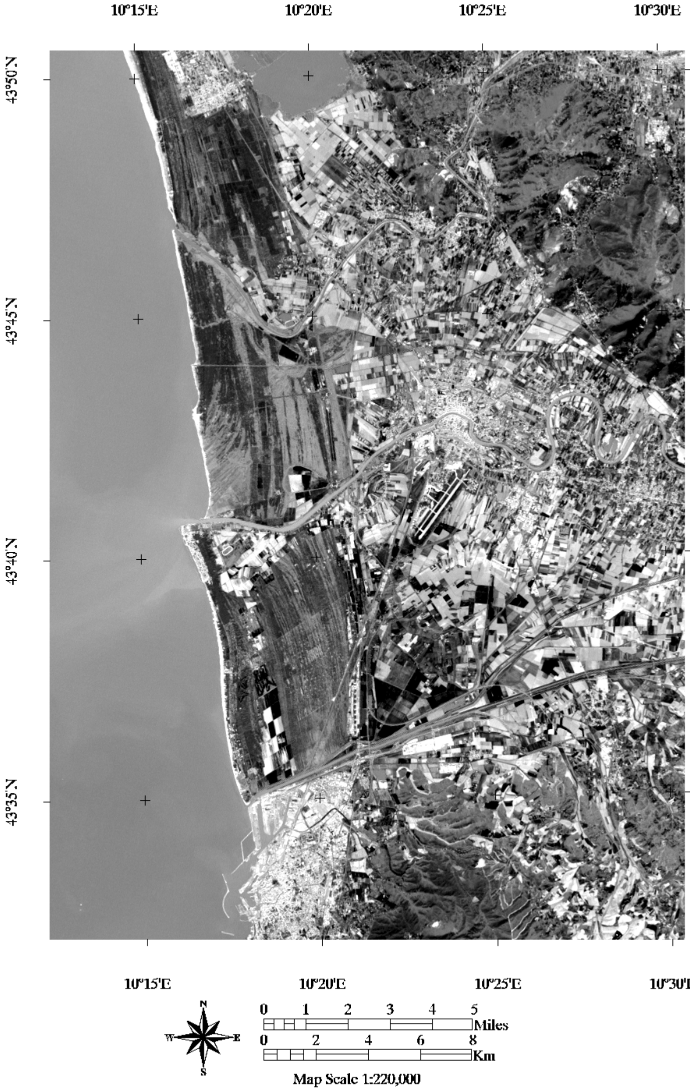

PC3_Pisa_L7_15February2001

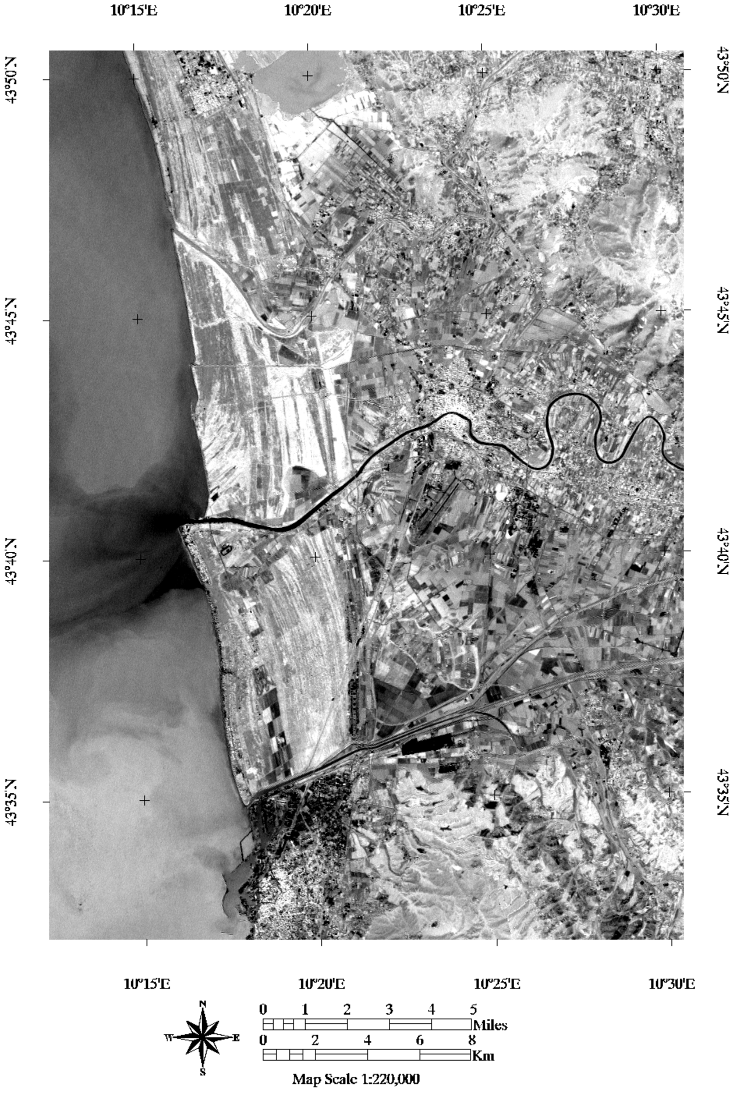

PC1_Pisa_l7_02February2002

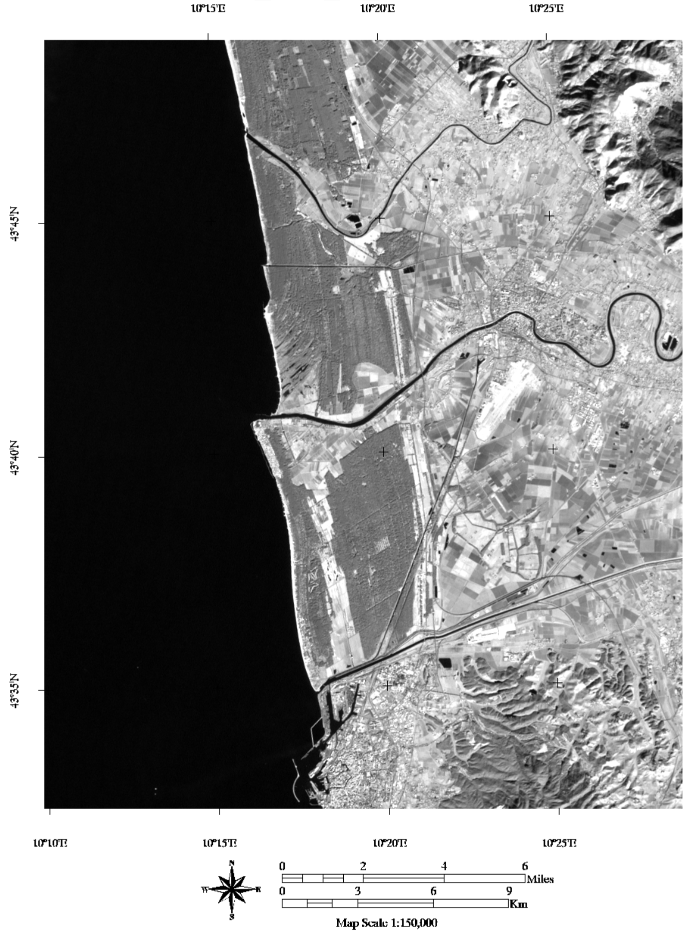

PC2_Pisa_l7_02February2002

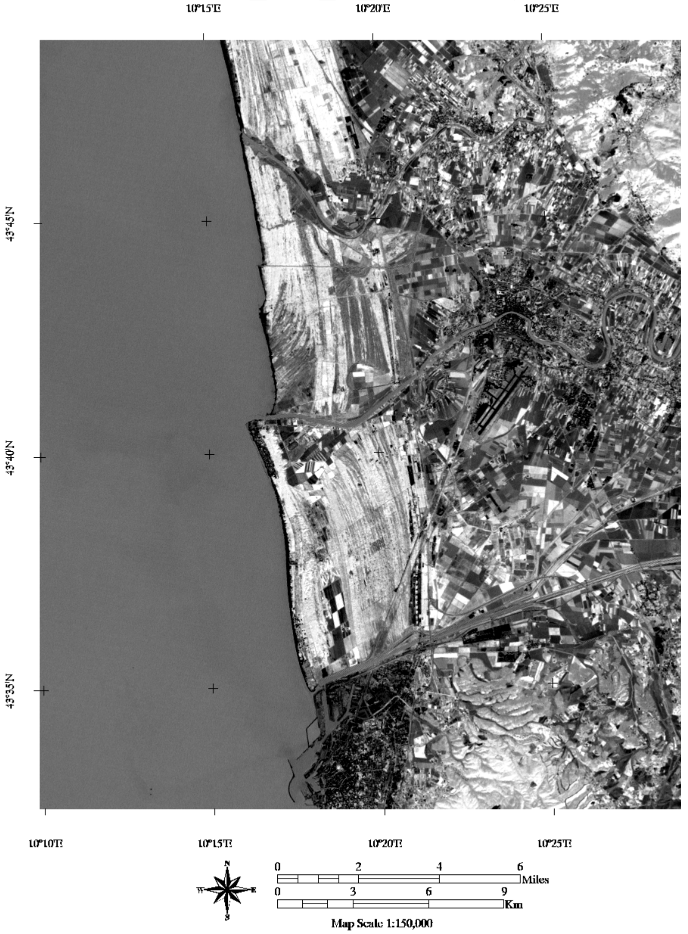

PC3_Pisa_l7_02February2002

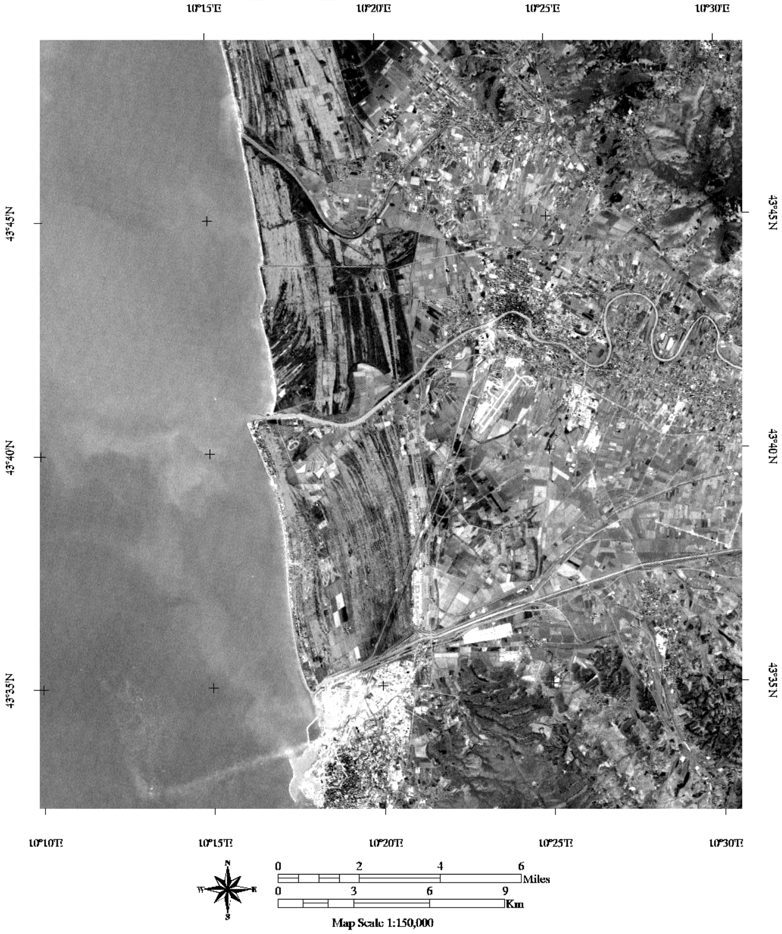

PC1_Pisa_L7_30September2002

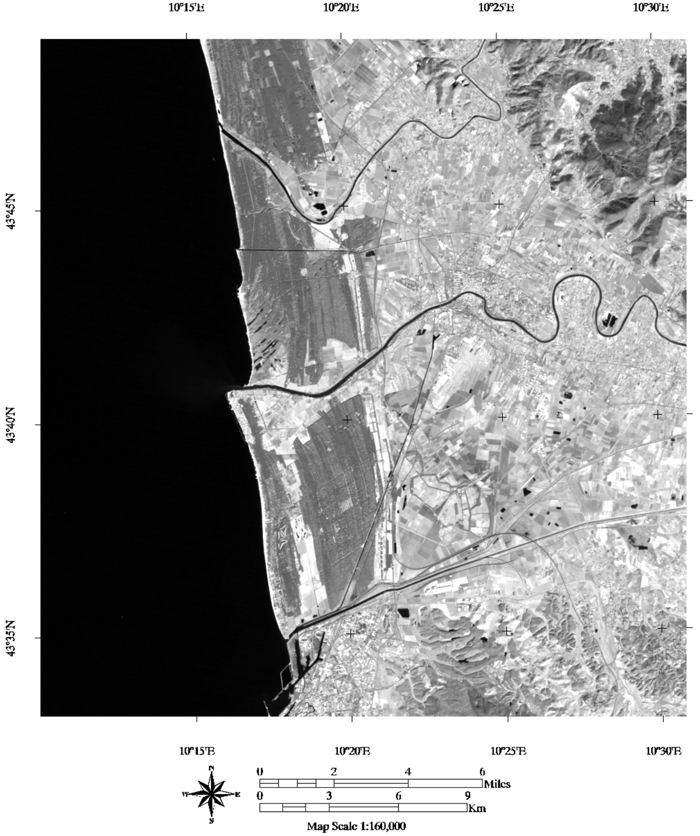

PC2_Pisa_L7_30September2002

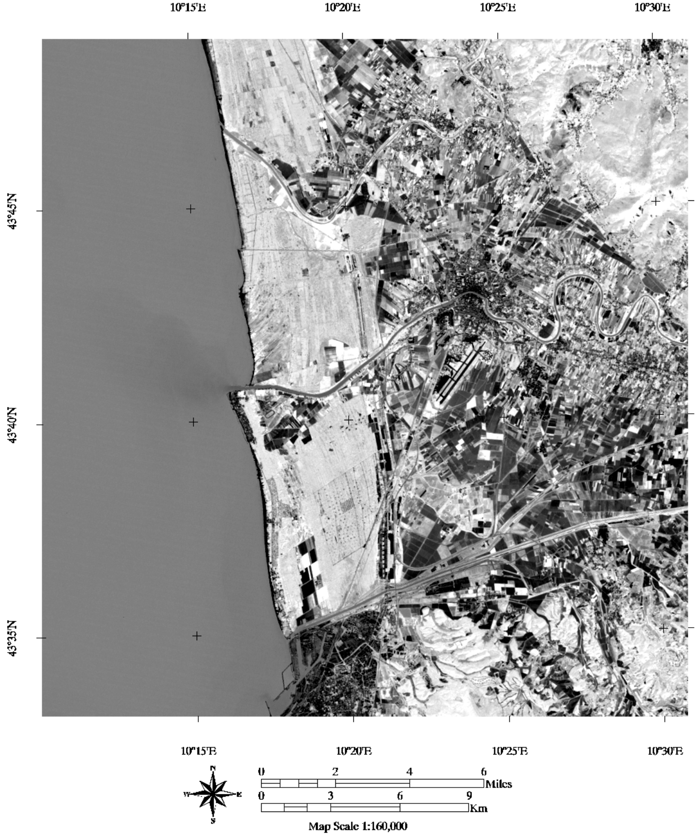

PC3_Pisa_L7_30September2002

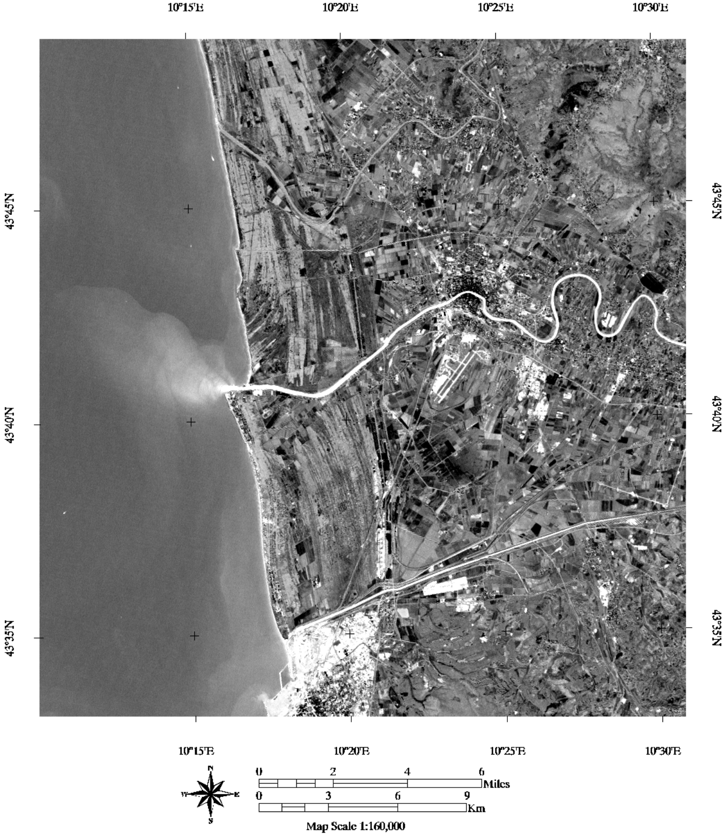

PC1_Pisa_L8_10September2015

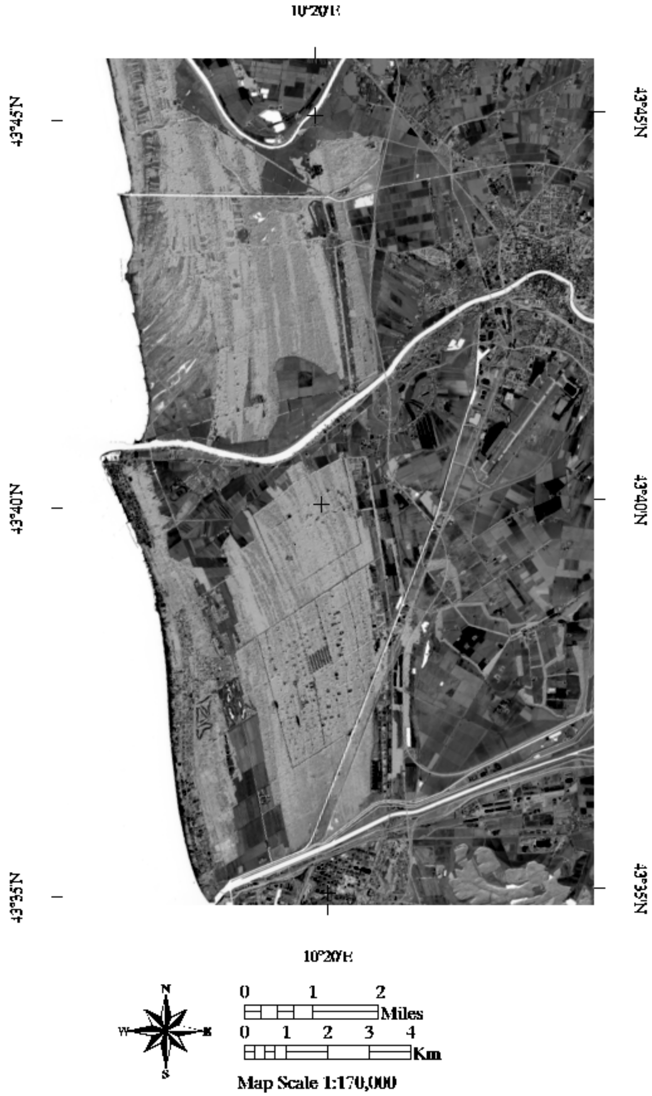

PC2_Pisa_L8_10September2015

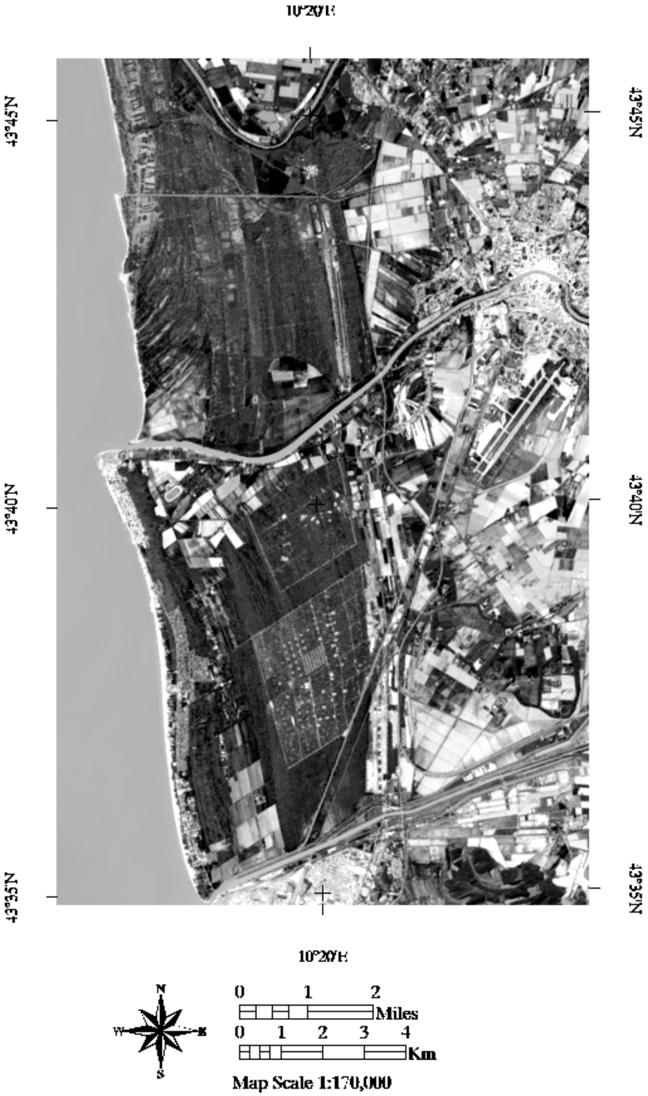

PC3_Pisa_L8_10September2015

PC1_Pisa_ASTER_19September2004

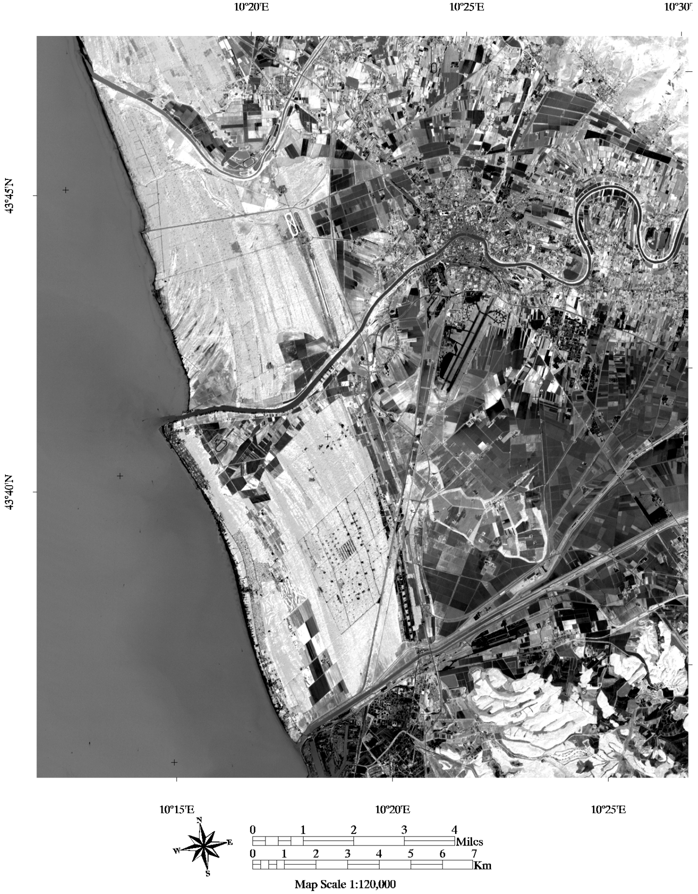

PC2_Pisa_ASTER_19September2004

PC3_Pisa_ASTER_19September2004

PC1_Pisa_ASTER_21September2008

PC2_Pisa_ASTER_21September2008

PC3_Pisa_ASTER_21September2008

PC1_Pisa_ASTER_06August2011

PC2_Pisa_ASTER_06August2011

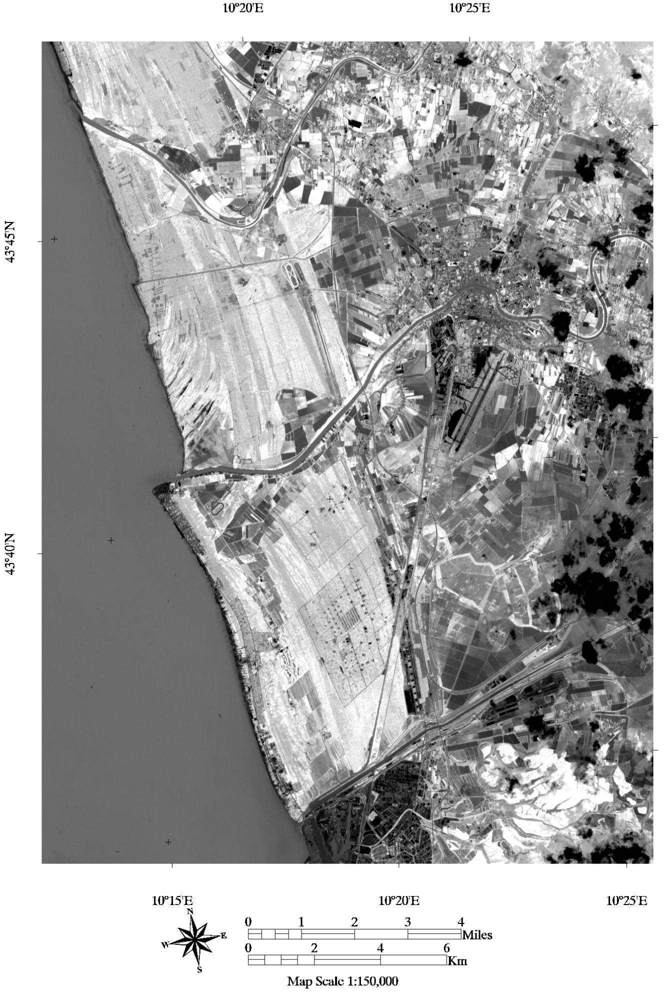

PC3_Pisa_ASTER_06August2011

PC1_Pisa_ASTER_08August2012

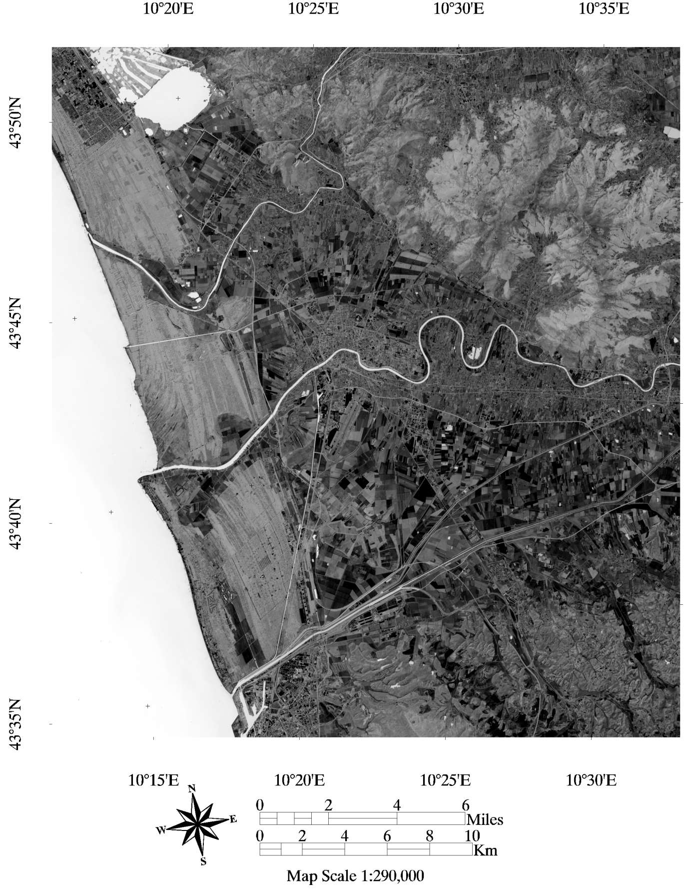

PC2_Pisa_ASTER_08August2012

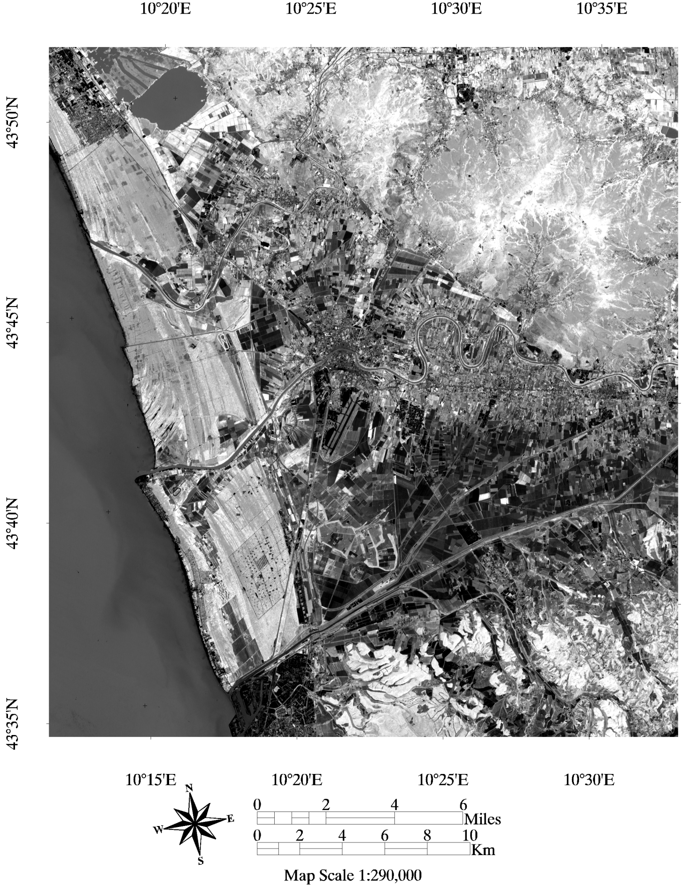

PC3_Pisa_ASTER_08August2012

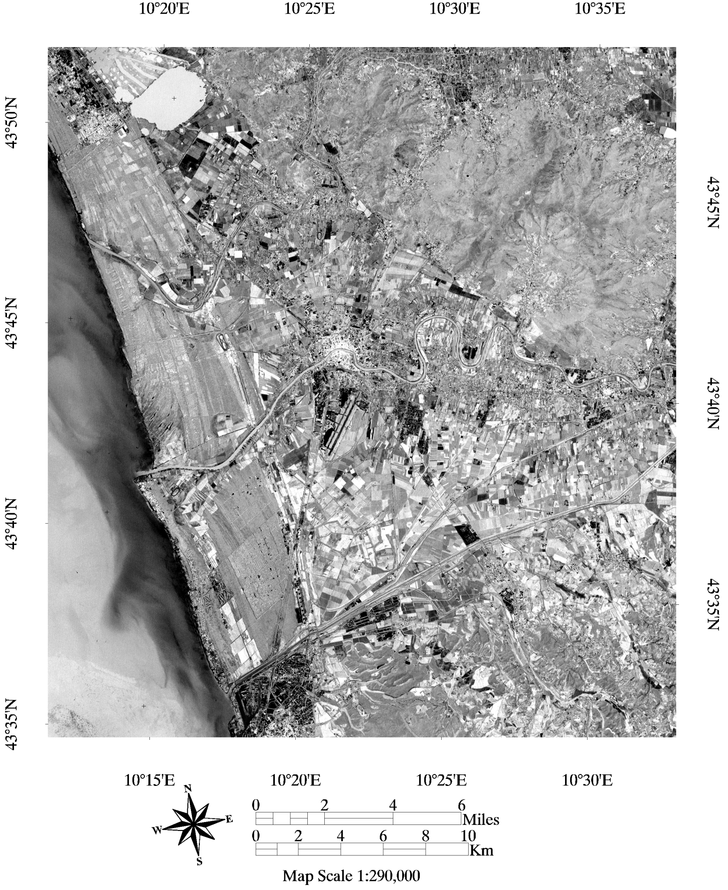

PC1_Pisa_Sent2a_24July2015

PC2_Pisa_Sent2a_24July2015

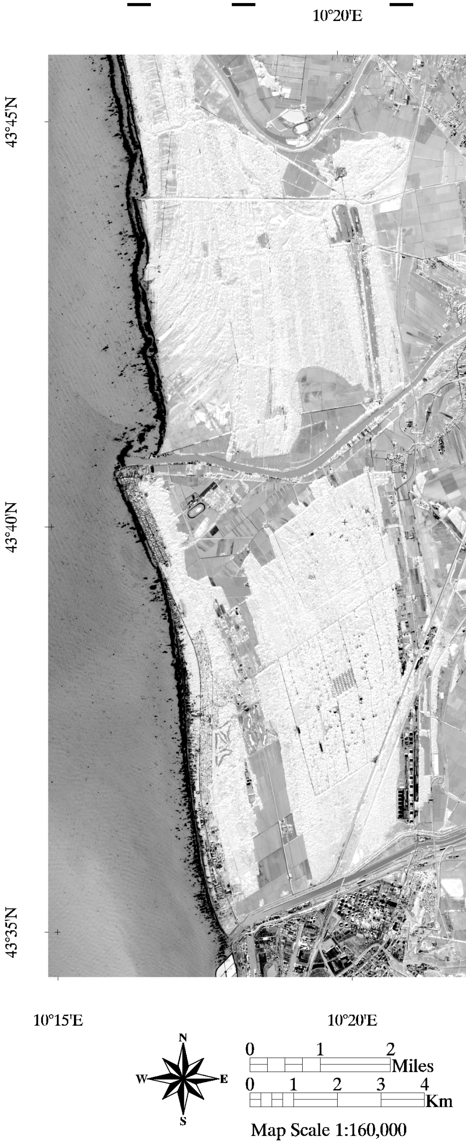

PC3_Pisa_Sent2a_24July2015


PC1_Pisa_Sent2a_13January2016


PC2_Pisa_Sent2a_13January2016

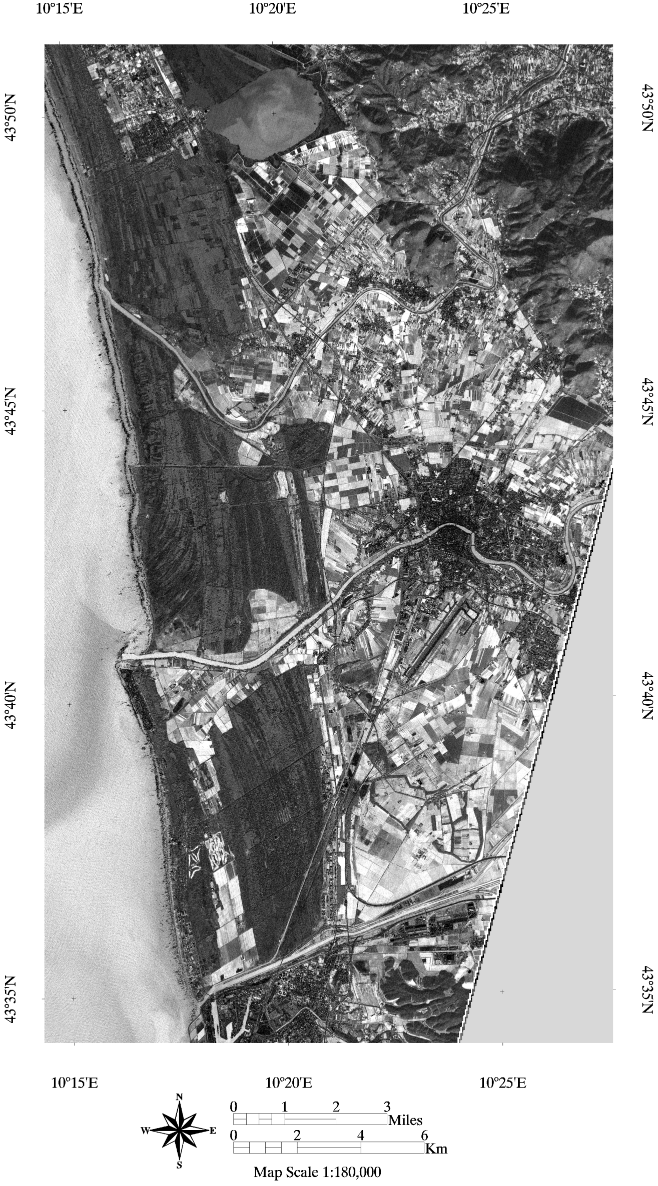
PC3_Pisa_Sent2a_13January2016

PC1_L7_Po_13_October_1999

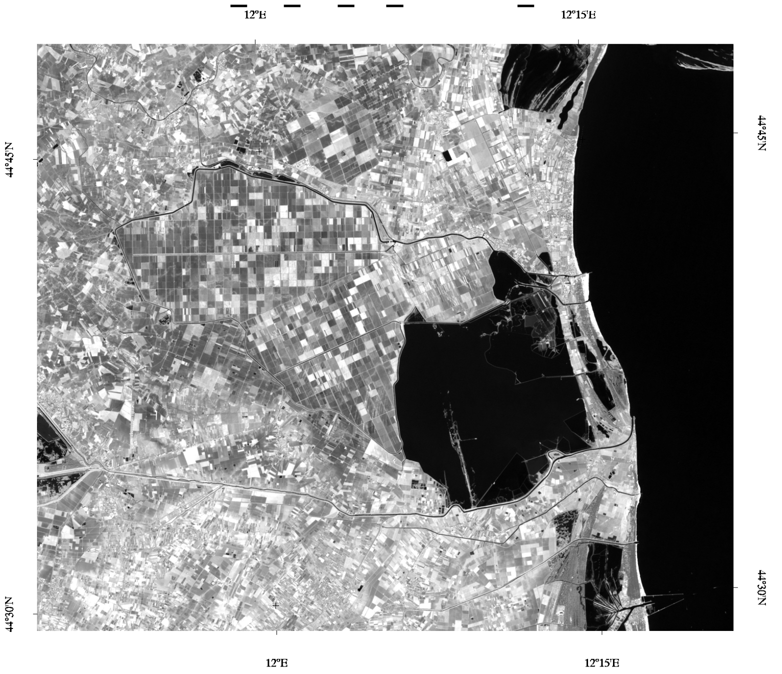

PC2_L7_Po_13_October_1999

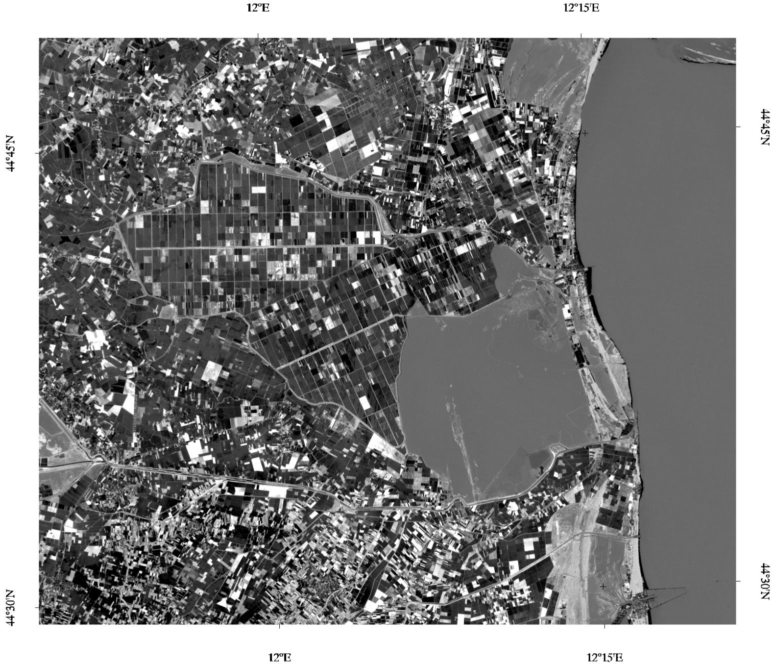

PC3_L7_Po_13_October_1999

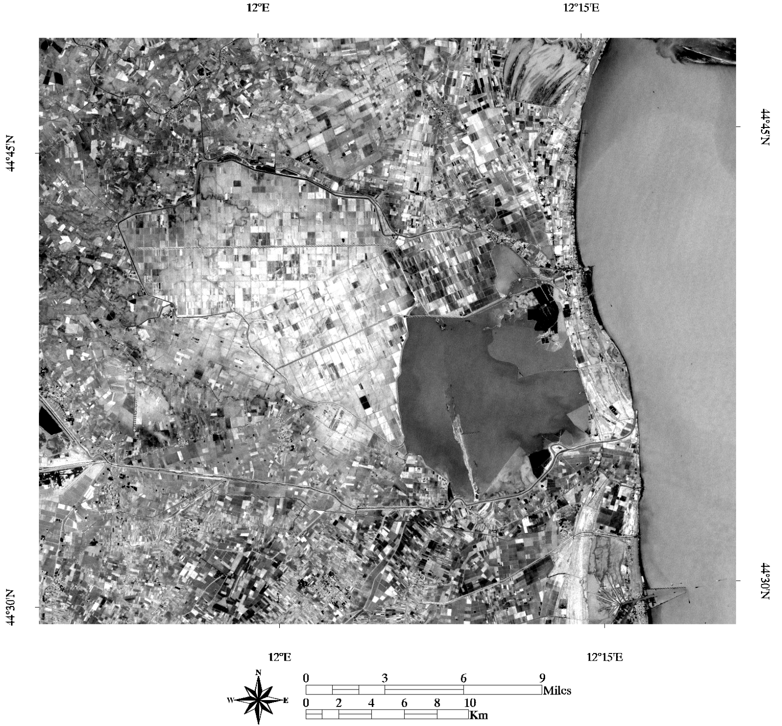

PC1_L7_Po_15_ February_2001

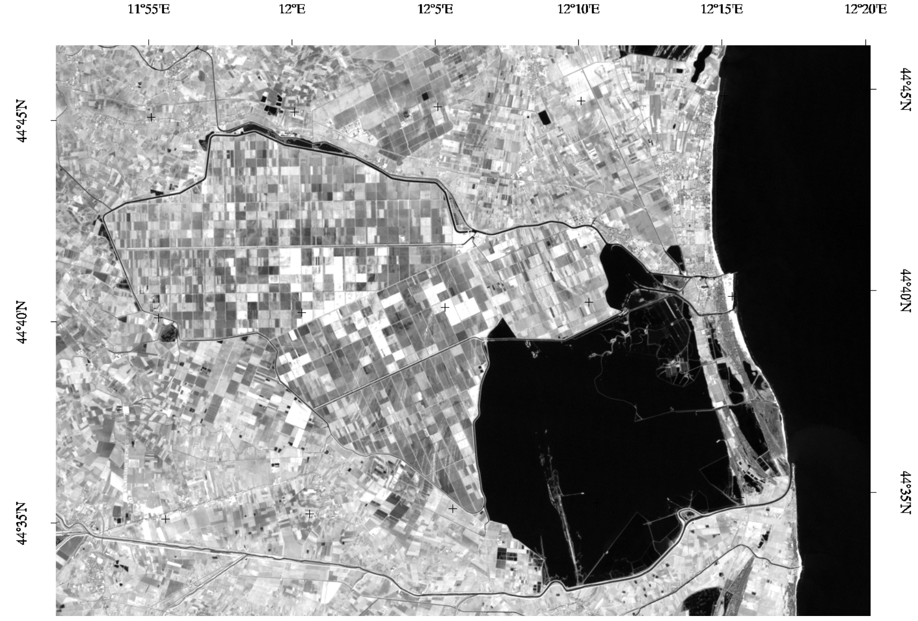

PC2_L7_Po_15_ February_2001

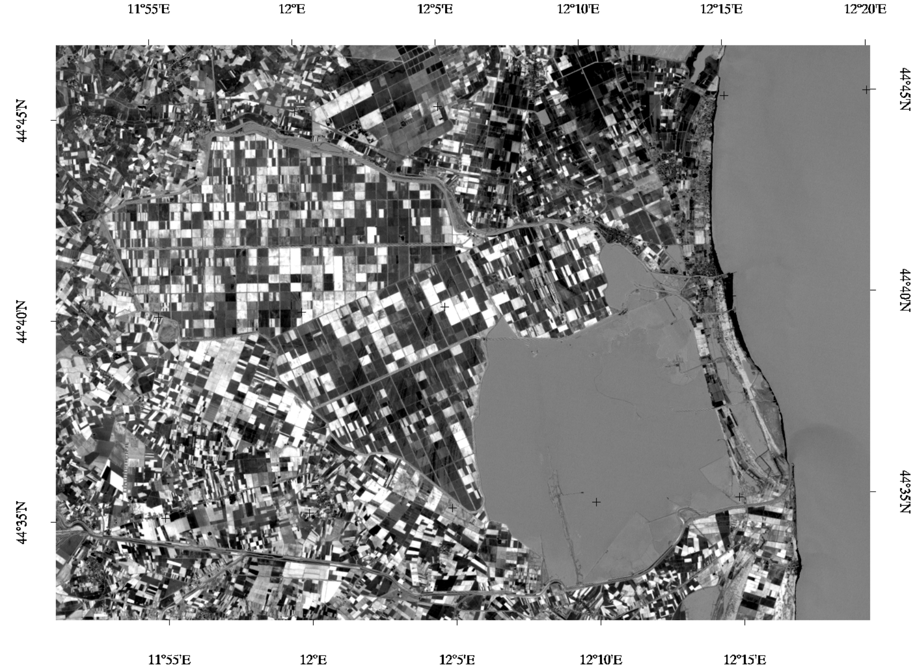

PC3_L7_Po_15_ February_2001

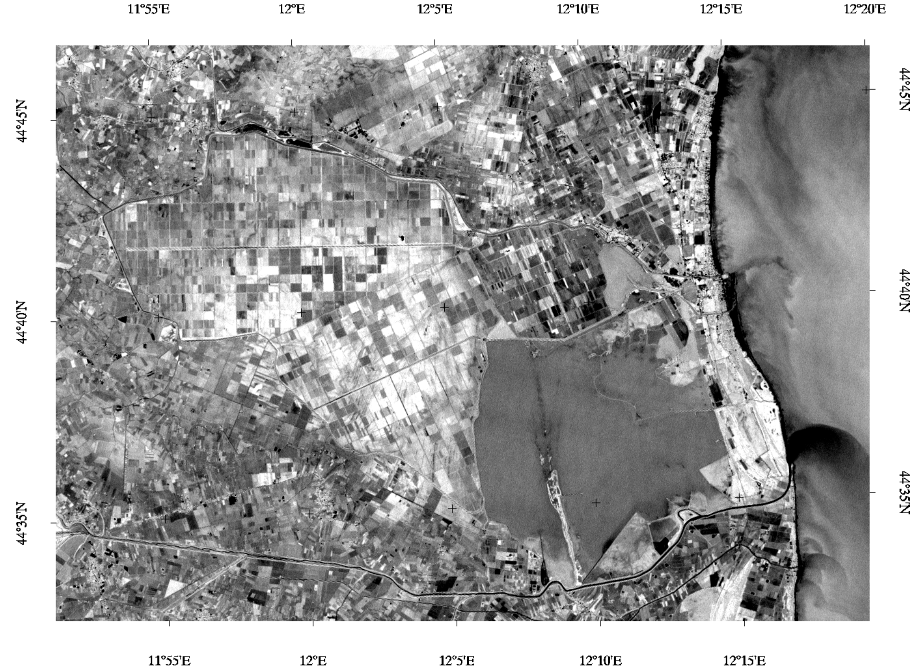

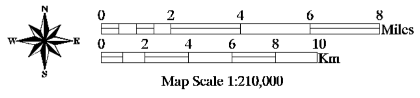

Map Scale 1:210,000

PC1_L7_Po_13_August_2002

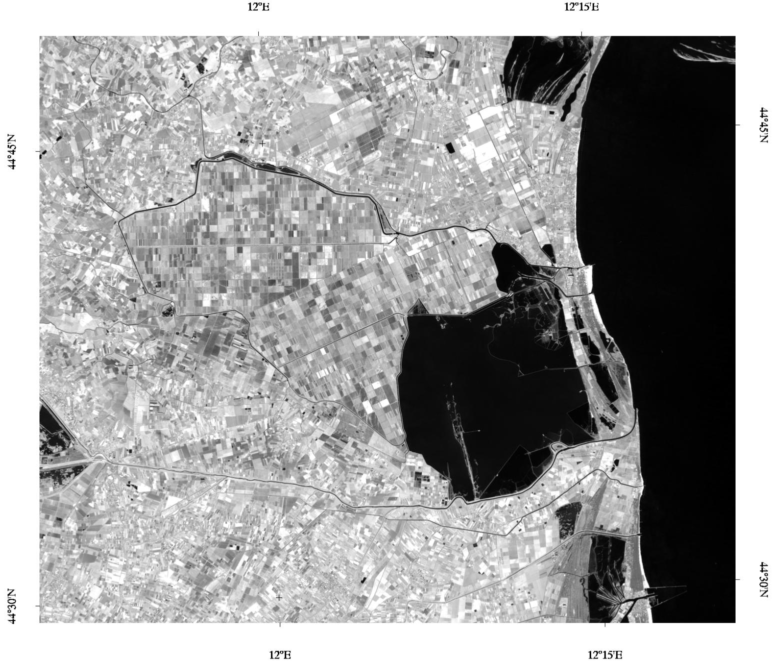

PC2_L7_Po_13_August_2002

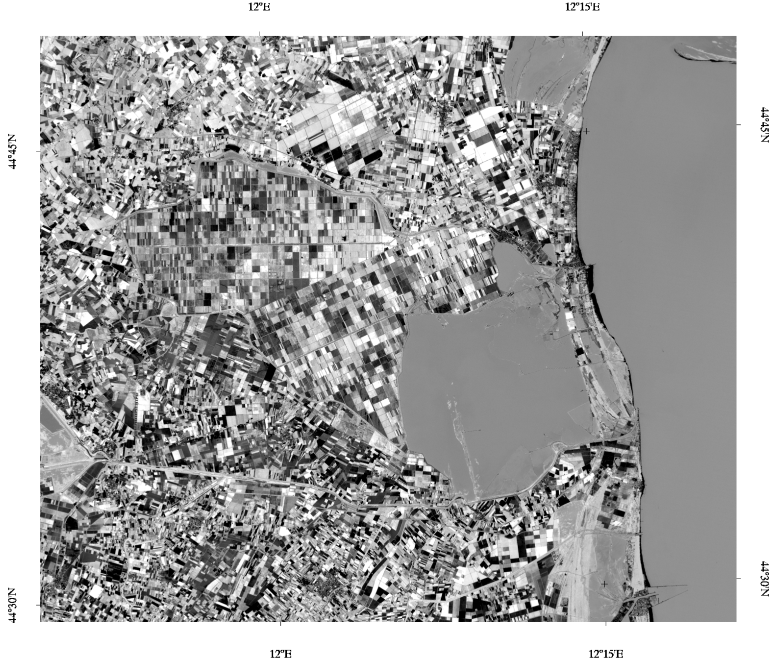

PC3_L7_Po_13_August_2002

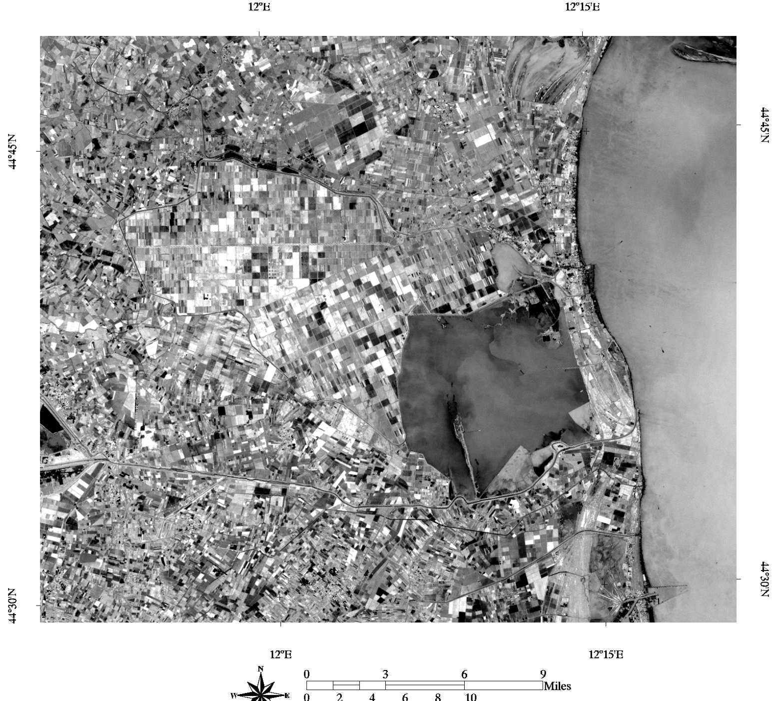

PC1_L7_Po_30_ September_2002

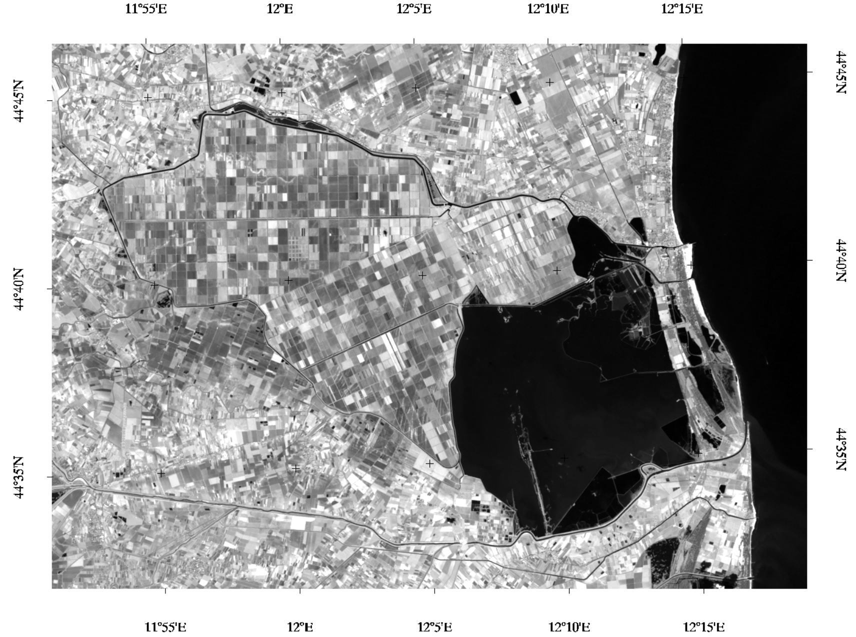

PC2_L7_Po_30_ September_2002

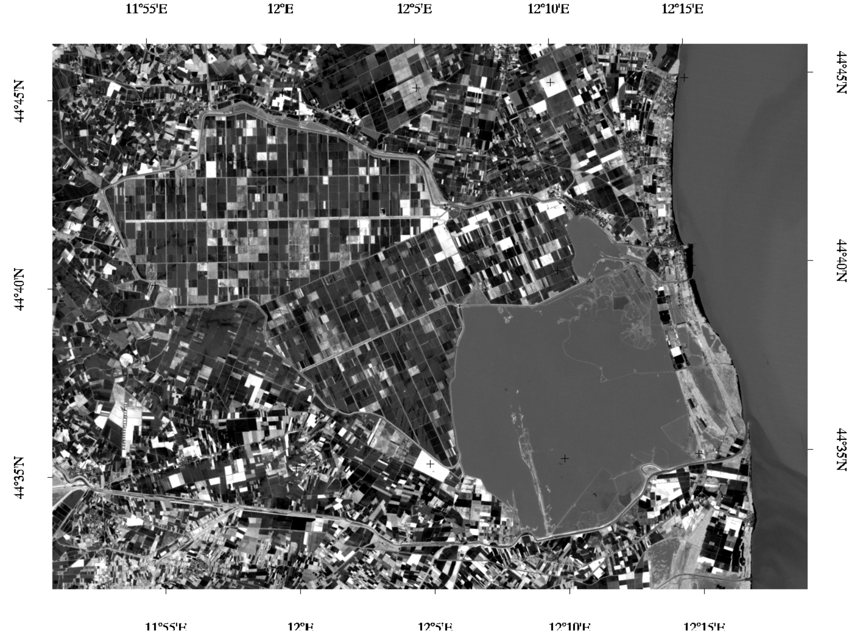

PC3_L7_Po_30_ September_2002

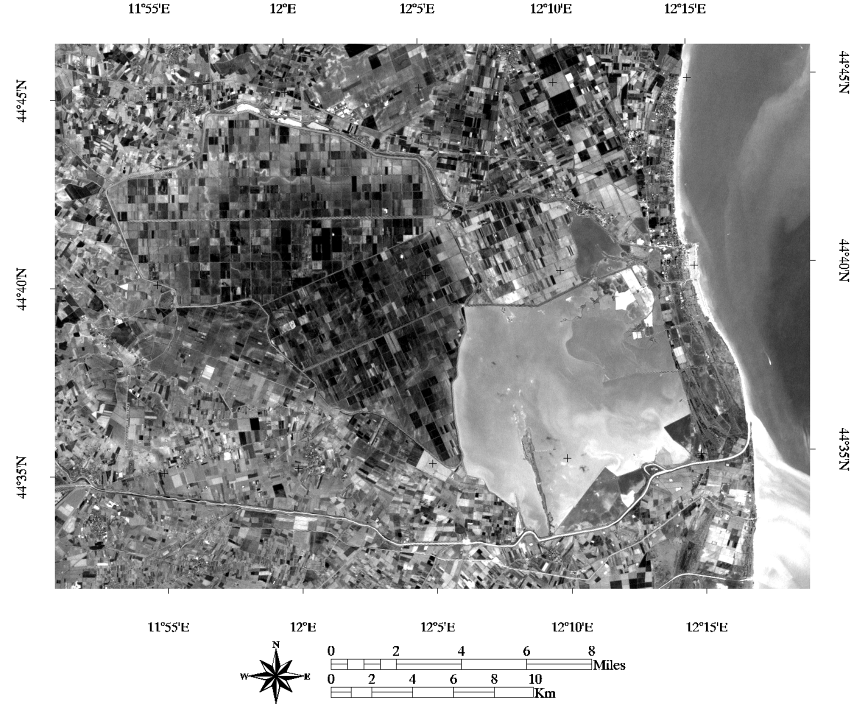

PC1_L7_Po_21_February_2003

PC2_L7_Po_21_February_2003

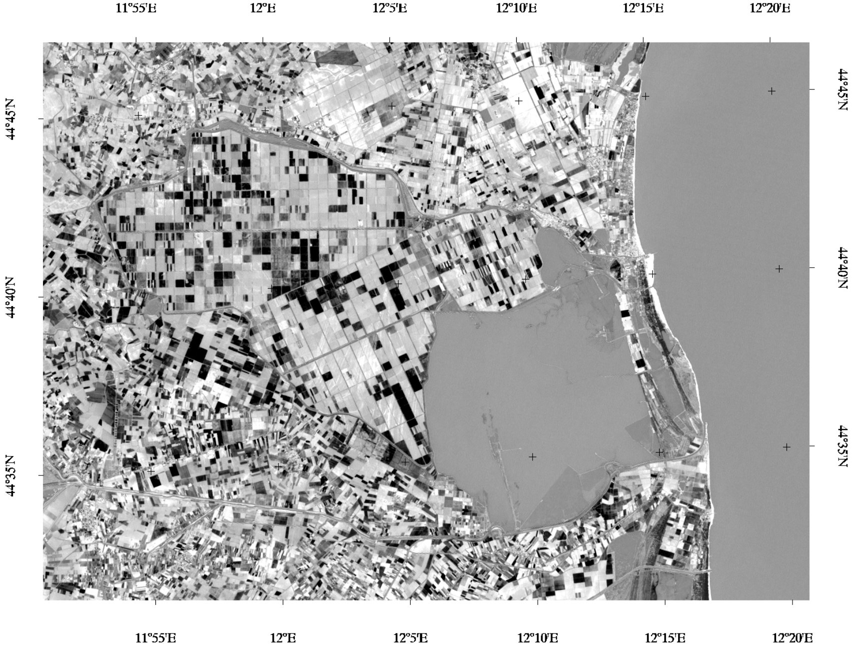

PC3_L7_Po_21_February_2003

PC1_Po_L8_18March2015

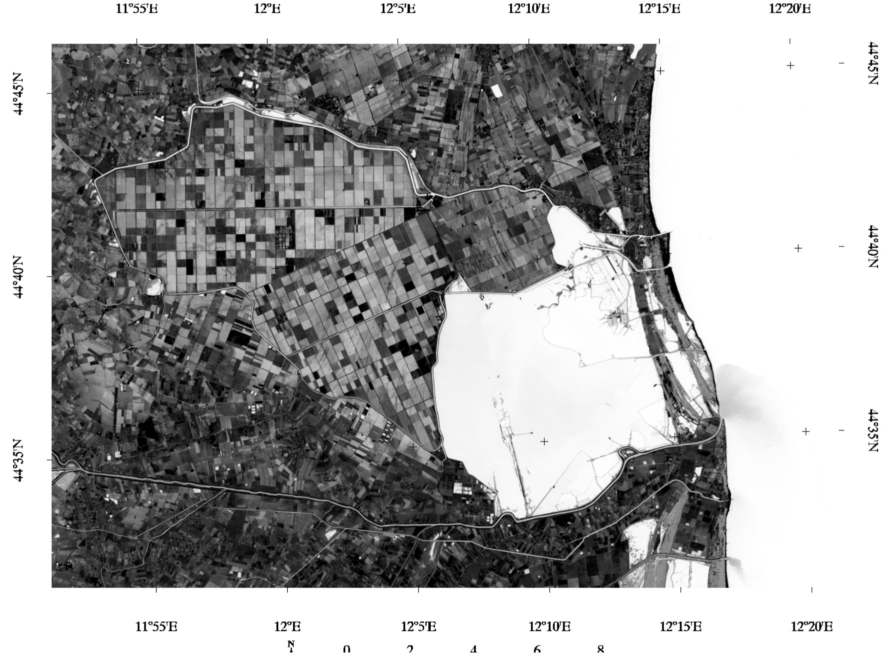

PC2_Po_L8_18March2015

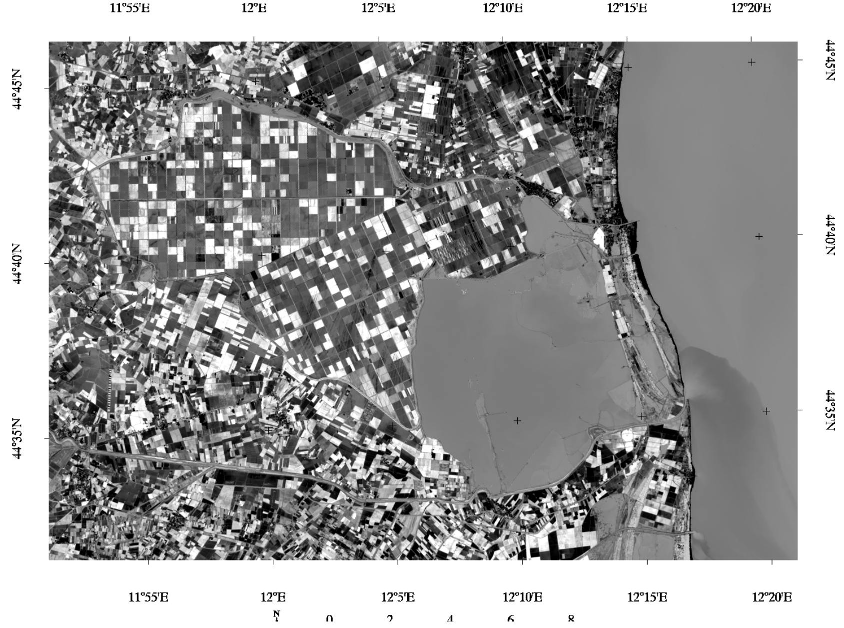

PC3_Po_L8_18March2015

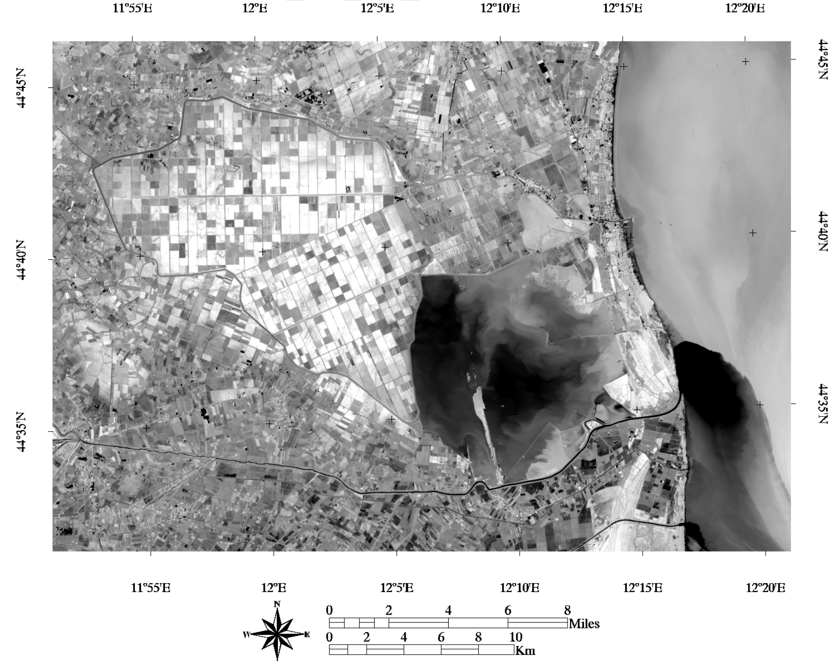

PC1_Po_L8_12October2015

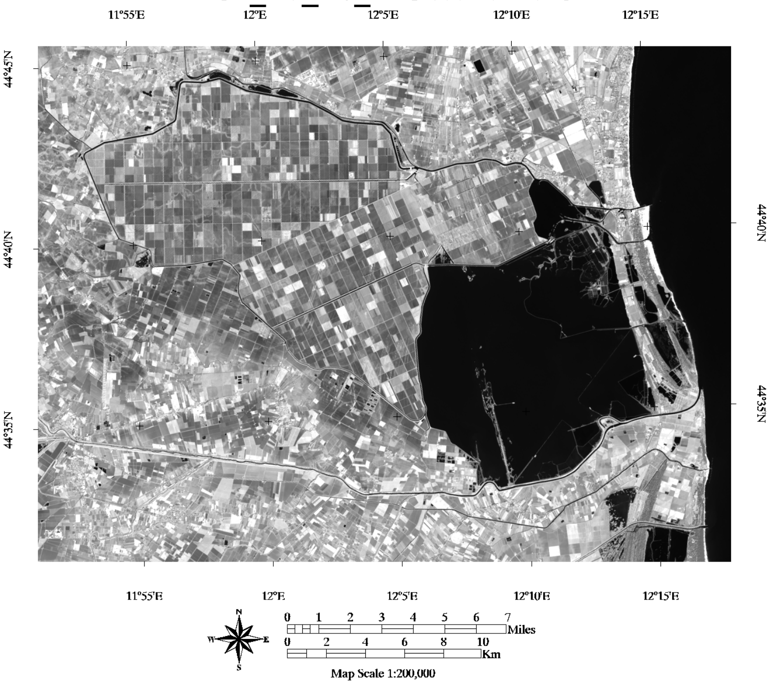

PC3_Po_L8_12October2015

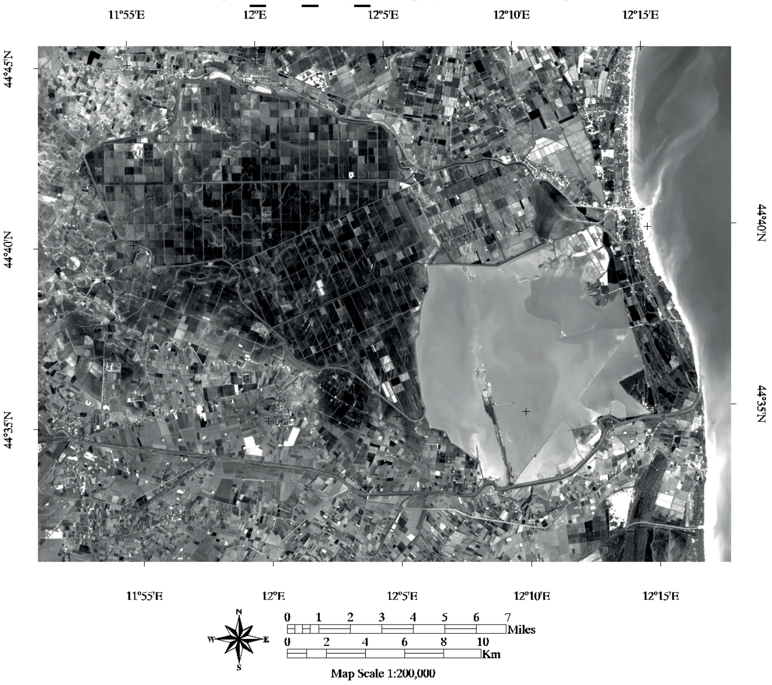

PC2_Po_L8_12October2015

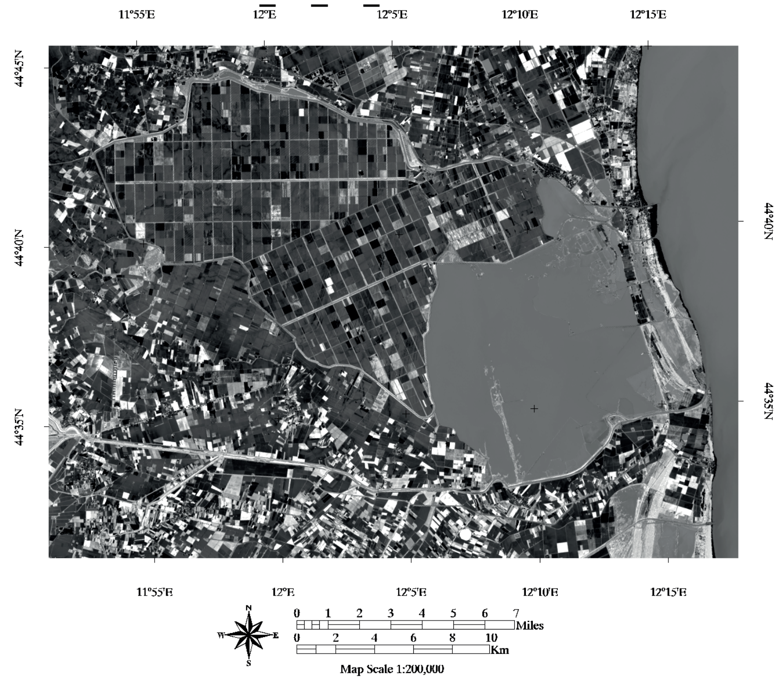

PC1_Po_L8_16January2016

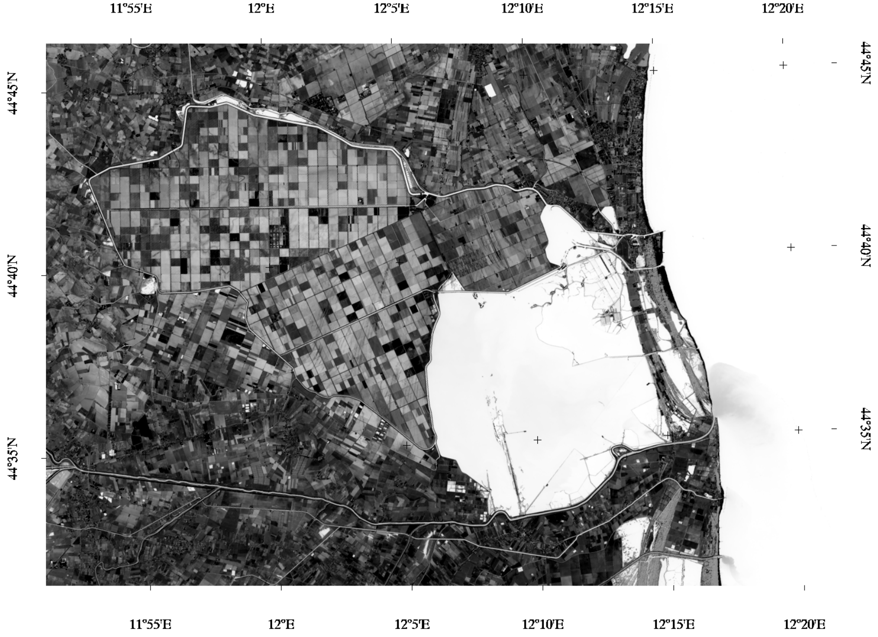

PC2_Po_L8_16January2016

PC3_Po_L8_16January2016

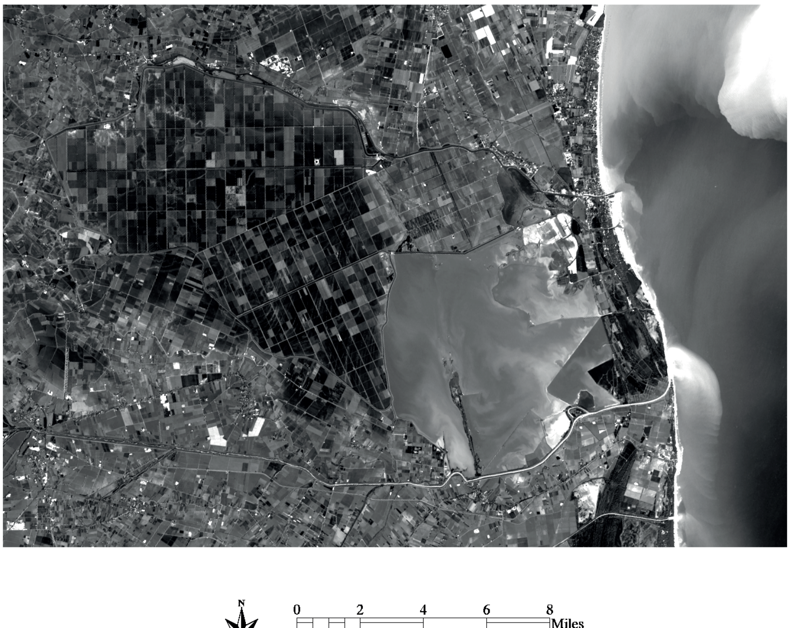

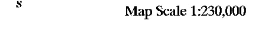

PC1_ASTER_Po_13oct2001

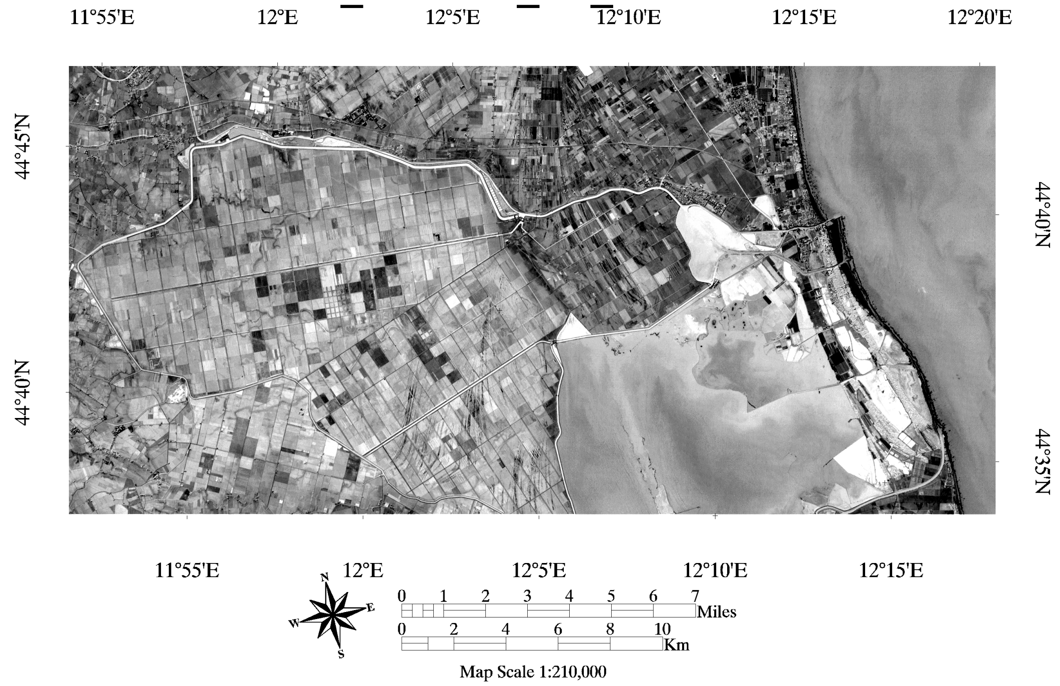

PC2_ASTER_Po_13oct2001

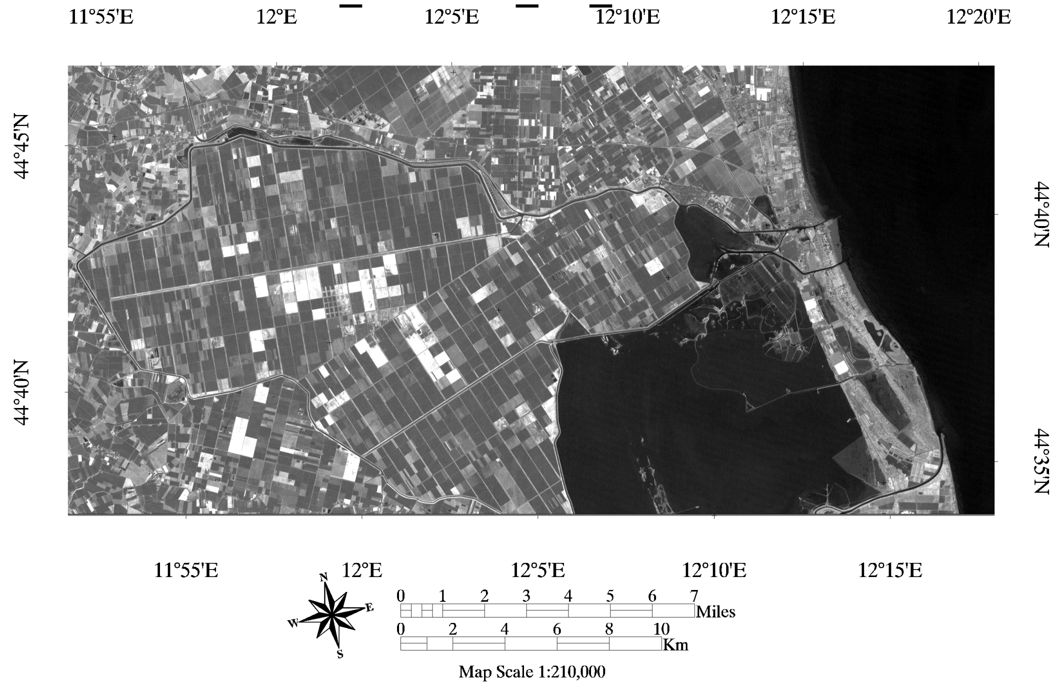

PC3_ASTER_Po_13oct2001

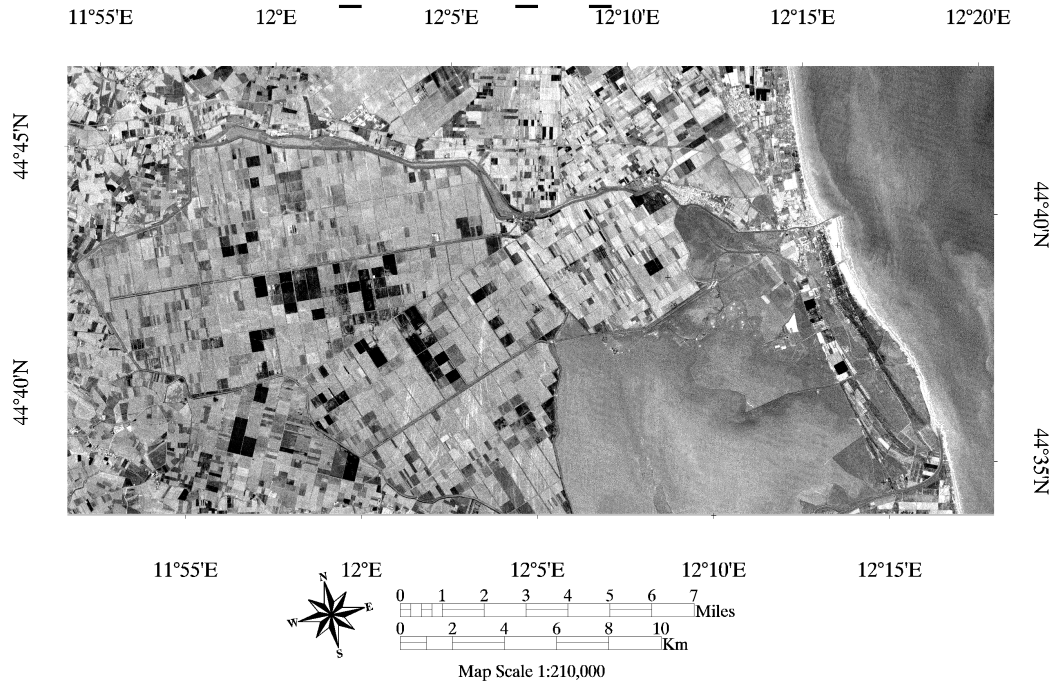

PC1_ASTER_Po_10Oct2007

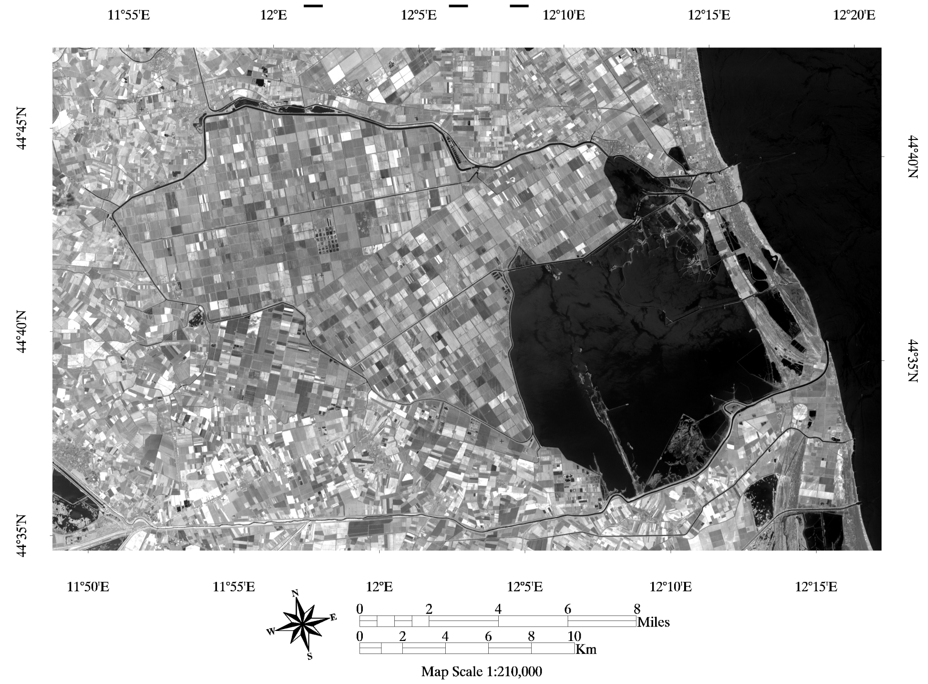

PC2_ASTER_Po_10Oct2007

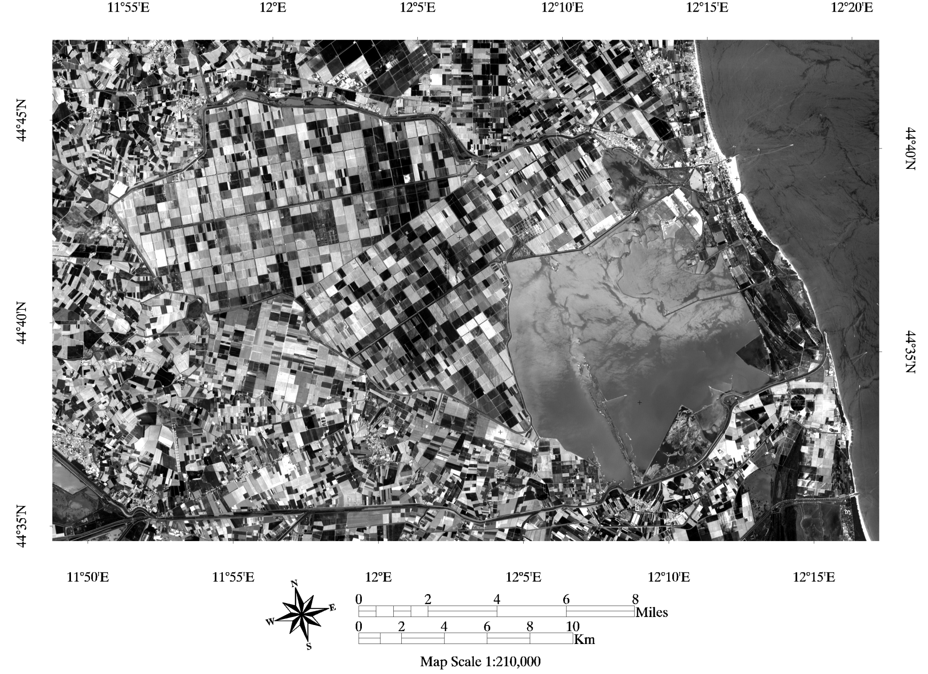

PC3_ASTER_Po_10Oct2007

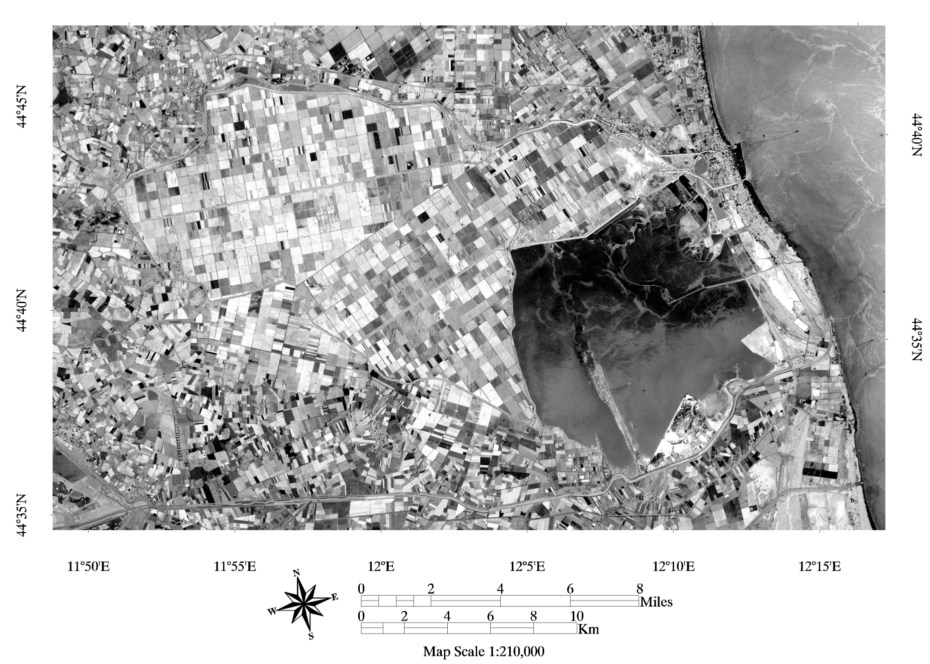

PC1_Sentinel2a_Po_18June2016

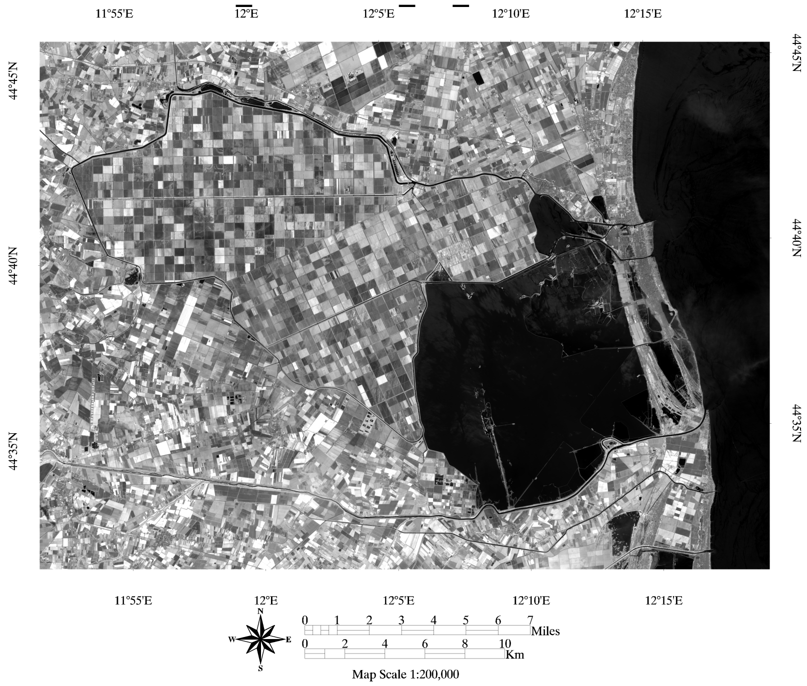

PC2_Sentinel2a_Po_18June2016

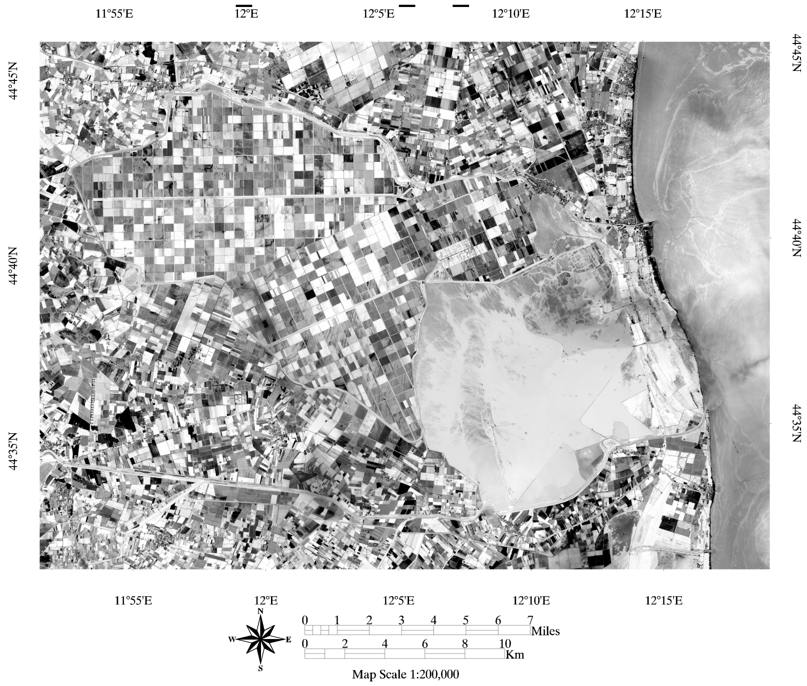

PC3_Sentinel2a_Po_18June2016

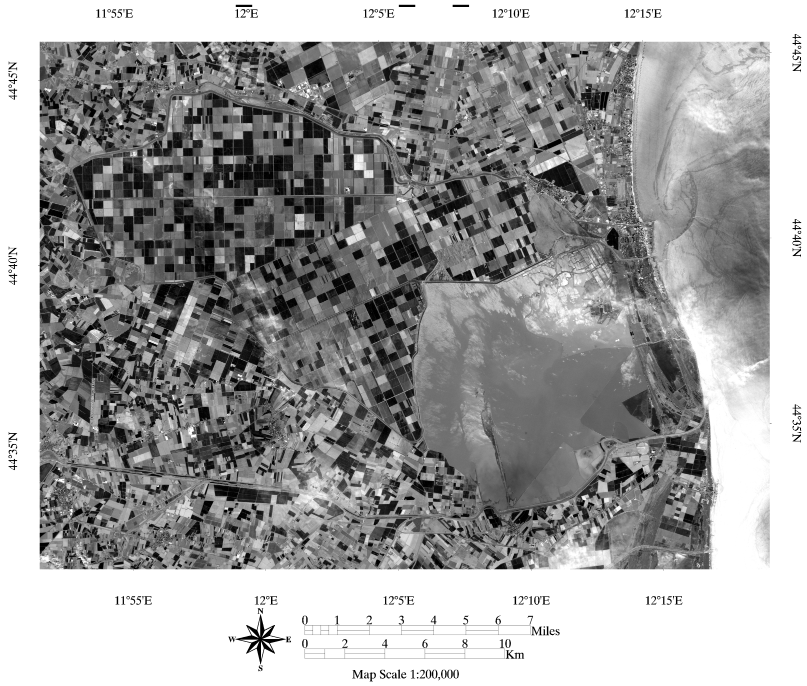

PC1_Sent2a_Po_13August2015

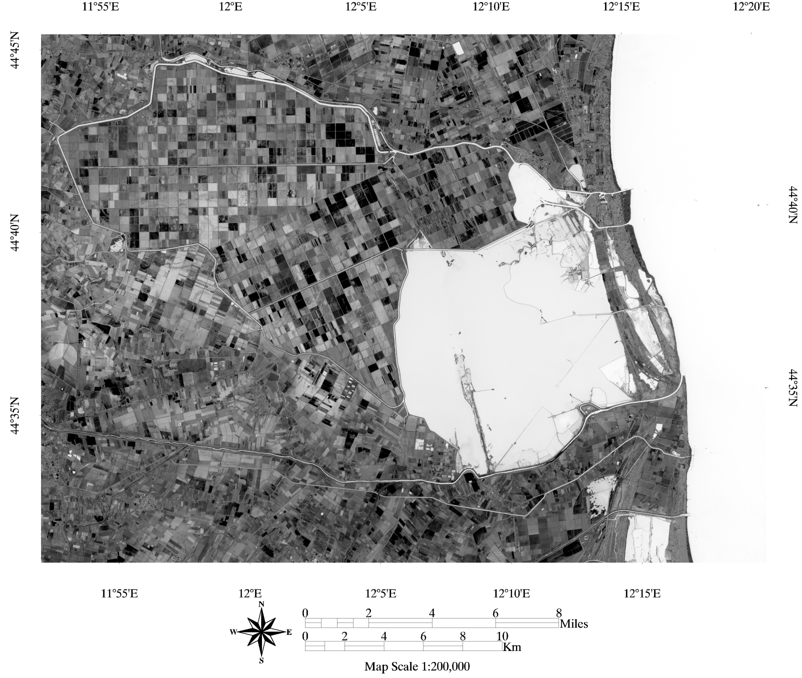

PC2_Sent2a_Po_13August2015

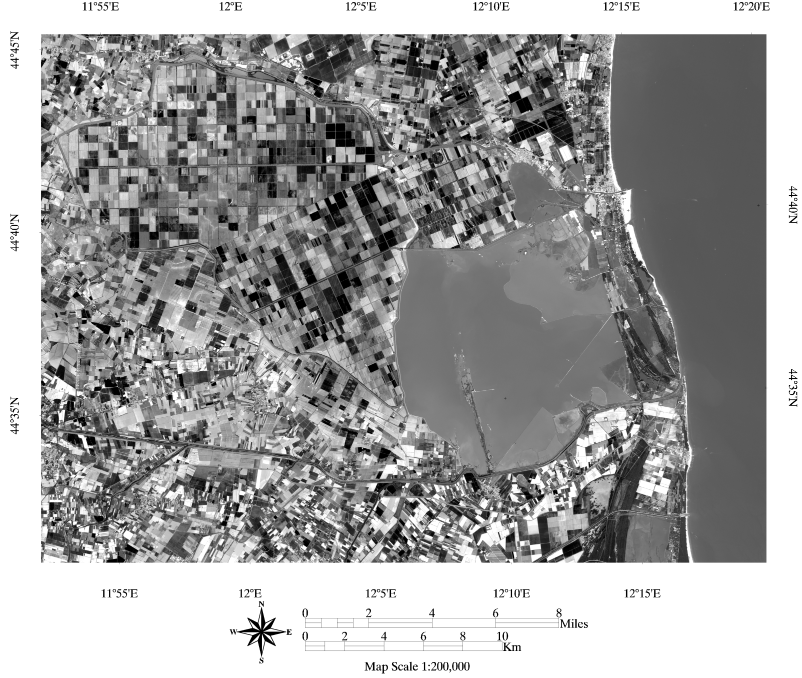

PC3_Sent2a_Po_13August2015

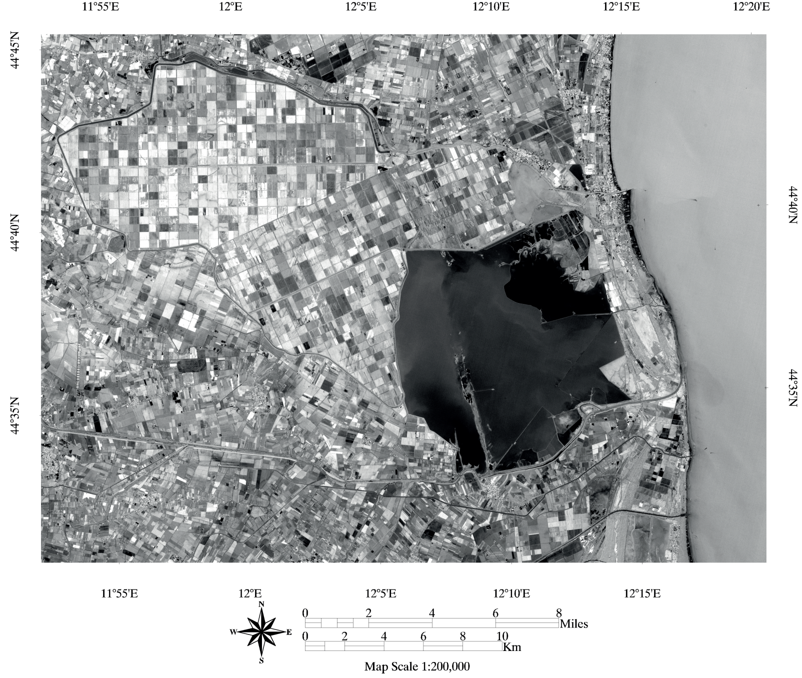

PC1_Po_Sent2a_12Sept2015

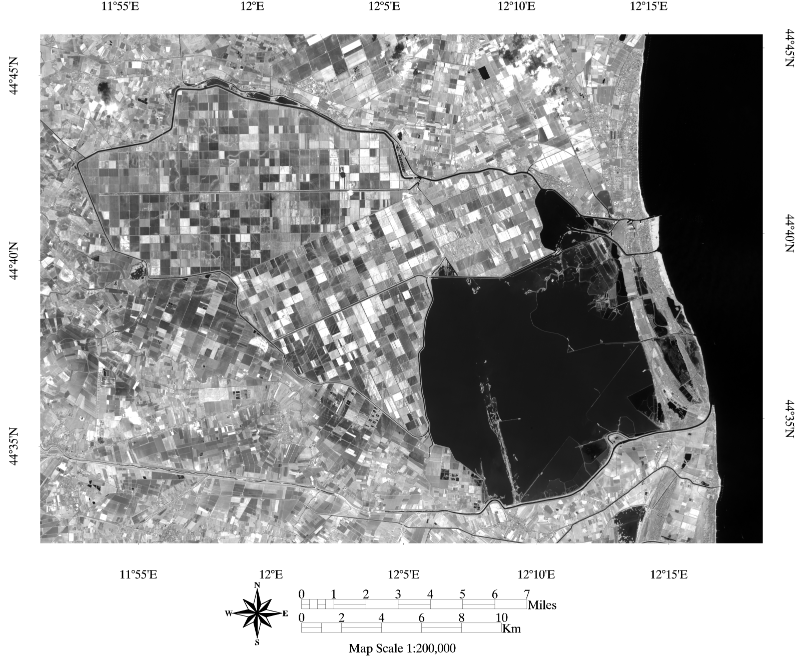

PC2_Po_Sent2a_12Sept2015

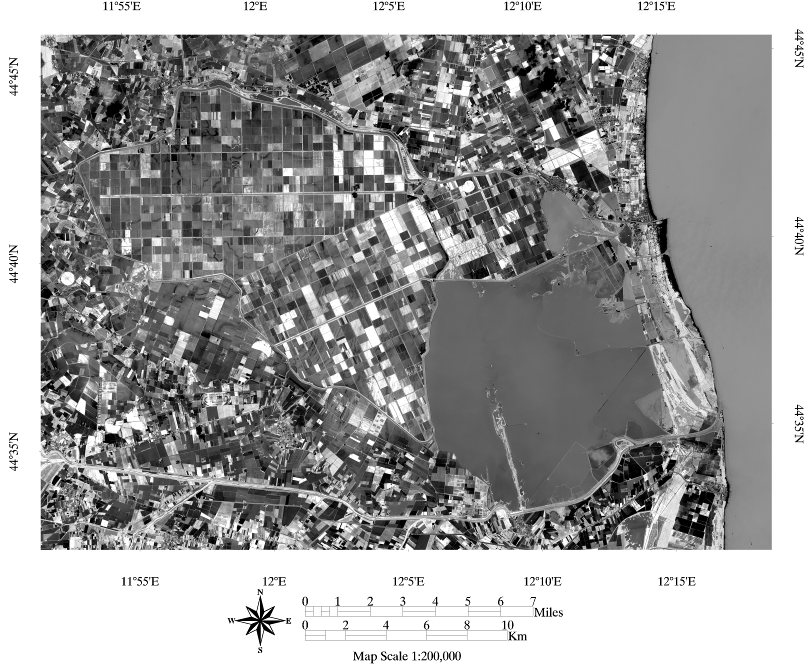

PC3_Po_Sent2a_12Sept2015

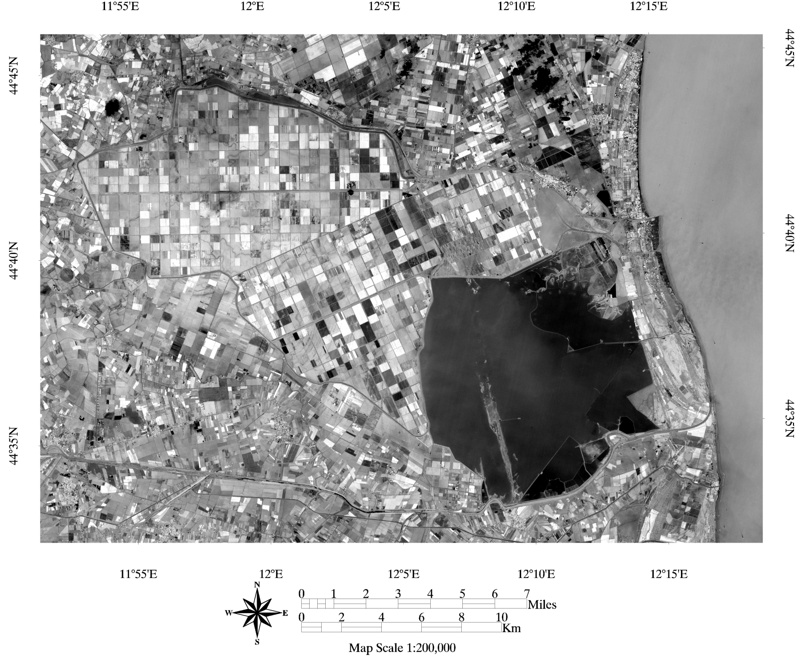


PC1_PO_HYPERION_07June2001

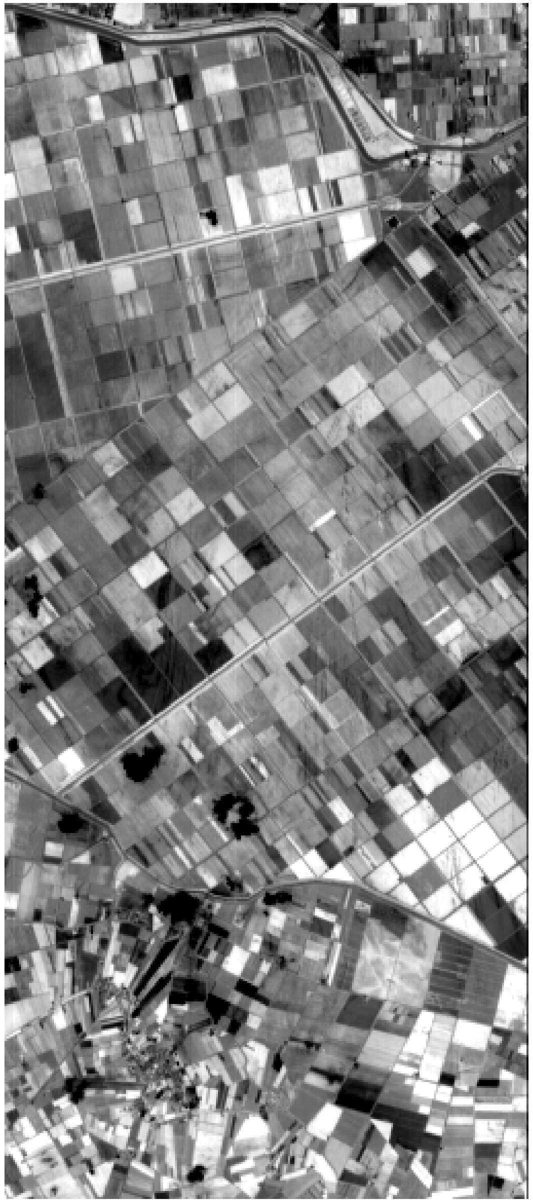
PC2_PO_HYPERION_07June2001

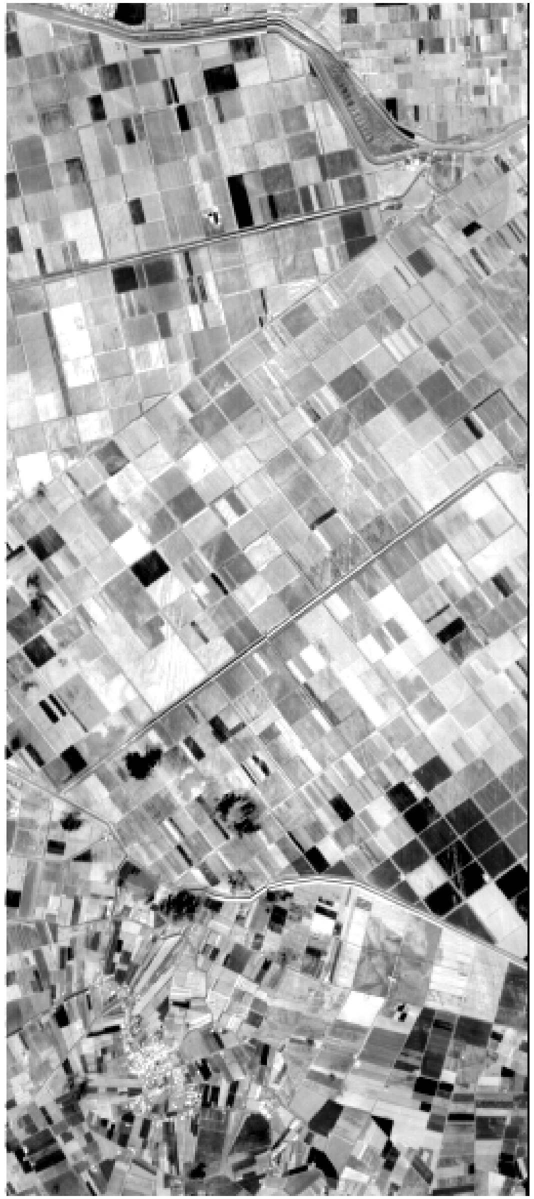
PC3_PO_HYPERION_07June2001

PC1_PO_HYPERION_07January2006

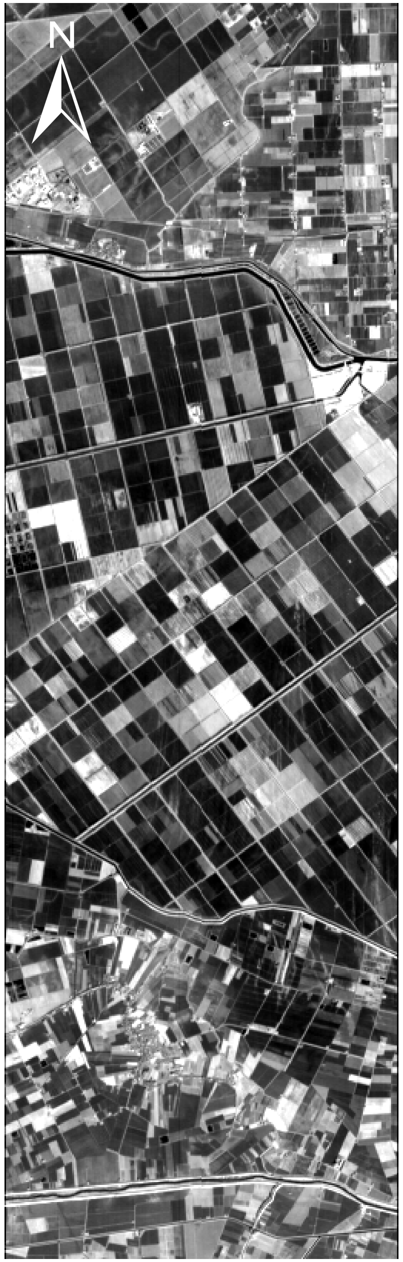

PC2_PO_HYPERION_07January2006

PC3_PO_HYPERION_07January2006

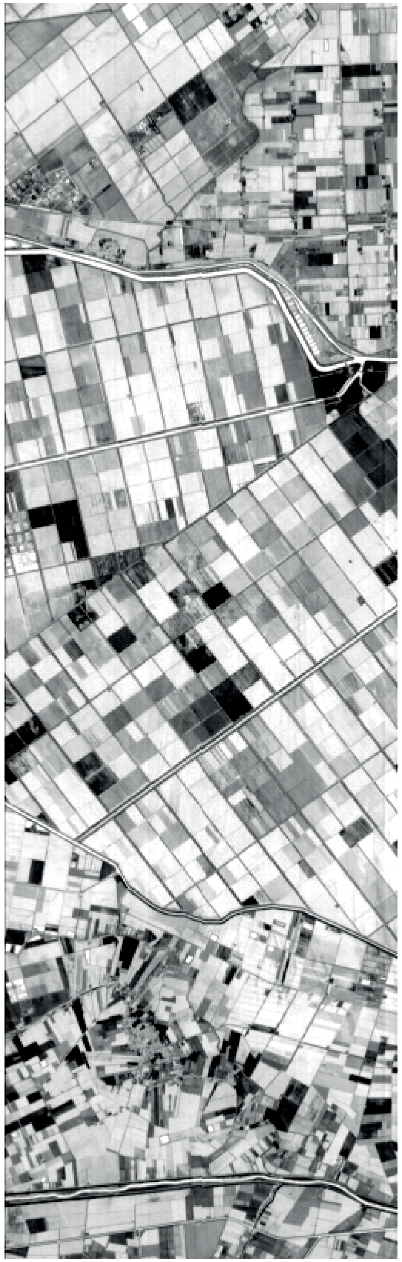

754_Landsat7_02February2002

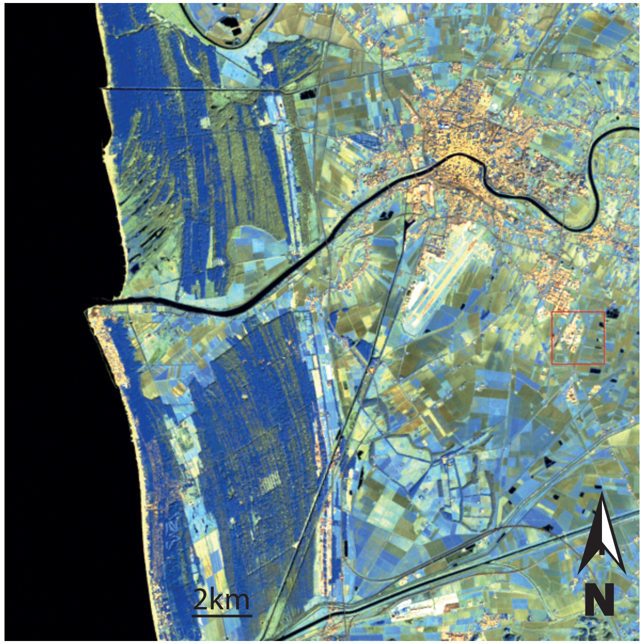

752_Landsat8_10September2015

324_Sentinel2a_13January2016

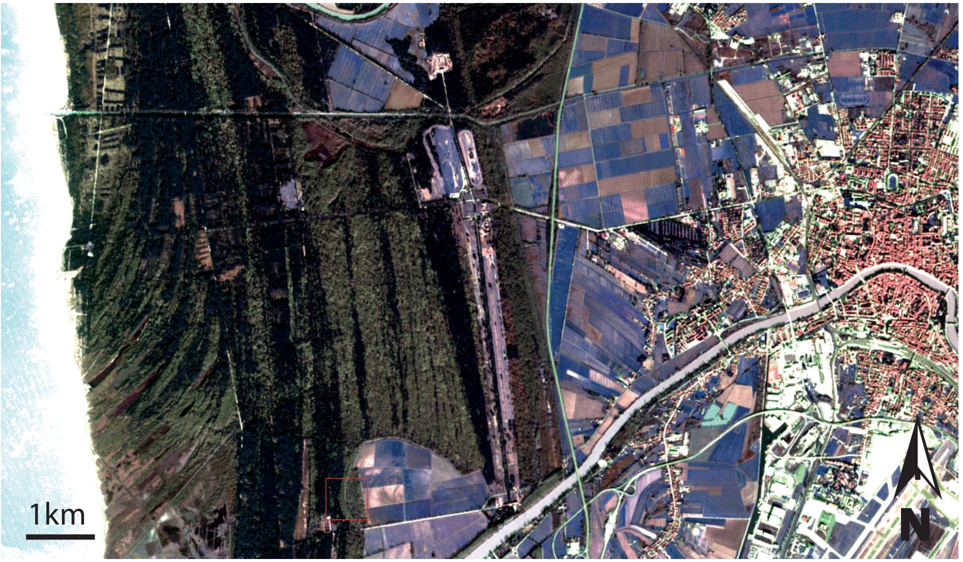

123N_ASTER_19September2004

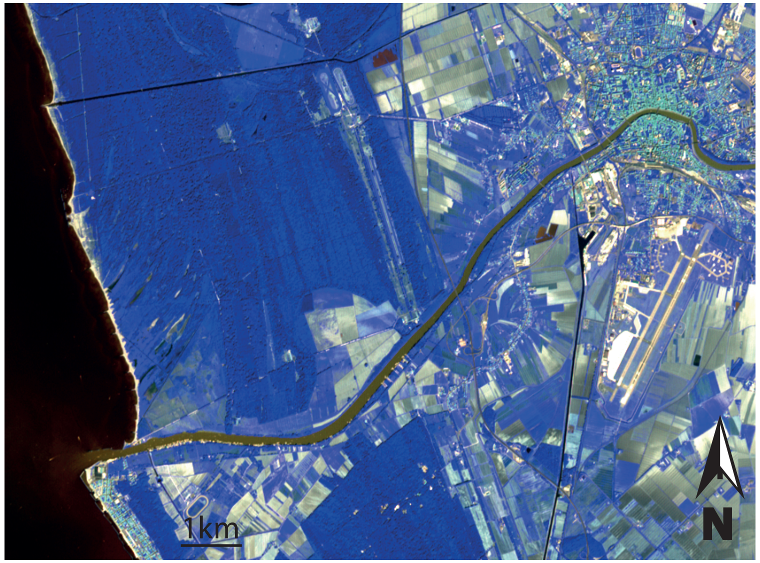


754__Landsat7_08October1999


752_Landsat8_12October2015

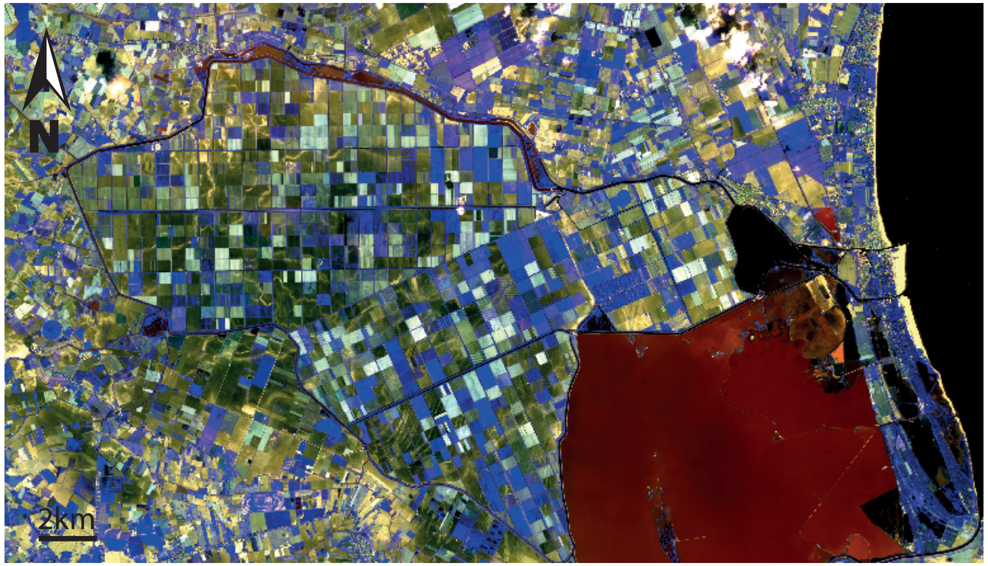
348__Sentinel2a_12September2015

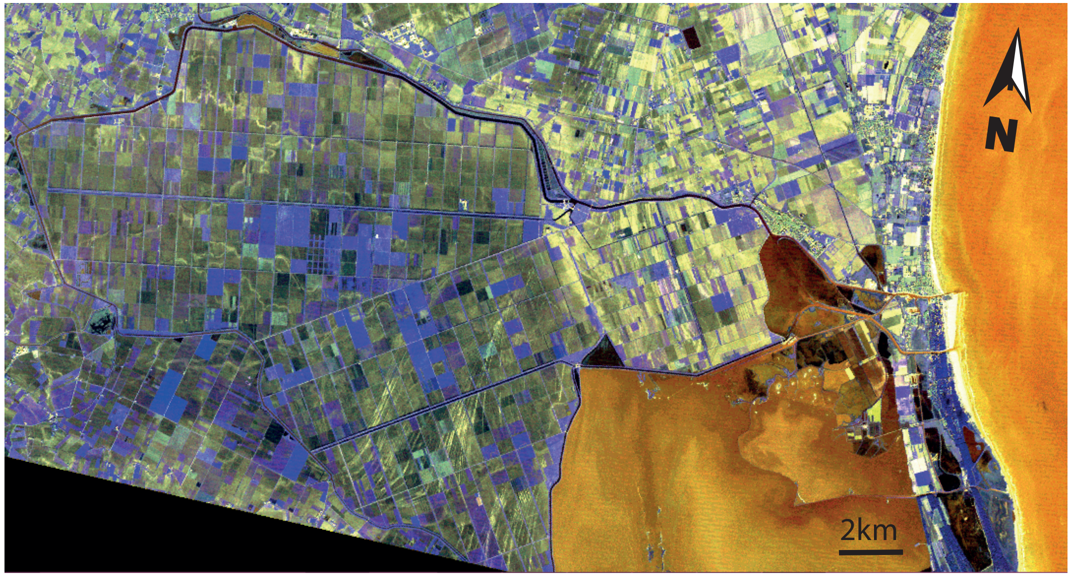
123N__ASTER_13October2001

APPENDIX B

STRATIGRAPHIC LOG AND PHOTOGRAPHIC REPORT OF VIBRACORES

(Pisa Plain and Mezzano Valley study areas)

Core_**CobraTSP1**

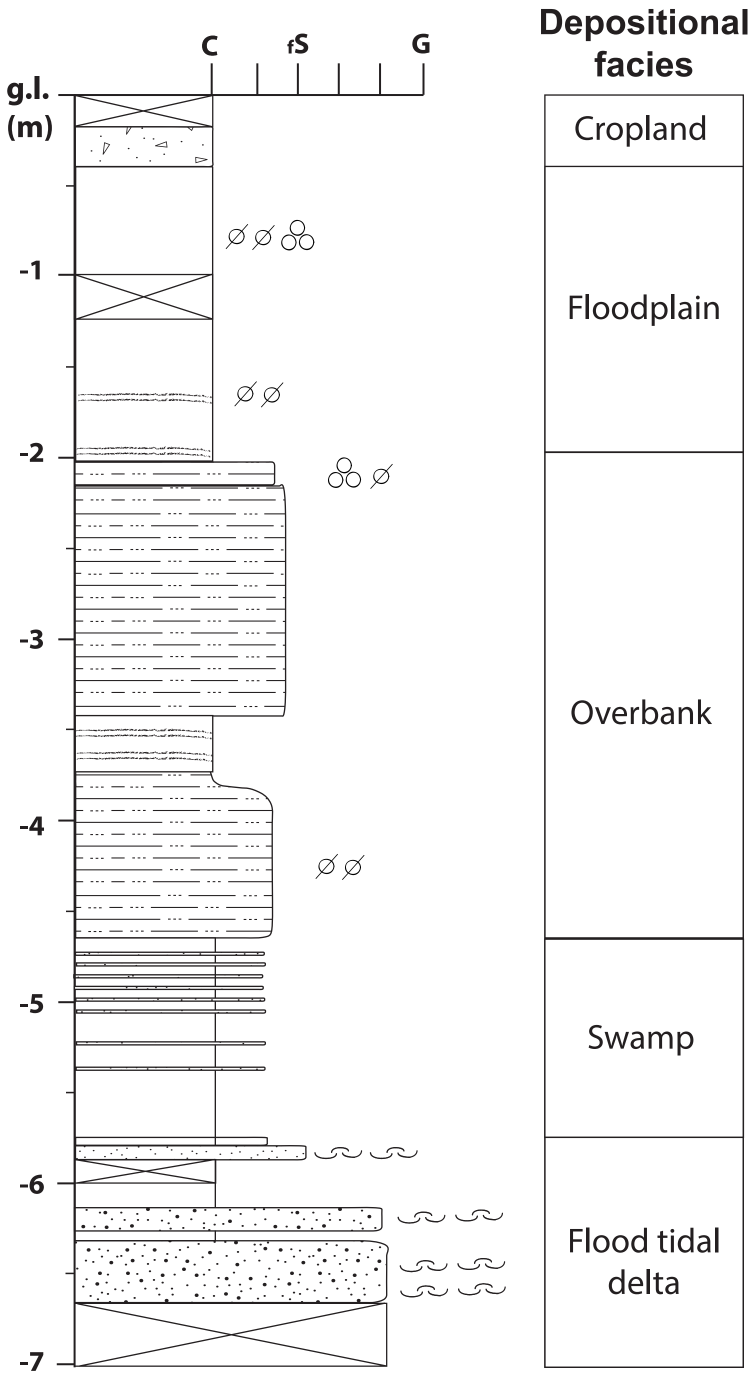

Legend

- ▨ Plough land
- ☐ Clay
- ▨ Silt, silty Clay
- ▨ Sandy silt-silty Sand
- ▨ Sand
- Calcareous nodules
- Redoximorphic features
- Mollusc fragments
- Organic-rich deposits

Placement:

Pisa-SanRossore
on trace, bright portion
coord.UTM-WGS84:32T 609660.037E-4842558.000N
g.l.= 0,58 m a.s.l.

Photographic report

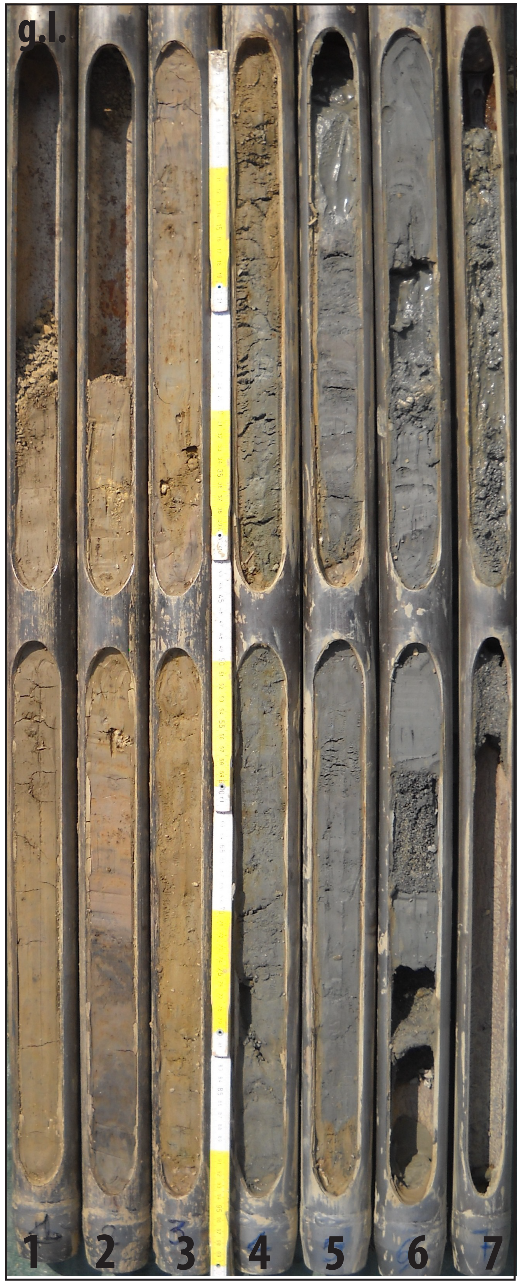

Core_**CobraTSP2**

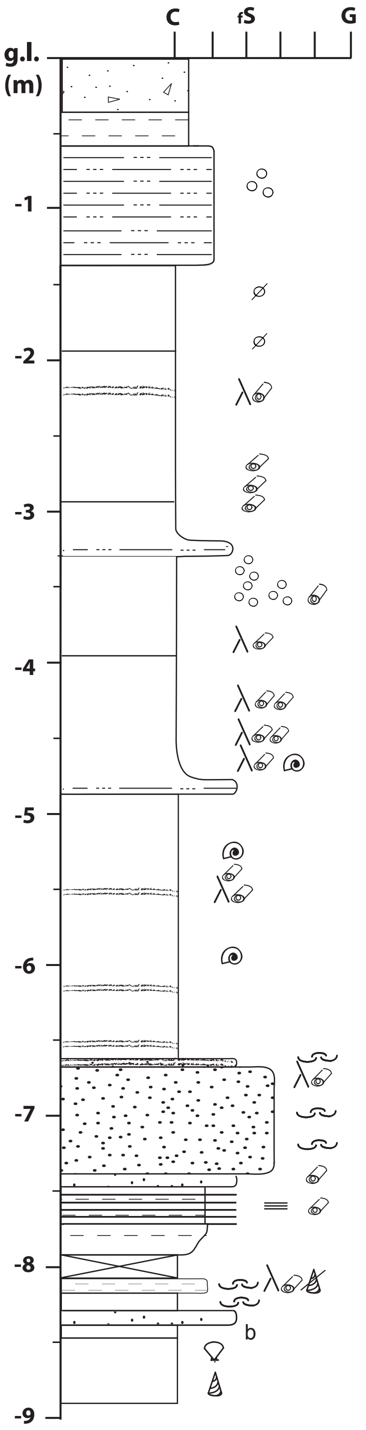

Depositional facies

- Crop land
- Overbank
- Floodplain
- Swamp
- Poorly-drained floodplain
- Swamp
- Fllood-tidal delta
- Lagoon

Legend

- Plough land
- Clay
- Silt, Silty clay
- Sandy silt-silty Sand
- Sand

- Calcareous nodules
- Redoximorphic features
- Mollusc fragments
- Marine bivalves
- Marine gastropods
- Freshwater gastropods
- Plant fragments and wood
- Organic-rich deposits

Placement:

Pisa-San Rossore
on trace, darkest portion
coord.UTM-WGS84: 609780.950E-4841894.100N
g.l.= 0,88m a.s.l.

Photographic report

Core_CobraTSP3

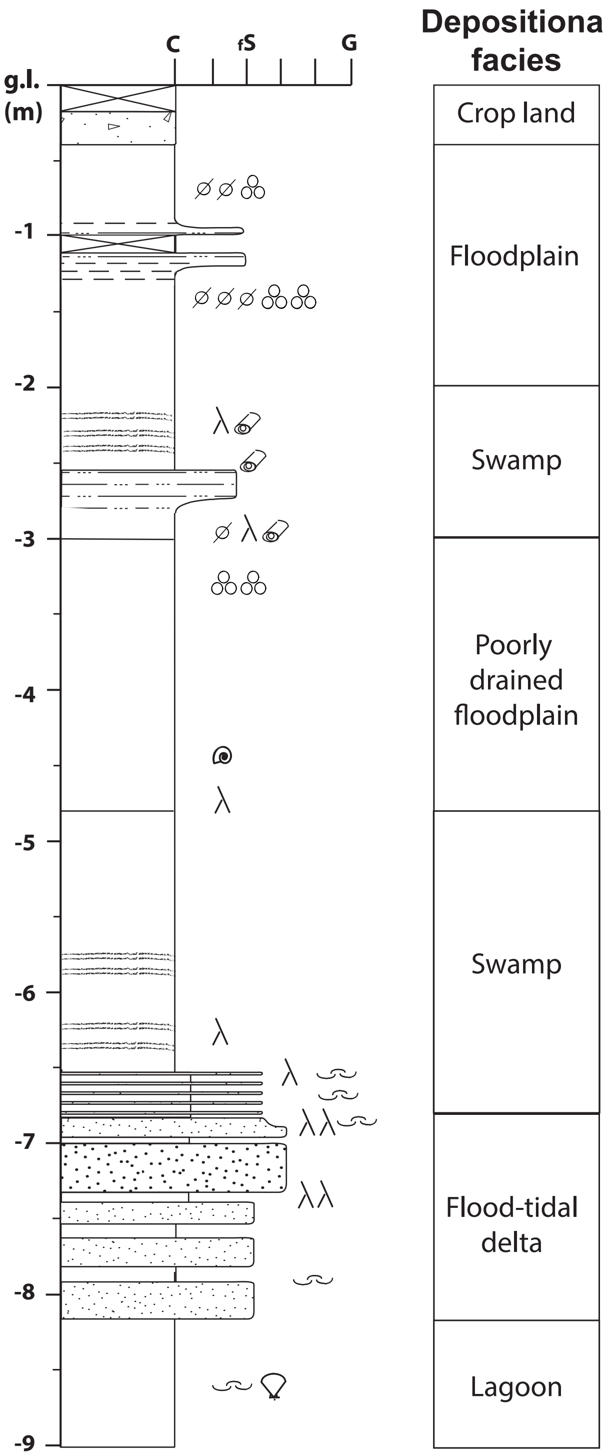

Legend

- Plough land
- Clay
- Silt, Silty clay
- Sandy silt-silty Sand
- Sand

- Calcareous nodules
- Redoximorphic features
- Mollusc fragments
- Marine bivalves
- Marine gastropods
- Freshwater gastropods
- Plant fragments and wood
- Organic-rich deposits

Photographic report

Placement:

Pisa-San Rossore
on trace, darkest portion
coord.UTM-WGS84: 609800.950E-4841927.000N
g.l.= 1,03m a.s.l.

Core_**CobraTSP4**

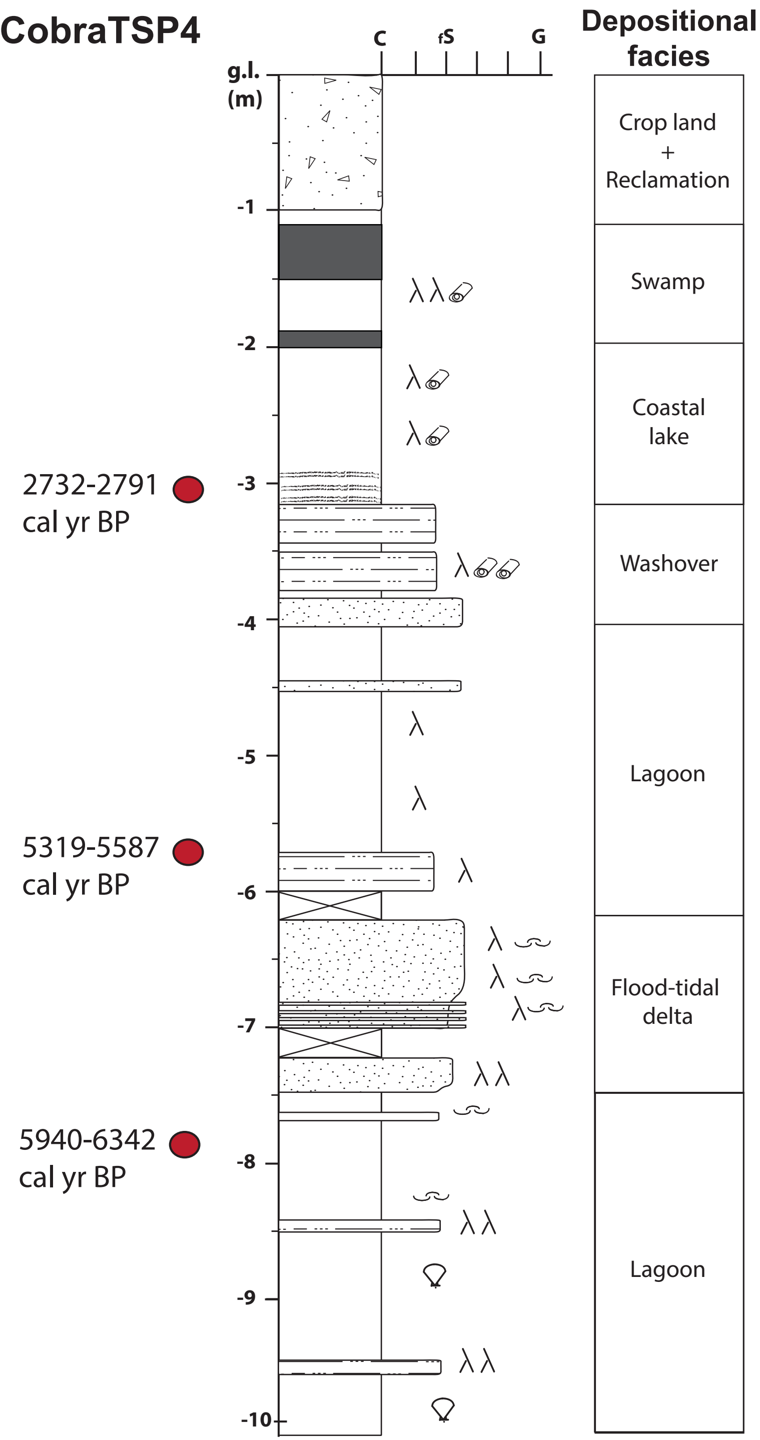

Legend

- Plough land
- Clay
- Silt, Silty clay
- Sandy silt-Silty sand
- Sand
- Peat
- Mollusc fragments
- Marine bivalves
- Marine gastropods
- Freshwater gastropods
- λ Plant fragments and wood
- Organic-rich deposits

Placement:

Pisa-San Rossore, E of the beachridge on trace, bright portion

coord.UTM-WGS84: 608409.950E-4842253.900N

g.l.= 0,24m a.s.l.

Photographic report

Core_**CobraTSP5**

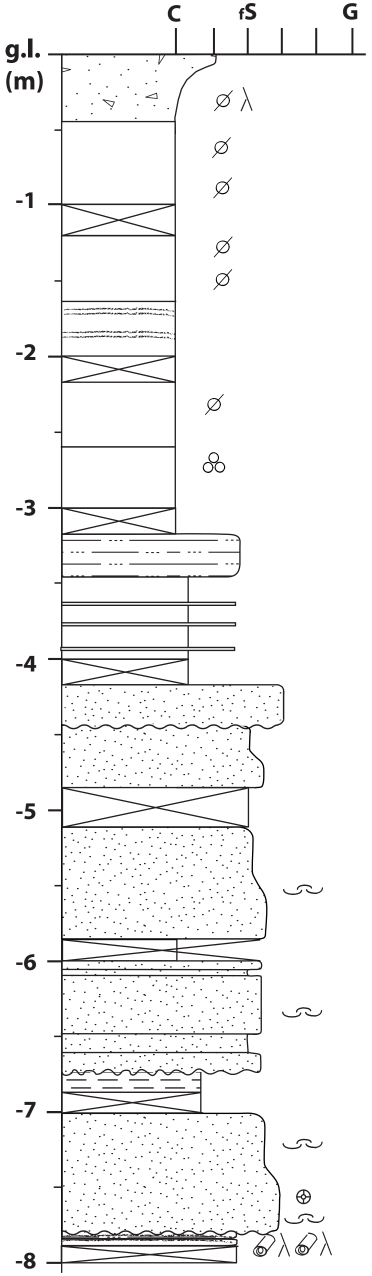

Depositional facies

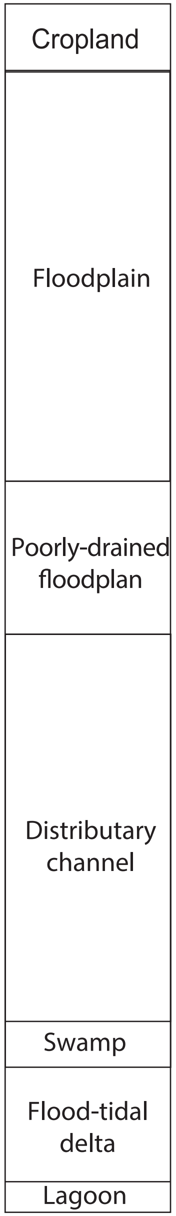

Legend

- Plough land
- Clay
- Silt, Silty clay
- Sandy silt-Silty sand
- Sand
- Calcareous nodules
- Redoximorphic features
- Mollusc fragments
- Corals
- Plant fragments and wood
- Organic-rich deposits
- Erosive surface

Placement:
San Rossore _Pisa
on trace
coord.UTM-WGS84: 609389.050E-4841797.900N
g.l.= 0,95m a.s.l.

Photographic report

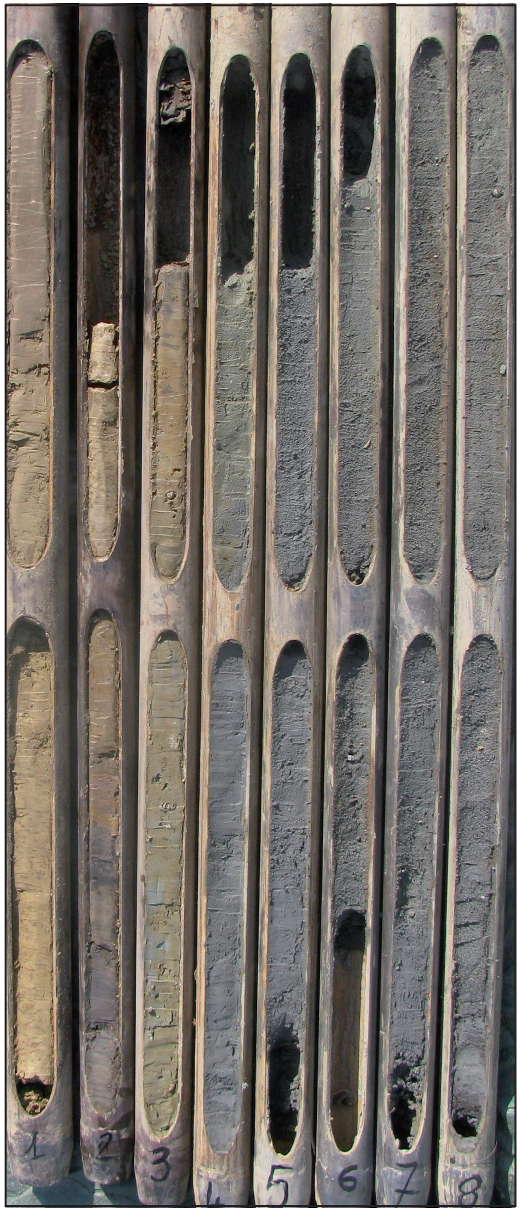

Core_**TSC1**

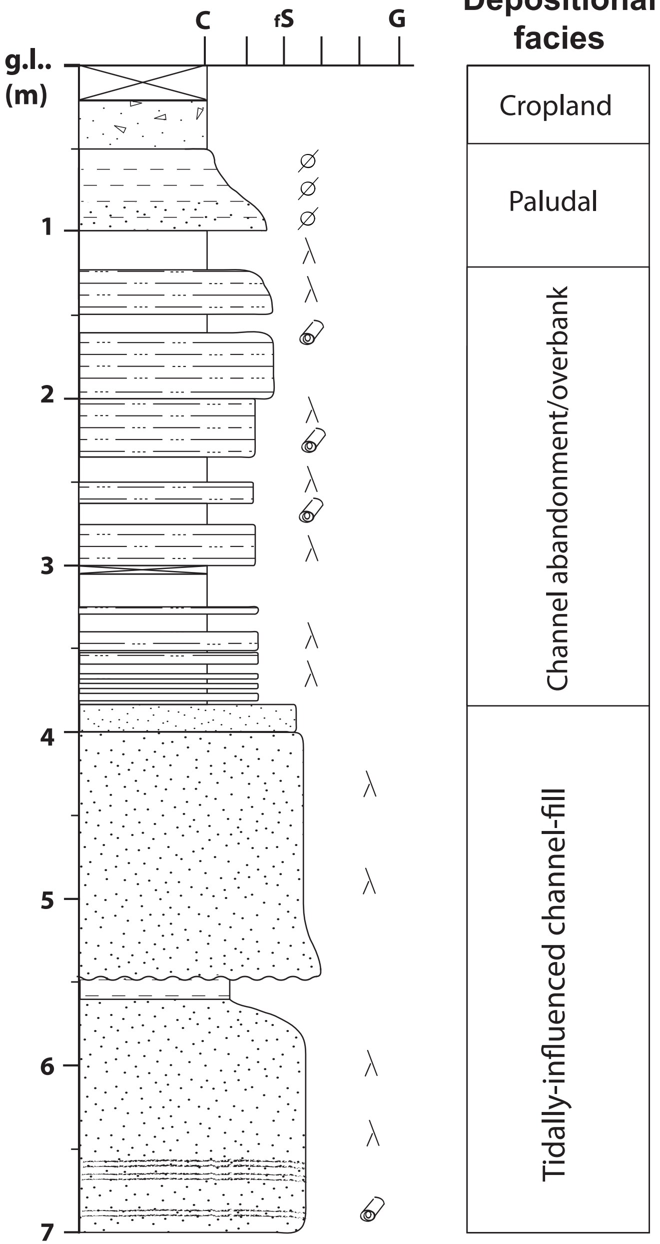

Legend

- Plough land
- Clay
- Silt, Silty clay
- Sandy silt-silty Sand
- Sand
- ∅ Redoximorphic features
- Mollusc fragments
- Brackish bivalves
- Marine gastropods
- Freshwater gastropods
- λ Plant fragments and wood
- Organic matter enrichment
- Erosive surface

Photographic report

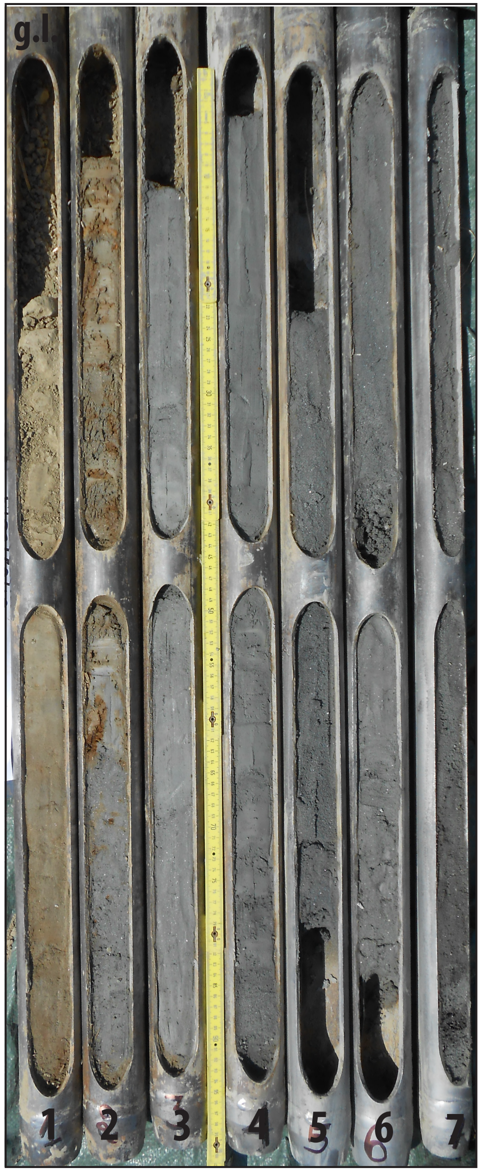

Placement:
Mezzano Valley
on trace, bright portion
coord.UTM-WGS84: 736495.235E-4955777.000N
g.l.= 1.48m b.s.l.

Core_**TSC2**

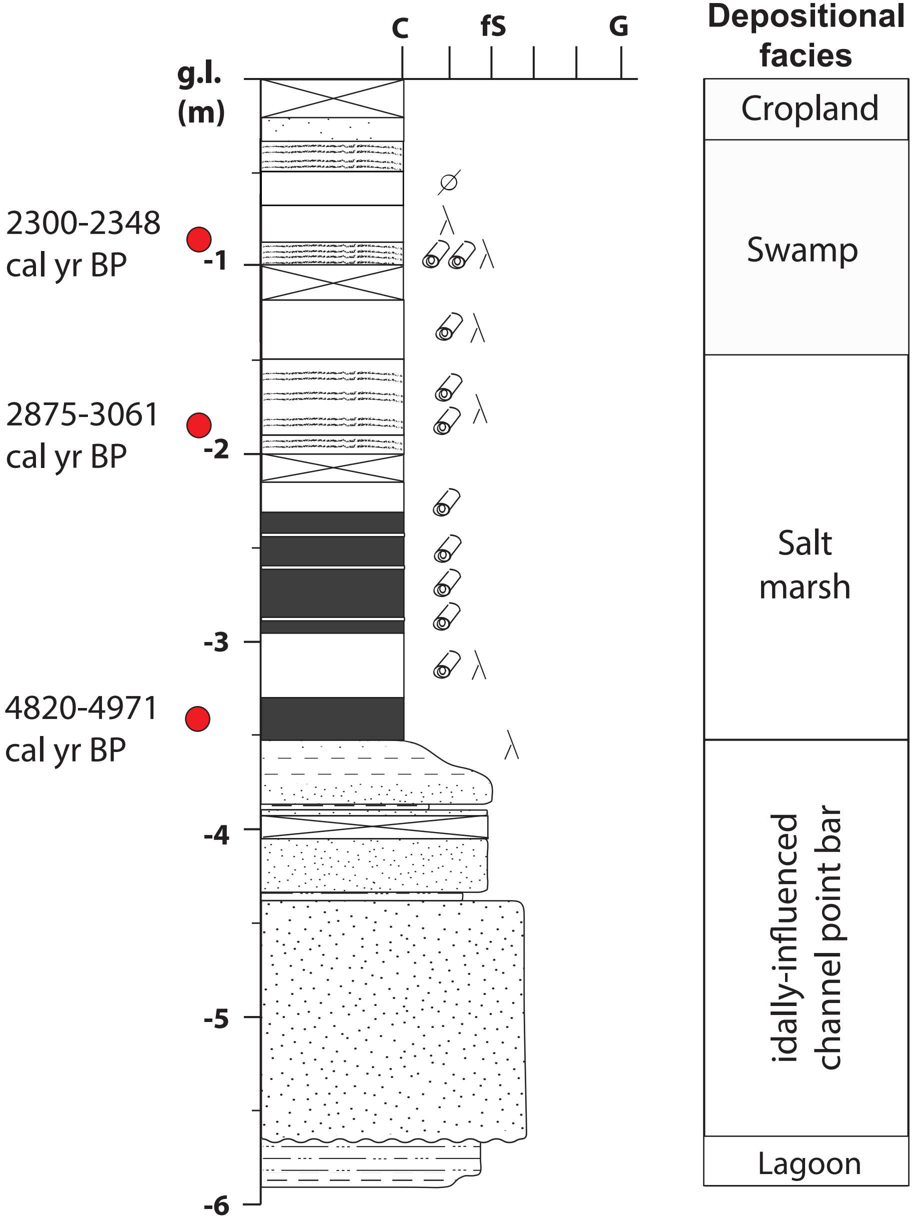

Legend

- ▨ Plough land
- □ Clay
- ▤ Silt, Silty clay
- ▤ Sandy silt-Silty sand
- ▨ Sand
- ■ Peat
- ∅ Redoximorphic features
- — Organic matter enrichment
- 〰 Erosive surface

Photographic report

Placement:
Mezzano Valley
outside trace
coord.UTM-WGS84: 736.500,295E-4955496.000N
g.l.= 0,88m a.s.l.

Core_TSC3

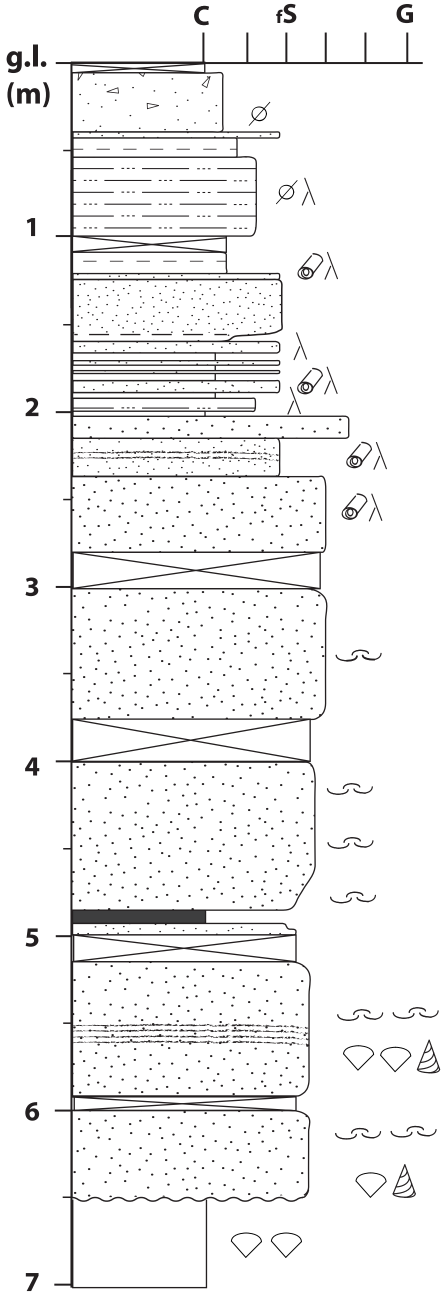

Depositional facies

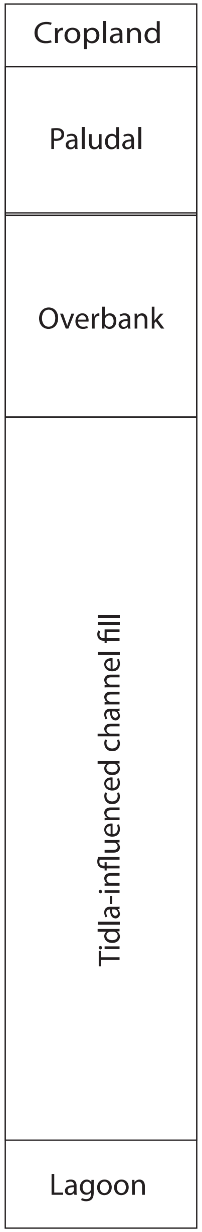

Legend

- ▨ Plough land
- ☐ Clay
- ▤ Silt, Silty clay
- ▤ Sandy silt-Silty sand
- ▩ Sand
- ■ Peat
- ∅ Redoximorphic features
- Mollusc fragments
- Brackish bivalves
- Marine gastropods
- Freshwater gastropods
- λ Plant fragments and wood
- Organic-rich deposits
- 〰 Erosive surface

Photographic report

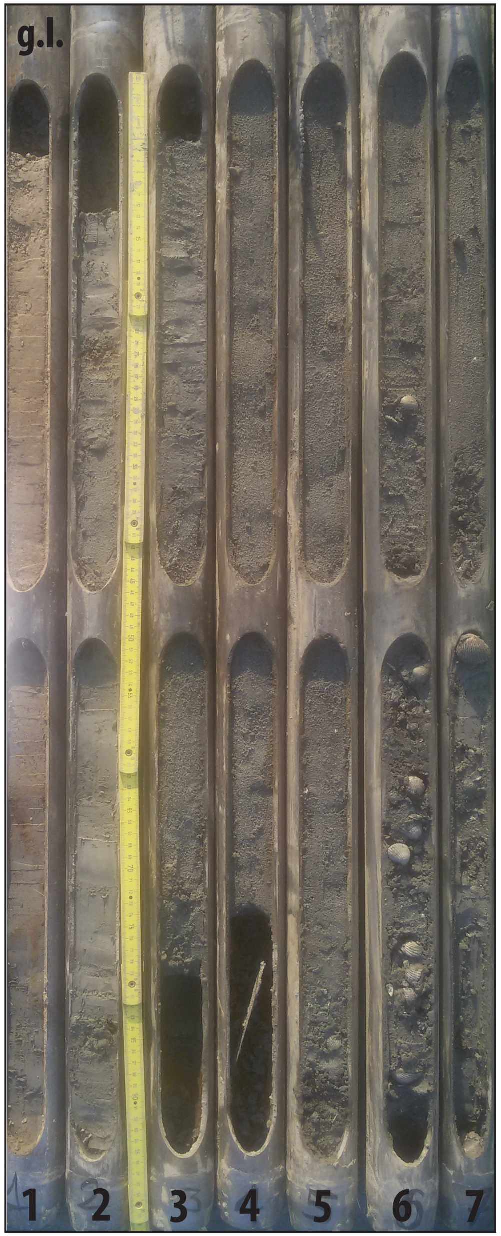

Placement:
Mezzano Valley
on trace, bright portion
coord.UTM-WGS84: 738256.973E-4950916.553N
g.l.= 3,53m b.s.l.

Core_**TSC4**

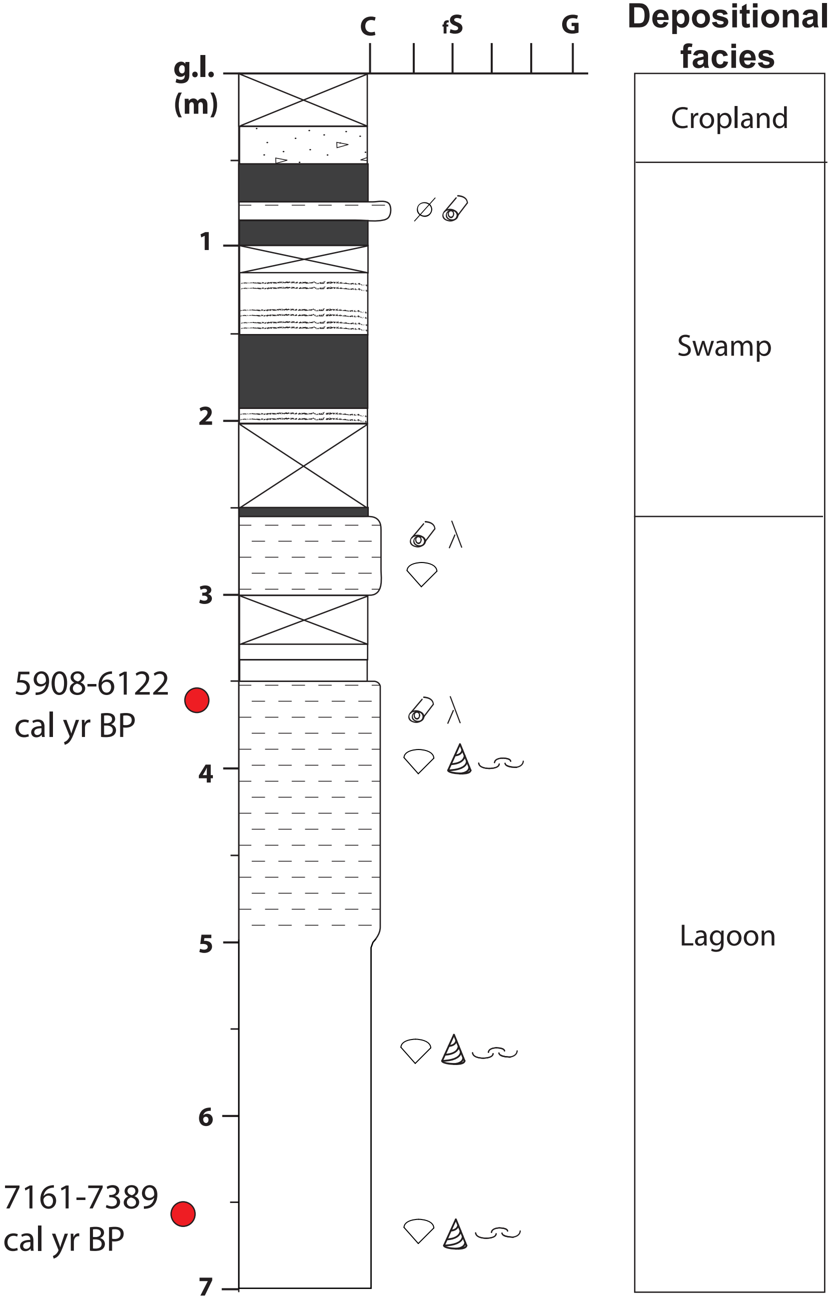

Legend

- Plough land
- Clay
- Silt, Silty clay
- Peat
- Redoximorphic features
- Mollusc fragments
- Brackish bivalves
- Marine gastropods
- Plant fragments and wood
- Organic-rich deposits

Photographic report

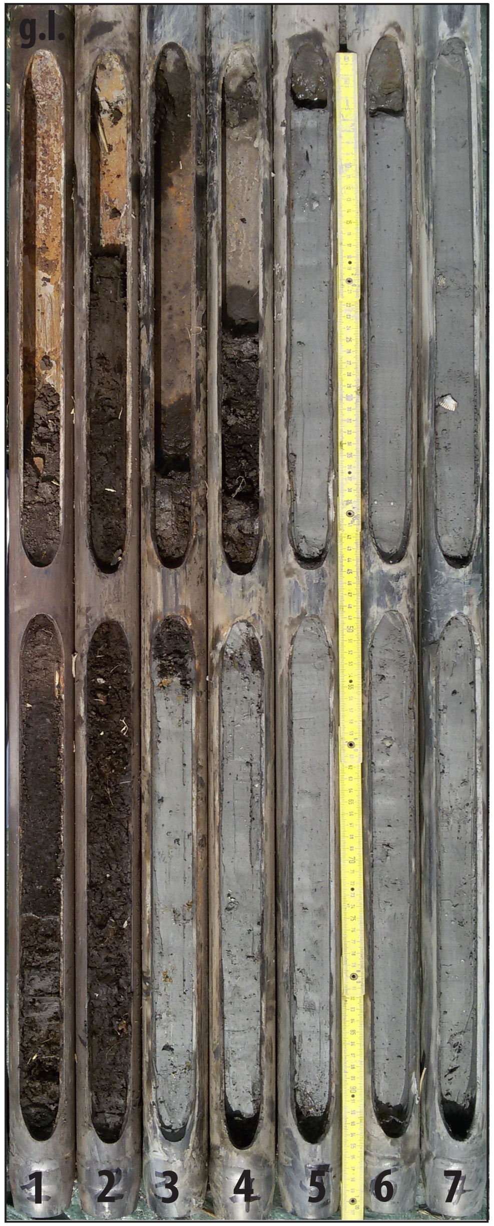

Placement:
Mezzano Valley
outside of track
coord.UTM-WGS84: 738059.457E-4950952.866N
g.l.= 3,43m b.s.l.

Core_**TSC5**

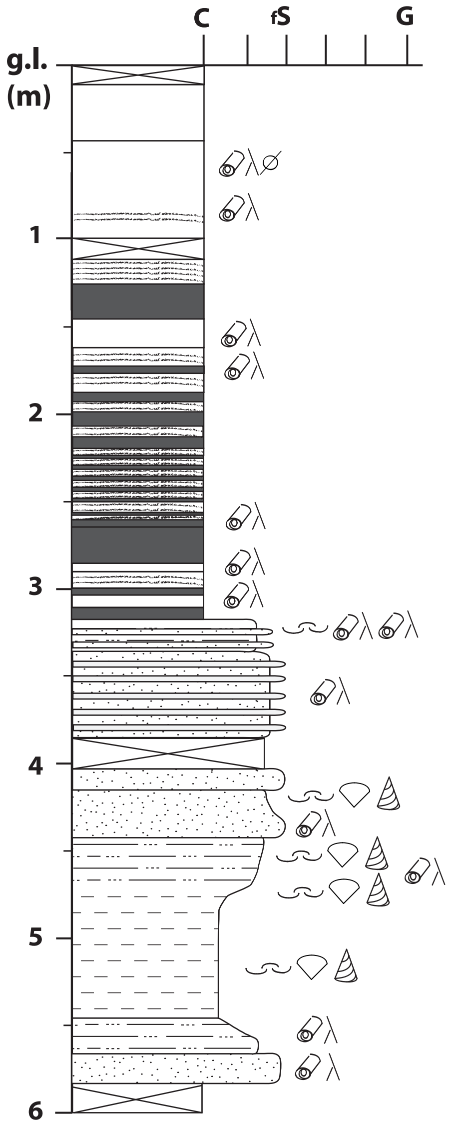

Depositional facies

Legend

- ⊠ Plough land
- ▢ Clay
- ▤ Silt, Silty clay
- ▤ Sandy silt-Silty sand
- ░ Sand
- ■ Peat
- ∅ Redoximorphic features
- ∼ Mollusc fragments
- Brackish bivalves
- Marine gastropods
- Freshwater gastropods
- λ Plant fragments and wood
- Organic-rich deposits

Photographic report

Placement:
Mezzano Valley
outside of track
coord.UTM-WGS84: 736634,765E-4955788,000N
g.l.= 3,21m b.s.l.

Core_**TSC6**

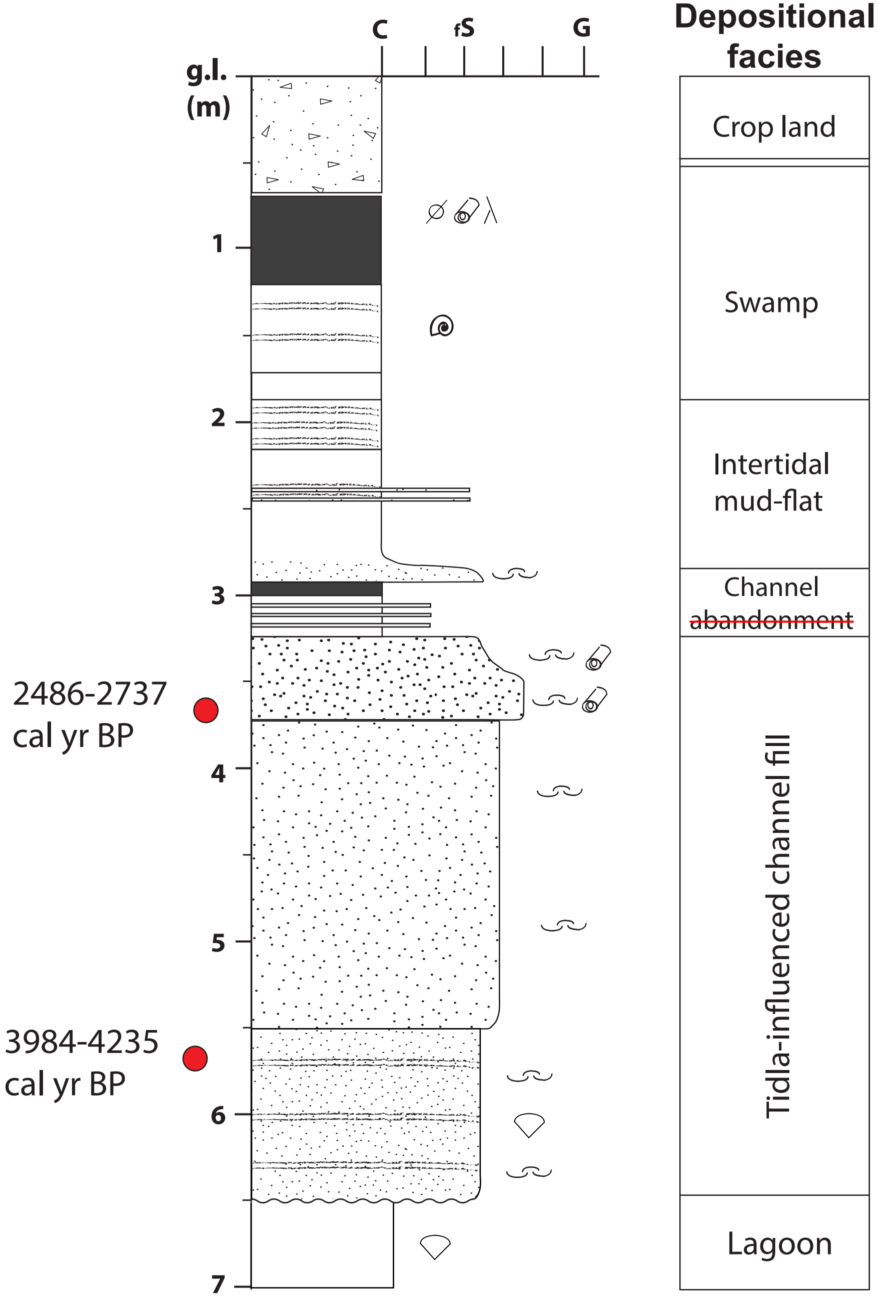

Legend

- Plough land
- Clay
- Silt, Silty clay
- Sandy silt-Silty sand
- Sand
- Peat

- Redoximorphic features
- Mollusc fragments
- Brackish bivalves
- Freshwater gastropods
- Plant fragments and wood
- Organic-rich deposits
- Erosive surface

Photographic report

Placement:
Mezzano Valley
on track, dark portion
coord.UTM-WGS84: 738411.571E-4950882.024N
g.l.= 3,76m b.s.l.

APPENDIX C

PUBLISHED PAPER

(Pisa Plain)

Atti Soc. Tosc. Sci. Nat., Mem., Serie A, 122 (2015)
pagg. 79-88, fig. 5; *doi: 10.2424/ASTSN.M.2015.22*

Giovanni Sarti (*), Veronica Rossi (**), Serena Giacomelli (**)(***)

THE UPPER PLEISTOCENE “ISOLA DI COLTANO SANDS” (ARNO COASTAL PLAIN, TUSCANYITALY): REVIEW OF STRATIGRAPHIC DATA ANDTECTONIC IMPLICATIONS FOR THE SOUTHERN MARGIN OF THE VIAREGGIO BASIN

Abstract - *The Upper Pleistocene “Isola Di Coltano Sands” (Arno Coastal Plain, Tuscanyitaly): Review of Stratigraphic Data Andtectonic Implications for the Southern Margin of the Viareggio Basin.* We present and discuss previously published stratigraphic and chronological (mainly archaeological remains) data about the “Isola di Coltano Sands”(ICS), with the support of unpublished core stratigraphies and taking into account the geological frame of the Arno coastal plain.

ICS outcrops in the southern portion of the extensional Viareggio Basin, forming three isolated small-sized reliefs rising up to 15 m above the present-day Arno coastal plain on both sides of the Arno River.

We document that the deposits outcropping north of the Arno River (Palazzetto site) reasonably belong to the Holocene prograding beach-ridge system to which they are physically juxtaposed. Indeed, both sedimentological and morphological characteristics indicate that the Palazzetto sands were exclusively formed by wind-related processes, likely occurred during the late Holocene according to the presence of Eneolithic artefacts.

Conversely, the common presence of *Mousterian* artefacts at the Castagnolo and Coltano sites, located south of the Arno River, documents an age older than 40 kyr (upper Pleistocene) for these reliefs. Moreover, new stratigraphic data show that ICS are constituted by alluvial deposits with evidences of repetitive fluvial erosion episodes. All these features, indicate that ICS can be reasonably included into the Late Pleistocene Vicarello Formation, widely outcropping along the southern margin of the Leghorn Hills. In this context, an estimated age ranging between MIS 6 and MIS 3 can be hypothesized for the ICS.

However, the occurrence of Upper Pleistocene reliefs formed by alluvial deposits (Coltano and Castagnolo sites) in the southern portion of the Arno coastal plain seems to conflict with the acknowledged interpretation of the area as an extensional, subsiding setting. Moreover, the sharp morphological boundary dividing the flat Holocene coastal plain from the Quaternary Leghorn Hills is roughly coincident with the SW-NE transpressive fault (Sillaro line) that subdivides the subsiding area (Viareggio Basin, to which the Arno plain belongs) from the uplifting area (Leghorn mounts).

Thus, our review of the available stratigraphic and chronological data strongly suggests the occurrence of a geological connection between the southern portion of the Arno coastal plain, specifically of the Castagnolo and Coltano reliefs, and the Leghorns Hills where the Vicarello Formation outcrops. This connection, which may have strong consequences on the geo-tectonic interpretation of the study area, and the formation age of ICS needs to be better investigated in the future with new high-resolution tectonic and absolute chronological data.

Keywords - Facies analysis, sea-level change, Holocene, Late Pleistocene, incised valley, Arno plain, extensional basin, subsidence, Coltano sands, Vicarello Formation.

Riassunto - *Le sabbie del Pliestocene superiore di Isola di Coltano (Pianura costiera dell’Arno, Toscana, Italia): revisione dei dati stratigrafici ed implicazioni tettoniche per il margine meridionale del Bacino di Viareggio.* Nel lavoro sono discussi i dati stratigrafici e cronologici riguardanti le “Sabbie dell’Isola di Coltano” (ISC), con il supporto di stratigrafie di sondaggio inedite e tenendo conto del quadro dell’evoluzione stratigrafico deposizionale della pianura costiera a sud dell’Arno.

ISC affiorano nella porzione meridionale del Bacino estensionale di Viareggio, e formano tre rilievi di piccole dimensioni con un’elevazione fino a 15m sull’attuale piana costiera dell’Arno in entrambi i settori del Fiume Arno.

I depositi affioranti a nord del Fiume Arno (sito di Palazzetto) sono attribuiti al sistema progradante di cordoni costieri olocenici ai quali sono fisicamente giustapposti. Le caratteristiche sedimentologiche e morfologiche indicano con evidenza l’origine eolica delle sabbie di Palazzetto depositatesi in età tardo olocenica, in accordo con la presenza di industrie Eneolitiche. Di contro, la diffusa presenza d’industrie Musteriane nei siti di Castagnolo e Coltano, ubicati a sud del Fiume Arno, documenta un’età non più giovane di 40.000 anni (Pleistocene superiore) per questi depositi. Inoltre, nuovi dati stratigrafici acquisti nell’ambito del progetto CARG alla scala 1/50000 del Foglio Pisa indicano che le ISC sono costituite da depositi alluvionali con evidenze di ripetuti episodi di erosione fluviale. Tutte queste caratteristiche, contestualizzate nel quadro stratigrafico tardo-Quaternario del sottosuolo e degli affioramenti dell’area di studio, indicano che le ISC possono essere incluse ragionevolmente nella Formazione di Vicarello del tardo Pleistocene, ampiamente affiorante lungo il margine meridionale delle Colline Livornesi. In questo quadro può essere ipotizzata per le ICS un’età stimata compresa tra il MIS6 e il MIS3. La presenza di rilievi di origine fluviale di età tardo plesitocenica (siti di Castagnolo e di Coltano) nella porzione meridionale della pianura costiera dell’Arno sembra in contrasto con l’interpretazione largamente condivisa che individua nell’area un’settore estensionale e subsidente. Infatti, il limite morfologico netto che separa la piana costiera olocenica dalle Colline Livornesi pre-Oloceniche è all’incirca coincidente con la nota faglia transpressiva SW-NE (Linea del Sillaro) che suddivide l’area subsidente (Bacino di Viareggio, al quale appartiene la pianura dell’Arno e dunque anche le ICS) dall’area in uplift (Monti Livornesi).

L’analisi dei dati disponibili suggerisce viceversa l’esistenza di una connessione tra la porzione meridionale della piana costiera dell’Arno,

---

(*) Dipartimentodi Scienzedella Terra University of Pisa via Santa Maria 53 - Italy sarti@dst.unipi.it

(**) Dipartimento di ScienzeBiologiche, Geologiche e Ambientali, University of Bologna, Piazza di Porta San Donato 1, Italy - veronica.rossi4@unibo.it; serena.giacomelli3@unibo.it

(***) Dipartimento di Fisica e Scienze della Terra “Macedonio Melloni” University of Parma, Parco Area delle Scienze, 7/A - serena.giacomelli@unipr.it

in particolare dei rilievi di Castagnolo e Coltano, e le Colline Livornesi, dove la Formazione di Vicarello affiora. Il significato di questa relazione, che può avere forti conseguenze sull'interpretazione geotettonica dell'area di studio necessita di ulteriori approfondimenti stratigrafici, tettonici e cronologici.

Parole chiave: Analisi di facies, variazioni del livello del mare, Olocene, Tardo Pleistocene, valle incisa, pianura dell'Arno, bacino estensionale, subsidenza. Sabbie di Coltano, Formazione di Vicarello

INTRODUCTION

According to Fancelli *et al.*,(1986), the"Isola di Coltano Sands"(ICF) forms three small-sized and isolated morphological reliefs rising up to 15 m above the present-day western portion of the Arno coastal plain, on both sides of the Arno river course (Figure 1). Following Lazzarotto *et al.* (1990), the "Isola di Coltano Sands" has been included within the Vicarello Formation (VF), which is Late Pleistocene in age and outcrops widely along the southern margin of the Arno plain, in correspondence of the Pisa and Leghorn foothills. Recently, in the context of the geological mapping (CARG) project of the Pisa Plain to scale 1:50,000 (Sheet 273), the northernmost outcrop of the "Isola di Coltano Sands" (Figure 1, Palazzetto site) has been included in the late Holocene coastal dune unit (Carosi *et al.*, in press). This interpretation is supported by the physically connection between the Palazzetto outcrop and the innermost coastal dune ridge. Furthermore, the Palazzetto succession is exclusively made up of fine sands showing clear evidences of aeolian shaping, such as blow-out and cross stratification, and contains Eneolithic artefacts (Carratori *et al.*, 1994) according to the Etruscan age of the innermost beach-ridge (Pranzini, 2001).

From a tectonic point of view, the occurrence of two late Pleistocene reliefs (Coltano and Castagnolo sites, Figures 1 and 2) seems to conflict with the widely acknowledged interpretation of the Arno coastal plain as an area subject to tectonic-driven subsidence (Mariani & Prato 1988; Pascucci, 2005).

Aim of this work is to furnish a stratigraphic review of the "Isola di Coltano Sands" (ICS) and discuss the tectonic implications deriving by its peculiar stratigraphic-depositional arrangement, focusing on: *i)* the onlap relationships between the Holocene deposits and the "Isola di Coltano Sands", rising up above the Arno coastal plain and *ii)* the mainly fluvial nature of the "Isola di Coltano Sands".

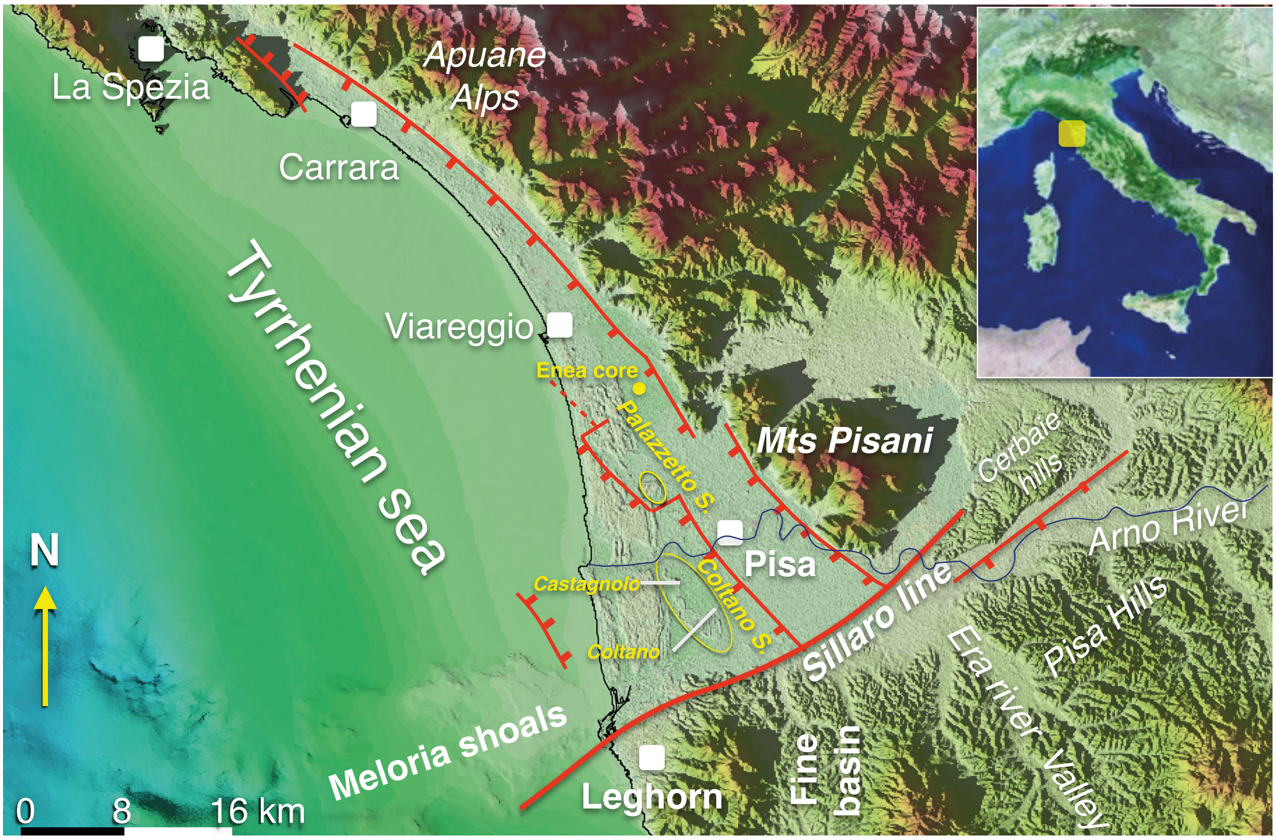

Figure 1 - Location map of the Arno coastal plain and surrounding areas. The main tectonic lineaments connected with the extensional Viareggio Basin are shown (from Pascucci, 2005). ICS reliefs are highlighted by yellow circles. Location of the Enea core is also reported.

Tectonic setting

The Arno coastal plain (Figure 1) constitutes the southern inshore portion of the NW-SE Viareggio extensional basin (Viareggio Basin-VB) that is about 20 km wide and 25 km long. It is bordered by the Pisa Mountains to the northeast, by the Meloria–Maestra shoal to the southwest, and by the Pisa and Leghorn Hills to the southeast.

The VB is one of the several extensional basins that formed since the late Messinian (ca. 7 Ma), in response to the opening of the Tyrrhenian Sea and the counter-clockwise rotation of the Apennine foredeep-foreland system (Malinverno & Ryan, 1986; Patacca *et al.*, 1990; Argnani *et al.*, 1997; Pascucci, 2005). Seismic analyses, integrated with stratigraphy from several deep-wells, document the occurrence of a 3000 m-thick succession of clays and sands ranging in age between the late Messinian and the Holocene and filling the onshore portion of VB (Mariani & Prato, 1988; Pascucci, 2005).

The southern boundary of the VB is marked by the NE-SW transversal lineament known as Livorno-Sillaro line (Bortolotti, 1966), which runs at the Leghorn and Pisa foothills. Several historical earthquakes, recorded few km seaward of the Leghorn city, testify that the Sillaro line is a still active transpressive fault (Ghelardoni, 1965; Cantini *et al.*, 2001; Cerrina Feroni *et al.*, 2001).

These data, and particularly the huge thicknesses of the basin-fill sedimentary succession, indicate that the extensional-subsiding nature of the VB mainly generated the sedimentary space-accommodation.

Depositional evolution

The Arno coastal plain is a wide (ca. 450 km2) and flat (05%) low-lying area, faced to the west by the Tyrrhenian Sea and bounded by the Versilia coastal plain and Pisa Mountains to the north, and Pisa and Leghorn Hills to the south.

The overall late Quaternary depositional evolution of Italian subsiding coastal plain areas has been strongly influenced by the Milankovitch-scale glacio-eustatic fluctuations (Fancelli *et al.,* 1986; Aguzzi *et al.*, 2005, 2007; Pascucci, 2005; Amorosi *et al.*, 2008a,b). A relatively wide set of data, coming from continuous boreholes drilled in the last ten years, shows an alternation of continental and coastal-shallow marine deposits in the uppermost 100 m of the Arno coastal plain. Within this depositional framework two incised-valley systems (IVFs, Sarti, 2012; Sarti *et al.*, 2015), 5-8 km wide and more than 30 m depth, represent the most prominent stratigraphic feature (Figure 3). The uppermost incised valley system (IVS) began to form, close to the modern Arno River course, at the transition to the Last Glacial Maximum (MIS 3-2). This incised valley partially cut the post-valley fill deposits of the oldest IVS, which developed in a southern position during the Middle Pleistocene (probably during MIS 8). The incised-valley fill (IVF) sequences accumulated during two interglacial phases (MIS 1 and MIS 7, respectively), and display similar facies architecture. Each IVF exhibits a fining-upward tendency, with a basal lag of fluvial gravels sharply overlain by transgressive, mud-dominated coastal plain and estuarine deposits that progressively onlap onto the valley flanks. Whereas the inundation of the interfluves is almost coincident with maximum marine ingression in both IVSs, a record of the highstand succession is observed uniquely above the uppermost valley fill, due to the erosive processes that followed the MIS 7 interglacial. Around 8000 cal yr BP an extensive surface comprised between the Pisa Mountains and the innermost outcropping beach-ridge was flooded, leading to the development of a 6 km-wide lagoon basin recorded in the subsurface by *Cerastodema*-rich, highly compressible m-thick silty clays (locally known as "pancone"). These lagoon deposits occur between ca. 20-5 m below sea level and show lateral transition to rich-organic swamp silty clays (Benvenuti *et al.,* 2006; Rossi *et al.*, 2011). In response to the following phase of decelerated sea-level rise (Lambeck *et al.,* 2004a, 2011), the uppermost prograding portion of the Arno coastal plain has been deposited (Amorosi *et al.,* 2013a; Figure 3). Specifically, a 10-15 m thick fluvio-deltaic succession, composed of predominant clays and silts encasing lenticular sand bodies (Amorosi *et al.,* 2013a), records the siltation of the lagoon and the progradation of the modern Arno delta-coastal plain system under prolonged conditions of relatively stable sea-level (Lambeck *et al.,* 2004a, 2011).

Stratigraphy of "The Isola di Coltano Sands"

At the Coltano site (Figures 2, 4), several hand-man cores driven down to 2 m below the ground surface document a monotonous succession of yellow decarbonated silty clays (Carosi *et al.,* in press), while more sandy deposits are observable moving northward at the Castagnolo site (Figure 2). At both sites no evidences of aeolian shaping are recorded. In contrast, several roughly flat surfaces separated by small escarpments are observed, suggesting repetitive erosional events of fluvial origin (Figure 4c).

On the basis of these sedimentological, stratigraphic and morphological features, we consider not reliable the interpretation of ICS as aeolian deposits (Fancelli *et al.*, 1986;Lazzarotto *et al.,* 1990), according to Carosi *et al.* (in press). Indeed, the available data are

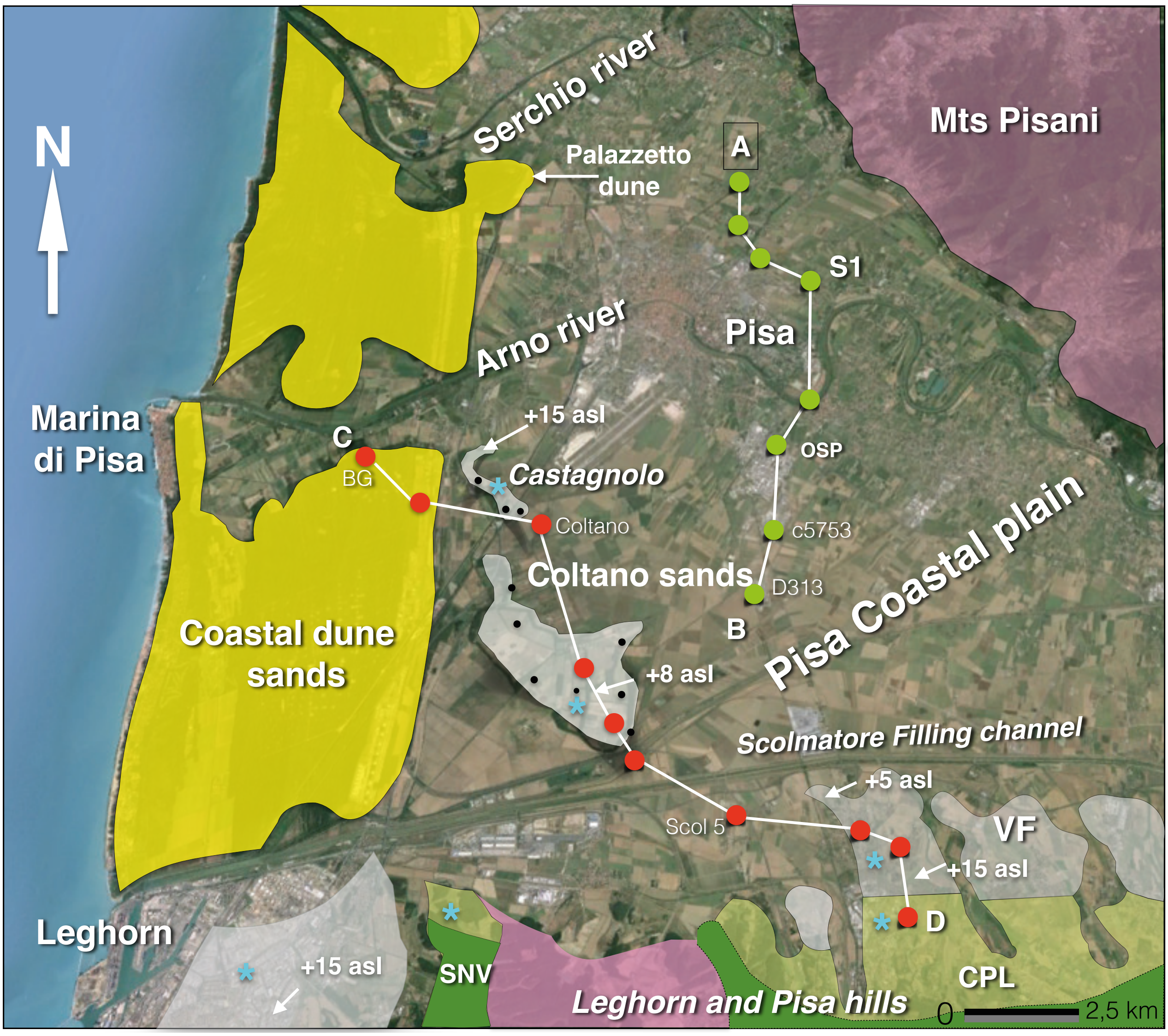

Figure 2 - Simplified geological sketch map of the study area (slightly modified from Carosi *et al.,* in press-CARG Sheet 273). It is worth to note that the Palazzetto relief is included into the late Holocene coastal dune unit, whereas Castagnolo and Coltano outcrops belong to the Upper Pliestocene Vicarello Formation. Location of the continuous cores (red and green circles) and the section traces, both reported in Figures 3 and 4, are also shown.

Keys: CPL, Casa Poggio ai Lecci Conglomerate and Sands, Middle Pleistocene in age. - SNV, Nugola Vecchia Sand, Lower to Middle Pleistocene in age. - In pink are reported the Pre-Quaternary deposits. - Small black circles: hand-man cores; - Light blue stars: *Mousterian* sites.

indicative of overbank and/or channel-related depositional environments similarly to what is suggested for the Late Pleistocene VF sands and silts (Lazzarotto *et al.*, 1990). These deposits unconformably lie onto the Middle Pleistocene deposits of "Casa Poggio ai Lecci" Fm, occurring along the Pisa and Leghorn foothills (Figure 2).

THE ICS INFERRED AGE

The widespread occurrence of *Mousterian* artifacts (Menchelli, 1984; Grifoni Cremonesi & Tozzi, 1995) within the Coltano and Castagnolo reliefs indicates an age older than 40 ky BP (Grün & Stringer, 1991) and represents the more robust chronostratigraphic data available by now (Marroni *et al.*, 1990; Federici & Mazzanti, 1995; Mazzanti, 2000). *Mousterian* artifacts

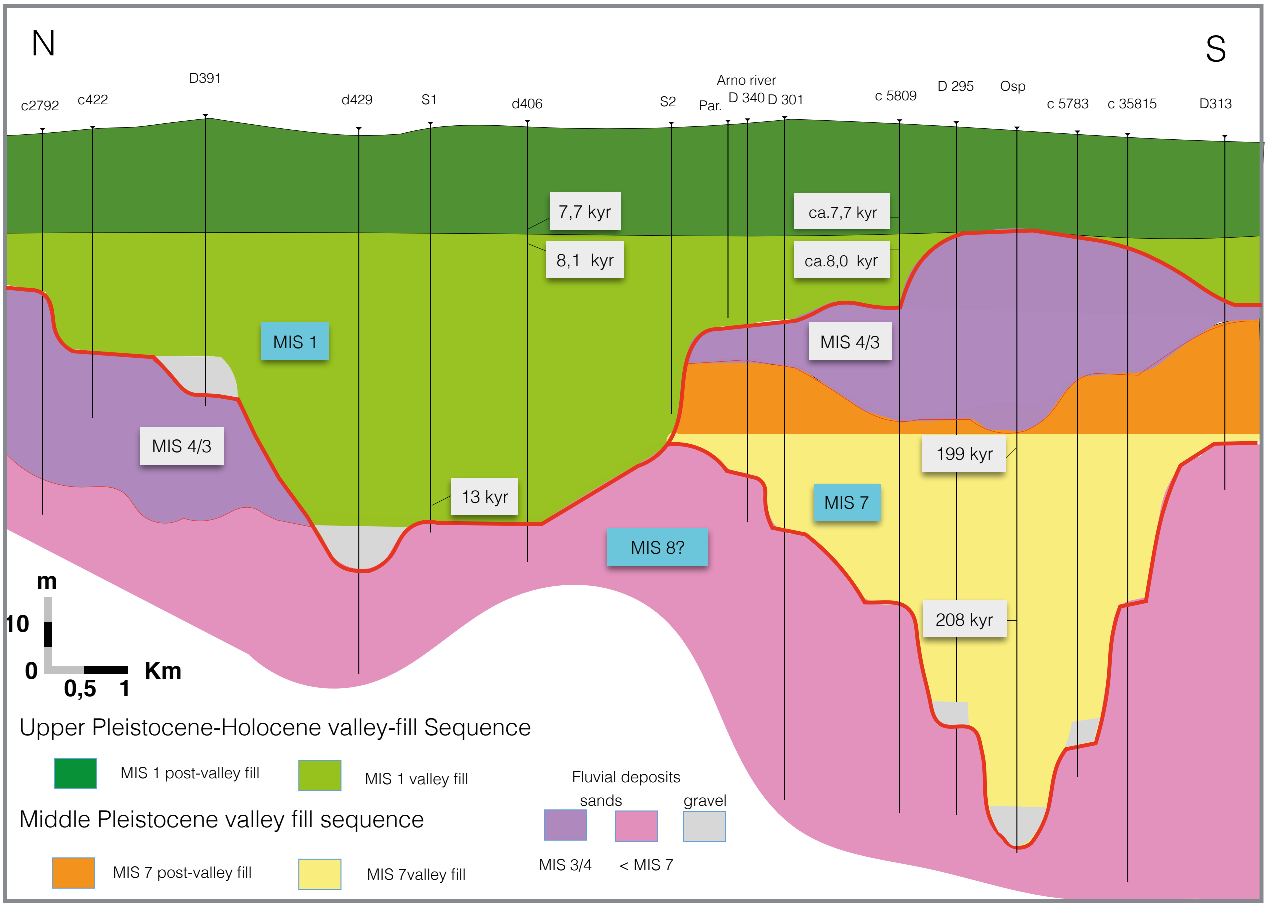

Figure 3 - Representative cross-section of the two incised-valley systems identified within the uppermost 100 m of Quaternary deposits buried beneath the Arno coastal plain. Subdivision into main stratigraphic units and their interpretation in terms of MIS are shown. The radiocarbon ages from the upper Pleistocene-Holocene incised-valley fill are reported as calibrated years BP, while the ages from the middle Pleistocene incised-valley fill are ERS data (dating from Amorosi *et al.*, 2013b, 2014; Sarti *et al.*, 2015). Section traces and sedimentary cores location are reported in Figure 2 (green dots).

(Figure 2) are also found along the Leghorn foothills on the top of the VF deposits, strengthening the belonging of the “Isola di ColtanoSands” to the VF (Lazzarotto *et.al.,*1990)

Other chronological information can be inferred through stratigraphic correlations of ICS with the Arno plain subsurface units.Several authors correlate the “Isola di Coltano Sands” with the “Limi fluviali-palustri” unit that in turn overlies the “Conglomerati dell’ Arno e del Serchio da Bientina” attributed to MIS 4 (Fancelli *et al.*, 1986; Della Rocca *et al.,* 1987; Federici & Mazzanti, 1995; Baldacci, 1999). This stratigraphic interpretation seems to agree with the age of the *Mousterian* findings and, according to Federici & Mazzanti (1995) and Mazzanti (2000), refines the age of the VF to the MIS 3 (older than 40 kyr but younger than MIS4; Ciampalini & Sammartino, 2007).

However, the reliability of this stratigraphic framework was criticized by Aguzzi *et al.* (2005), showing that the coarse-grained interval (“Conglomerati dell’Arno e del Serchio da Bientina”) used as subsurface stratigraphic marker (Fancelli *et al.,* 1986) is the result of a lithological correlation among conglomerates of different ages (Aguzzi *et al.,* 2007). This fact is relievable in the map reporting the isobaths of the “Conglomerati dell’Arno e del Serchio da Bientina” (see Figure 5 in Fancelli *et al.*, 1986), where the depth of the conglomerates lower boundary broadly ranges from 20 m to more than 200 m below the ground level. Moreover, stratigraphic analysis of continuously cored boreholes performed in the Arno coastal plain confirms the presence of conglomerate layers at different stratigraphic positions partially connected to the IVSs development (Figures 3, 5).

To sum up, in the absence of new specific dates the only reliable ICS chronologicalconstrains are represented by the *Mousterian* artifacts older than 40 ky (the ICS

Figure 4 - The ICF at Coltano southern Hill area (See Fig. 2 for the location). View is from SE. a) panoramic view of Coltano hill and the surrounding coastal plain area; b) particular of the escarpment; c) view from SW of the top of Coltano hill, not the flat morphology.

youngest age limit) and the Middle Pleistocene “Conglomerati di Casa Poggio ai Lecci” Fm, on which the VF rests on(the ICS older age limit). Subsurface date (Figure 5) show that the ICS erode the post-valley fill succession of MIS 7 age. Basing on that the older age limit of ICS can be restricted to MI7/6.

THE “ICS PARADOX”: STRATIGRAPHIC AND TECTONIC IMPLICATIONS

In order to discuss the tectonic implications deriving from the occurrence of the ICS reliefs in the Arno coastal plain the following key-points should be keep in mind:

i. the assumed, general subsiding-extensional tectonic framework of the Arno coastal plain;
ii. the ICS depositional age that should be not younger of 40 kyr and not older of Middle Pleistocene (likely younger of MIS 7);
iii. the morpho-stratigraphic position of Coltano and Castagnolo reliefs, which rise up to 15 m above the modern plain that is still aggrading;
iv. the onlap of Holocene deposits onto the ICS reliefs.

As widely documented by both outcrop and subsurface data, the late Quaternary stratigraphy of several coastal and deltaic areas was mainly controlled by the interplay between glacio-eustatic and tectonic signa-

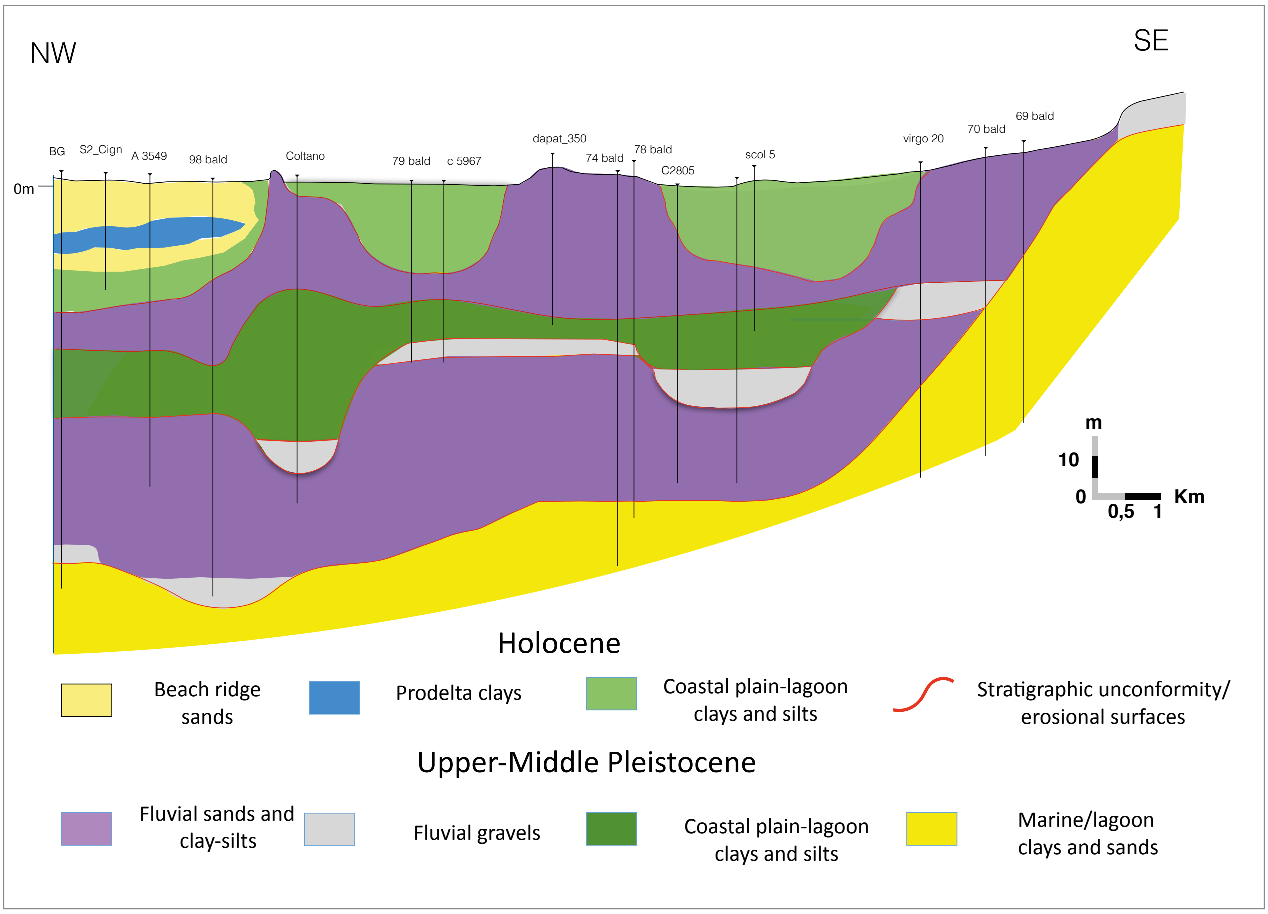

Figure 5 - Stratigraphic section showing the facies architecture of the Holocene-Middle Pleistocene depositional succession, buried beneath the southern portion of the Arno coastal plain. Interpreted stratigraphic relationships between ICS and the formations outcropping along the southern margin of Leghorns Hills are also proposed. Section trace and sedimentary cores location are reported in Figure 2 (red dots).

tures (Mazzini *et al.,* 1999; Amorosi *et al.,* 2008a,b, 2009; Carboni *etal.*, 2010; Milli*et al.,*2013; Breda *et al.,* in press). According to the available literature (Ludwigh *et al.*, 1996; Waelbroech *et al.,* 2002; Siddal *et al.*, 2003; Ferranti *et al.,* 2006) during the MIS3, the age attributed by several authors to the formation of ICS reliefs (Federici & Mazzanti, 1995; Mazzanti, 2000), the sea level was ca. 50-70 m lower than the present-day.

Therefore, the MIS 3 coastline and, consequently, the MIS 3 base level should be shifted tens of km seaward from the modern position even taking into account the relatively low gradient of the Pisa-Leghorn sea platform.

These independent and more generic considerations confirm how much is weak the interpretation of the ICS reliefs as aeolian depositional bodies. Indeed, fossil dunes several meters higher than the present-day aggradational floodplain and detached tens of km from their coeval shoreline would represent a morpho-stratigraphic paradox.

However, the “ICS paradox” is not even resolved by the new facies interpretation of Coltano and Castagnolo sandy deposits as the result of fluvial depositional processes (Carosi *et al.,* in press), because it implies a rate of aggradation so high to still exceed (up to 15 m) the present-day topography. Specifically, MIS 3 fluvial bodies that accommodate to a -50/-70 m base level (Waelbroech *et al.,* 2002) cannot emerge above the modern alluvial-coastal plain formed in equilibrium with the present-day base level.

In this respect, other stratigraphic speculations can be exploited. Following the aforesaid discussion, all chronological attributions related to glacial phases occurring between 40 kyr and the Middle Pleistocene (i.e., MIS 4, MIS 6) should be excluded because their sea-level values are always significantly lower than the present day.

On the other hand, the Mediterranean mean sea-level value attributed to the Last Interglacial -MIS 5e (ca. 6±3 m above s.l.; Lambeck *et al.,* 2004b) could fit with the altimetric quote of the ICS reliefs. Although a Last Interglacial age for amalgamated fluvial deposits so close to the present shoreline (less than 8 km; Figures 1, 4) is unlikely, we cannot totally rejected this interpretation to date. Indeed, along the N Tuscan coastline MIS 5e deposits show a complex distribution due to different tectonic conditions. A marine terrace containing the MIS 5 Senegalese fauna outcrops few km south respects to Coltano and Castagnolo sites (Leghorn terrace in Figure 1; Ciampalini *et al*., 2006), while marine deposits radiometric dated to the MIS 5 and MIS 7 occur at ca. 65-75 m of depth few km north of the Arno River, in the Serchio coastal plain (Enea Core in Figure 1;Carboni*et al.,* 2010).

In this regard, a new light could be shed on the issue of ICS formation if we reconsider the structural-tectonic context of the southern part of the Arno plain and, specifically, if the two reliefs are considered not detached from the Leghorn hills structural unit, where VF deposits extensively outcrop along the margins at quotes ranging between 5-30 meters (Figure 2). Moving northward from the Leghorn hills, which are subject to a weak uplift since the end of MIS 5e (MIS 5e beach deposits outcrop at 15m; Ciampalini *et al.,* 2006), to the Coltano and Castagnolo reliefs the present-day morphology could be the result of a series of erosional events, mainly related to the last glacial sea-level lowering (MIS 5d-MIS 2; Waelbroech *et al.,* 2002) and to the following transgressive postglacial (MIS 1) valley fill processes.

This interpretation determines strong implications on the tectonic arrangement of the southernmost portion of the VB and on the role of the transpressive Sillaro fault running along the Pisa and Leghorn foothills. Indeed, the transition zone connecting the uplifting Leghorn and Pisa hills and the subsiding Arno coastal plain (VB southernmost sector)seems to not coincide with the morphological hills escarpment, as the ICS morpho-stratigraphic features at Coltano and Castagnolo sites imply that this part of the coastal plain likely belongs to the Leghorn hills structural unit.

The consequent question should be where is the exact location of the area connecting the uplifting or not subsiding zone with the true subsiding one. If our argumentations are correct, this area must be necessarily located north of the northernmost VF outcrops (the Castagnolo site; Figures 1 and 2).

On the basis of these observations, the transition zone may be reasonably shifted northward in correspondence of the present-day Arno river course. However, it is clear that our stratigraphic reconstructions will need to be crosschecked with new absolute dating on ICS deposits (e.g., OSL-Optically Stimulated Luminescence dating on sands) and high-resolution tectonic data, in order to assess the reliability of our hypothesis.

Conclusions

The revision of stratigraphic and depositional features of the ICS, in the context of the late Quaternary subsurface and outcrop stratigraphy, shed new light on the tectonic interpretation of the southern margin of the Viareggio Basin. The following key-points summarize our conclusions:

1) The comparison among Late Pleistocene-Holocene sea-level curves, the fluvial nature of ICS and the ICS estimated age is not compatible with the interpretation of a true subsiding context (southern portion of Viareggio Basin);
2) ICS outcrops at the same quote (about 5-15 m) of the VF that constitutes the Leghorn foothills and the Viareggio Basin southern margin;
3) The ICS is geologically connected to the margin of the Leghorns Hills (VF) and likely formed during the glacial periods occurring between MIS 6-MIS 3;
4) The present-day morphology is the inheritance of Late Quaternary strong erosive processes linked to sea-level fall cycles, as also documented in the subsurface by repetitive incised valley fill sequences;
5) Further subsurface and outcropping stratigraphic data along with new tectonic-seismotectonic data and absolute ages on ICS deposits are needed to resolve the "ICS paradox" and define a more accurate geo-tectonic model for the Arno plain southern area.

Acknowledgments

The authors are indebted with Giancarlo Molli and Gianni Zanchetta for their helpful suggestions.

REFERENCES

Aguzzi M., Amorosi A., Colalongo M.L., Lucchi M.R., Rossi V., Sarti G., Vaiani S.C., 2007. Late Quaternary climatic evolution of the Arno coastal plain (Western Tuscany, Italy) from subsurface data. *Sedimentary Geology* 202(1): 211-229.

Aguzzi M., Amorosi A., Sarti G., 2005. Stratigraphic architecture of Late Quaternary deposits in the lower Arno Plain (Tuscany, Italy). *Geologica Romana* 38: 1-10.

Amorosi A., Rossi V., Scarponi D., Vaiani S.C., Ghosh A., 2014. Biosedimentary record postglacial coastal dynamics: high-resolution sequence stratigraphy from the northern Tuscan coast (Italy). *Boreas* 43: 1-16.

Amorosi A., Bini M., Giacomelli S., Pappalardo M., Ribecai C., Rossi V., Sammartino I., Sarti G., 2013a. Middle to late Holocene environmental evolution of the Pisa coastal plain (Tuscany, Italy) and early human settlements. *Quaternary International* 303: 93-106.

Amorosi A., Rossi V., Sarti G., Mattei R., 2013b. Coalescent valley fills from the late Quaternary record of Tuscany (Italy). *Quaternary International* 288, 129-138.

Amorosi A., Lucchi M.R., Rossi V., Sarti G., 2009. Climate change signature of small-scale parasequences from Lateglacial–Holocene transgressive deposits of the Arno valley fill. *Palaeogeography, Palaeoclimatology, Palaeoecology* 273(1): 142-152.

Amorosi A., Pavesi M., Lucchi M.R., Sarti G., Piccin A., 2008a. Climatic signature of cyclic fluvial architecture from the Quaternary of the central Po Plain, Italy. *Sedimentary Geology* 209(1): 58-68.

Amorosi A., Sarti G., Rossi V., Fontana V., 2008b. Anatomy and sequence stratigraphy of the late Quaternary Arno valley fill (Tuscany, Italy). In: Amorosi A., Haq B.U., Sabato L. (Eds.), Advances in Application of Sequence Stratigraphy in Italy. GeoActa, Special Publication, vol. 1, 55-66.

Argnani A., Bernini M., Di Dio G.M., Papani G., Rogledi S., 1997. Stratigraphic record of crustal scale tectonics in the Quaternary of the Northern Apennines (Italy). *Il Quaternario* 10: 595-602.

Baldacci F., 1999. Struttura e piezometria del 1° acquifero artesiano in ghiaie della Pianura Pisana. *Atti Società Toscana Scienze Naturali*, *Memorie Serie A* 106: 91-101.

Benvenuti M., Mariotti-Lippi M., Pallecchi P., Sagri M., 2006. Late-Holocene catastrophic floods in the terminal Arno River (Pisa, Central Italy) from the history of a Roman riverine harbour. *The Holocene* 16(6): 863-876.

Bortolotti V., 1966. La tettonica trasversale dell’Appennino I. – La linea Livorno – Sillaro. *Bollettino della Società Geologica Italiana* 85: 529-540.

Breda A., Amorosi A., Rossi V., Fusco F., in press. Late-glacial to Holocene depositional architecture of the Ombrone palaeovalley system (Southern Tuscany, Italy): sea-level, climate and local factors control in valley-fill variability. *Sedimentology*. doi: 10.1111/sed.12253.

Cantini P., Testa G., Zanchetta G., Cavallini R., 2001. The Plio–Pleistocene evolution of extensional tectonics in northern Tuscany, as constrained by new gravimetric data from the Montecarlo Basin (lower Arno Valley, Italy). *Tectonophysics* 330(1): 25-43.

Carboni M.G., Bergamin L., Di Bella L., Esu D., Cerone E.P., Antonioli F., Verrubbi, V., 2010. Palaeoenvironmental reconstruction of late Quaternary foraminifera and molluscs from the ENEA borehole (Versilian plain, Tuscany, Italy). *Quaternary Research* 74(2): 265-276.

Carosi R., Montomoli C., PertusatI P.C., FrassI C., Leoni L. & Sarti G. (in press) - Carta Geologica d’Italia alla scala 1:50.000. Foglio 273- Pisa.

Carratori L., Ceccarelli Lemut M.L., Frattarelli Fischer L., Garzella G., Greco G., Grifoni Cremonesi R., Tozzi C., 1994. Carta degli elementi naturalistici e storici della Pianura di Pisa e dei rilievi contermini, scala 1: 50.000. In: Mazzanti R. (Ed.), La pianura di Pisa eirilievi contermini la natura e la storia. *Memorie della Società Geografica Italiana* 50, Roma .

Cerrina Feroni A. ,Leoni L., Martelli L., Martinelli P., Ottria G., Sarti G., 2001. The Romagna Apennines, Italy: an eroded duplex. *Geological Journal* 36(1): 39-54.

Ciampalini A., Sammartino F., 2007. Le industrie musteriane e le Sabbie di Ardenza (Livorno). *Quaderni del Museo di Storia Naturale di Livorno* 20: 27-45.

Ciampalini A., Ciulli L., Sarti G., Zanchetta G., 2006. Nuovi dati geologici del sottosuolo del “Terrazzo di Livorno”. *Atti Società Toscana Scienze Naturali*, *Memorie Serie A* 111: 75-82.

Della Rocca B., Mazzanti R., Pranzini E., 1987. Studio geomorfologico della Pianura di Pisa. *Geografia Fisica e Dinamica Quaternaria* 10, 56-84.

Fancelli R., Grifoni R., Mazzanti R., Menchelli S., Nencini C., Pasquinucci M., Tozzi C., 1986.EvoluzionedellaPianura di Pisa. In: Mazzanti R., Grifoni Cremonesi R., Pasquinucci M., PultQuaglia A.M. (Eds.), Terre e Paduli. Reperti, documenti, immagini per la storia di Coltano. Bandecchi e Vivaldi, Pontedera (Pisa), 23-29.

Federici P.R., Mazzanti R., 1995. Note sulle pianure costiere della Toscana. *Memorie della Società Geografica Italiana* 13: 165-270.

Ferranti, L., Antonioli, F., Mauz, B., Amorosi, A., Dai Pra, G., Mastronuzzi, G., Monaco C., Orrù P., Pappalardo M., Radtkei U., Rendaj P., Romano P., Sansò P., Verrubbi V., 2006. Markers of the last interglacial sea-level high stand along the coast of Italy: tectonic implications. *Quaternary International* 145: 30-54.

Ghelardoni R., Giannini E., Nardi R., 1965. Ricostruzione paleogeografica dei bacini neogenici e quaternari della bassa valle dell’Arno sulla base dei sondaggi e rilievi sismici. *Memorie della Società Geologica Italiana* 7: 91-106.

Grifoni Cremonesi R., Tozzi C., 1995. Gli insediamenti dal Paleolitico all’età del Bronzo. In: Mazzanti R. (Ed.), La Pianura di Pisa e di rilievi contermini, Provincia di Pisa, 153-182.

Grün R., Stringer C.B., 1991. Electron spin resonance dating and the evolution of modern humans. *Archaeometry* 33: 153-199.

Lambeck K., Antonioli F., Anzidei M., Ferranti L., Leoni G., Scicchitano G., Silenzi S., 2011. Sea level change along the Italian coast during the Holocene and projections for the future. *Quaternary International* 232(1): 250-257.

Lambeck K., Antonioli F., Purcell A., Silenzi S., 2004a.Sea-level change along the Italian coast for the past 10,000 yr. *Quaternary Science Reviews* 23(14): 1567-1598.

Lambeck K., Antonioli F., Purcell T., Stirling C., 2004b. MIS 5.5 Sea level in the Mediterranean and inferences on the global icevolumes during late MIS 6 and MIS 5.5. In: Proceedings of the 32nd International Geological Congress, Florence. Italy.

Lazzarotto A., Mazzanti R., Nencini C., 1990. Geologia e morfologia dei Comuni di Livorno e Collesalvetti. *Quaderni del Museo di Storia Naturale di Livorno*11: 1-85.

Ludwig W., Probst J.L., 1996. A global modelling of the climatic, morphological, and lithological control of river sediment discharges to the oceans. IAHS Publications-Series of Proceedings and Reports-Intern. Assoc. Hydrological Sciences 236: 21-22.

Malinverno A., Ryan W.B.F., 1986. Extension in the Tyrrhenian sea and shortening in the Apennines as a result of arc migration driven by sinking of the lithosphere. *Tectonics* 5: 227-245.

Mariani M., Prato R., 1988. I bacini neogenici costieri del margine tirrenico: approccio sismico-stratigrafico. *Memorie della Società Geologica Italiana*41: 519-531.

Marroni M., Mazzanti R., Mercini C., 1990. Geologia e morfologia delle colline Pisane. *Quaderni del Museo di Storia Naturale di Livorno* 11(1): 1-40.

Mazzanti R., 2000. Geomorfologia del bacino versiliese-pisano con particolare riferimento alla “gronda del lupi”, scarpata fossile che separa le colline livornesi, con i loro terrazzi eustatici, dalla pianura alluvionale di Pisa. *Atti Società Toscana Scienze Naturali*, *Memorie Serie A,* 107: 169-189.

Mazzini I., Anadon P., Barbieri M., Castorina F., Ferreli L., Gliozzi E., Mola M.,Vittori E., 1999. Late Quaternary sea-level changes along the Tyrrhenian coast near Orbetello (Tuscany, central Italy): palaeoenvironmental reconstruction using ostracods. *Marine Micropaleontology* 37(3): 289-311.

Menchelli S., 1984. Contributoallo studio del territorio pisano: Coltano e l'ex Padule di Stagno. *Studi classici orientali* 32: 255-270.

Milli S., D'Ambrogi C., Bellotti P., Calderoni G., Carboni M.G., Celant A., Ricci V., 2013. The transition from wave-dominated estuary to wave-dominated delta: the Late Quaternary stratigraphic architecture of Tiber River deltaic succession (Italy). *Sedimentary Geology* 284: 159-180.

Pascucci V., 2005. Neogene evolution of the Viareggio Basin, Northern Tuscany (Italy). *GeoActa* 4: 123-138.

Patacca E., Sartori R., Scandone P., 1990. Tyrrhenian basin and Apenninic arcs: kinematic relations since late Tortonian times. *Memorie della Società Geologica Italiana* 45: 425-451.

Pranzini E., 2001. Updrift river mouth migration on cuspate deltas: two examples from the coast of Tuscany (Italy). *Geomorphology* 38(1): 125-132.

Rossi V., Amorosi A., Sarti G., Potenza M., 2011. Influence of inherited topography on the Holocene sedimentary evolution of coastal systems: an example from Arno coastal plain (Tuscany, Italy). *Geomorphology* 135(1): 117-128.

Sarti G., 2012. La macro area: la Pianura di Pisa. In: Civita M. & Redini M. (Eds.), Tutela della costa pisana dall'ingressione marina. Graffiti Pisa, 63-95.

Sarti G., Amorosi A., Rossi V., 2015. Late Quaternary multiple incised-valley systems buried beneath the Pisa Coastal Plain (Tuscany, Italy). INQUA 27 July–2 August 2015, Nagoya, Japan,T01763 (01279).

Siddall M., Rohling E.J., Almogi-Labin A., Hemleben C., Meischner D., Schmelzer I., Smeed, D.A., 2003. Sea-level fluctuations during the last glacial cycle. *Nature* 423(6942): 853-858.

Waelbroeck C., Labeyrie L., Michel E., Duplessy J.C., McManus J.F., Lambeck K., Balbon E., Labracherie M., 2002. Sea-level and deep water temperature changes derived from benthic foraminifera isotopic records. *Quaternary Science Reviews* 21(1): 295-305.

(*ms. pres. il 00 mese 0000; ult. bozze il 00 mese 0000*)